COMPARATIVE STUDY OF BRINE TREATMENT USING A FUNCTIONALIZED NANOFIBRE AND AN ION EXCHANGE RESIN

By

EMMANUEL OLUSEYI OMONIYI

Thesis submitted in fulfilment of the requirements for the degree

Master of Technology: Chemistry

in the

Faculty of Applied Sciences

at the

Cape Peninsula University of Technology

Supervisor: Prof Nico Van Der Walt
Co-supervisor: Prof Leslie Petrik

Bellville
June 2015

DECLARATION

I, Emmanuel Oluseyi Omoniyi, declare that the contents of this thesis represent my own work, and that the thesis has not been submitted before for any degree or academic examination in any other university. Furthermore, it represents my own opinions and not necessarily those of the Cape Peninsula University of Technology.

_____ _____

Signed **Date**

ABSTRACT

In this study, comparative sorption studies of the major metal ions (Mg^{2+}, Ca^{2+}, K^{+} and Na^{+}) in the brine wastewater were performed on hydrophilic materials (PAN nanofibre, PAN+TiO_2 nanofibre, PAN+ZEOLITE nanofibre) and Purolite S950 resin to investigate their uptake performances. For this purpose, PAN nanofibre was electrospun and subsequently doped with 3 wt% each of titanium dioxide and zeolite respectively, in controlled experimental conditions in order to improve its performance. This was followed by the characterization of the respective hydrophilic materials (PAN, PAN+TiO_2 and PAN+ZEOLITE nanofibres) using Fourier Transform Infrared Spectroscopy (FT-IR); Scanning Electron Microscopy (SEM) and X-ray Diffraction (XRD). SEM showed that the incorporation of titanium dioxide or zeolite into the PAN structure made the surface rougher than that of the ordinary PAN nanofibre and FT-IR revealed the peaks belonging to titanium dioxide and zeolite respectively, showing the inorganic materials are within the PAN structure. The XRD analysis complemented the FT-IR of the nanofibres by revealing the peaks characteristic of titanium dioxide and zeolite are present on the PAN structure.

Batch sorption experiments were carried out to investigate the sorption properties of PAN, PAN+TiO_2 and PAN+ZEOLITE nanofibres for Mg^{2+}, Ca^{2+}, K^{+} and Na^{+} ions from brine wastewater. Comparative batch studies using PAN, PAN+TiO_2 and PAN+ZEOLITE nanofibres were carried out using Purolite S950 resin as the standard. Parameters which include contact time, effect of temperature, pH, sorbent dose, sorption isotherms were studied in the sorption experiments to understand the sorption phenomena, loading capacity of the sorbents (nanofibres and resin) and the sorption kinetics for Mg^{2+}, Ca^{2+}, K^{+} and Na^{+} ions from the simulated brine solutions.

The results from the comparative batch studies revealed that the Purolite S950 resin was effective in the removal of the divalent metal ions (Mg^{2+} and Ca^{2+}) over the other metal ions, thereby depicting good selectivity towards Mg^{2+} and Ca^{2+} ions. The removal by the Purolite S950 resin followed the order: $Mg^{2+} > Ca^{2+} > K^{+} > Na^{+}$. The binding capacity to the divalent metal ions is influenced by the aminophosphonic acid functional group attached to the resin.

Langmuir and Freundlich sorption isotherms were employed to evaluate the parameters by fitting the model equations to data obtained from the batch experiments, and the sorption mechanism for Mg^{2+}, Ca^{2+}, K^{+} and Na^{+} was found to follow the Langmuir isotherm model. The sorption capacities for Mg^{2+}, Ca^{2+}, K^{+} and Na^{+} ions were indicating that the monolayer adsorption occurred on all the sorbents.

Purolite S950 resin had faster kinetics than the nanofibres showing that the sorption equilibrium could be reached within 60 minutes, compared to the sorption equilibrium of 120 minutes by the nanofibres. The sorption kinetics of Purolite S950 resin and the nanofibres were also analysed for both pseudo-first order and pseudo-second order mechanisms. The pseudo-second order kinetics gave the best correlation of the experimental data.

Thermodynamic parameters (ΔG°, ΔH° and ΔS°) of the sorption process were evaluated; the result showed the sorption processes were endothermic for all the sorbents. This showed the sorption of the metal ions onto the sorbents would be favourable at high temperature. Also, the positive values of the free energy change (ΔG°) revealed the sorption process onto the sorbents was non-spontaneous and thermodynamically unfavourable.

The order of efficiency and performance of the sorbents can be given as: Purolite S950 resin > PAN+ZEOLITE > PAN+TiO_2 > PAN.

ACKNOWLEDGEMENTS

I express my utmost gratitude to God Almighty for making this project a reality. I am particularly grateful for his abundant grace and mercy throughout the course of this study.

I also express my sincere appreciation to my supervisor Professor Nico Van Der Walt for accepting me for this program, and for his devoted time and excellent guidance throughout the duration of this research project. To my co-supervisor, Professor Leslie Petrik, for giving me an opportunity to be part of the Environmental and Nano Sciences Research Group (ENS) and for her encouragement, guidance, unwavering support and nourishment given to me throughout the period of this research project.

I would also like to express my appreciation to the entire Chemistry Department, CPUT. I wish to thank Mrs Dawn Petersen for her administrative assistance at all times, and also the academic staff; Dr Francois Wewers, Dr S. Olatunji, Mrs Shirley Le Roux, etc, for their assistance and kind gestures. To the technical staff of Analytical Chemistry Laboratory, Cape Peninsula University of Technology; most especially, Mrs Zandile Mthembu, for her assistance and co-operation in acquiring chemicals and the use of certain equipment in the laboratory; Gillian Fennessy-Yon, for her willingness to help at all times. My gratitude also goes to the entire administrative and technical staff of Environmental and Nano Sciences Research Group (ENS), at the University of the Western Cape; Averil Abbott, Vanessa Kellerman, Ilse Wells and Rallston Richards for their assistance throughout the course of this research. I also appreciate the co-operation from the post-doctoral fellows; Dr Olanrewaju Fatoba, Dr Bernardus Barnard, Dr Godfrey Madzivire and colleagues in the Environmental and Nano Sciences Research Group.

I also gratefully acknowledge the efforts of my particular friends especially Chris Samakinde for his kind gestures and assistance throughout the duration of my study. I wish to say thank you to Akintunde Awe for his encouragement, motivation and for being there at all times. To Wasiu Afolabi and Jimoh Tijani for their willingness to help at all times.

My sincere gratitude also goes to my siblings; Bukola Adeyemo, Fisayo Olagunju, Oluwagbenga Omoniyi and Tayo Omoniyi and for their love and prayers and support as always.

Finally, I would like to appreciate my mother, Mrs Faramade Adunni Omoniyi, for the uncommon affection, love and financial support throughout my study.

DEDICATION

This Project is dedicated to

Almighty God

The source of all inspirations

TABLE OF CONTENTS

LIST OF FIGURES

LIST OF TABLES

APPENDICES

GLOSSARY

AMD: Acid mine drainage

BWRO: Brackish water reverse osmosis

C_e: Equilibrium concentration of the sorbate (mg/L)

DMEA: Dimethylethanolamine

DMF: Dimethylformamide

DVB: Divinylbenzene

DWA: Department of Water Affairs

EFC: Eutectic freeze crystallization

ED: Electrodialysis

EDR: Electrodialysis reversal

FT-IR: Fourier Transformed Infrared Spectroscopy

ICP-OES: Inductively Coupled Plasma-Optical Emission Spectroscopy

MED: Multi-effect-distillation

MSF: Multi-stage-flash

MF: Microfiltration

MFI: ZSM-5

MOR: Mordenite

NF: Nanofiltration

PAN: Polyacrylonitrile

PAN+TiO_2: PAN doped with titanium dioxide

PAN+ZEOLITE: PAN doped with zeolite

PS: Polystyrene

Q_e: Amount of metal ions sorbed at equilibrium (mg/g)

RO: Reverse Osmosis

SBA: Strong-based anion

SEM: Scanning Electron Microscopy

SRO: Spiral-wound reverse osmosis

SWRO: Sea water reverse osmosis

TDS: Total dissolved solid

TOC: Total organic carbon

TRO: Tubular reverse osmosis

UF: Ultrafiltration

VC: Vapour compression

WHO: World Health Organisation

XRD: X-ray Diffraction

ZLD: Zero liquid discharge

CHAPTER ONE

1.0 Introduction

The increased level of environmental contamination as a result of industrial development is posing a great threat to the global environment. The industrial processes involved in the extraction of metals or, generally speaking, all the processes involving metals in their productive cycle generate significant metal ions pollution. Refining, mine drainage, metal industries, electroplating, dye and leather industries, landfill leachate, domestic effluents and agricultural run-off, all generate wastewater that contain metal ion contaminants.

The pollution of water by heavy metals and toxic elements has made water treatment the subject of much interest. Therefore, researchers have suggested a cost-effective process, such as ion exchange, to remove these metals from wastewater by using naturally-occurring and synthetic materials (Szostak, 1989; Zamzow & Murphy, 1992; Zoumis *et al.,* 2000).

1.1 Background to the water scarcity problems

The mining industry has been under immense pressure to recycle and re-use water so as to minimize the intake of fresh water from the rivers and from the water utility companies and eliminate the continuous decantation of polluted mine water into the environment and local river systems (Bell *et al.,* 2001). The practice of the mining industries in the past decades has been the continuous pump-outs of the increasing volume of underground mine water into the river systems (Schoeman & Steyn, 2001). This has subsequently resulted in the pollution of the surface and ground water bodies, the soil and the surrounding vegetation in the mining and the catchment areas. The rise in pollution and salinity of the water makes the surface water supply unsafe for drinking, environmental and agricultural purposes. Because of the shortage of fresh water supplies and also, the increasing concern over the effect of heavy metals in the environment, certain water reclamation technologies have been studied and harnessed to various extents and these include ion exchange, chemical precipitation, membrane filtration, reverse osmosis, carbon sorption and co-precipitation/sorption (Kurniawan *et al.,* 2006; Wang *et al.,* 2003).

Water treatment processes, for example, at power stations currently include water recovery through desalination, ion exchange regeneration for water softening to yield boiler feed water and cooling systems which produce blow-down water.

In the mines, on the other hand, desalination, especially reverse osmosis, treats rising underground water to potable levels. Meanwhile, desalination technologies have difficulties associated with managing the inorganic waste products (sludges and brines) that are produced. Majority of the treatment systems yield brines that are of relatively high concentration and invariably are expensive to dispose or to convert into useful by-products. Brines are hypersaline waters that contain high concentrations of toxic elements and salts. They are problematic effluents created by desalination processes such as Reverse Osmosis (RO), electrodialysis (ED), used for coal and gold mining, evaporative cooling power stations and process industries. Such brines are also found in nature in the interior of the earth, and they are also found on the earth's surface as by-products of mining, gas production and oil production (Ndlovu-Yalala, 2010). Brines and salinity build-ups are the resultant effect of the drive to save water through recycling and other recovery processes. The contamination by heavy metal also exists in aqueous waste streams from mining operations. They pose a great risk of metal contamination in groundwater and surface water. Heavy metals are not biodegradable and they accumulate in living organisms, giving rise to various diseases and disorders, e.g., headaches, nausea, vomiting, abdominal pain, neurological disorders, insomnia, forgetfulness, liver damage, lung insufficiency, dizziness, etc, (Jain *et al.,* 2004; Sekar *et al.,* 2004; Iqbal *et al.,* 2007). Therefore, the removal and recovery of heavy metals has become one of the most prominent aspects of environmental research.

Notable development has been made in the past few years with upgraded desalination technologies in industry and mining. Meanwhile, the desalination technologies that are available are outrageously expensive or unsatisfactory due to the long term liability and the dangers brines pose to water resources. Low efficiency in the removal of trace levels of metal ions has been the main limitation. It is therefore important and highly imperative to develop cost effective ways and total integrative solutions to manage brines for long term sustainability relative to pre-treatment, beneficiation, disposal and concentration of the brines. The wastewater treatment selection method is based on the concentration of waste and the cost of treatment. Sorption by ion exchange resin is one of the popular methods for the removal of major, minor and heavy metals from the wastewater and aqueous media (Yavuz *et al.,* 2003).

Various methods have been used to recycle and remove heavy metals from aqueous solutions such as electrochemical treatment, sorption, membrane separation, ion exchange, chemical precipitation, etc, (Miretzky *et al.,* 2006; Shoushtari *et al.,* 2006; Shin *et al.,* 2004; Tahaei *et al.,* 2008). Among all these, sorption is one of the most common and simple methods.

The sorption of metals ions can be achieved by employing polymer materials containing functional groups, for example, amidoxime, tetrazine, phosphoric, carboxyl and amino, etc, (Neghlani *et al.*, 2011), to form strong complexes with metal ions through the coordination reaction. Sorption of metals onto these materials is dependent solely on the functional groups present on the sorbent surfaces.

In recent times, the electrospinning method has been a simple and versatile technique being widely applied to produce nanofibres. The electrospun nanofibres possess numerous interesting characteristics such as high porosity, small interfibrous pore size, and most importantly much larger specific surface in comparison to conventional fibres (Fenglin *et al.*, 2013). The high specific surface makes nanofibres better sorbents (Ma *et al.*, 2006), which have high sorption rates and capacities than other types of materials such as conventional fibres, foams and resins, etc, (Saeed *et al.,* 2008). Thus, nanofibres, modified by introducing functional groups on their surface, could be applicable for the removal and recovery of metals from aqueous solutions.

1.2 Objectives of the study

Processes involved in the treatment of brine (evaporative concentration and other concentration processes, electrolysis, eutectic freeze crystallization-EFC) require the removal of Ca^{2+} and Mg^{2+}. Environmental pollutants like the Ca^{2+}, Mg^{2+} and Na^{+} ions in the waste water have to be recovered and removed, and this has received significant attention. The removal and recovery of these pollutants have health implications and high cost associated with it, for both industrial and domestic consumption. Therefore, the general objective of this study is to develop a super hydrophilic material to address the Ca^{2+} and Mg^{2+} ion contaminants in the brines as these affected the crystallization of NaCl during the eutectic freeze crystallization process in the treatment of brines and also, slow down the evaporation rate of brine from the evaporation pond.

This objective will be addressed by investigating the performance of the PAN and also the improved PAN doped with titanium dioxide (PAN + TiO_2) and zeolite (PAN + Zeolite) in removing the Ca^{2+} and Mg^{2+} from brine solutions and comparing its performance to the conventional commercial resin (Purolite S950). However, this study will seek to establish answers to the research questions:-

a) What is the best possible way to functionalize PAN nanofibre?
b) Can improved nanofibre enhance the brine evaporation rate?

c) How can the ion exchange capacity, equilibrium isotherms and kinetics investigation of the sorbents and solution interphase aid in understanding the interaction between the metal ions and functional groups on the sorbents?
d) How best to evaluate the sorbent/solution ratio: The optimum mass of metal ion uptake per volume effluent?
e) How does the ion exchange capacity of the improved nanofibre compare to that of the commercially-obtained chelating resin exchanger, in order to determine the efficiency of the nanofibres?
f) What is the effect of the competing ions, in observing how they influence metal removal?

1.3 Research Approach

Improved nanofibres (PAN + TiO_2 and PAN + Zeolite) will be used in the treatment of the simulated brine solutions which corresponds to the brines from the Emalahleni Water Reclamation desalination plant. This plant is fed by the acidic and saline mine waters from four different coal mines in the Witbank area which are Greenside Colliery, Klein Kopje Colliery, South Witbank Colliery and the Navigation Colliery. Parameters including pH of the solution, contact time, sorbent dose, effect of concentration and batch sorption experiments will be studied to comprehend the sorption phenomena, the loading capacity of the nanofibre, and the kinetics of sorption of Ca^{2+} and Mg^{2+} from the brine solutions.

The research overview will include the following:

a) Doping of the Polyacrylonitrile nanofibre (PAN nanofibres with titanium dioxide and zeolite and its characterization);
b) Comparative batch sorption experiments comparing Polyacrylonitrile (PAN) nanofibres, doped Polyacrylonitrile nanofibres using the Purolite S950 resin as the standard.

1.4 Problem Statement

The disposal of brines known as hypersaline waters has been a challenge to South African power utilities and mines due to the large volumes generated and the high concentration of

contaminants in the wastewaters. Brine discharge is a problematic effluent from water desalination processes, coal and gold mine drainage, oil and gas production and evaporative cooling in power stations and process industries. Water treatment plants, such as Emalahleni water treatment plant near Mpumalanga, have provided a challenge of how to recover residue water left in the brines and to develop a process to produce saleable by-product from brines. Such brines are usually mixtures of many salts and dissolved materials, and disposal is environmentally problematic and costly. The evaporation ponds method was found to be the most efficient and the cheapest method that can be used to reduce the volume of concentrated salt stream from the reverse osmosis process. But water reclamation plants are experiencing a problem with the rate of evaporation; they generate more brine in reverse osmosis process than what can be evaporated effectively in the evaporation ponds. It is therefore highly imperative to develop a means of enhancing the evaporation rate of the brine.

1.5 Delimitation of Research

In the current study, the following areas will be investigated:

1. Treatment of the brine with cationic resins in simplifying the brine mixture.

2. Doping of PAN nanofibre with titanium dioxide, zeolite and their characterization.

3. Comparative batch sorption experiment of the Purolite S950 resin and improved polyacrylonirile nanofibre.

4. Simulated solutions of calcium chloride, magnesium chloride potassium nitrate and sodium chloride based on the composition and concentrations of the brine (major cations) that would be used.

1.6 Thesis Outline

The remaining parts of the thesis will be divided into the following chapters:

Chapter 2: Literature review

A detailed review of literature about the generation of brines and their effects on the environment, the methods of treatment employed in the brine waste water treatment, ion

exchange mechanism and sorption process as an alternative means for the treatment of waste water, and the application of PAN nanofibres will be discussed.

Chapter 3: Methodology

Sample preparation procedure for the electrospinning of Polyacrylonitrile nanofibres, doped PAN with titanium dioxide and zeolite and the subsequent characterization of the fibres using Scanning Electron Microscopy (SEM), Fourier Transform Infra-red Spectroscopy (FT-IR) and XRD.

Batch sorption experiments will be presented with concise experimental procedures as well as important formula for various calculations.

Chapter 4: Results and Discussion:

The basis of discussion in this chapter will involve the outcome of the characterization of the plain and doped Polyacrylonitrile nanofibres where the degree of functionalization will be assessed and presented. Sorption behaviours of PAN nanofibre and doped nanofibres will also be shown. The graphs and results describing the kinetics, sorption and the equilibrium of the sorption process for both Purolite S950 resins and the nanofibres will be discussed.

Chapter 5: Conclusion and Recommendations

Conclusion on the metal-removal capacity of the sorbents and especially the performance of the doped nanofibres will be assessed and discussed. Directions for future work will also be suggested. Recommendations will also be made and irregularities noted.

CHAPTER TWO

2.0 Literature Review

It is very important here to discuss water scarcity and pollution, brines, the nanofibre materials and properties, their background in use as sorbents as well as their applications. This section is going to present the relevant information on the use of nanofibre as an alternative sorbent in wastewater treatment such as brines.

2.1 Water Scarcity and Pollution

There have been many debates about the water crisis, but the obvious reality is that 1.2 billion people do not have access to safe and affordable water for their domestic use, according to the World Health Organization (WHO). Not very well documented is the fact that most of the 900 million people in the rural areas that have an income below the one-dollar-per-day poverty mark do not have access to water for their livelihoods and this has significant impact on the people's well-being. The lack of access to safe drinking water and good sanitation, with poor personal hygiene, results in health implications, especially through diarrhoeal diseases, which is estimated to cost the lives of 2.18 million people, three-quarters of whom are children younger than the age of 5 years, annually, and also, a yearly universal burden of disease estimated as 82 million disability adjusted life years (Pruss *et al.*, 2002). Water scarcity could be defined to be a situation when an individual does not have access to safe and affordable water to satisfy his or her needs for the purpose of drinking, washing or their livelihoods generally; such individual is said to be water insecure (Rijsberman, 2006). And when a large amount of people in a particular location are water insecure for a notable period of time, such an area can be referred to as water scarce (Rijsberman, 2006). Water forms the basic essence of life as it is required in various aspects of life that is, human consumption, industrial use and agriculture. Its scarcity brings enormous problems for people and societies (Pereira *et al.*, 2002). We all must be prepared to become involved in the preservation of natural water sources. The available natural water bodies do not have enough capacity to meet the increased water demands and also have limited capacity to receive pollutant charges of the effluents from the alarming expansion of industrial, urban and agricultural uses. In the areas where water scarcity are prominent, the water resources are already degraded, or put under degradation processes both in quality and quantity, this in turn adds to the shortage of water. There are still water conflicts in water-stressed areas among local settlements and authorities

on the preservation of natural ecosystems. Urban and domestic uses and/or, activities that alleviate poverty and hunger, for example, the uses in the industry, food production and energy are being given foremost priority while the preservation protocols are ignored.

Water scarcity may be a consequence of a range of processes and these may be as a result of natural causes (arid and semi-arid climates and droughts), it may also be induced by human activities (desertification and water management), or may be the consequence of the interaction of both (Pereira *et al.*, 2002). Figure 2.1 shows the arid and semi-arid regions of the world.

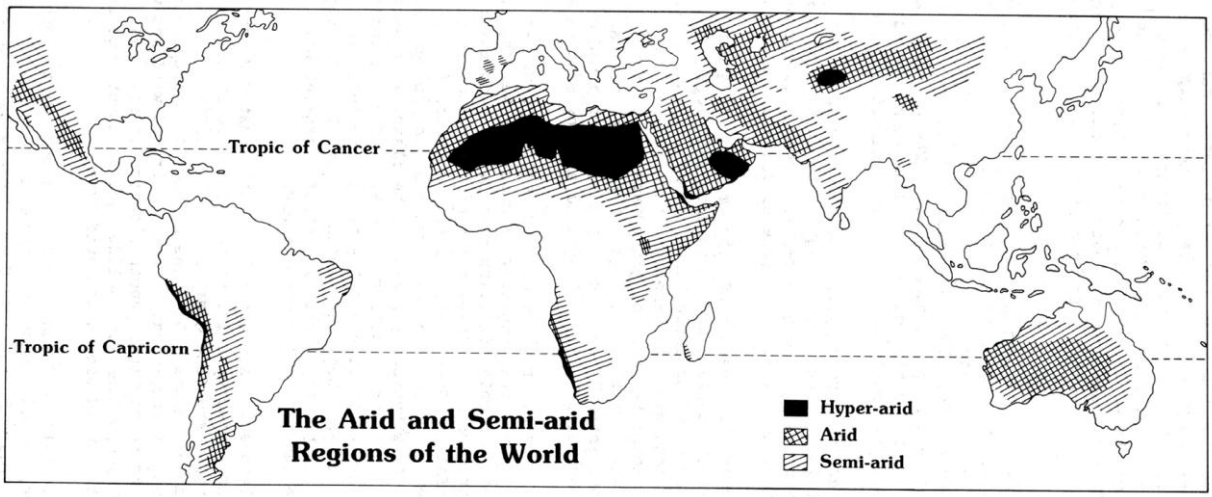

Figure 2.1: The arid and semi-arid regions of the world
(Hufschmidt & Kindler, 1991)

Preservation of water is crucial all around the world. The Republic of South Africa is a semi-arid country with the problem of water shortages and the rate of population increase has resulted in an increase in fresh water demands. To begin with, countries that do not have much water would suffer serious future consequences if subjected to any pollution. The fresh water supply in South Africa is almost stretched to its limit (Schlacher & Wooldridge, 1996). Less than 10% of rainfall in South Africa is available as surface water, which is one of the lowest conversion ratios in the world (Anon, 1986). Rainfall distribution varies in a significant manner and water resource availability is uneven having approximately 60% of river flow being generated from 20% of the land area (east coast). Ground water resources in South Africa are also limited. The ground water sources over-abstraction associated with the deep pump irrigation has resulted in minimized supply of freshwater to communities and subsequently results in the drying up of lakes and rivers.

South Africa is categorized currently as a water-stressed country, having an annual availability of fresh water of less than 1700 m^3 per capita which is the index for water stress. According to one of the indicators defining water scarcity called the Falkenmark indicator or water stress index, calculating water availability per person can serve as a measure defining water scarcity if it is known how much water is needed to satisfy a person's need (Falkenmark *et al.*, 1989). Falkenmark *et al.*, (1989) proposed 1700 m^3 of renewable water resources per capita per year as the threshold, based on the evaluations of water requirements in the household, industrial, agricultural and energy sectors, including the needs of the environment. Therefore, countries which cannot sustain this renewable water supplies figure are said to be water stressed. Also, when the supply falls below 1 000 m^3 it is said to be water scarcity, and below 500 m^3, an absolute scarcity. Figure 2.2 illustrates water scarcity in 2030 using Falkenmark indicator.

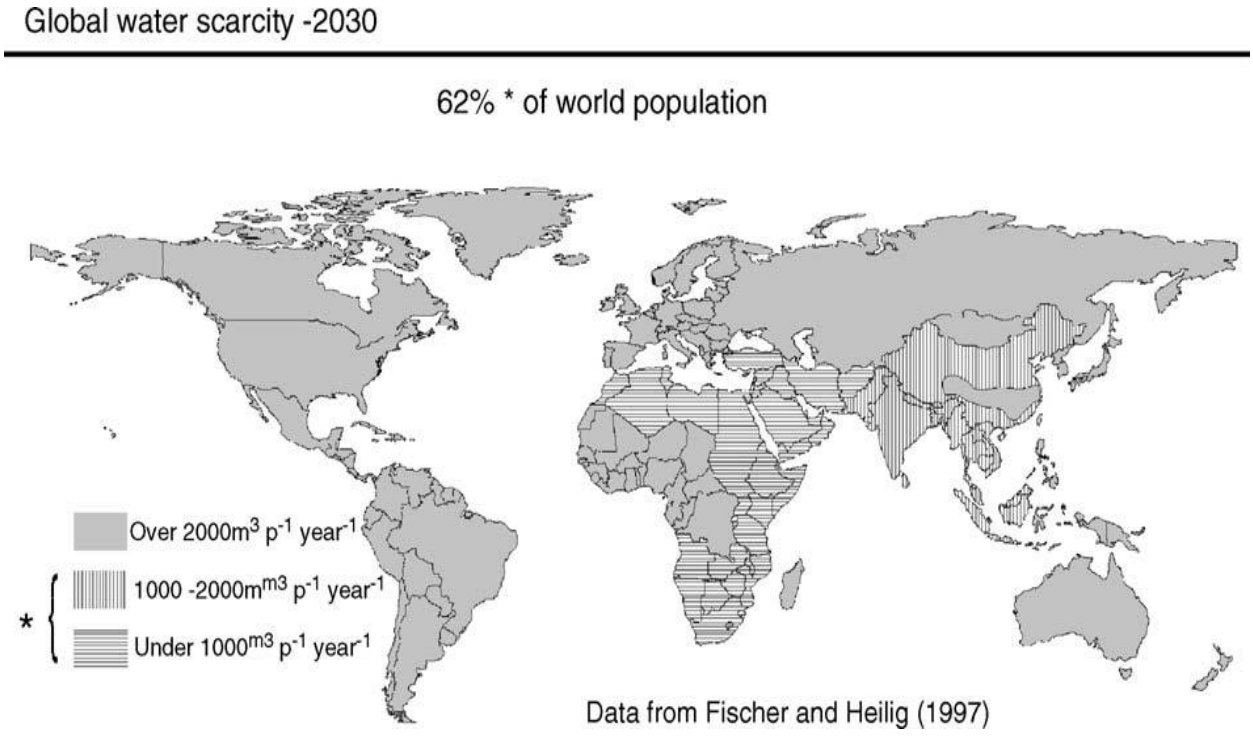

Figure 2.2: Water scarcity in 2030 based on the Falkenmark indicator.
(Source: Wallace, 2000).

The current calculation by the Food and Agricultural Organization (FAO) is 1.154 m^3 per capita per year. South Africa's vast expanses are considered arid and semi-arid land with 65% of the country receiving an inadequate rainfall, less than the minimum amount of rainfall required for successful farming in dry land (<500 mm/year) (Anon, 1986). The consistent lack of adequate rainfall has resulted in an increase in water demand, and this is experienced in

rural and urban communities, which may possibly result in more conflict in its allocation and invariably, a further stress on water resource leading to scarcity. Typical conflicts can be said to be that existing between consistently growing urban areas using water for agriculture or a conflict existing between agriculture and the environment in the process of agricultural expansion or finding new resources to replace the ones given to the urban areas. Meanwhile, the sharp increase in the use of water and chemicals which fuelled the Green revolution has played a significant role in environmental degradation, and also threatened the water resource base upon which we depend for food and livelihoods (Rijsberman, 2006).

In South Africa, water pollution comes majorly from the mining industries. Industrial power plants handle large volumes of process waters that are contaminated with chemicals, metal ions, and other materials (Feng, 2004). The pollution caused to the scarce water resources of South Africa as a result of mining is one of the serious challenges being faced by the country. The mining sector contributes between 20-30% of mineral sales of South Africa, which is the second largest exporter of coal in the world as well (Lloyd, 2002). The generating technology in South Africa depends largely on coal-fired power stations, with about a million tons of coal being the source of energy supplying South African homes. The supply of electricity makes up 25% of the final energy demand of the South African economy (Lloyd, 2002). The major heavy metal-containing waste that comes directly from the coal mining operations even years after the closure of the mine, is acid mine drainage (AMD) and because of the proximity of mining sites to the natural streams, thousands of kilometres may be affected and consequently, toxic metal pollutants enter the waterways. Both the underground mine systems of coal as well as gold mine are interconnected and depend on collective and responsible mine-water management to sustain their separate operations (Bell *et al.*, 2001). Most mine-water is pumped to the surface to allow continuous deep underground mining operations. Some of the water is then stored and treated, before reuse and the remaining water is normally released into surrounding streams and rivers as mine-brine waste water or AMD. The rise in pollution and salinity of the surface water makes it unfit for drinking, agriculture or environmental purposes. South Africa is currently on the campaign to increase and improve the quality and quantity of potable water both for industrial and domestic uses. As a result, potable water demand levels are soaring, which eventually might lead to scarcity. Major factors contributing to water scarcity in South Africa range from pollution of water resources through mining activities (brines and AMD) and limited fresh water supplies, population growth and increased demand for water from mining, the industry and domestic sectors (Rijsberman, 2006). For this demand to be met, water reclamation has been imperatively

identified as a viable alternative to augment the supply of water. Sources subject to reclamation have been identified and these include underground and mine waters, industrial waste waters, brackish, saline and brine wastewaters.

2.2 Brine

Brine is wastewater saturated with dissolved salts such as potassium, calcium, sodium, sulphates, chlorides and nitrate ions and high total dissolved solids (< 1,500 mg/kg TDS)(El-Manharawy & Hafez, 2003). It is formed through water treatment when Tubular Reverse Osmosis (TRO) is employed to treat wastewater as the situation is at the Emalahleni water treatment plant. Brine is a concentrated stream that contains a total dissolved solids (TDS) greater than 36 g/L. Brine is water saturated or nearly saturated with salt, while natural brines are waters that contain very high to an extremely high concentration of dissolved constituents such as elements, molecules and ions. It is also considered that brines are those waters more saline, or more concentrated in dissolved materials, than sea water (35 grams of dissolved constituents per kilogram of sea water) (Sonqishe *et al.,* 2009). Also, brine can contain concentration of salt more than five times greater than the salt content of average sea water (Sonqishe *et al.,* 2009). Brines are basically of commercial interest, especially in the production of table salt. Brines also occur in nature and are found in the earth's interior and also on the earth's surface as a by-product of mining, salt lakes, gas production and oil production. Brine wastewater is a by-product of various water treatment processes such as desalination, power generating stations. There is a need for proper handling when disposed because of its potential to pollute the groundwater and also, cause water pollution which results in levels of salinity in excess of the Department of Water Affairs (DWA)'s limits (Gunther *et al*., 2008). The feed source of South African brine that is produced from coal-mining industries in the Witbank region is an excessive volume of groundwater with a quantifiably high salt concentration from coal mines that is either associated with sulphate, calcium, magnesium (neutral type of water), or that is slightly acidic (containing Fe, Mn and Al metals)(Ndlovu-Yalala, 2010).

2.2.1 Brines Sources

The brine wastewater source that will be studied in this research is an effluent waste stream from the Emalahleni Water Desalination plant; this plant uses reverse osmosis technology. This plant gets its feed from four different coal mines in the Witbank area which are

Greenside Colliery, Klein Kopje Colliery, South Witbank Colliery and the Navigation Colliery. The waste water is pumped from these coal mines to the Emalahleni Water Reclamation plant. The quality of water from these mines is rich in the basic constituents like calcium, magnesium, sulphate ions for neutral type of water and the slightly acidic type which is associated with manganese, aluminium and iron metals. Klein Kopje colliery has 12 million m^3 of stored underground mine water currently which is estimated to be generating at a rate of 14 ML/d (Annandale *et al.,* 2002). The Emalahleni Water Desalination Plant offers the privilege to study this kind of brine having in mind that in the process of its purification, it concentrates the salts and at the same time handles large volumes of saline water therefore showing the need for an environmentally-sound method of disposal. The high volume of mine water being generated and its high concentration gives the chance to try cost-effective sorbents that have high sorption capacity with greater kinetics.

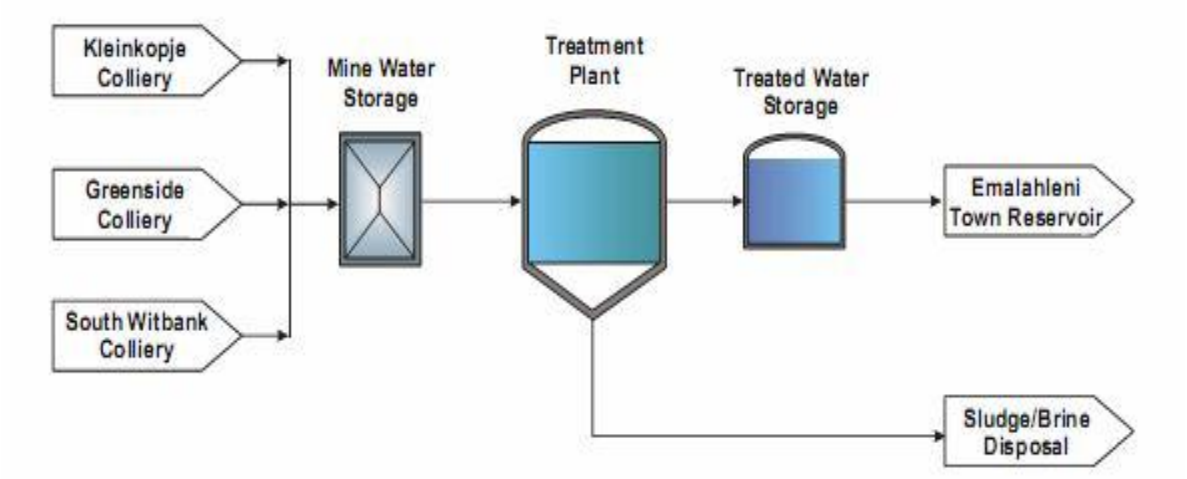

Figure 2.3: Schematic diagram of the Emalahleni desalination plant.

This next section will describe the sources of brine waste water streams from the power stations, coal mines and desalination processes in detail.

2.2.1.1 The Brines from Power Stations

The most abundant source of energy in South Africa is coal, which is a low grade bituminous coal that has a low heat value with high content of ash (Willis, 1987).

The power generating company in South Africa, Eskom, depends on coal-fired power stations in order to produce 90% of its electricity and for the purpose of logistics, the power stations were situated near the coal mines (Willis, 1987). Annually, over 100 million tons of coal is

being used by Eskom (Willis, 1987). In South Africa, coal mining is relatively cheap compared to the rest of the world. The costs are about four times higher in Europe. Therefore, the low costs have enhanced the country's prosperity and the chances for development. In the power stations, the cooling towers utilize the process of evaporation in order to release heat from process water, and to keep the salt concentration's balance, a part of the water is taken off to be replaced with fresh water. The blow-down water, which is the water discarded, has characteristics such as hardness and high concentration of salt, majorly calcium carbonate ($CaCO_3$) and calcium sulphate ($CaSO_4$) (Stratton and Lee, 1975). Blow-down water also has high turbidity and conductivity, and a pH range between 9.6 – 10.5 (Khedr, 2008). Treatment is needed to soften and remove the salt, so that the standard of water can be brought to an acceptable level for use in the plant. At certain power stations like the Tutuka Power Station, feed water is composed of neighbouring coal mine's water produce and the site's cooling water blowdown which is 50% cooling water and 50% mine water (Khedr *et al.,* 2008; Burhrmann *et al.,* 1999). Recovery is carried out using a combination of full scale membrane applications including Electrodialysis Reversal (EDR) and Spiral-wound Reverse Osmosis (SRO). A highly concentrated saline solution is produced as by-product of the EDR and SRO processes during the regeneration of the membranes. Conventionally, regenerating material with excess sodium chloride (NaCl) is used to regenerate cation exchange water softeners, whereby the sodium ions replace the magnesium and calcium ions which are trapped on the ion exchange resin. This subsequently leads to the production of calcium and magnesium chlorides. However, materials in the regenerant wastes are soluble and they contribute greatly to the TDS when discharged into the water course.

2.2.1.2 Saline Waters from Coal Mines

In South Africa, coal is mined in the Free State, Gauteng, Kwazulu-Natal and Mpumalanga provinces. In the 1930s and 1940s, the mining methods used in the coal mines were responsible for most environmental problems, especially the practice of pillar robbing (Pereira *et al.,* 2002). The northern Free State and Mpumalanga are the provinces where the majority of coal deposits are found. Generally in Mpumalanga, it is found at shallow depths and thick seams unlike Kwazulu-Natal, where the seams are deeper and thinner, only that they are of higher quality. Since it is found at shallow depths in Mpumalanga, it is easier and cheaper to mine, therefore, it is the most cost-effective and efficient way of generating electricity. Most coal mines in the Mpumalanga province have a water quality characteristic of calcium-magnesium-sulphate rich, neutral water type (refer to table 2:1; Annandale *et al.,* 2002) while

certain mines have more problems of acidic types of water that gives pH's below 3, also, saline mine waters have a TDS at about 4000 mg/L with a conductivity that varies between 2000 μS/cm and 6500 μS/cm, and acidity is associated with manganese, iron and aluminium concentrations (Gunther *et al*., 2008; Buhrmann *et al.,* 1999).

Table 2.1: Mine water quality from 3 coal mines in Witbank

Water	Electrical Conductivity (mS/m)	pH	Mg^{2+} (mg/L)	Ca^{2+} (mg/L)	Na^{+} (mg/L)	K^{+} (mg/L)	Cl^{-} (mg/L)	SO_4^{2-} (mg/L)	HCO_3^{-} (mg/L)
Tweet fontein Colliery, Kleinkopje	227	7.1	196	405	47	-	32	1524	68
Landau Colliery	156	6.0	19	287	7	11	3	998	10
Jacuzzi Colliery, Kleinkopje	288	6.4	170	555	46	-	19	1986	142

(Ndlovu-Yalala, 2010)

It is imperative that the underground coal mines deal with the excess quantities of underground water (Buhrmann *et al.,* 1999). Presently, no accurate measures exist of the total volumes of water contained in old underground workings, neither of the rate at which additional water affected is accumulating (Annandale *et al.,* 2002). The mines keep expanding and so, there is a continuous influx of water into the mine which raises an urgent need for water to be pumped out. Meanwhile when mining activity is over at a particular section, it is closed and the pumping machine is evacuated. And when the mine roof collapses, the aquifer breaks which results in underground water flowing into the mine. It was estimated in 1992 that 130,000 tons of salt were discharged from coal mines, and 200,000 tons discharged from the gold mines (Annandale *et al.,* 2002). Therefore, at an average total dissolved salts concentration of 2 g/L, this would mean an annual discharge of some 65 million m^3 of water from the coal mines, and 100 million m^3 from the gold mines. Still, it is expected that these volumes will increase with time (Annandale *et al.,* 2002).

2.2.1.3 Brines from the Desalination Processes

In most arid nations where structural shortage of water is a constant phenomenon, desalination becomes the solution for water scarcity. Countries like Israel, Cyprus and Jordan

which have exploited their sources of natural water and having no more sources to exploit resort to desalination process as an escape route.

Desalination is a separation process which is used to reduce the dissolved salt content of saline water to a usable level. Three liquid streams are involved in all desalination processes: the saline feed-water (brackish water or seawater), low-salinity product water, and the very saline concentrate (brine or reject water) which must be disposed of.

The volume of concentrate produced from a particular desalination plant is a factor of the recovery rate of the desalination process. However, in the desalination processes, one of the demerits is that seawater reverse osmosis (SWRO) plants can yield a concentrate which is two times more concentrated than the feed waters; on the other hand, the yield concentrate from the distillation process may have salt concentration of only 10% (Tsiourtis, 2001; Mauguin & Corsin, 2005). Brackish water reverse osmosis plants (BWRO) yielded 25% of the total feed water (Awerbuch & Weekes, 1990), in the case of groundwater reverse osmosis plants (RO), the yield is between 10-25% of the total feed water (Alaabdula'aly & Al-Saati, 1995). The membrane performances which are generally acceptable for water recovery yields fall in the region between 30-60% for Sea Water Reverse Osmosis (SWRO), 60-85% for Brackish Water Reverse Osmosis (BWRO), 85-97% for BWRO with concentrators and 95-99.5% for salt rejection (Wangnick, 2002). In spite of energy consumption, the key criterion for implementing the RO technology is the volume of concentrate produced in the process. The volume of concentrate generated is much more critical for inland RO plants situated in areas distant from the ocean (Oren *et al.,* 2010). Water quality of RO concentrate from industrial sites however, can be different from the municipal concentrates. For instance, mine-contaminated groundwater treatment sites have a high concentration of calcium (>1000 mg/L), silica (>200 mg/L) and sulfate (>4500 mg/L) in addition to metals (Subramani *et al.*, 2012.). The presence of sparingly soluble salts in RO concentrate from municipal wastewater treatment plants, results in the total organic carbon (TOC) also being high (>30 mg/L) (Lee *et al.,* 2009). Concentrate generated from the membrane desalination processes has basic characteristics of high TDS and minimal quantity of process-added chemicals. The salinity range 2000 – 5000 mg/L of the brackish waters can be reduced to drinking quality at a cost of approximately $0.75 - $1.00 per 1000 gallons compared to the range of $3.00 - $5.00 per 1000 gallons of seawater desalination costs. Most importantly, the two commercial technologies are based on the membrane and thermal processes. Membrane processes include reverse osmosis (RO), microfiltration (MF), electrodialysis (ED), nanofiltration (NF), and ultrafiltration (UF). While thermal processes include multi-effect distillation (MED), multi-

stage flash evaporation (MSF) and vapour compression distillation (VC) (Tang & Yong, 2008). These systems are chosen based on the costs of operation, the effluent stream type and the energy consumption. The multi-stage flash evaporation (MSF) and RO processes have been the most widely adopted for both seawater and brackish water desalination, both making up 84% of the total installed capacity (Turek, 2004) (Figure 2.4). Also, desalination plants have treated different concentrations of raw water, mostly seawater and brackish water (Turek, 2004).

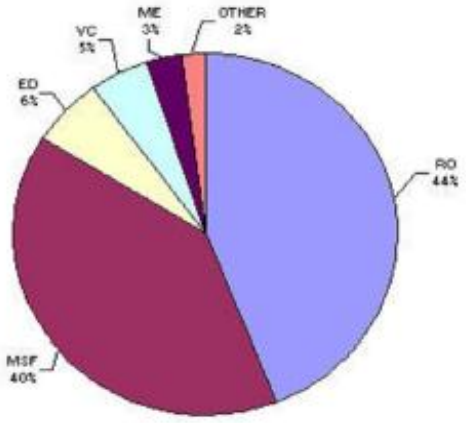

Figure 2.4: The installed desalination capacity methods
(RO = 44%; MSF = 40%; ED = 6%; VC = 5%; ME = 3%; Other =2%).

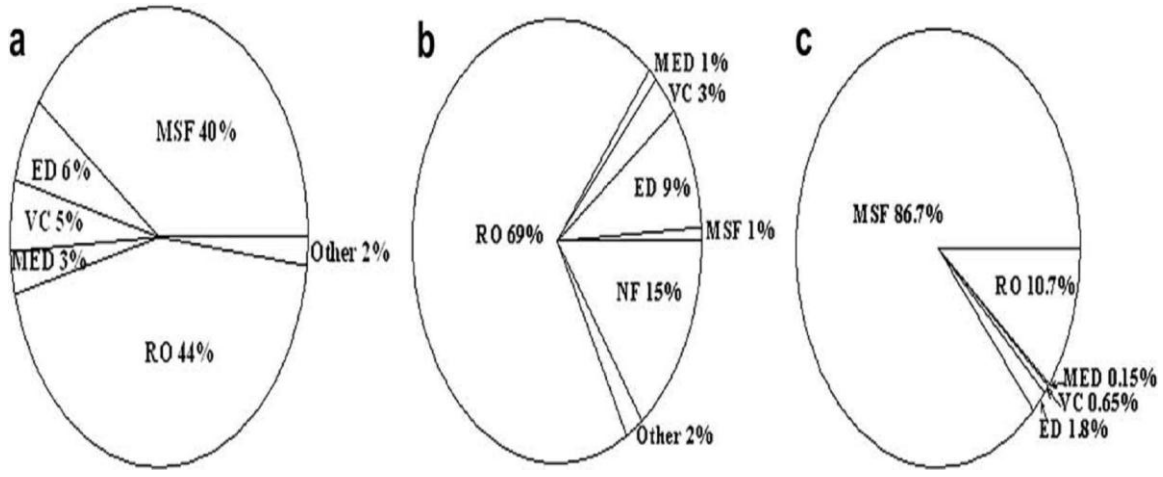

Figure 2.5: Desalination production capacity by process technology distribution
(a) All over the world, (b) In the United States (c) In the Middle East (Arabia, Kuwait, Oman, United Arab Emirates, Qatar and Bahrain (Greenlee *et al.*, 2009)

2.2.2 Thermal Processes-based Treatment Technologies

For many centuries, thermal desalination has been the main distillation process for production of fresh water, but in the 1950s, large-scale drinking water distillation plants began to operate.

About 75% of the total desalination plants today use some variation of the Thermal desalination processes owing to its simplicity and global applicability (Abufaved & El-Ghuel, 2001). The efficiency of the distillation cycle is dependent on the difference in temperature of the surrounding seawater at the intake to the discharged effluent. Lower differential temperature results in higher efficiency of the system and subsequently results in lower power consumption.

Water is generally evaporated and the vapour that results condenses and is received as fresh water. The multi-effect evaporator gives out latent heat by the condensing water and this is used to evaporate water at a lower pressure in a separate vessel, referred to as an "effect" (El-Dessouky *et al.,* 1998). Evaporation by multi-stage-flash (MSF) takes place by superheating water under pressure, and then the pressure is released. As a result of pressure release, water evapourates spontaneously until it cools down to the boiling point. This heated water is subsequently passed through a succession of chambers called "stages" at lower pressures. As a result of many effects or stages addition, energy consumption of these processes is reduced, therefore, the names "multi-effect" and "multi-stage flash" are derived. Steam of 1 kg can produce approximately 15 kg of potable water (Khawaji *et al.,* 2008). Middle East countries initiated the design and implementation of thermal distillation. At first, they used multi-effect distillation (MED) and later developed a process known as multi-stage-flash (MSF) distillation (Greenlee *et al.,* 2009). The thermal desalination technology is being overtaken by the development of membrane processes in the Middle East since 1960s because of new plant installations. However countries in the Middle East still use thermal desalination due to easily accessible fossil fuel resources and poor water quality of the local feed water. Thermal desalination helps when feed water is more concentrated at high temperatures (Greenlee *et al.,* 2009). Distillation can remove 99.5% impurities from water but the cost is quite capital-intensive for the treatment of large volumes of water and also, more energy-consuming than reverse osmosis systems, but as it requires less pre-treatment of the water, it is therefore given more consideration (Khawaji *et al.,* 2008). It is a good process for the removal of heavy metals, sodium, nitrates, hardness, dissolved solids, bacteria and many organics.

2.2.3 Membrane Processes Treatment Technologies

The two basic types of membrane desalination processes are: Reverse Osmosis (RO) and electrodialysis (ED). In the case of reverse osmosis, pressure is applied and forces water to pass through a membrane overcoming the natural osmotic pressure of water in flowing from

region of high concentration to low concentration, to divide the water into a dilute product stream and a concentrated brine stream (i.e. water molecules are forced by the pressure to flow against the osmotic gradient through a series of membranes that are permeable to water but that trap salt). Water molecules pass through the membrane while contaminants are flushed along the surface of membrane and come out as concentrated brine in a separate stream. RO membranes have a negatively charged surface and repel negatively charged ions or molecules and more cations are then present near the membrane surface, thus an electric potential that is known as the Donnan potential, is created (Greenlee *et al.,* 2009). The Donnan potential helps in repelling ions by the membrane; meanwhile, divalent ions or increasing salinity decreases the effect of Donnan potential on salt rejection.

Typically, Reverse Osmosis membranes achieve sodium chloride rejections of 98 – 99.8%.

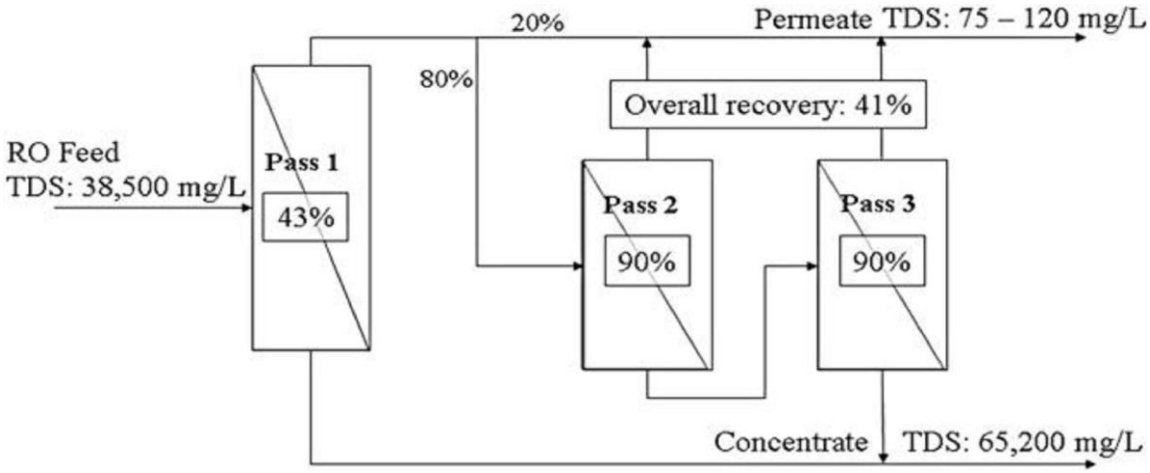

Figure 2.6: Schematic diagram illustration of a typical Reverse Osmosis (RO) plant.
(Greenlee *et al*., 2009)

Every box in Figure 2.6 represents one RO pass and their respective recovery (in %) (Greenlee *et al.,* 2009). In electrodialysis (ED), contaminants are removed from water by using an electric field to pull ionic impurities through ion-selective membranes, away from the purified water. The ED process is effective for salt removal from feed water because the cathode attracts the sodium ions and the anode attracts chloride ions.

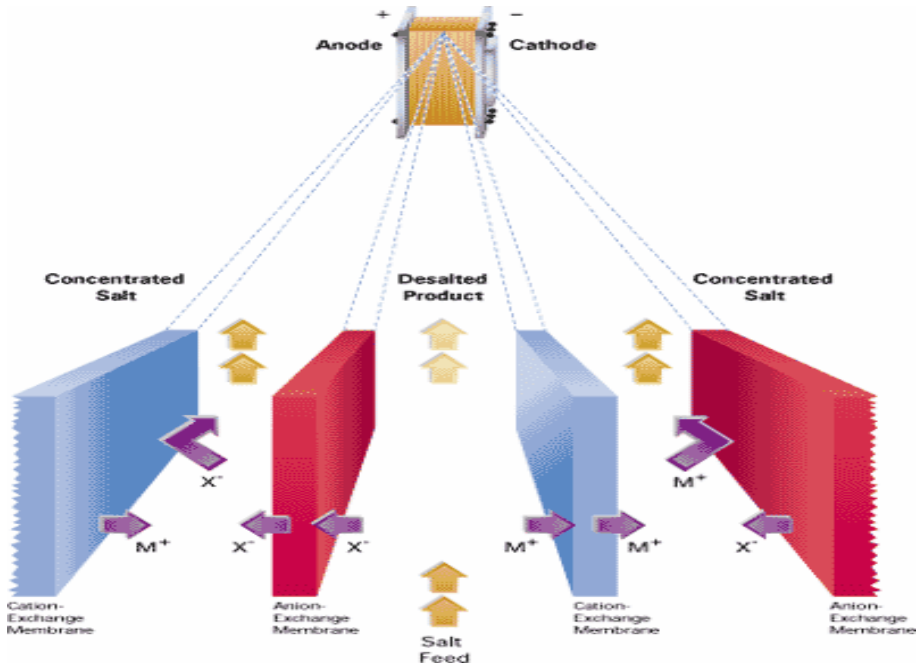

Figure 2.7: Diagrammatic scheme of an electrodialyzer having two cell pairs. (Valerdi-Perez *et al*., 2000).

Figure 2.7 illustrates the electrodialysis (ED) process, the migration of ions is triggered by an electric field. As a result, water is desalinized and becomes fresh (Valerdi-Perez *et al.,* 2000). The recovery rate is high and the ED process can remove 75 to 98 % of total dissolved solids from the feed water (Chamier, 2007). ED however has its disadvantages. There is a limitation to the amount of contaminants it can remove. For example, it cannot remove pyrogens, organics and elemental metals that have weak or non-existent surface charges because they are attached to the membranes. It also requires skilled operators and routine maintenance. According to Korngold *et al*., 2009, detergents and certain colloids may get attached to the pores of the membrane thereby reducing their ionic transport ability, thus, there is a need for constant cleaning of the membranes. Brine concentration can be increased by electrodialysis from 1.5% - 10% in trying to reduce the brine effluent volume and disposal costs (Korngold *et al.,* 2009). Setbacks are however experienced with ED when laboratory-grade water is being produced owing to the precipitation of $CaSO_4$ on the surface of the membrane during the concentration (Korngold *et al.,* 2009). There is a need for the treatment technologies improvement owing to the high demand for these processes caused by the scarcity of fresh water. It becomes imperative to validate and implement the desalination processes to reduce or treat the concentrate effluent.

2.2.4 The Impact of Brine on the Environment

The impact of the desalination process on the environment has been an aspect of desalination that has been ignored. Certain methods are employed in the disposal of brine and each one has merits and demerits and of course, an interplay of factors which include local available resources, cost, impact on the environment and technology. Meanwhile, major environmental issues affecting a desalination plant include brine disposal, energy considerations and the location of the plant. Obviously, plant location becomes an issue in a situation where the selection of site must be determined by considering the energy supply availability and the proximity to feed water intake, site for brine disposal and water end-user (Svenson, 2005). The residues of water-softening chemicals (lime), flocculation (iron and aluminium silicates, sulphates), antiscalants, disinfectants (sodium hypochlorite, chlorine) and antifoaming agents are all contained in the brine reject streams. The primary make-up of reject brine to salinity and high TDS levels in water is the combination of magnesium, sodium, calcium and chloride, which can have harmful effects for livestock and human consumption. Water pollution is the consequence of land disposal which results when concentrated brine is discharged into sources of fresh water and unprotected wells. The composition of brine has a major effect on the environment, as the degree of salinity in soil truncates crop growth, which is shown by the reduction in the growth of plants, leaf colour, darkening and scorching of shoots. The growth of most plants reduces due to the increase in the osmotic pressure as a result of the presence of salts in the soil and soil water. This is because the dissolved salts increase the osmotic potential in the soil water and subsequently increase the energy needed by the plants in the extraction of water from soil. High concentration of solute present in the soil solution is good for favourable physical properties in the soil, while a high concentration of sodium and chloride in clay soil reduces aeration, soil permeability and triggers dispersion of soil particles and could bring about an alteration in the electrical conductivity of soil, invariably changing the sodium sorption ratio (SAR) and subsequently induces specific ion toxicity (Ndlovu-Yalala, 2010). The surface discharge of reject brine from inland desalination plants could have a negative impact on soil and groundwater (Rao *et al.,* 1990; Mohamed *et al.,* 2005 and Al-Faifi *et al.,* 2010). Certain other researchers have reviewed the impact of reject brine composition and conditions on marine life (Lattemann & Hopner, 2005; Sadhwani *et al.*, 2005).

2.2.5 The Disposal of Brine

Disposal of brines has been a major problem facing inland desalination plants owing to many factors such as: Environmental regulations aimed at protecting the environment from continued pollution, the increase in the volume of brine rejects being generated and the alarming costs associated with wastewater desalination in an attempt to augment fresh water supplies and the cost of disposal in an environmentally friendly manner. The desalination process produces the highest amount of brine wastewater with about 20-50% of the total feed water flowing as reject brine. The amount of brine produced, as a percentage of the feed water, depends on the choice of the method, initial salinity of feed water and factors affecting the choice of disposal method. The factors that influence the selection of a disposal method were identified by Mickley *et al.,* (1993) and these include volume of the concentrate, constituent of the concentrate, physical or geographical location of the concentrate discharge point, availability of the receiving site, public acceptance, capital and operating costs and possible facility expansion.

The major methods of brine disposal according to Glater *et al.,* (2003) are: deep well injection, evaporation ponds, and solar ponds, they are not however applicable to large volumes of wastewater. There are various other options for the disposal of brine waste water; they are waste minimization, disposal into surface water bodies, disposal into municipal sewers, pumping into specially designed evaporation ponds, thermal evaporation towards the zero liquid discharge (ZLD), concentration into solid salts and irrigation of plants tolerant to high salinity (halophytes). Brine disposal at inland sites is generally limited to three categories namely: deep well injection, evaporation ponds and solar ponds (Ahmed *et al.,* 2001). Water pollution results when hypersaline brine is discharged into the sources of fresh water and unprotected wells as a result of the negative impact of land disposal.

2.3 Nanofibres

Electrospinning is a technology that is broadly used for an electrostatic fibre formation which makes use of electrical forces to produce polymer fibres using polymer solutions of both natural and synthetic. This has witnessed a great increase in the research and commercial awareness for the past few decades (Ahn *et al.,* 2006). The electrospinning process gives capabilities that are unique for the production of novel natural nanofibres and fabrics whose pore structure is controllable (Zussman *et al*., 2003). Electrospinning has gained much

attention this last decade for its versatility in spinning a wide range of polymeric fibres and of course, its ability to produce fibres consistently in the submicron range which is difficult to achieve by merely using standard mechanical fibre-spinning technologies (Reneker *et al.,* 2000). With interesting characteristics like smaller pores and higher surface areas than regular fibres, electrospun nanofibres have been applied successfully in many fields, such as pharmaceutical, biotechnology, optical electronics, tissue engineering scaffolds nanocatalysis, filtration, environmental engineering, protective clothing, defence and security, biomedical and healthcare (Subbiah *et al.,* 2005; Welle *et al.,* 2007; Ramakrishna *et al.,* 2006). Electrospinning is overall, a simple and relatively robust technique in the production of nanofibres from a wide range of polymers. Electrospun nanofibres offer several advantages including, a very high surface-to-volume ratio, malleability, and tuneable porosity in order to conform to a wide range of shapes and sizes, also, the ability to control the composition of the nanofibre in order to achieve the desired results from its properties and functionalities. Recently, there is an increasing interest to technologically exploit the increase in the production of nanoscale fibres, especially for the nanofibrous scaffold fabrication from a wide range of synthetic and natural polymers for tissue engineering (Chong *et al.,* 2007). In spite of the many advantages offered by the electrospinning process, the rate of production of nanofibres has been a serious factor that limits their application. In order to increase the rate of production of these electrospun nanofibres, a new system has been studied by various research groups which consists of a two-layer electrospinning system, having the lower layer being a ferromagnetic suspension as well as the upper layer being a polymer solution and multiple spinnerets or systems of nozzle which are arranged in a matrix/circle/line and bubble electrospinning (a new bottom-up gas-jet electrospinning) (Theron *et al.,* 2005; Yarin & Zussman, 2004; Liu & He, 2007). Since a large quantity of fibres is needed for various applications, the scale-up of nanofibres is not feasible through the use of a single jet. Many researchers have therefore used a porous hollow tube so as to get multiple jets in which case the production rate is enhanced by increasing the number of holes and the tube length (Dosunmu *et al.,* 2006; Varabhas *et al.,* 2008). Despite the milestone achieved with the spun nanofibres and the electrospinning method, certain challenges need to be considered. Non-uniform cellular distribution and lack of cellular migration in the scaffold with increasing depth in the normal passive seeding conditions pose a major challenge in the use of electrospun mats and scaffolds in tissue engineering. The case of cellular infiltration into the architecture of the nanofibres is gaining attention owing to its potential in making further applications of electrospun meshes or scaffolds in various tissue engineering applications stagnant. Nanofibres are obtained in an inexpensive and simple manner through the

conventional electrospinning technique, but by this method at times, there is a build-up of meshes with tremendous fibre density. Reports have also shown that decrease in the electrospun fibre diameter leads to an increase in the number of fibre-to-fibre contacts per unit length as the mean pore radius in the mesh decreases (Eichhorn & Sampson, 2005).

2.3.1 Electrospinning history

The term "electrospinning", derived from "electrostatic spinning", has been in use relatively in recent times. It is an old technique which was first observed by Rayleigh in 1897 and was studied in detail on electrospraying by Zeleny in 1914 (Bhardwaj & Kundu, 2010). Formhals described an experimental set-up for polymer filaments production with the use of an electrostatic force and published a series of patents from 1934 to 1944 (Huang *et al.,* 2003). Antonin Formals conceived a bright idea for the fabrication of silk-like fibres. He based his idea on the knowledge whereby a dissolved solid in an electrical field will generate threads. The process for the fabrication of textile yarns where a voltage of 57 kV was used for electrospinning cellulose acetate with the use of acetone and monomethyl ether of ethylene glycol as solvents was the first patent on electrospinning (US Patent Number: 2116942) and the process was patented by Antonin Formhals in 1934 and also granted patents that are related (U.S. Patents 2116942, 2160962 and 2187306) in 1938, 1939 and 1940 respectively (Pawlowski *et al.,* 2004). The spinning process by Formhals consists of a movable thread collecting device to collect the threads in a stretched condition, in the manner like that of a spinning drum in conventional spinning (Subbiah *et al.,* 2005). His first patent however states that he has made a device that has the power to make the theoretical principle work in real practice and this is evident in some of the drawings he inserted in his patent. The figure 2.8 shows the schematic drawings by Antonin Formhals in his patent.

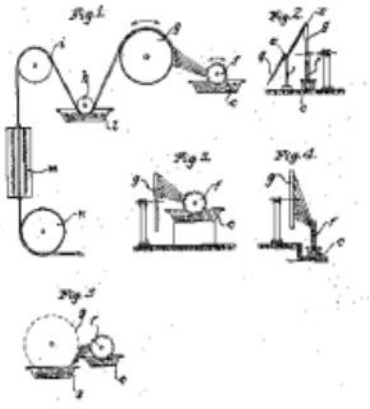

Figure 2.8: Schematic drawings by Formhals
(Formhals, 1939)

However, in the past 60 years, about 50 patents in electrospinning of polymer melts and solutions have been filed (Li & Xia, 2004). Also, a simple apparatus for electrical atomization and production of streams of highly electrified uniform droplets of about 0.1 mm in diameter was invented by Vonnegut and Newbauer in 1952 (Bhardwaj & Kundu, 2010). Shortly after this, an investigation into the dispersion of a series of liquids into aerosols under high electric potentials was done by Drozin in 1955, while Simons in 1966 was able to patent an apparatus for the production of non-woven fabrics which were ultra-thin and light in weight having different patterns using electrical spinning. While in 1971, an apparatus to electrospin acrylic fibres with diameters in the range of 0.05-1.1 μm was made by Baumgarten (Bhardwaj & Kundu, 2010). Now in recent years, the process of electrospinning has gained more attention as a result of an increased interest in the area of nanotechnology, even as fibrous structures of various polymers or ultra-fine fibres having diameters at the scale of submicrons or nanometers can be fabricated easily by the application of this process (Huang *et al.*, 2003).

The process of electrospinning has gained as much popularity due to the fact that more than 200 universities and institutes of research all over the world are carrying out research on the various aspects of the electrospinning process and of course, the fibre it produces. The number of patents for applications based on the electrospinning has also grown in recent years (Bhardwaj & Kundu, 2010). Certain organizations such as eSpin technologies, Kato Tech and NanoTechnics are all actively involved in reaping the benefits of the unique advantage offered by the electrospinning process, however, companies like Freudenberg and Donaldson Company have been making use of the electrospinning process in their air filtration products for the past 20 years (Ramakrishna *et al.*, 2006).

2.3.2 The Process of electrospinning

Electrospinning is a unique technique that uses electrostatic forces to produce ultrafine fibres from polymer solutions or melts to produce fibres with thinner diameter ranging from nanometer to micrometer, and a larger surface area than the ones obtained from conventional processes of spinning. A direct current voltage is however applied in the range of tens of kilovolts to generate the electrospinning. The principle of electrospinning works based on the principle that strong mutual electrical repulsive forces overcome weaker forces of surface tension in the charged liquid of the polymer, this works similarly to techniques such as electrostatic precipitators and pesticide sprayers (Chew *et al.*, 2006a). Two standard electrospinning set-ups are available currently, namely: vertical and horizontal. Meanwhile, as

a result of the expansion of this technology, more sophisticated systems have been developed by various research groups which are capable of fabricating a more complex nanofibrous structure in an efficient way and more controlled manner (Stankus *et al.,* 2006; Kidoaki *et al.,* 2005). An electrospinning system is made up of three major components namely: a spinneret, a high voltage power supply and a grounded collecting plate (often a plate, rotating mandrel or metal screen). This setup utilizes a high voltage source in order to inject charge of a particular polarity into a polymer solution or melt, and this is accelerated towards a collector of opposite polarity. The typical set up of electrospinning materials is shown in figure 2.9 (a and b).

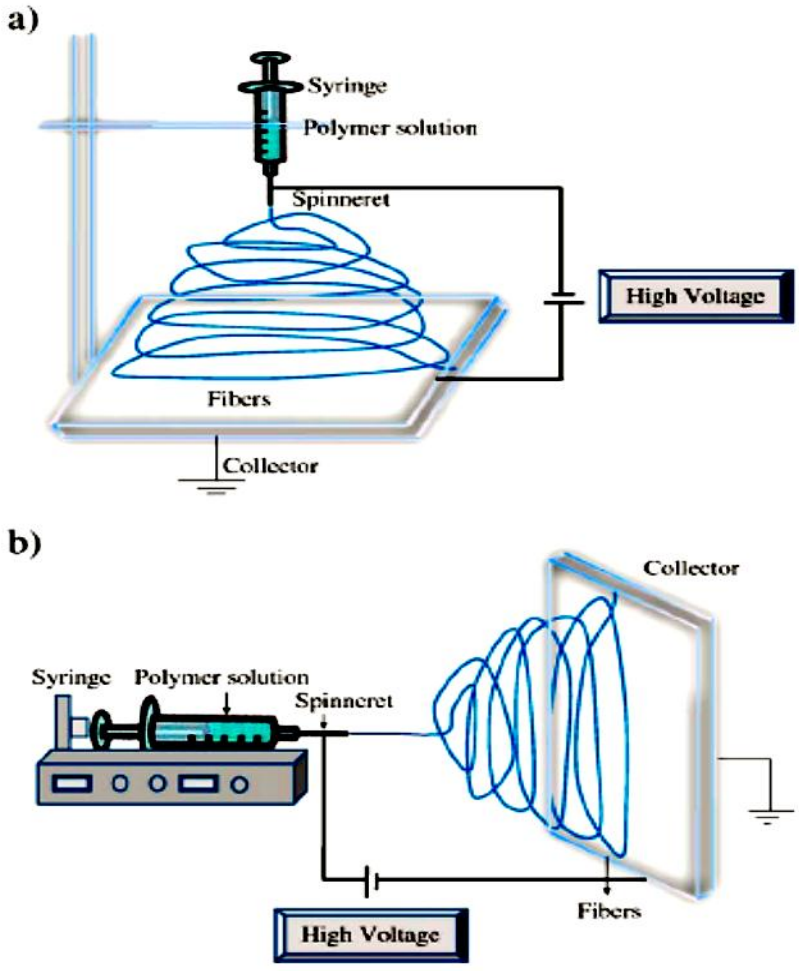

Figure 2.9: Schematic diagram for the electrospinning set up (a) Vertical set up and (b) Horizontal set up for electrospinning
(Bhardwaj & Kundu, 2010)

2.3.3 Fibre formation

The process is carried out at room temperature and atmospheric conditions (Sill & Recum, 2008). The majority of polymers are dissolved in certain solvents before the electrospinning process, after the dissolution is complete, the polymer solution is formed. This polymer fluid

is then sucked into the capillary tube for electrospinning. It is however advisable that the process be carried out in a chamber with a good ventilation system owing to the possible tendency of certain polymers to emit unpleasant or harmful smells (Huang *et al.,* 2003).

2.3.4 The polymers used in the electrospinning process

In the electrospinning process, a wide range of polymers are used and they are able to form very fine nanofibres within the submicron range and are used for various applications and processes. It has been reported that electrospun nanofibres are made from various polymers, namely: natural polymers, synthetic polymers and the blend of both with the inclusion of proteins (Ohgo *et al.,* 2003; Wnek *et al*., 2003), polysaccharides (Son *et al.,* 2004a,b) and even nucleic acids (Fang & Reneker, 1997). However, over 200 polymers have been successfully electrospun from various natural polymers and their characterizations are done based on their various applications (Jiang *et al.,* 2004a).

2.3.5 Synthetic and natural polymers

A wide range of polymers are being electrospun nowadays and the nanofibres from these electrospun nanofibres have been employed in various applications including, scaffolds, tissue engineering (Pham *et al.,* 2006), drug delivery (Kenawy *et al.,* 2002), sensors (Liu, H. *et al.,* 2004), protective clothing (Gibson *et al.,* 2001), fine filtration, adsorptive membranes (Sang *et al.,* 2008) and various biomedical applications (Bhardwaj & Kundu, 2010). In biomedical applications, naturally occurring polymers are better than the synthetic polymers because they exhibit better biocompatibility and low immunogenicity. A strong reason for using natural polymers in the electrospinning process is as a result of their inherent capacity for binding cells, this is because they carry protein sequences, such as RGD (arginine/glycine/aspartic acid) (Pierschbacher & Ruoslahti, 1984). Examples of typical natural polymers include fibrinogen, casein, gelatine, collagen, chitin cellulose acetate, chitosan, silk protein, etc. The type of scaffold fabricated from natural polymer gives a better clinical functionality.

Problems associated with the fabrication of some natural polymers are basically denaturation (Bhardwaj & Kundu, 2010). For synthetic polymers, they give an advantage over natural polymers as it is possible to tailor them to produce a wider properties range including, viscoelasticity and strength (mechanical properties), and the rate of desired degradation (Hakkarainen, 2002). Synthetic polymers employed in biomedical applications are

hydrophobic biodegradable polyesters, and have all been electrospun into nanofibrous scaffolds. Examples are polylactide (PLA) (Boland *et al.,* 2001), polyglycolide (PGA) (Fang & Reneker, 1997) and poly (Ý-caprolactone) (Ohkawa *et al.,* 2004a; Tan *et al.,* 2005a).

2.3.6 Copolymers

Electrospinning carried out with copolymers gives enhancement of properties of polymeric materials, which includes the tailoring of thermal stability, barrier properties and mechanical strength. As a result of the enhanced properties, it has been sought after for applications in engineering structure via methods like melt-blending, copolymerization and incorporation of inorganic filters (Wang *et al.,* 2005a). The concept of using copolymers is a viable scheme to generate entirely new materials with properties that are desirable when carried out in a proper way. The performance of copolymers-based electrospun scaffolds can be improved significantly as compared to homo-polymers (Bhardwaj & Kundu, 2010). Other properties like structure, morphology, pore size and distribution, biodegradability, mechanical properties and other physical properties can as well be altered by the use of copolymers in electrospinning (Bhardwaj & Kundu, 2010). For instance, the elastic poly (ethylene-co-vinyl alcohol) (PEVA) nanofibrous mat stiffens up after the addition of poly (glycolide) (PGA) for blend electrospinning (Kenawy *et al.,* 2002). A triblock copolymer containing PLA, p-dioxanone and PEG (PLA-b-DX-b-PEG), was synthesized by Saito et al., this unique block copolymer shows a good balance between the rate of degradation and hydrophilicity (Saito *et al.,* 2001). In the case of poly methyl methacrylate (PMMA), its thermal stability can be upgraded by the copolymerization of methyl methacrylate (MMA) with methacrylic acid (MAA). Poly(methacrylic acid) (PMAA) exhibits a higher degradation temperature as a result of the formation of acid anhydride upon heating, and its glass transition temperature is higher than PMMA (Ho *et al*., 1992; Huang & Chang, 2003).

2.3.7 Effects of electrospinning parameters

Processes involved in electrospinning are controlled by various parameters, and these are classified broadly into solution parameters, ambient parameters and process parameters. The solution parameters are: viscosity, molecular weight, surface tension and conductivity, while process parameters include the flow rate, distance from the tip to collector and the applied electric field. These parameters have a significant effect on the fibres morphology obtained through the electrospinning process. If these parameters are properly manipulated and

optimized, nanofibres of desired morphology and diameters can be derived (Chong *et al.,* 2007). Additionally, these variables extend to ambient parameters which include temperature and humidity of the surroundings which also play an important role in the determination of the diameter and morphology of the electrospun nanofibre (Li & Xia, 2004).

2.3.7.1 Viscosity

In the determination of fibre size and morphology during the spinning of polymeric fibres, the viscosity of the solution plays an important role. According to Bhardwaj & Kundu, (2010), there is no continuous fibre formation with a very low viscosity and with a very high viscosity, it becomes difficult to eject jets from the polymer solution, therefore, there is a need to optimize viscosity for electrospinning (Bhardwaj & Kundu, 2010). Different polymer solutions have different viscosity ranges at which spinning is carried out, and the maximum spinning viscosities have been reported by researchers to range from 1 to 215 poise (Baumgarten, 1971; Buchko et al., 1999). Research has shown in the study of polyethylene oxide (PEO) to study the formation of nanofibre in different viscosities, that the range between 1 and 20 poise is suitable for uniform nanofibre production by electrospinning (Fong *et al.,* 1999). There is a strong relationship between the concentration of the solution and solution viscosity, and this relationship alongside the fibre obtained has been investigated in a number of systems, these include poly(ethylene oxide) (PEO) (Huang *et al*., 2001a), poly(lactic-co-glycolic acid) (PLGA) (Kim *et al*., 2005a), poly (vinyl alcohol) (PVA) (Ding *et al*., 2002; Zhang *et al*., 2005b), poly (methylmethacrylate) (PMMA) (Gupta *et al*., 2005), poly (L-lactic acid) (PLLA) (Jun *et al*., 2003), polystyrene (Jarusuwannapoom *et al*., 2005), dextran (Jiang *et al*., 2004a) and gelatin (Ki *et al*., 2005). When the polymer solution is of very high viscosity, it exhibits longer stress relaxation times, this could inhibit the fracturing of ejected jets during electrospinning (Bhardwaj & Kundu, 2010). When the solution concentration of viscosity is increased, it results in a larger and more uniform diameter (Deitzel *et al*., 2001). The solution viscosity therefore plays an important role in the determination of the range of concentrations in obtaining a continuous fibre. With a low solution viscosity, there arises surface tension which leads to the formation of beads or beaded fibres, while above a particular concentration, a continuous fibrous structure is achieved and the morphology is affected by the solution concentration (Doshi & Reneker, 1995).

2.3.7.2 Concentration

For fibre formation to occur in the electrospinning process, certain minimum solution concentration is required. But at low solution concentration, what is obtainable is the mixture of beads and fibres, but when the concentration of the solution increases, there is a change in the shape of the beads from spherical to spindle-like and uniform fibres with increased diameters are finally formed owing to the higher viscosity resistance (Ryu *et al.*, 2003; Ki *et al.*, 2005). An optimum solution concentration is therefore required for the electrospinning process, because at low concentrations, beads are generated instead of fibres and at high concentrations, the continuous formation of fibres are prohibited as a result of the inability to maintain the flow of solution from the needle tip which results in the formation of larger fibres (Sukigara *et al.,* 2003). An attempt has been made by researchers to discover the relationship between the concentration of solution and fibre diameter, and a power law relationship was found, that when the solution concentration increases, fibre diameter also increases with gelatine electrospinning (Jun *et al.,* 2003).

2.3.7.3 Surface tension

Surface tension is also an important factor that affects the electrospinning process as a function of the solvent composition of the solution. When the surface tension of the nanofibre solution is reduced, fibres can be obtained without beads, meanwhile, different solvents might offer different surface tensions. In general, the high surface tension of a solution inhibits the process of electrospinning owing to the instability of the jets and the generation of sprayed droplets (Hohman *et al.,* 2001). Beads, droplets and fibre formation depends on the surface tension of the solution and spinning solution with lower surface tension helps the electrospinning process to occur at a lower electric field (Haghi & Akbari, 2007). It does not however mean that a lower surface tension of a solvent will be more suitable for electrospinning. But in essence, the determinant for the upper and lower boundaries of the electrospinning window is the surface tension, provided other variables are constant (Pham *et al.,* 2006).

2.3.7.4 Molecular weight

This is an important factor that has a notable effect on the electrical and rheological properties such as conductivity, dielectric strength, surface tension and viscosity (Haghi and Akbari, 2007). This important parameter affects the electrospun fibre morphology in the sense that, high molecular weight polymer solutions provide the suitable viscosity for fibre generation, and low molecular weight solution generate beads rather than fibres while high molecular weight solution delivers fibres with larger average diameters (Bhardwaj & Kundu, 2010). The

molecular weight of the polymer is the reflection of the number of entanglements of the polymer chains in a solution and this translates to its viscosity (Bhardwaj & Kundu, 2010).

2.3.7.5 Surface charge density/Conductivity

Most polymers are conductive except for some dielectric materials; also, the charged ions in the solution of the polymer have an effect in the jet formation. The type of the polymer, availability of the ionisable salts and the solvent used are the main determinants of solution conductivity (Bhardwaj & Kundu, 2010). As the electrical conductivity of the solution increases, the diameter of the fibres electrospun decreases. Meanwhile, a solution with low conductivity results in insufficient elongation of a jet by electrical force in order to produce a uniform fibre with the possibility of beads being observed (Bhardwaj & Kundu, 2010). Highly conductive solutions are extremely unstable in the presence of strong electric fields, this leads to a broad diameter distribution and dramatic bending instability (Hayati *et al.,* 1987). It is possible to obtain the electrospun nanofibre that has the smallest fibre diameter with highest electrical conductivity and the drop in diameter can be attributed to the increase in the electrical conductivity. The jet radius was observed to be inversely proportional to the cube root of the solution's electrical conductivity (Haghi & Akbari, 2007; Fong *et al.,* 1999).

2.3.8 Processing parameters in electrospinning

These are various process parameters involved in the electrospinning of the polymer solution to achieve the desired fibre standard.

2.3.8.1 The flow rate

This is an essential parameter as it affects the jet velocity and the rate at which the material is being transferred. It is more desirable and advisable to embark on a lower feed rate as this affords the solvent more time for evaporation (Yuan *et al*., 2004). The pore diameter and the fibre diameter increase with an increase in the flow rate of the solution; this is in the case of polystyrene (PS) fibres. Also, when the flow rate is altered, the morphological structure can also be changed slightly. High flow rate produces beaded fibres, this is due to lack of proper drying time before getting to the collector (Yuan *et al.,* 2004; Zuo *et al.,* 2005).

2.3.8.2 The applied voltage

The voltage applied to the solution is an important factor in the electrospinning process. It is after the threshold voltage is reached that fibre formation occurs. During this process, necessary charges are induced on the solution alongside the electric field, therefore, electrospinning is initiated. It has been experimentally proven that the shape of the initiating

drop changes depending on the spinning conditions including flow rate, viscosity and voltage (Baumgarten, 1971). However, there are certain controversies about the effect of the applied voltage in the electrospinning process. With the electrospinning of polyethylene oxide (PEO), it was shown that the electric field does not have as much significance on the fibre diameter (Reneker & Chun, 1996). It was suggested that there is more polymer ejection which facilitates the formation of a larger fibre diameter when higher voltages are applied (Demir *et al.,* 2002). Some researchers have reported that an increase in the voltage applied, or invariably increasing the strength of the electric field, will increase the electrostatic repulsive force on the fluid jet and this entirely narrows down the fibre diameter. Mostly, a higher voltage produces greater stretching of the solution as a result of the greater coulombic forces contained in the jet and a stronger electric field. All these result in the reduction of the fibre diameter and rapid solvent evaporation from fibres. There is also a greater possibility of the formation of beads (Pawlowski *et al.,* 2004; Buchko *et al*., 1999; Demir *et al.,* 2002; Haghi & Akbari, 2007).

2.3.8.3 The tip to collector distance

The tip to collector distance is another way or approach whereby the morphology and the fibre diameter are controlled. It has been observed that the minimum required distance is needed for the fibre to dry before reaching the collector, or else, beads have been observed in situations where the distance is too close or too far (Geng *et al.,* 2005). This parameter is not as significant compared to other parameters, this was observed in the electrospinning of gelatine (Ki *et al.,* 2005), poly (vinylidene fluoride) (Zhao *et al.,* 2005), chitosan (Geng *et al.,* 2005) and PVA (Zhang *et al.,* 2005b). Reports have shown that flatter fibres can be produced at closer distances, while rounder fibres have been obtained with an increase in distance and this is observed in the electrospinning of silk-like polymer having fibronectin functionality (Buchko *et al.,* 1999).

2.3.9 Effect of ambient parameters

Ambient parameters also play a major role in the electrospinning process, these parameters include temperature, humidity etc. Research studies have been conducted to investigate the effects of temperature and humidity on electrospinning. Certain studies showed the effect of temperature on the electrospinning of polyamide-6 fibres which ranged from 25 to 60 °C and discovered that an increase in temperature yields fibres with decreased fibre diameter, this decrease in diameter was attributed to the decrease in the viscosity of the polymer solution at

higher temperatures (Mit-Uppatham *et al.,* 2004). The relationship between viscosity and temperature is inverse and it has been shown that when humidity is increased, there is a formation of small circular pores on the fibre's surface; when humidity is increased further, the pores coalesce (Casper *et al.*, 2004).

2.4 Ion Exchange

Ion exchange is the exchange of ions between two phases (Alexandratos, 2008). Ion exchange materials can be defined as insoluble substances that contain ions which are loosely held and are capable of being exchanged with other ions in solutions that come in contact with them. These exchanges occur without any damage or physical alteration to the ion exchange material. Ion exchangers are defined as insoluble acids or bases that have salts which are also insoluble, this allows them to exchange either positively charged ions (cation exchangers) or negatively charged ions (anion exchangers). Other natural substances like proteins, cellulose, living cells and soil particles display ion exchange properties that play a vital role in their functions in nature. In the treatment of industrial waste effluents, sorption has been shown to be an effective way of treatment owing to many advantages including cost-effectiveness, availability, efficiency and simple mode of operation. The sorption process is recommended for the removal of low concentrations of metal ions in effluent wastes. In the sorption process, there is a sorbent which binds molecules through the means of physical attractive forces, chemical binding and ion exchange. The sorbent should be regenerable with ease, cheap and must be in large quantities for best result yield (Kunin, 1976). The factors affecting the sorption process of ion exchange include the affinity for sorption of targeted materials and the efficiency of desorption. Sorption efficiency of a target contaminant depends strongly on the sorbent-solute interactions; this can be improved by the attachment of a functional group onto the surface of the sorption site. This process involves two major steps which are sorption and desorption. The ion exchange process is meant to be reversible, in which case the sorbed solutes can be regenerated effectively. But the effectiveness of desorption diminishes for sorbents that are highly selective.

In the purification of water, the objective is often to soften the water or to generally get rid of the mineral content altogether. Ion exchange explains this process as flows through a bed of ion exchange material; unwanted ions are removed and subsequently replaced by the loosely-held ions on the surface of the sorbent material. Water is softened by using a resin containing

Na^+ cations but which binds Ca^{2+} and Mg^{2+} more strongly than Na^+. When the water goes through the resin, the resin attracts the Ca^{2+} and Mg^{2+} and gives off Na^+ making for "softer" water. If there is a need to remove the mineral content entirely then, it is made to pass through a resin which contains H^+ (which replaces all the cations) and then through a second resin which contains OH^- (which replaces all the anions). The H^+ and OH^- then react to produce more water. This process however, has some demerits because there are substances existing in some waters (for example, organic matter or Fe^{3+} ions) that are capable of contaminating the resin. Generally, the advantages of the process (durability of resins, cheap maintenance etc.) are more than the disadvantages. Also, the process is environmentally friendly because it deals only with substances already existing in water. The primary use of synthetic resins is for purifying water, they are also employed for various other applications which include separating out some elements. When the resin is treated with a regenerant, it releases the targeted ions into solution which implies the recovery of the metal ions and simultaneously recovering the exchange capacity of the resin for it to be re-used.

Ions on the ion exchanger can be exchanged for the same stoichiometric equivalent of the other ions which are of the same sign, as the ion exchanger comes in contact with solution containing the ions. Equations 2.1 and 2.2 explain how the ion exchange process is a diffusion process and is also selective, which means it captures the counter ions in preference to other ions of the same sign contained in the solution. Also, the efficiency and usefulness of an exchange material lie in its ability to regenerate quickly without any loss in quality and capacity.

$$2\mathbf{X}\text{-Na} + MgCl_2\,(aq) \rightarrow \mathbf{X}_2\text{-Mg} + 2NaCl\,(aq)\ \text{(cation exchange)} \qquad (2.1)$$

$$2\mathbf{X}\text{-Cl} + Na_2SO_4\,(aq) \rightarrow \mathbf{X}_2\text{-}SO_4 + 2NaCl\,(aq)\ \text{(anion exchange)} \qquad (2.2)$$

The above reactions show the solid phase which is the resin designated as X, also, the ions that participate in the exchange which include Na^+ and Ca^{2+} for cation exchange, while Cl^- and SO_4^{2-} are for anion exchange, all these are referred to as the counter ions. Within the resin framework, the counter ions move about freely and are replaceable by other ions of the same charge. The ions existing in the solution that have the same charge as that of the ion exchanger are referred to as the co-ions. Cation exchangers are the carriers of exchangeable cations while carriers of exchangeable anions are the anion exchangers.

Advancements have been made in ion exchange concepts that have led to the development of specialized polymeric systems designed to selectively remove undesirable ions. Water softening using sodium aluminosilicate cation exchange resin was the first industrial

application of ion exchange reported in 1905. Today, there have been various applications of ion exchange across industries including water treatment (heavy metal ions removal, water softening, deionization, etc.), biomedical, chemical synthesis, food processing, hydrometallurgy, chromatography and synthetic fibre production (Economy *et al*., 2002, Greig, 2000).

The basis of a wide variety of chemical processes which involve removal of ions, substitution and separation is formed through ion exchange. For separation, different ions are separated in accordance to their respective affinities existing between them and the resin as the solution runs through the resin-packed column. For substitution however, the ions on the resin which are of insignificant or no commercial value at all are replaced with valuable ions. There are many applications of ion exchange but most importantly, it is often employed in the ultra-pure water production. Ion exchange materials are most efficiently used in the treatment of waste streams when an unwanted substance of relatively low concentration is to be removed from the waste stream. The technologies of ion exchange have been beneficial in their ability to remove highly diluted contaminants and the fact that ion exchange techniques are insensitive to the variations in concentration and flow (Zagorodgni, 2006). Furthermore, ion exchange processes have an edge over other separation techniques, especially when the targeted substance must be removed from diluted solutions with low or no residuals. Another advantage of ion exchange materials is that it has found wide applications in pharmaceutical and food industries. Despite being chemically active, they are also highly stable physically and chemically, therefore, they do not cause any contamination of the product (Zagorodgni, 2006). These materials are responsible for most of the analytical procedures, isolation and purification processes which are now being used generally in the pharmaceutical field (Winters & Kunin, 1949).

The applications of ion exchange materials in chemical analysis are wide; they also differ from the industrial application. In medicine, they are still under investigation, as research is ongoing on the prospects of a controlled drug release. In this case, some ion exchange materials can be incorporated into the pharmaceutical formula to effect delay of drug consumption by the body. As a result of high chemical stability, these polymer materials do not cause any discomfort or harm when taken as pills.

Owing to the role of the polymeric ion exchange resins have to play in water treatment and their potentials of application in other areas, the following sections will focus more on them,

as well as the synthesis of ion exchange resins. Their properties and application will be discussed in detail.

2.4.1 Ion Exchange Resin

Ion exchange can be defined as the exchange of ions between the substrate and the medium surrounding it. When an ion exchange reaction is reversible, it is said to be most useful, because the ion exchanger can be reused many times (Hubicki & Kołodyńska, 2012). Ion exchange resins are solid materials which are insoluble and carry exchangeable cations and anions on fixed sites (Helfferich, 1962). The resin structure is characterized generally by the pore-size distribution of spherical beads, and also, the cross-linking degree that exists between the polymer chains in the bead. Resins are mostly available in the moist bead granular or powdery form having a particle size distribution which ranges from 0.3 – 1.2 mm and the structure could either be a gel or macroporous. A three-dimensional covalent network exhibited by the conventional ion-exchange beads are bonded to the exchange groups. This network protects the material structure integrity, while bound ions give either cationic or anionic exchange sites. Figure 2.10 shows the structure of a cation exchange resin.

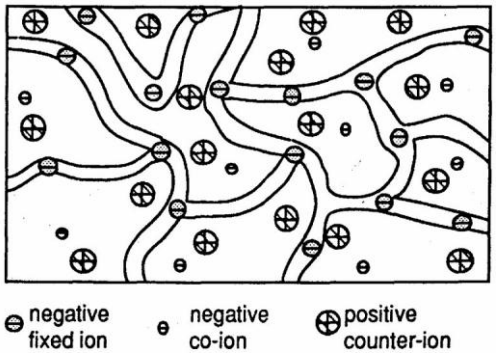

Figure 2.10: A structure of cation exchange resin
(Zagorodgni, 2007)

Around 1930, ion exchange resins (carbonaceous exchangers) were developed so as to harness their exchange capacity (almost one-third of the entire ion exchange capacity of a modern resin) in the treatment of industrial water (Harland, 1994). A number of shortcomings were associated with this class of resins including lack of uniformity, low chemical and physical stability. However, progress was later made by the upgrade of these exchangers with higher exchange capacity, better chemical, thermal and physical stability. In the sorption process, metal ions are loaded onto the surface of the resin and eluted with the right eluent, and the amount of the metal ion sorbed on the resin is a function of the concentrations of the

ligands and the competing metal ions, the resin binding capacity and contact time (Helfferich, 1962). Greater binding capacity of the resin leads to greater capacity of the resin to subdue some ligands' stability, which means, higher binding capacity leads to the sorption of metals ions in less stable complexes than metal-resin complex and also free metal ions. A common disadvantage of the ion exchange process is slow kinetics. Meanwhile, when the resin porosity is increased or bead size is decreased or by crosslinking can boost the kinetics when the accessibility of the polymer supported ligands to the metal ions. Table 2.1 shows the outline of some of the available resins with their functional groups

Table 2.2: Some resins with their functional groups, binding sites and metal ions separated with them

Resin	Binding Sites	Functional group	Separated metal ions	References
Retardion 11A8	Amphoteric	Quartenary ammonium group and carboxylate	Cd^{2+}	Samczy ski & Dybezy ski, 1997
Poly(4-vinylpyridine)	Bidentate	Aminophosphonate	Cu^{2+}, Mg^{2+}, Ca^{2+}, Pb^{2+}, UO_2^{2+}, Zn^{2+}, Cd^{2+}	Wu & Lau, 1996
Amidoxime	Amphoteric	Hydroxylamine	Fe^{3+}, U^{6+}, Pb^{2+}, Cu^{2+}, Zn^{2+}, Cd^{2+}	Colella et al., 1980; Egawa & Kabay, 1992.
Chelex 100	Tridentate	Iminodiacetate	Cr^{3+}	Gode & Pehlivan, 2003.
Amberlite IR-122	Monodentate	Sulphonate	Cd^{2+}, Pb^{2+}, Zn^{2+}	Wu & Lau, 1996
Amberlite CG 50	Bidentate	Carboxylate	Cr^{3+}, Cr^{6+}	Pesavento et al, 1994
Sephadex SP C-25	Sulphonate	Monodentate	Cd^{2+}, Pb^{2+}, Zn^{2+}	Wu & Lau, 1996

Ion exchangers can be divided into two groups, namely organic and inorganic according to their composition.

(i) Organic ion exchangers

Most organic resins are made up of a three-dimensional network matrix of macromolecular hydrocarbon chains, which usually consist of a copolymer of styrene and divinylbenzene (DVB), the crosslinking being provided by the DVB. The characteristics of the resin are a function of the ion-exchange groups present on the matrix. Generally speaking, the resin can therefore be categorized into three groups namely: cation exchangers (having strong acid and weak acid groups), anion exchangers (having strong base and weak base groups) and selective chelating groups (specific ion exchangers) (Bolto & Pawlowski, 1987).

The chelating resins are materials having chelating or complexing groups on their surface and they selectively remove particular metal ions from the complex solutions through chelating groups which have high affinity for the targeted metal ion. The preparation of most of the chelating resins is based on a two-step synthesis process:

(a) Insertion of an appropriate functional group on the polymeric support surface or polymer activation.
(b) Ligand immobilization of particular suitability by condensation reaction or coupling reaction (Garg et al., 1998).

Chelating agents form complexes with metal ions only in particular pH ranges. Now if a water sample contains a metal ion and passes over a chelating resin at certain pH values, then the metal ion forms a chelate with the chelating agent on the polymeric support and is therefore retained by the resin excluding the impurities which pass through. This is explained in Figure 2.11.

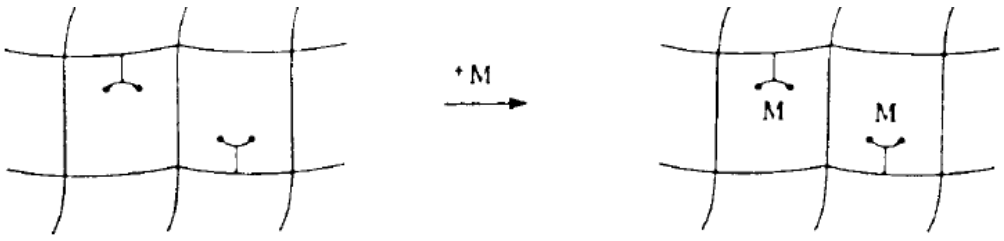

Figure 2.11: Sorption of metal by chelating resin.
(Garg et al., 1998)

During the elution process, the eluent chosen helps in the removal of the metal ion from the chelate site of the resin. This can be achieved by changing the pH through the use of acids. This helps in trying to regenerate the resin and therefore, chelating resins can be reused.

(ii) Inorganic ion exchangers

Zeolites and clay minerals are characteristic representatives of the group of inorganic materials which are crystalline hydrated aluminosilicates of alkali and alkaline earth cations with an open, infinite and three-dimensional structure. There are two main types of zeolites, synthetic and natural minerals and they can lose and gain water reversibly and also exchange extra framework cations, these are carried out without any alteration to the crystal structure (Mumpton, 1999). The components, ion exchange capacity and channel diameter for different clay minerals, synthesized and natural zeolites are shown in Table 2.2.

Table 2.3: Clay minerals, synthetic and natural zeolites components and exchange capacities

Species	Idealized Formula	Exchange capacity (eq/kg)	Channel diameter (nm)
Faujasite	$(Na_2,K)[(AlO_2)_{64}(SiO_2)_{128}].256\ H_2O$	5.02	0.74
Clinoptilolite	$(Ca,Na_2,K_2)_3[(AlO_2)_6(SiO_2)_{30}].24H_2O$	2.62	0.24 – 0.61
Quartz	Dense lattice (3-D)	0.05	-
Chabazite	$Ca_2[(AlO_2)_4(SiO_2)_8]_2.13H_2O$	4.95	0.37 - .042
Montmorillonite	Double layer lattice	0.70 – 1.00	-
Analcite	Silicates (expanding) $Na_{16}[(AlO_6)_{16}(SiO_2)_{32}]._{16}H_2O$	4.95	0.69
Muscovite	Double layer lattice silicates (non-expanding)	0.10	-
Kaolinite	Single layer lattice silicates	0.03 – 0.15	-

The precise geometrical structure of zeolites allows them to differentially sorb neutral molecules according to their structure and sizes, this is known as molecular sieving. It is this ability that is responsible for many industrial applications such as gas and liquid phase operations with zeolites for reforming reactions, drying in petrochemical cracking and separation of hydrocarbon. Zeolites have attracted the attention of scientists for their use commercially in sorption, ion exchange, catalytic properties and molecular sieves (Zhao *et al*., 2007).

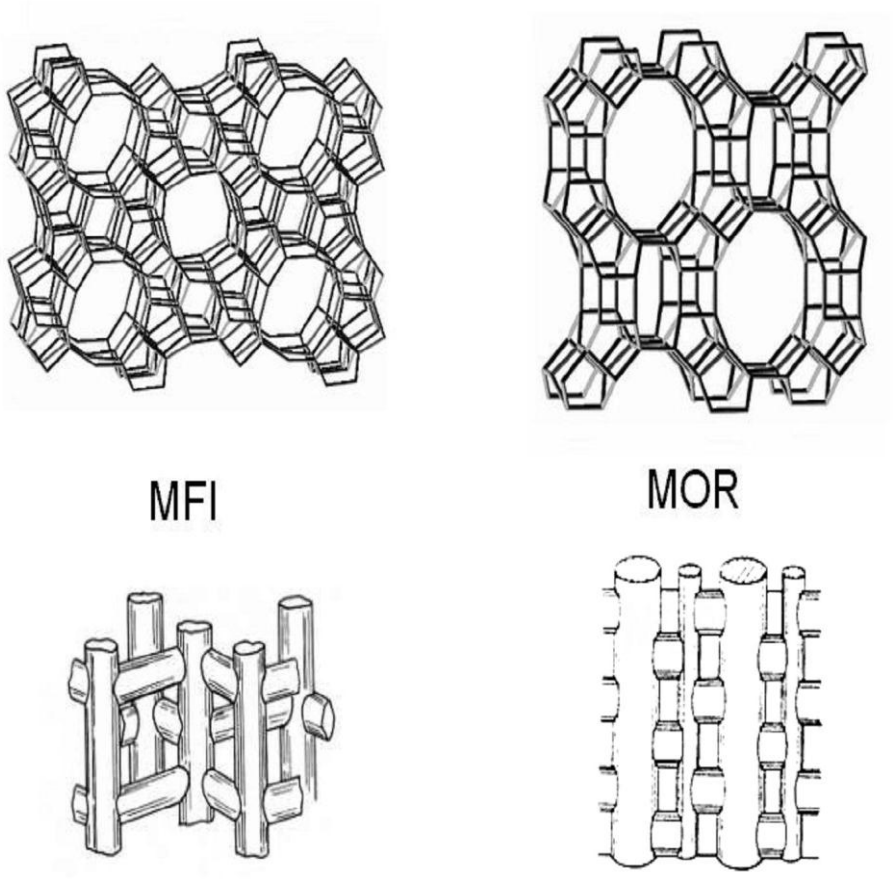

Figure 2.12: Some examples of the framework and pore system of zeolite: MOR and MFI topologies
(Housin, 2003)

The graphical representation of zeolite framework and pore systems in Figure 2.12 shows voids and channels in zeolites which explain the properties of zeolite.

Zeolites are three-dimensional frameworks of silicate (SiO_4) tetrahedral whereby the four oxygens of each tetrahedron are shared with the adjacent tetrahedral. The disadvantages of zeolites compared to resins for conventional ion exchange applications can be attributed to their structure, chemical instability in high and low pH and slow kinetics.

The two types of ion exchange resins (organic and inorganic) are able to sorb in any solution they are placed in, but just to a certain degree. As a result of the polymer chains molecules flexibility, sorbate ions can infiltrate into the polymer where the sorption occurs. The main disparities between sorption and ion exchange processes are the size of the potential energy barrier and the desorption process accompanying the ion exchange. Furthermore, sorption processes involve weak Van de Waals forces, contrary to the strong Coulombian forces

involved in ion exchange. The capacity of sorption is affected by factors including the pore structure, active groups, polarity of sorbent, etc. (Ndlovu-Yalala, 2010).

Titanium dioxide (TiO_2) is also an important inorganic solid adsorbent which is characterized by its resistance to thermal degradation and high mechanical properties, compared to other bio sorbents or organic adsorbents (Naiya *et al*., 2009). TiO_2 particularly gives other several advantages when it is applied as an adsorbent for the removal of metals. As an oxide, it is widely studied and used as a model mineral for its high chemical stability and negligible solubility over a wide pH range (Georgaka & Spanos, 2010). Titanium dioxide (TiO_2) offers an ideal point of zero charge (Bourikas *et al*., 2001); as a result, it becomes easy to embark on sorption studies on both positively and negatively charged surfaces of titanium dioxide over a wide pH range (Olsson *et al*., 2003; Vandenborre *et al*., 2007).

It is important to know that titanium dioxide exists in two major polymorphic forms namely, anatase and rutile. However, the surface area for the anatase powder is greater than that of rutile, and for this reason, anatase is used in most applications (Henrich & Cox, 1994). In recent times, titanium dioxide has been relevantly studied as a photocatalyst and offering several advantages in the purification of water in the presence of UV-radiation (Legrini *et al*., 1993).

In certain studies, the sorption study of copper species on the surface of titanium dioxide revealed that the uptake of copper increased with increasing pH and was constant for higher pH values (Kim *et al*., 2003).

Titanium dioxide has also found other applications in solar energy conversions (Hagfeldt & Graetzel, 1995), photocatalyst (Zhang *et al*., 2003), photochromic devices (Moser *et al.*, 1998) and sensors (Mohammadi *et al*., 2007).

2.4.2 Ion Exchange Resin Synthesis

Suspension polymerization is the conventional method for the preparation of porous polymeric materials with the addition of a monomer / monomer mixture and a monomer-soluble initiator to a stirring reactor that contains water with a low amount of steric stabilizer (Gun'ko *et al*., 2005). The copolymerization of styrene and divinylbenzene (DVB) (Figure 2.13), is the process employed in the synthesis of majority of ion exchange resins. The basic matrix of the resin is provided by the styrene molecules and the DVB crosslinks the polymers to enable the toughness and insolubility of the resin. The degree of crosslinking in the three-dimensional arrangement of the resin is vital owing to the fact that it helps in the determination of the internal pore structure.

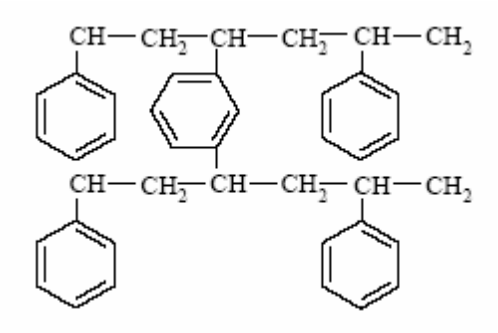

Figure 2.13: Styrene-divinylbenzene copolymer

Styrene-divinylbenzene (DVB) copolymer is formed by suspension polymerization. It is the addition of the monomer mixture and its dispersion into small droplets in a vigorously agitated solution which is kept at a stipulated temperature for polymerization (usually 85 ºC – 100 ºC) (Chanda & Roy, 2006). The addition of stabilizer prevents the agglomeration of droplets and the droplets' size depends on the solution viscosity, the stabilizer and the agitation. The droplets are transformed into polymer beads of the gel-type polymer matrix, as the polymerization progresses. As polymerization ends, polymer beads having pores in their structures are obtained and these are activated chemically for performance as ion exchangers. Activated groups are attached to the resins to give chemical functionality in the bead. They have a constant electrical charge balanced by oppositely charged ions of the same equivalence, and these ions freely exchange with other ions of identical charge. For instance, the sulphonation process is used to attach sulphonic acid groups to the beads.

Strong acid cationic exchange resins are produced by the sulphonation of styrene-DVB copolymer beads. Sulphuric acid is used to functionalize the copolymer beads at elevated temperature (150 ºC) and pressure with the use of a swelling solvent to achieve a particular degree of sulphonation (Harland, 1994). Due to steric effects, the sulphonic acid group occupies the para-position, and the high pressure is to ensure an effective increase in the boiling temperature of the solvent so that the copolymer beads are kept swollen at a higher temperature than the normal boiling point of the swelling solvent while no harm is done to the beads. When the reaction is complete, the resin is therefore hydrated and recovered after the conversion into a metal salt is achieved.

For weak acid cation exchange resins, their preparation is done by the copolymerization of an acid anhydride or an organic acid with a crosslinking agent. This is commonly achieved by the combination of an acrylic or methacrylic acid with divinylbenzene or with a compound that has at least two vinyl groups as shown in Figure 2.14.

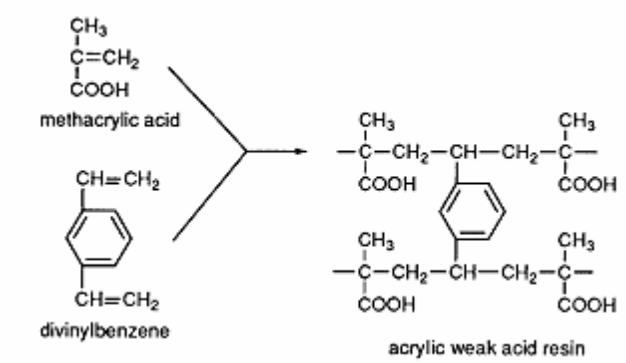

Figure 2.14: Acrylic carboxylic cation exchange resin.

Similarly, strong-based anion (SBA) exchange resins are prepared by the chloromethylation of styrene-DVB copolymer, this is followed by the amination of the product with a tertiary alkyl amine as shown in Figure 2.15. However, there is a slight difference with the activation of SAC resin because the amount of DVB used is less to allow a more porous bead. Also, the type of amine used is a determinant of the resin's functionality. Trimethylamine (TMA) is the commonly used amine that creates a type 1 SBA exchanger, while the use of dimethyl ethanolamine (DMEA) gives a type 2 anion resin (Harland, 1994).

The resin matrix rigidity is provided by the crosslinking agent (divinylbenzene), which also provides the resistance to swelling. The swelling ability of the resin, the mesh width of the matrix and the counter-ions mobility within the resin are being determined by the degree of cross-linking. As a result, highly cross-linked resins are generally harder and more resistant to mechanical strain; but are brittle, show slower diffusion rates and are susceptible to oxidation (Harland, 1994).

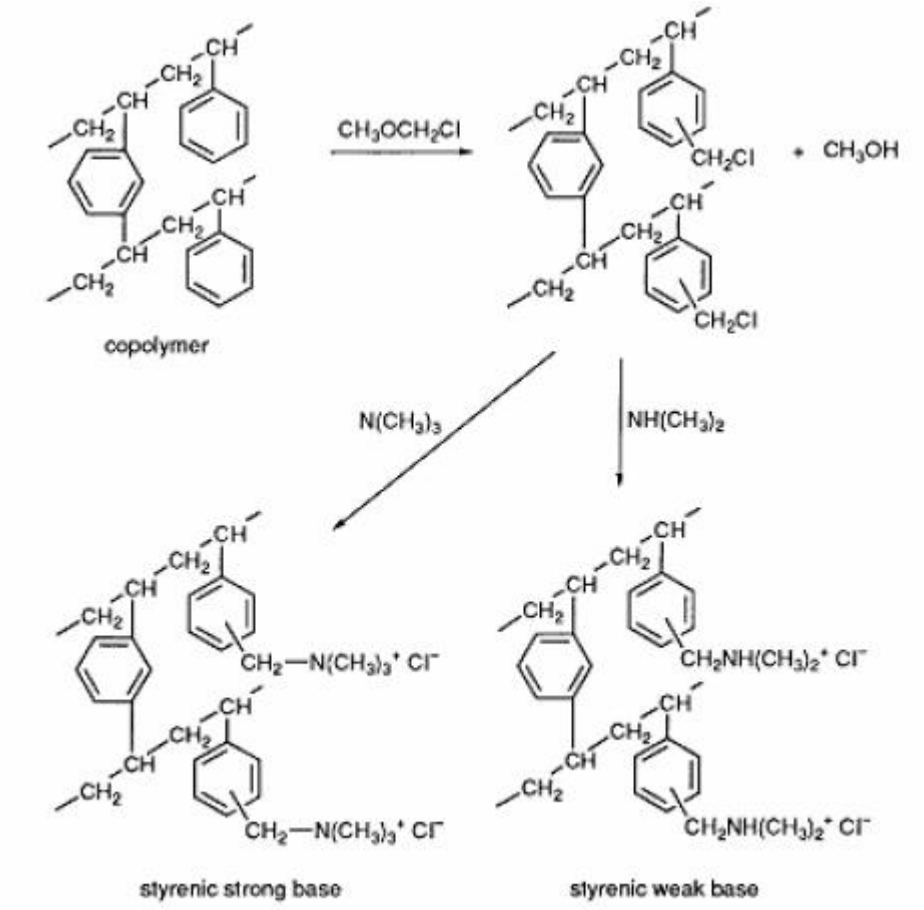

Figure 2.15: Synthesis styrenic anion exchange resins.

2.4.3 The Properties of Ion Exchange Resins

Both synthetic and natural materials exhibit ion exchange abilities. The major difference is their capacities in their sorption properties which differentiate them as ion exchangers. Table 2.3 shows both the physical and chemical properties of ion exchange resins.

Table 2.4: Properties of ion exchange resins

CHEMICAL	PHYSICAL
Ionic form	Surface area
Ion exchange capacity	Particle size
Type of functional group	Pore size and morphology
Cross-linking degree	Physical structure and morphology
Type of matrix	Partial volume when swollen

(Harland, 1994)

2.4.3.1 Physical properties

i. Porosity

Porosity is defined as the ratio of volume of voids to total volume of the resin. Conventional resin porosity ranges from 20% to 50%, but ranges from 5% to 50% in the macroporous resin (Calmon, 1984). The electrolyte of the solution, the degree of cross-linking and the manufacturing process influence the shape and size distribution of pores in the ion exchange resin particle. In order to achieve a large surface area, there should be an incorporation of a large number of small pores into the resin through suspension polymerization process, this is discussed in section 2.4.2. Most importantly, the major contribution to the overall surface area is being accounted for by the micropores with diameters lesser than 2 nm, this is followed by mesopores having diameters ranging from 2 to 50 nm (Sing *et al.*, 1985). In the case of macropores, they contribute insignificantly to the overall surface area because at low pressures, they act as transport pores for the molecules of the sorbate in diffusing from the bulk into the particle interior (Calmon, 1984). For microporous resins, porosity forms their major property and this allows ions of high molecular weight to diffuse in and out of the resin beads (Lieser, 1979). Specific surfaces of typical porous and non-porous sorbents are given in Table 2.4.

Table 2.5: Specific surfaces of typical porous and non-porous sorbents

POROUS		NON-POROUS	
Sorbent	**Specific surface (m^2/g)**	**Sorbent**	**Specific surface (m^2/g)**
Bone char	60 - 80	ZnO pigment	1 - 10
Asbestos	17	TiO_2 pigment	70 - 80
Polymeric macroreticular	100 - 600	Carbon black	100
Activated carbon	1200		
Granular carbon	500 - 2000		
Silica gel	200 - 600		
Zeolite	300 - 600		

Porous materials' application depends on the intimate contact with a surface which supports the active sites, as it is in ion exchange, solid phase synthesis, sorption, catalysis and chromatography (Calmon, 1984). During ion exchange, the active groups are on the surface of the resin particles and also in the pores within the particles. This is where selectivity comes into play because pores of different sizes receive the ions within their range. Ions of smaller sizes are thereby exchanged, while the larger ones cannot because they cannot access the relevant sites.

ii. Particle size

Particle size plays an important role in the separation efficiency, hydraulic expansion, ion exchange kinetics and pressure drop. Ion exchange resin particle sizes usually range from 0.04 – 1.2 mm, but the most common size being in the range 0.3 - 0.85 mm for large scale applications (Harland, 1994). The process of ion exchange is basically a diffusion process which is controlled by mass transfer resistance which depends solely on the nature of the resin as well as the particle size.

iii. Colour, Density and Mechanical Resistance

Colours can be used in categorizing ion exchangers. While the strongly acidic cation exchange resin and weakly acidic condensation type resins are brown, the acrylic and methacrylic acid polymers are white. The degree of cross-linking is the determinant for colour density in the resin matrix. The resin physical appearance can be categorized into gel resins and macroporous resin. Gel resins are usually shiny beads and clear to transmitted light, while the macroporous resins are dull beads of translucent appearance.

The real density of any resin in whatever form (dry or swollen) is dependent on the resin structure, type, ionic form, degree of crosslinking and swelling capacity. Dry and water-free resins have smaller density for anion exchangers (1200 kg/m3) compared to cation exchangers (about 1400 kg/m^3). It is however more practical to use the water-swollen resin density owing to its use in the prediction of hydrodynamic behaviour in the column or fixed bed system. It is important to note that bulk density is different from the density of the swollen resin, swollen resin's water content is about 40 – 60% and the densities are important for operation purposes (Harland, 1994). The resin's structure determines the mechanical strength, therefore, the mechanical strength varies based on the structure of the resin and this also contributes to the wear resistance of the resin. When the degree of cross-linking is increased, the mechanical strength of the resin also increases. The mechanical strength however decreases upon regeneration with concentrated acid and base.

iv. Physical Structure

Ion exchange resins are divided into five categories, based on their physical structures.

***Gel Resins*:** These were the first organic ion exchangers with an essentially homogenous distribution of water throughout the matrix of the resin (Bolto & Pawlowski, 1987). Figure 2.16a shows the gel resin. They do not have permanent porosity, but the pores are formed when the resin swells up in water resulting in the homogenous distribution of water all through the matrix of the resin (Kunin, 1976). The resulting pores formed are small-sized micropores and mesopores (20-50 A^o) per unit volume which results in higher capacity. When the resin undergoes drying, the pores collapse and cease from existence in the dry state. The distance between the polymer chains and the crosslinks is the determinant of the pore structures and this varies with the cross-link level of the polymer, the operating condition and the polarity of the solvent. Gel resins give certain advantages: they have a greater mechanical and chemical stability, have higher loading capacities and react faster in the functionalization reactions (Desilva, 1999).

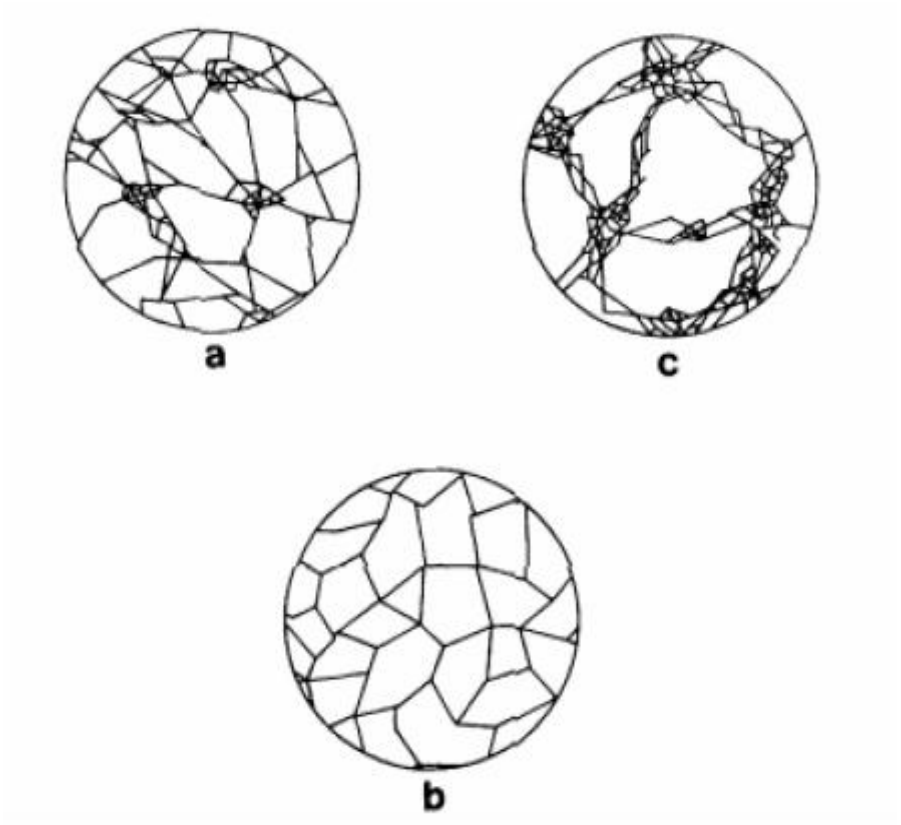

Figure 2.16: Polymeric chains distribution in ion exchangers: (a) gel-microporous resin; (b) gel-isoporous resin; (c) macroporous resin

***Microporous Resin*:** Polymer particles which are manufactured with a low crosslinking level are referred to as microporous (Figure 2.16b). Rates of exchange can be improved when smaller particles are used, providing a larger surface area. The powdered ion exchangers are fine particles, although when they are in a coagulated form, they cause a high pressure operation loss. Due to this loss, they cannot be used in a column system (Bolto & Pawlowski, 1987).

***Macroporous Resin*:** As the name implies, macroporous resins (Figure 2.16c) are made with large pores which are permeable to interior exchange sites. Their process of manufacture leaves a network of pathways throughout the bead, with a heterogeneous structure made up of two phases: (a) the gel regions which are made of dense polymer chains and a low solvent amount, and (b) the macroscopic pores which are permanent and contains solution similar to the ambient region. It is a structure that allows the active portion of the bead to have a high level of divinylbenzene crosslinking and not affect the exchange kinetics.

2.5 Sorption Isotherms

The relationship existing between the amount sorbed and concentration is known as the sorption isotherm, and these are basic requirements for the design of the sorption system used in the removal of pollutants.

Sorption isotherms are mathematical models which describe the distribution of sorbed pollutant (sorbate species) on the sorbent (q_{eq}) and the pollutant in solution (C_{eq}) at a constant temperature, based on a set of assumptions that are related to the homogeneity and heterogeneity of the solid surface, the type of coverage, and the possibility of interaction between the sorbate species (Kelesoglu, 2007). The most frequently used two-parameter models in literature describing the non-linear equilibrium are the Langmuir and the Freundlich models.

2.5.1 The Freundlich Isotherm Model

The Freundlich isotherm illustrates physical sorption from liquids, and a brief empirical equation used to represent sorption data is called the Freundlich equation. The Freundlich model assumes neither homogenous site energies nor limited levels of sorption. The empirically derived Freundlich isotherm is given in equation 2.3.

$$q = k_f (C_e)^{\frac{1}{n}} \quad (2.3)$$

Where q = Amount sorbed per unit weight of sorbent at equilibrium (mg/g)

C_e = Equilibrium concentration of sorbate in solution after sorption (mg/L)

K_f = Empirical Freundlich constant or capacity factor [(mg/g)*(mg/L)^n]

1/n = Freundlich exponent

The exponent 1/n is an index of the diversity of free energies associated with the sorption of the solute by multiple components of a heterogenous sorbent. When 1/n = 1, the isotherm is linear, this means the system's free energy is constant at all sorbate concentrations. Meanwhile, when 1/n < 1, the isotherm is concave and sorbates are bound with weaker free energies, but when 1/n > 1, the isotherm is convex and there is more presence of the sorbate in the sorbent which enhances the free energies of further sorption (Schwarzenbach *et al*., 2003). The Freundlich isotherm model is a good fit for an sorption system which implies there is almost no limit to the amount sorbed and there is also a multilayer sorption. Freundlich

equation (2.4) is applied to a particular case by plotting ln q_e against ln C_e from the logarithmic form of equation 2.3.

$$lnq_e = \left(\frac{1}{n}\right) lnC_e + lnk_f \quad (2.4)$$

Where q_e is the amount sorbed (mg/g), C_e is the equilibrium concentration of the sorbate (mg/L), K_f [(mg/g)*(mg/L)^n] and n is the Freundlich constants related to sorption capacity and sorption intensity, respectively (Freundlich, 1926). ln q_e versus ln C_e linear plots would give the value of 1/n as slope and k_f as an intercept. The value of k_f can be used as alternative measure of sorption capacity, while 1/n determines the sorption intensity.

2.5.2 The Langmuir Model

Langmuir derived an alternative equation on the basis of the nature of the process of sorption from solution. The Langmuir sorption isotherm was developed assuming that;

- Monolayer sorption occurs.
- There is a fixed number of accessible sites on the surface of the sorbent, all of which have the same energy.
- Sorption is reversible.
- Lateral interactions do not occur among the sorbates.

The Langmuir model is probably the best known and the most widely applied sorption isotherm, which has established good agreement with various experimental data and is given in equation 2.5:

$$q_e = \frac{q_o b C_e}{1 + bC_e} \quad (2.5)$$

where q_e is the amount sorbed (mg/g), C_e is the equilibrium concentration of the sorbate (mg/L), and parameters q_o and b are Langmuir constants related to maximum sorption capacity (mg/g) (monolayer capacity) and bonding energy of sorption (L/mg), respectively, which are functions of the characteristics of the system as well as time. The linearized form of the Langmuir equation is given in equation 2.6.

$$\frac{1}{q_e} = \frac{1}{q_o} + \frac{1}{bq_oC_e} \quad (2.6)$$

Plots of 1/qe versus 1/Ce were obtained from the linearized form of the Langmuir equation. The values of monolayer capacity (q_0) and Langmuir constant (b) have been evaluated from the intercept and the slope of these plots.

It is possible to correlate the sorption capacity with the variation of surface area and porosity of the sorbent. The higher the surface area and pore volume, the higher the capacity of sorption. The Langmuir equation is applied for homogenous surfaces, therefore, it can be deduced that at a low concentration of the sorbate, it reduces a linear isotherm effectively, thus, follows Henry's law. On the other hand, at high concentrations of the sorbate, it predicts a constant monolayer sorption capacity.

2.6 Thermodynamic Parameters of Sorption

It is important to understand the changes expected to occur in the designing of sorption columns or batch sorption systems and how fast they take place. How fast the reaction is can be calculated by kinetic studies. However, the change in the reaction that is expected during this process requires knowledge of thermodynamic parameters. It is assumed in thermodynamic concepts that energy cannot be gained nor lost in an isolated system, but the entropy change is the driving force (Ho, 2003). The three key thermodynamic parameters that must be considered to determine the process include: the enthalpy of sorption (ΔH^o), entropy change (ΔS^o) and free energy change (ΔG^o) as a result of the transfer of a unit mole of solute from the solution onto the solid-liquid interface. The enthalpy change is an important thermodynamic function which is useful whenever there is a differential change occurring in the system. When the value of ΔH^o is negative, it is an exothermic process, and a positive value indicates an endothermic process. Another important thermodynamic parameter is the entropy change ΔS^o. The parameter ΔS^o investigates the spontaneity of the sorption process. ΔH^o and ΔS^o values were obtained using equation 2.7 (Vadivelan & Kumar, 2005):

$$lnK_d = \frac{\Delta S^o}{R} - \frac{\Delta H^o}{RT} \quad (2.7)$$

Where R = Universal gas constant (8.314 J/mol.K)

T = Absolute solution temperature (K)

K_d = Distribution coefficient

K_d (distribution coefficient) can be calculated by equation 2.8.

$$K_d = \frac{q_e}{C_e} \quad (2.8)$$

Where q_e = Amount sorbed per unit weight of solid (mg/g), (mol/g)

C_e = Equilibrium concentration of solute in solution (mg/g), (mol/g)

The values of ΔH^o and ΔS^o can be calculated from the slope and intercept of the plot between ln K_d versus 1/T respectively.

The free energy change is also an important thermodynamic parameter involved in the sorption process and can be calculated from equation 2.9.

$$\Delta G^o = -RT \ln K_d \quad (2.9)$$

Where ΔG^o: Gibbs Free energy change; R: Universal gas constant (8.314 J/mol.K); T: Temperature (K)

2.7 Kinetics of Sorption

In the design of industrial sorption columns, it is necessary to achieve the prediction of batch sorption kinetics. The nature of the sorption process is dependent on the physical and chemical features of the sorbent system and on the conditions of the system. Researchers have previously used different kinetic models including Elovich kinetic equation, Lagergren's pseudo first order, pseudo second order and parabolic diffusion model, so as to predict the mechanism of the sorption process. In all these models, the sorption kinetics was often described by the Lagergren's pseudo first order model (Mall and Upadhyay 1998). The second order model is now currently being widely used for the sorption systems for its good representation of the experimental data for most of the systems involving sorbent and sorbate.

2.7.1 Lagergren's Pseudo First Order Kinetics

This model has been widely used to predict the kinetics of metal ion sorption. The kinetics of metal sorption that follows the pseudo first order model is given by Ho & McKay, (1998) in equations 2.10 and 2.11:

$$\frac{dq}{dt} = k_1(q_e - q) \quad (2.10)$$

$$log(q_e - q) = logq_e - \left(\frac{k}{2.303}\right) \times t \quad (2.11)$$

Where q: amount of metal sorbed at any time (mg/g); q_e: amount of metal sorbed at equilibrium time (mg/g); k_1: Pseudo first order rate constant (min^{-1})

The value of k_1 can be obtained from the slope of the linear plot of log (q_e – q) versus time (t).

2.7.2 Pseudo second order model

In a situation when the q_e obtained from the first order reaction is not the same as the one derived experimentally, the second order equation (2.12) is applied in order to obtain k_2 (Ho & McKay, 1998).

$$\frac{dq}{dt} = k_2(q_e - q)^2 \qquad (2.12)$$

Where q = Amount of metal sorbed at any time (mg/g); q_e = Amount of metal sorbed at equilibrium time (mg/g); k_2 = Pseudo second order rate constant (g/mg.min)

When equation (2.12) is integrated under the boundary conditions of t = 0 to t = t and q = 0 and q = q_e gives the equation (2.13):

$$\frac{t}{q_t} = \left(\frac{1}{k_2 q_e^2}\right) + \left(\frac{1}{q_e}\right) \times t \qquad (2.13)$$

The plot between t/q versus t makes it possible to obtain q_e and k_2.

2.8 Summary

Desalination technologies have been employed and implemented in order to provide a solution to the water scarcity problems and improve fresh water supplies. These alternative technologies are however accompanied with a major challenge by the formation of a concentrated brine stream which is difficult and costly to dispose. The concentration of the brine produced is directly proportional to the percentage recovery. The composition of these brines is major cations, anions and trace elements. The particular elements of interest are major cations including: calcium, magnesium, potassium and sodium. These cations are present in high concentrations in the brine mixture. Different desalination technologies employed in the treatment of brine streams have resulted in overwhelming quantities of brines being generated. Hydrophilic adsorbents like the nanofibres have offered promising characteristics in terms of their kinetics and large surface area which enable them to remove complexed and dissolved metals from the contaminated stream. These hydrophilic adsorbent materials can have cationic or anionic exchange sites or complexing agents and the factors that determine separations are dependent on their affinities for the metal ions and different stabilities of the complexes.

CHAPTER THREE

3.0 Experimental Methods

3.1 Ion Exchange Resin, PAN and Other Materials

The chelating cation exchange resin Purolite S950 and the anion exchange resin PPA500Plus (from The Purolite Company, Bala Cynwyd, USA), PAN polymer, titanium dioxide (TiO_2), Dimethylformamide (DMF) and zeolite Y (from Zeolyst International, Valley Forge, USA), were used in this study. The Purolite S950 is a macroporous aminophosphonic acid chelating resin, designed for the removal of cations of toxic metals such as lead, copper and zinc from industrial effluents at low pH. At somewhat higher pH values, calcium, magnesium and barium, as well as the toxic metals cadmium, nickel, and cobalt are strongly complexed and may be separated from quite high concentrations of univalent cations. Purolite S950 is highly selective (under appropriate conditions) for a range of both heavy metal and common divalent ions. Therefore, its use can be recommended where it becomes necessary to remove calcium or magnesium in order to avoid possible precipitation, or where its selectivity for a particular range of metals offers advantages. The physicals properties, specifications and general descriptions of Purolite S950 resins as reported by the suppliers are shown in Table 3.1.

Table 3.1: General description and properties of resins

	Purolite S950
Functional group	Aminophosphonic
Matrix	Macroporous polystyrene crosslinked with divinylbenzene
Polymer Structure	Macroporous
Capacity	26 g/l (Calcium)
Specific gravity	1.13
Ionic form	Na^+

3.1.1 Sampling

The brine wastewater used in this study was a third-stage reverse osmosis effluent taken from the Emalahleni water reclamation plant in Mpumalanga province. This brine was filtered using a 0.45 μm pore membrane filter paper with the aid of a manual pumping device. The filtered brine sample was preserved with 3 drops of concentrated HNO_3 acid for approximately 100 mL of sample. The sample was subsequently preserved at 4 °C until analysis for cations using inductively-coupled plasma-optical emission spectroscopy (ICP-OES).

3.1.2 Chemicals Used

The chemicals used in this study are described alongside their grade and supplier in Table 3.2 below:

Table 3.2: Chemicals used

Chemicals	Percentage Purity	Suppliers
Acetic acid	98%	Merck Chemicals
Calcium chloride	99%	Merck Chemicals
Magnesium chloride	98%	Merck Chemicals
Potassium nitrate	99%	Merck Chemicals
Sodium chloride	99%	Merck Chemicals
Sodium hydroxide	99%	Merck Chemicals
Hydrochloric acid	32%	Merck Chemicals
Nitric acid	55%	Merck Chemicals
Ammonium acetate	99%	Sigma Aldrich
DMF	99.5%	B & M Scientific
Titanium dioxide	99.5%	Sigma Aldrich

3.1.3 Stock Solutions Preparation

The major metal ion concentration in the effluent collected from the Emalahleni treatment plant was determined and the concentration range of 100 – 1000 mg/L $MgCl_2$, KNO_3, NaCl and $CaCl_2$ solutions used in experiments were prepared. All the solutions were prepared from analytical grade chemicals and the solvent used was deionized water. 1000 mg/L stock solutions of magnesium ions (Mg^{2+}), potassium ions (K^+), calcium ions (Ca^{2+}) and sodium ions (Na^+) were prepared by dissolving 8.365 g of $MgCl_2$. $2H_2O$; 2.586 g of KNO_3; 3.668 g of $CaCl_2.2H_2O$ and 2.541 g of NaCl in 1 litre of deionized water respectively. Subsequently, working solutions of Mg^{2+}, K^+, Ca^{2+} and Na^+ containing 100 – 500 mg/L were prepared by appropriate dilution of the stock solution before use.

3.2 Instrumentation

An atomic absorption spectrophotometer (AAS), model PU9100 Philips AAS, was used for the quantitative determination of sodium. An inductively coupled plasma optical emission spectrophotometer (ICP-OES) was used for the quantitative determination of the concentration of magnesium, potassium, calcium and sodium ions. A Philips PANalytical instrument with a pw3830 x-ray generator operated at 40 kV and 25mA was used for X-ray diffraction (XRD) analysis for the determination of the crystal structures of the adsorbents. The Perkin-Elmer Spectrum 100 FT-IR spectrometer was used for the infrared spectra measurement. The surface morphology of PAN, PAN+TiO_2, PAN+Zeolite and the resin was examined by the scanning electron microscope (Hitachi X650, Scanning Electron Micro analyser) at 10-20 kV before and after sorption. The pH measurement was carried out using a glass electrode (micro ohm pH meter), the calibration of the pH meter was done using standardized Merck buffer solutions (pH 4, pH 7 and pH 9). The GFL model water bath shaker was used for shaking the metal solutions at desired temperatures.

3.3 Preparation of 8 wt% Polyacrylonitrile (PAN)

50 mL of DMF was transferred into a schott bottle. An oil bath was heated to a temperature of 90 $^{\circ}$C, and the schott bottle having the 50 mL DMF was placed inside the oil bath and firmly clamped at the bottleneck with the content being stirred by a magnetic stirrer. The set-up was

allowed to stabilize for about 15 minutes so that the oil bath and the solvent in the schott bottle would have the same equilibrium temperature of 90 $^{\circ}$C. PAN of a mass of 4.1043 g was transferred into the schott bottle containing the DMF and stirring was continued for about an hour. Thereafter, the schott bottle was removed from the oil bath and the solution was stirred without heating for 24 hours.

3.3.1 Electrospinning of Polyacrylonitrile (PAN) Nanofibre

The prepared mixture in section 3.3 was sucked into two syringes, and the syringes were placed into the pump with the flow rate set at 0.4 mL per hour and a voltage of 25 kV was applied across the two syringe needles to electrospin the content onto a collector of aluminium foil. The electrospinning parameters were determined based on the information in the literature as regards electrospinning. The electrospinning condition was set at a temperature of 27 $^{\circ}$C and the distance between the needles of the syringes and the collector was 15 cm. The droplet was ejected out of the needle under the high voltage and accelerated towards the collector in the external electrostatic field and therefore collected on the aluminium foil surface as a nanofibrous mat. The solution surface tension was overcome by the electrical force at the surface of the drop solution, and therefore resulted in the stretching and elongation of the polymer solution into nanofibres. Figure 2.9 shows the schematic set-up for electrospinning.

3.3.2 Doping of Polyacrylonitrile (PAN) with Titanium dioxide (TiO_2)

A 3 wt.% concentration of titanium dioxide was achieved by weighing 1.5391 g of titanium dioxide (TiO_2) and subsequently transferred to the prepared solution in section 3.3 and the mixture was stirred for 24 hours to achieve an even mixture. The resulting mixture was electrospun using the technique described in section 3.3.1. But the flow rate was reduced to 0.2 mL per hour owing to the fact that the mixture had thickened.

3.3.3 Doping of Polyacrylonitrile (PAN) with Zeolite

A 3 wt.% concentration of zeolite was also achieved by weighing 3.078 g of Zeolite Y and transferred to the prepared solution in section 3.3 and the mixture was stirred for 24 hours to achieve an even mixture. The resulting mixture was electrospun using the technique described in section 3.3.1. But the flow rate was reduced to 0.2 mL per hour.

3.4 Brine Baseline Study

3.4.1 Conversion of S950 Resin to the Ammonium form

A 20 mL column was filled with the S950 resin (in the Na^+-form) to the 15.0 mL mark. The sodium ion was eluted by the passage of 150 mL of 1.0 M ammonium acetate solution through the column. The last 5 mL eluate was tested for sodium in a flame of an atomic absorption spectrophotometer (AAS), to see whether the flame was colourless, showing that sodium is completely removed from the resin in the column.

3.4.2 Behaviour of Calcium, Magnesium, Potassium and Sodium on Purolite S950 Resin

The major ions under investigation in the Emalahleni brine are calcium, magnesium, potassium and sodium respectively. The contents of the major elements in the brine mixture are used to calculate the volume (10 mL) of the solution to be passed through the resin, which must be in total milli-equivalence of a 10 mL resin column. An Emalahleni brine solution containing calcium, magnesium, potassium and sodium ions was passed through the 15 mL S950 purolite resin (NH_4^+-form) column and ten samples of 10 mL fractions were collected from the beginning of the sorption step. Each fraction was diluted to the mark in a 250 mL volumetric flask with deionized water and the content of the elements of each fraction was determined.

3.5 Nanofibre Characterization

3.5.1 SEM Analysis

A scanning electron microscope device (Hitachi X650, Scanning Electron Micro analyser) at 10-20 kV was used to examine the surface morphology of the PAN, PAN+TiO_2 and PAN+Zeolite nanofibres respectively, before and after doping.

3.5.2 FT-IR Analysis

The infra-red spectra of PAN, PAN+TiO_2 and PAN+Zeolite nanofibres were carried out with the FT-IR spectrometer to determine if any functional groups are present.

3.5.3 Determination of Cation Exchange Capacity for Purolite S950 Resin

An approximately 5 g of resin was placed in a column and converted to the hydrogen form by the passing 1 L of 1 M HNO_3 through the column. The resin was thoroughly rinsed with excess deionized water to strip the resin of any excess acid; this was then drained and air-dried. From the 5 g resin sample prepared, approximately 1.0 g was weighed and transferred into a dry 250 ml Erlenmeyer flask, fitted with a stopper, and exactly 200 mL of standardized 0.1 M NaOH solution already prepared in 5 % NaCl was added. A stopper was placed on the flask and the sample was set aside overnight. 50 mL aliquot of the supernatant solution was then back-titrated to the colourless end point of phenolphthalein with standard 0.1 M HCl. The hydrogen ions which were initially available in the resin phase were equivalent to the volume of acid needed to produce a permanent colouration (Fisher & Kunin, 1955).

3.6 Sorption Experiments

The capacity of sorption of PAN, PAN+TiO_2 and PAN+Zeolite nanofibres toward Ca^{2+}, Mg^{2+}, Na^{+} and K^{+} ions from metal ion solutions was investigated by batch sorption experiments, with their respective performance compared to the Purolite S950 resin.

In the investigation of the sorption behaviour of these polymers, synthetic solutions were used without the interference of the trace metal ions in the brine waste water. The first set of experiments were carried out with Ca^{2+}, Mg^{2+}, Na^{+} and K^{+} solutions at the concentration of 100 mg/L in deionized water. The desired pH for each solution was attained by using 0.1 mol/L acetic acid and 0.05 mol/L sodium hydroxide solutions.

3.6.1 Batch Sorption Experiment

The batch sorption experiment for the metal ions (Ca^{2+}, Mg^{2+}, Na^{+} and K^{+}) using a model solution was carried out in a 100 mL plastic bottle using a tray action shaker. Fixed amounts of resin and the nanofibres (0.1 g) were contacted for 8 hours with 50 mL metal ion solution of variable concentration and pH at 25 °C. Blank solutions were treated in a similar manner without the adsorbent and the concentrations were recorded as initial concentration at the end of each operation. The residual concentration of the metal ions (Ca^{2+}, Mg^{2+}, Na^{+} and K^{+}) in the solution after the treatment were thereafter measured by ICP-OES. The quantity of metal

ion adsorbed (q, mg/g), (q, meq/g), (q, mmol/g) and percent sorption (% A) were calculated as shown by (Equations 3.1, 3.2, 3.3 and 3.4) respectively.

$$q(mg/g) = \frac{(C_o - C_f) \times V}{M} \quad (3.1)$$

$$q(meq/g) = [\frac{q(mg/g)}{Equivalent\ weight\ of\ M^{n+}}] \quad (3.2)$$

$$q(mmol/g) = \frac{(C_o - C_f) \times V}{Mr \times M} \quad (3.3)$$

$$Sorption\ (\%) = \frac{(C_o - C_f)}{C_o} \times 100 \quad (3.4)$$

Where q is the amount of metal ion adsorbed expressed in (mg/g) or (meq/g) or (mmol/g), C_o is the initial metal ion concentration, C_f is the final metal ion concentration (mg/L), V is the volume (L) of solution, M is the mass of the adsorbent used (g). Equivalent weight of M^{n+} is the formulae weight divided by the charge on metal ion, and Mr is the atomic mass of the adsorbed metal ion (Sang et al., 2008).

3.6.2 Effect of contact time

The contact time experiments were conducted using a model solution at 25 °C in different plastic bottles with covers. The bottles were shaken for different time intervals at constant temperature. Fixed masses of adsorbents (0.1 g each for nanofibres or resins) were contacted with 25 mL of 100 mg/L of the metal ions (Mg^{2+}, Ca^{2+}, Na^{+} and K^{+}) in solution and the phases were separated by filtration after a specified time. The supernatant solution was then collected for analysis by ICP-OES. The experiment was carried out in quadruple under similar conditions.

3.6.3 Sorption Isotherm (Effect of concentration)

The effect of concentration was carried out in a series of 100 mL plastic bottles. The bottles were filled with 25 mL of different initial concentrations that varied from 100 to 500 mg/L while the temperature and adsorbent mass were kept constant. After the equilibration time was reached, the phases were separated by filtration and analysed using the ICP-OES. Blank solutions were also given a similar treatment, but devoid of the adsorbent, and concentrations at the end of each operation were recorded as the initial concentration. The data obtained was used to determine the quantity adsorbed at equilibrium (sorption capacity), q_e, of the adsorbent. The experiment was carried out in quadruple under similar conditions.

3.6.4 Sorption Kinetics

The sorption kinetics experiments were performed by using adsorbent of a fixed mass (0.1 g each for nanofibres and resins) in contact with 25 mL of 100 mg/L of the metal ions (Mg^{2+}, Ca^{2+}, Na^{+} and K^{+}). At different time intervals, the samples were taken and filtered. The subsequent filtrate portions were analysed using the ICP-OES. This experiment was carried out in quadruple under similar conditions.

3.6.5 Effect of Adsorbent dose

The batch equilibration method was used to measure the metal ion binding capacity by varying the adsorbent mass. Different dry adsorbent amounts (0.1 - 0.5 g for nanofibres and 0.1 - 0.5 g for resins) were contacted with 25 mL of 500 mg/L of the metal ion solutions (Mg^{2+}, Ca^{2+}, Na^{+} and K^{+}) for 8 hours at 25 $^{\circ}$C with constant shaking. After the completion of the equilibration time, the supernatant solution was analysed by ICP-OES. All test samples were run in quadruples.

3.6.5 Effect of pH

The effect of pH was carried out using the batch technique. 0.1 g each of the sorbents was placed into a series of 100 mL plastic bottles, where 25 mL of 500 ppm of each metal solution had been placed. Prior to the addition of the adsorbents, the metal ions solutions were adjusted to the various pHs in the pH range of 2-7, by carefully adjusting the pH with 0.1 mol/L acetic acid and 0.05 mol/L sodium hydroxide solutions. The mixture was shaken for 8 hours at 25 $^{\circ}$C. When the equilibration was completed, the supernatant solution was collected and

analysed by the ICP-OES. All test samples were run in quadruple. Blank solutions were also treated in a similar manner without the adsorbent and the concentration at the end of the operation was recorded as initial concentration.

3.6.6 Effect of Temperature

The effect of temperature was also studied by the batch equilibration method. This was achieved by placing 0.1 g of the sorbents (the nanofibres and the resin) into the plastic bottles, where 25 mL of 500 ppm of each metal ion solution had been placed, at constant pH. The mixture was shaken for 1 hour at different temperatures (25 $^{\circ}$C, 35 $^{\circ}$C, 45 $^{\circ}$C and 55 $^{\circ}$C). After the equilibration time was reached, the supernatant solution was analysed by ICP-OES. All the test samples were carried out in quadruple under the same conditions. The data obtained was used to calculate the enthalpy change (ΔH°), entropy change (ΔS°) and the free energy change (ΔG°).

CHAPTER FOUR

4.0 Results and Discussion

4.1 Nanofibre Characterization

The characterization of the nanofibre was carried out by the use of the following methods: X-ray diffraction (XRD), Fourier Transform Infra-Red (FT-IR) spectroscopy, Scanning Electron Microscopy (SEM). The sorption capacities of the nanofibres and the resin were compared while the variable factors affecting sorption such as temperature, pH, sorption isotherm, sorbent dose, contact time and sorption kinetics were also carried out. The outcome of these investigations is discussed in this section.

4.1.1 Doping of PAN and FT-IR spectra Analysis

The 8 wt.% PAN nanofibre described in section 3.3 was doped with titanium dioxide (TiO_2) and zeolite respectively, at a 3 wt.% concentration under constant stirring at room temperature for 24 hours to make the solution dissolve evenly. The electrospinning of the PAN nanofibre, PAN+TiO_2 nanofibre and PAN+ZEOLITE nanofibre was achieved by the process described in section 3.3.1.

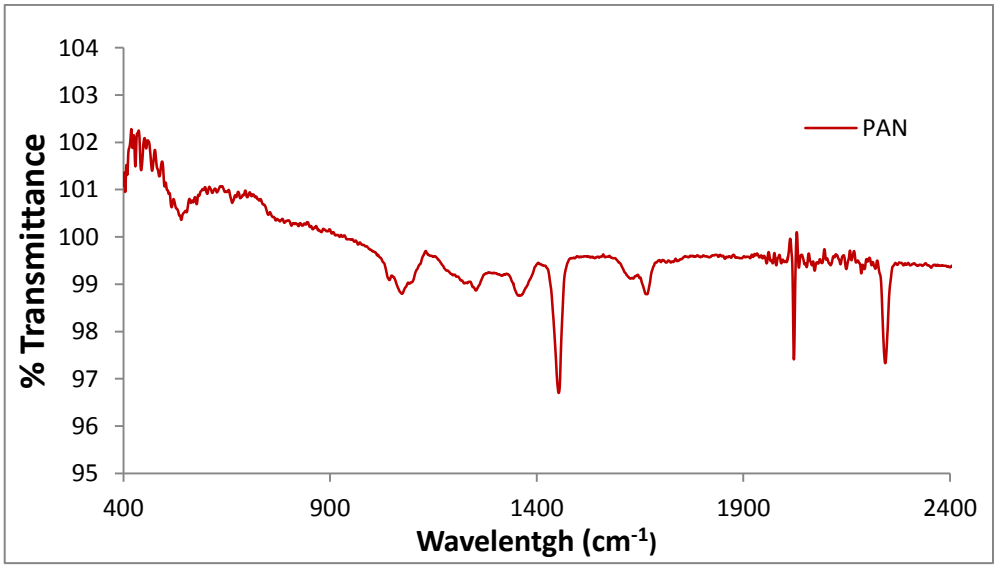

Figure 4.1: The FT-IR spectrum of PAN nanofibre

The FT-IR spectrum of PAN in Figure 4.1 exhibits the characteristic bands of nitrile (C≡N) at about (2 250 cm^{-1}), carbonyl (about 1 725 cm^{-1}) and this indicates that PAN is a copolymer.

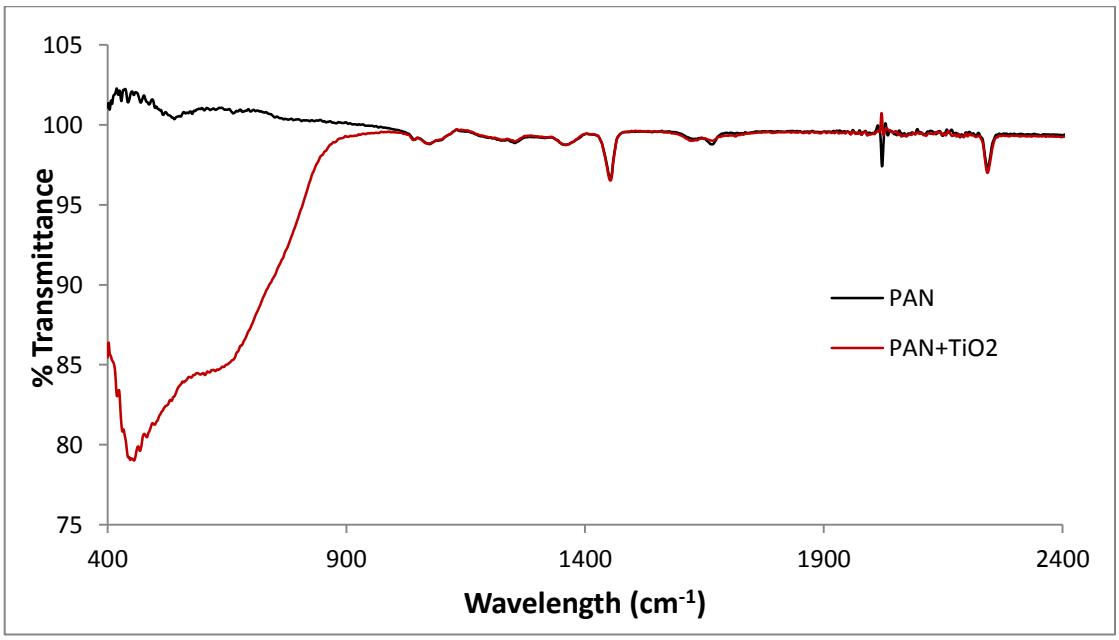

Figure 4.2: FT-IR spectra for PAN and PAN+TiO_2

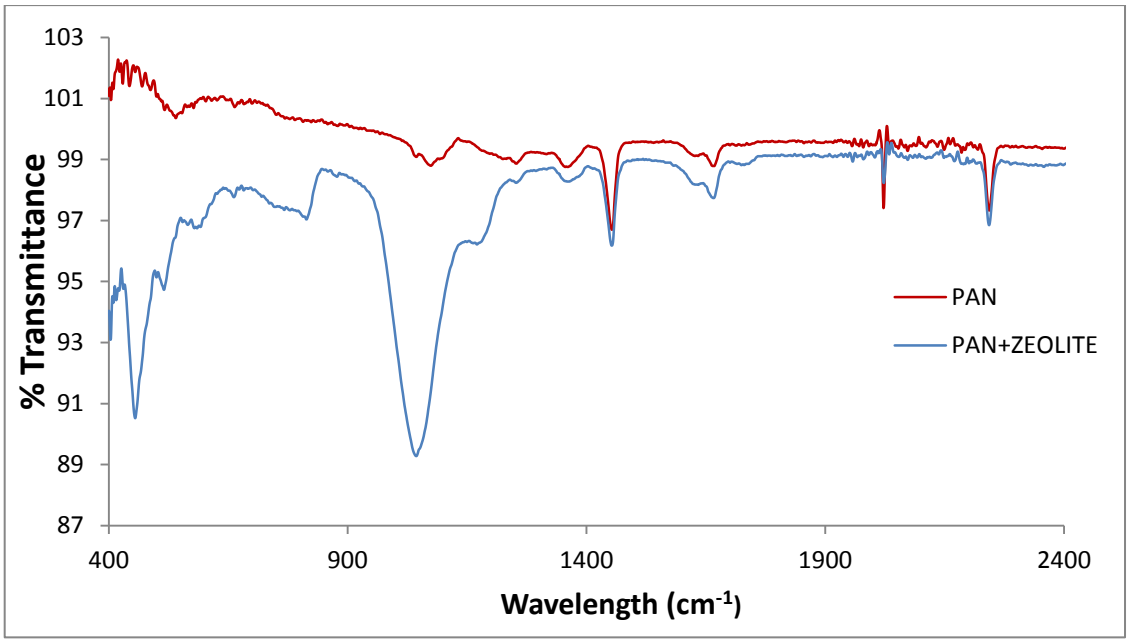

Figure 4.3: FT-IR spectra for PAN and PAN+ZEOLITE

The FT-IR spectrum of the PAN doped with titanium dioxide (TiO_2) as shown in Figure 4.2, also exhibits the characteristics of PAN spectrum with no major changes in the magnitude of the peaks as depicted in the FT-IR spectra of the respective nanofibres. The incorporation of titanium dioxide (TiO_2) revealed a broad peak at about 470 cm^{-1}. The same applies to the incorporation of zeolite into the PAN structure. For the zeolite incorporated in PAN however, as shown in Figure 4.3, the peak at 460 cm^{-1} is assigned to the insensitive internal structure

TO_4 (T = Si or Al), which is the characteristic tetrahedrall bending peak of zeolite Y (Holmberg *et al.,* 2003). The peak at 685 cm^{-1} is assigned to external linkage symmetrical stretching, while the peak around 1055 cm^{-1} signifies the external linkage asymmetrical stretching of zeolite Y (Holmberg et al., 2003). Generally, the FT-IR spectra match well with the absorption peaks characteristic of zeolite Y discussed in past literature (Flanigen *et al.,* 1971)

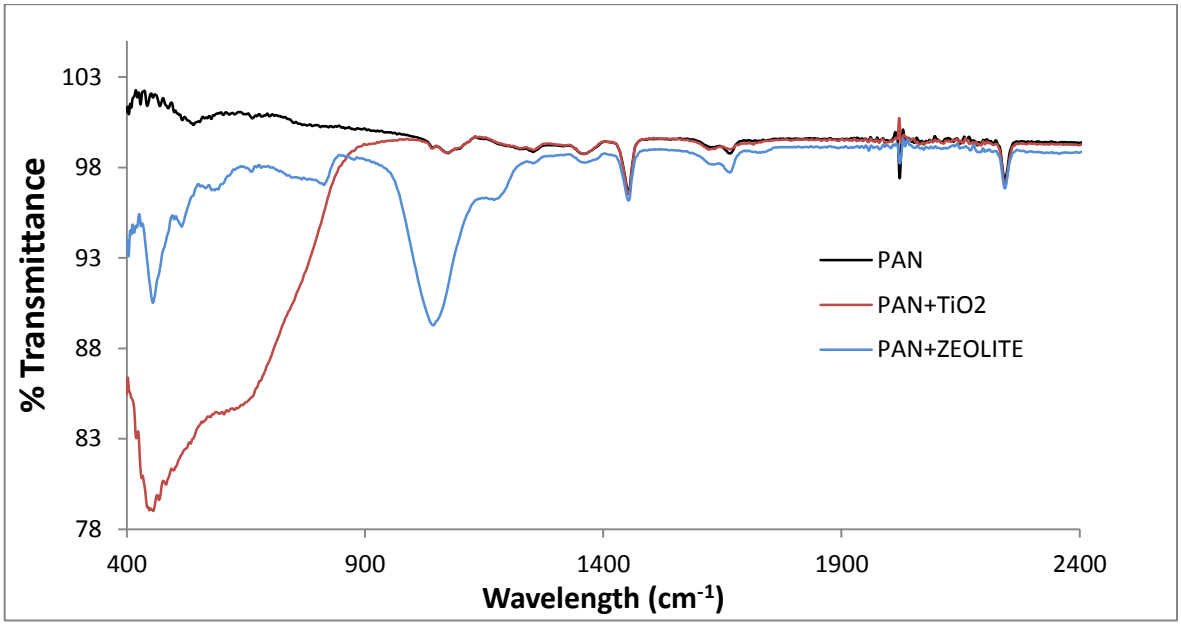

Figure 4.4: The FT-IR spectra of (a) PAN, (b) PAN+TiO_2 and (c) PAN+ZEOLITE

The Figure 4.4 depicts the FT-IR spectra of the three nanofibres. The spectra for PAN+TiO_2 and PAN+ZEOLITE are almost the same with that of PAN, with the slight difference being the result of the addition of titanium dioxide and zeolite respectively.

4.1.2 XRD Analysis

In Figure 4.5, the graph shows the XRD spectra of PAN nanofibre, PAN+ZEOLITE nanofibre and zeolite Y samples. The peaks of the XRD analysis presented in Figure 4.5 were compared with standard spectra to identify the corresponding mineral phase using Joint Committee on Powder Diffractive Standards (JCPDS) data for zeolite materials. It can be seen from the XRD spectrum of PAN that it forms two major peaks. The first sharp peak was observed at 16.54 theta degrees, while the second peak happens to be a broad hump between 20 and 38 theta degrees. But the PAN+ZEOLITE spectrum shows all the peaks of the zeolite Y structure labelled as “Y”, including the peak of PAN at 16.53 theta degrees, with a reduced intensity of all the peaks, owing to the incorporation of zeolite into the PAN lattice. As a result, it is

evident that the zeolite is incorporated in the PAN fibres. This further complements the FT-IR spectrum of PAN+ZEOLITE in Figure 4.3, where the PAN structure remains intact and the peaks associated with the zeolite Y structure also reflect. The zeolite Y XRD spectrum reveals all the peaks of zeolite Y with a pronounced intensity. All the peaks associated with zeolite Y align well in the XRD spectra of PAN+ZEOLITE and zeolite respectively.

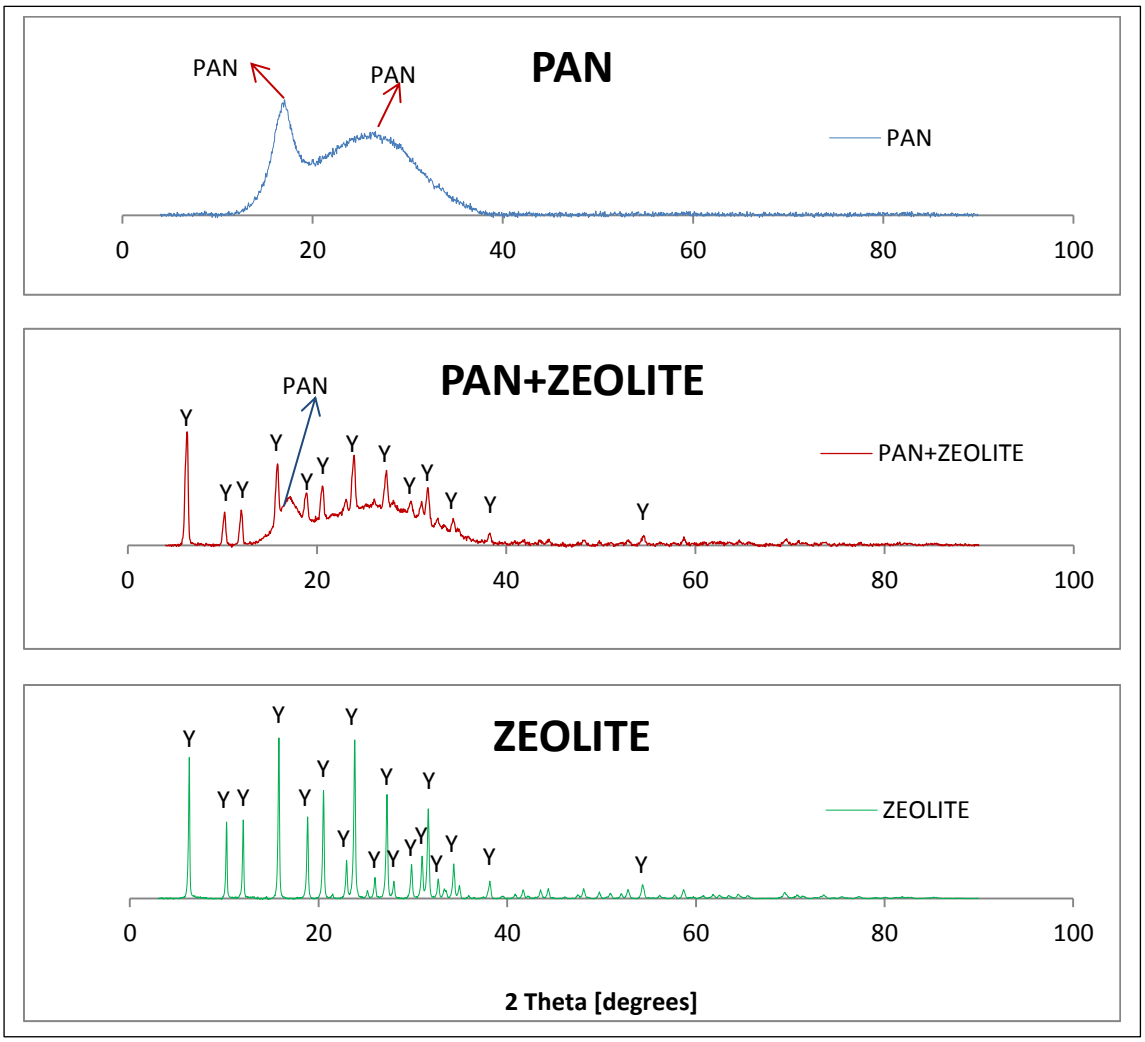

Figure 4.5: XRD patterns of PAN, PAN+ZEOLITE and ZEOLITE.

Figure 4.6 shows the XRD patterns of PAN+TiO_2 and TiO_2. The peaks labelled as " T " are the peaks associated with titanium dioxide (TiO_2). However, in the XRD analysis of titanium dioxide (TiO_2) and PAN+TiO_2 as shown in Figure 4.6, it can be seen that all the peaks of titanium dioxide also reflected in the XRD spectrum of PAN+TiO_2 and the two major peaks associated with PAN emerged at 17.17 and 27.22 theta degrees respectively. This XRD result makes it clearly evident that TiO_2 was successfully incorporated into the PAN fibres without any degradation.

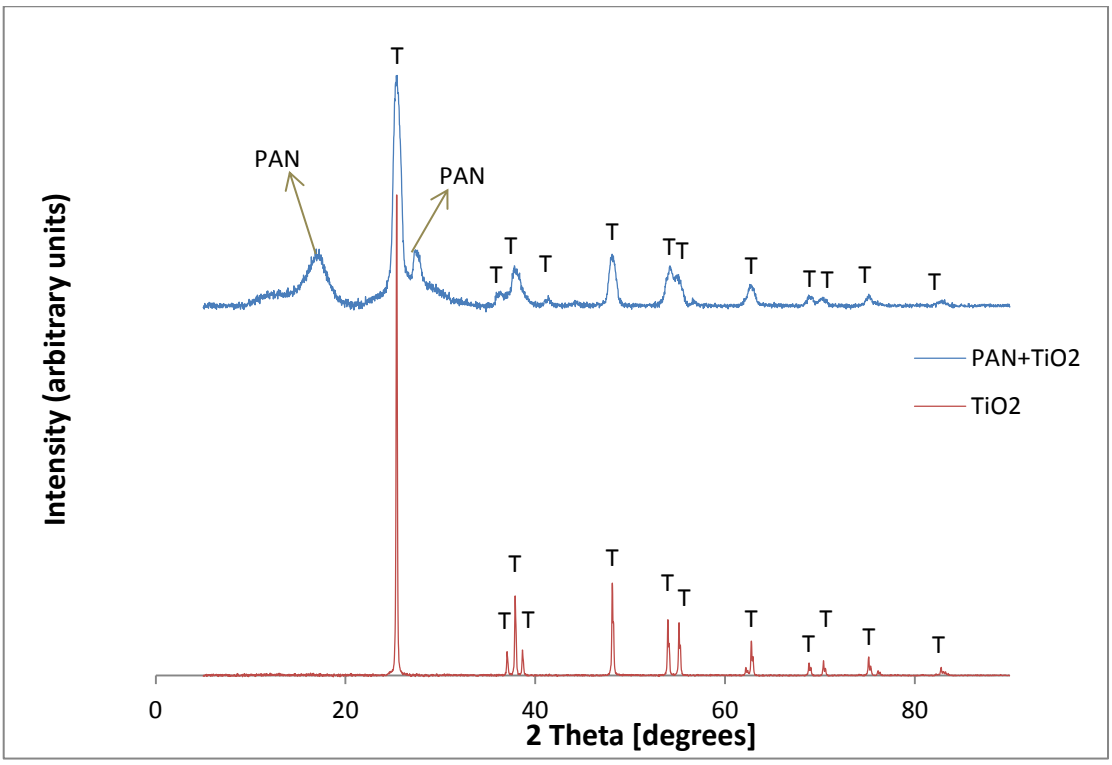

Figure 4.6: XRD patterns of PAN and PAN+TiO_2

4.1.2 SEM Images

The surface morphology of PAN, PAN+TiO_2 and PAN+ZEOLITE nanofibres was examined by using a scanning electron microscope. The surfaces of the nanofibres were examined before and after doping. Figure 4.7 shows the SEM images of PAN nanofibres as made at different magnifications (a) and (b) respectively.

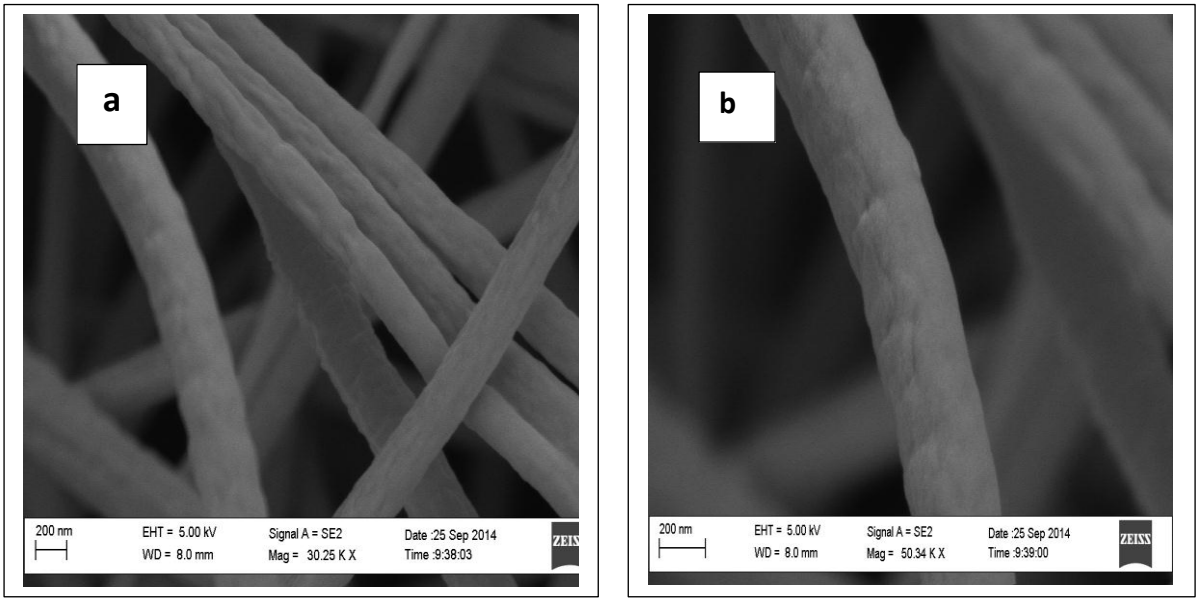

Figure 4.7: SEM images (a) and (b) showing the PAN nanofibre surface morphologies at different magnifications before sorption.

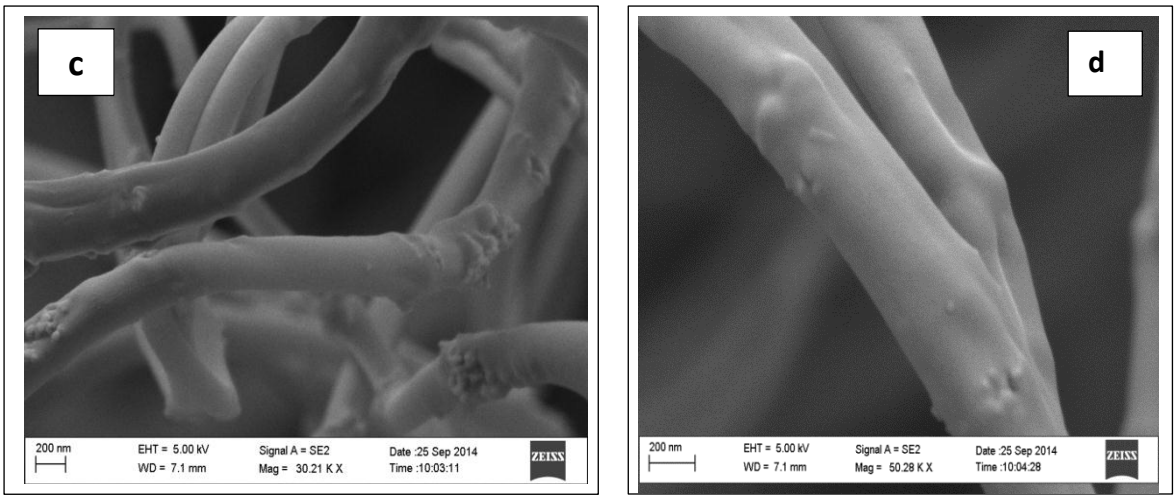

Figure 4.8: SEM images (c) and (d) showing the PAN+TiO_2 nanofibre surface morphologies at different magnifications before sorption.

Before the sorption experiment, the smooth nature of the PAN nanofibres can be seen in the Figure 4.7 for both magnifications. Also, when PAN was doped with titanium dioxide (TiO_2) as shown in Figure 4.8, it is obvious to notice the undulating nature of the nanofibre. This can be attributed to the incorporation of titanium dioxide (TiO_2) into the PAN nanofibre matrix, as it is evident in the uneven distribution of TiO_2 throughout the nanofibre structure.

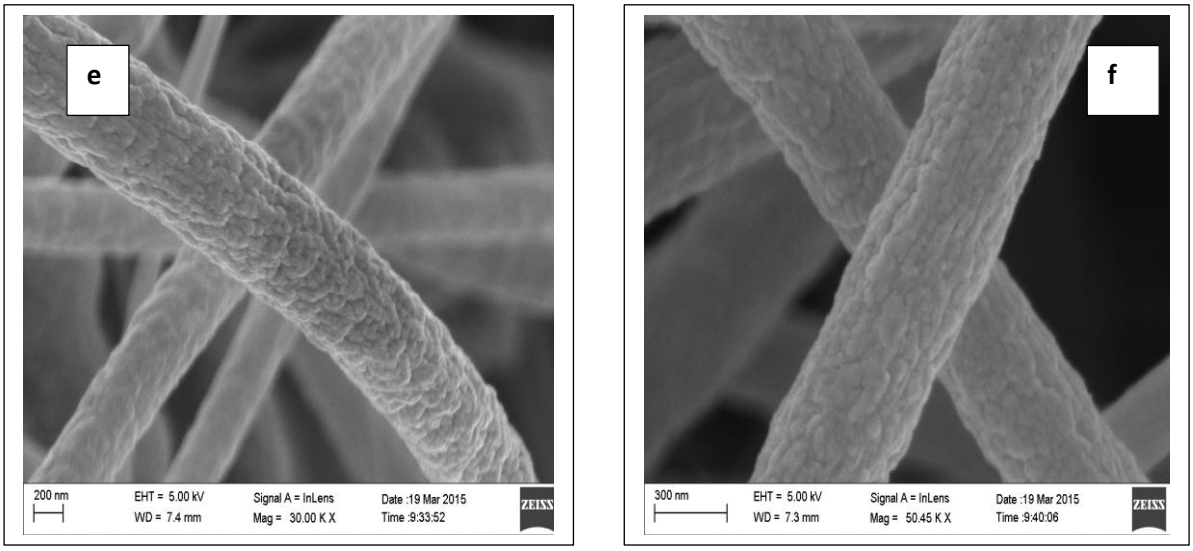

Figure 4.9: SEM images showing the PAN+ZEOLITE nanofibre surface morphologies at different magnifications (e) and (f) before sorption.

Figure 4.9 shows the PAN+ZEOLITE nanofibre SEM images with the strands of the nanofibres being predominantly rough throughout on its entire surface due to the incorporation of zeolite particles into the PAN fibres.

In Figure 4.10, after the sorption upon PAN, there was no degradation whatsoever visible on the nanofibres but rather, the PAN nanofibre appears rougher than it was prior to sorption. For

PAN+TiO_2 in Figure 4.11, some nanofibre strands appear very similar to the way it was before the sorption, but surfaces appeared smoother. Also in the case of PAN+ZEOLITE nanofibre in Figure 4.12, the strands of the polymer also appear slightly rougher than it was before the sorption.

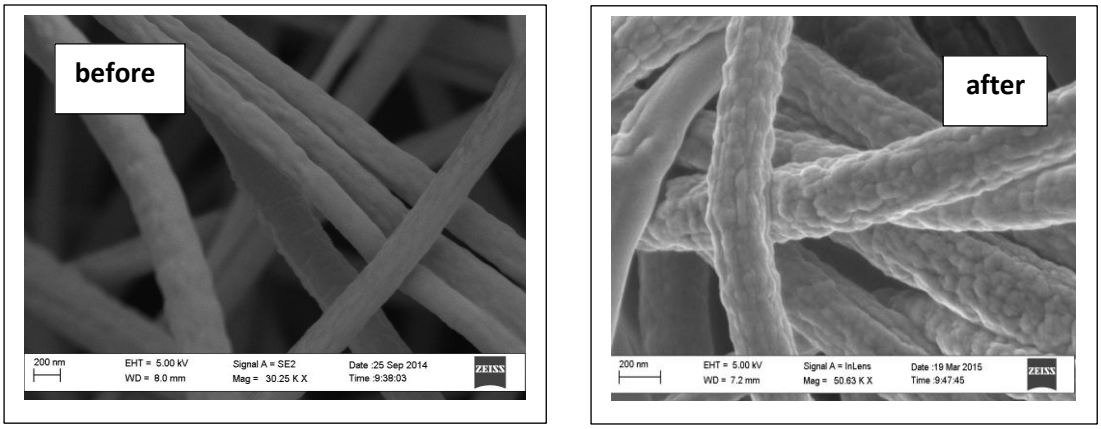

Figure 4.10: SEM images showing PAN nanofibres before and after sorption.

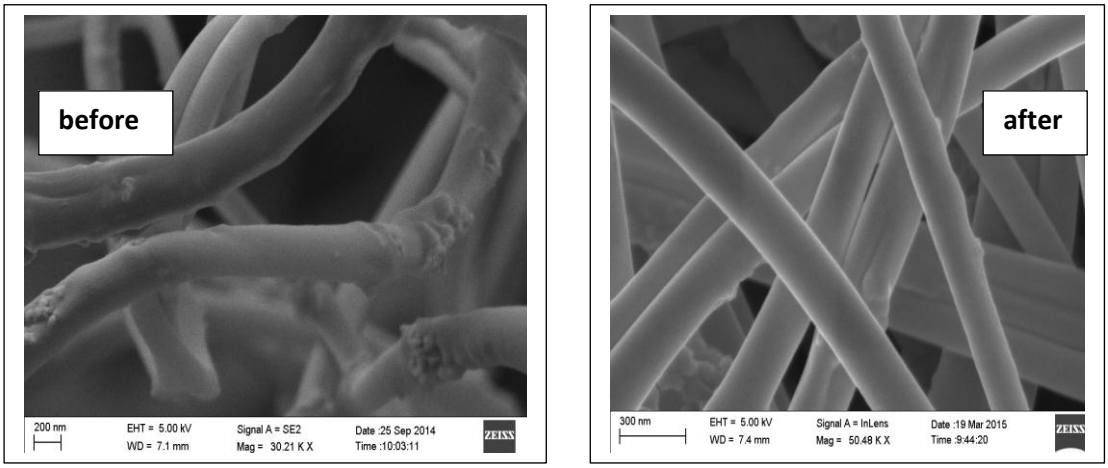

Figure 4.11: SEM images showing PAN+TiO_2 nanofibres before and after sorption.

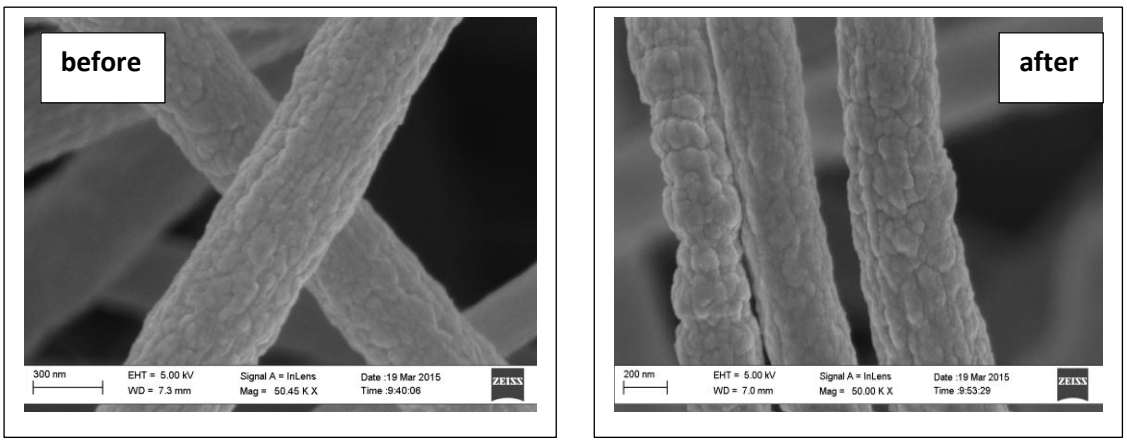

Figure 4.12: SEM images showing PAN+ZEOLITE nanofibres before and after sorption.

4.2 The Batch Sorption Experiments

Different solutions were synthetically prepared in the range of 100 – 1000 mg/L to imitate the brine effluent generated from the Emalahleni water reclamation plant in the batch sorption experiments for the sorption of Mg^{2+}, Ca^{2+}, K^{+} and Na^{+}. Purolite S950 resin and the nanofibres (PAN, PAN+TiO_2 and PAN+ZEOLITE) were employed to carry out the batch sorption experiments. The effect of various parameters such as the temperature, sorbent dosage, pH of the solution, contact time, sorption isotherm and the sorption kinetics were investigated for the sorption of Mg^{2+}, Ca^{2+}, K^{+} and Na^{+} ions from the solutions.

4.2.1 The effect of sorbent dose

Sorbent dose is an important parameter which influences the extent of metal uptake from the solution by varying the sorption mass. For the various metal ions (Mg^{2+}, Ca^{2+}, K^{+} and Na^{+}), the initial concentration of the aqueous feed solution was 500 mg/L. The experiment was conducted with the metal ion solutions being shaken separately with the various masses of the resin or the nanofibres for 8 hours (the procedure can be seen in section 3.6.5).

The results of the effect of the Purolite S950 resin dosage on the sorption of Mg^{2+}, Ca^{2+}, K^{+} and Na^{+} ions from their separate solutions are shown in Table 4.1 and Figure 4.13.

Table 4.1: The effect of resin mass on the sorption of Mg^{2+}, Ca^{2+}, K^{+} and Na^{+} ions from the individual solutions by Purolite S950 resin.

Resin mass (g/25 mL)	Mg^{2+} sorption (%)	Ca^{2+} sorption (%)	K^{+} sorption (%)	Na^{+} sorption (%)
0.1	25.4	11.4	0.4	11.4
0.2	45	50.6	0.6	12
0.3	76	80.6	0.8	12.6
0.4	86.8	91.8	0.8	13
0.5	97.4	97.8	0.8	13.4

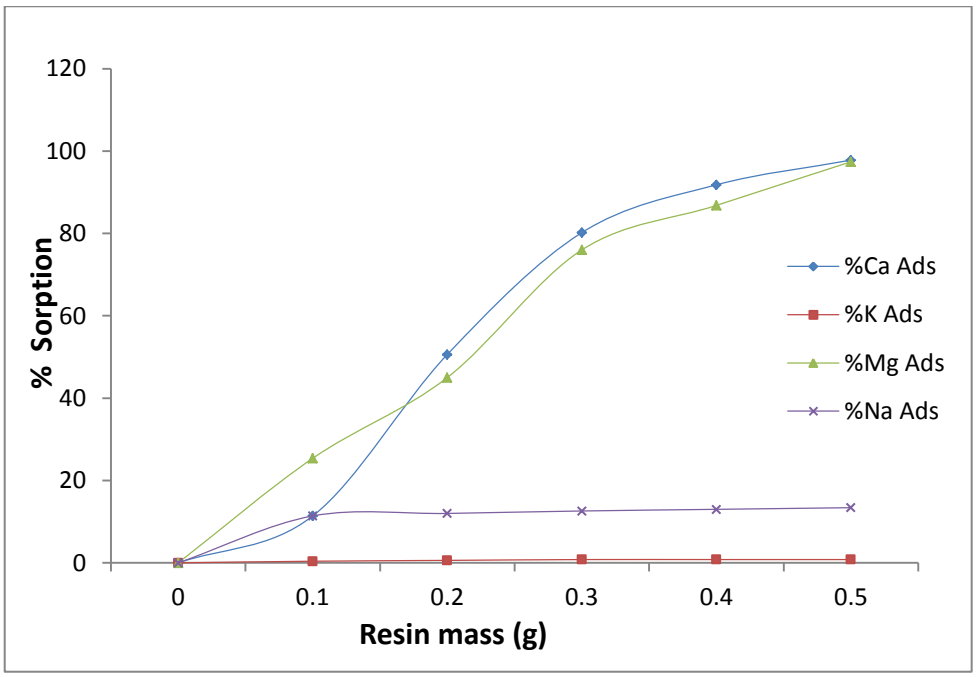

Figure 4.13: The effect of resin mass on the sorption of Mg^{2+}, Ca^{2+}, K^{+} and Na^{+} by Purolite S950 resin
(Metal ion concentration, 500 mg/L; Temperature, 25 °C; volume, 25 ml; contact time 8 hours)

In this experiment, the metal ion concentration (500 mg/L) and the time (8 hrs) were kept constant while the resin mass was varied between 0.1 and 0.5 g. The amount of metal ion uptake increased from 25.4 and 11.4 to 97.4 and 97.8 % sorption for Mg^{2+} and Ca^{2+} ions respectively, as a result of the increase in the resin mass from 0.1 g to 0.5 g. A similar trend was observed for K^{+} and Na^{+} ions where the uptake of metal ions increased from 0.4 and 11.4 to 0.8 and 13.4 % sorption respectively. The K^{+} ion sorption by the resin was limited to between 0.3 g and 0.5 g / 25 mL, while Ca^{2+} and Mg^{2+} ions reached the zenith for the resin amount of 0.5 g / 25 mL. Based on these results, the optimum resin amount for both Ca^{2+} and Mg^{2+} was determined to be 20 g resin/L. Figure 4.13 shows clearly that the percentage sorption of the metal ions increased as the sorption dose increased from 0.1 g to 0.5 g. This increase can be attributed to the increase in the number of available sites as the dose of the sorbent is increased. The removal of metal ions increased with the increase in the Purolite S950 resin mass which reached its maximum at 0.5 g / 25 mL or 20 g resin/L. It is however reasonable that the near 100 % sorption of Mg^{2+} and Ca^{2+} from the solution is due to the availability of more exchange sites than the cations available in the solution. Maximum sorption is achieved when the exchange sites are exhausted; this means there are still more available exchange sites left on the resin capable of more sorption.

The nanofibre mass was also varied from 0.1 to 0.5 g in 25 mL metal ion solutions, the nanofibres include: PAN, PAN+TiO_2 and PAN+ZEOLITE. The results shown in Table 4.2 and Figure 4.14 reveal a slight increase in the metal ions sorption with an increase in the

sorbent dose. From these results, it can therefore be inferred that the optimum sorption amount was found to be 12 g sorbent/L for the sorption of Mg^{2+}, Ca^{2+}, K^{+} and Na^{+} ions by PAN nanofibres. Any further increase in the sorption dose showed little or no effect upon the percentage sorption of the metal ions from the solution, this is perhaps due to the saturation of the available exchange sites.

Table 4.2: Effect of the sorption dose on the sorption of Mg^{2+}, Ca^{2+}, K^{+} and Na^{+} ions from individual solutions by PAN nanofibres.

PAN mass (g / 25 mL)	Mg^{2+} sorption (%)	Ca^{2+} sorption (%)	K^{+} sorption (%)	Na^{+} sorption (%)
0.1	22.2	4.0	1.0	9.4
0.2	23.0	5.0	1.4	10.4
0.3	23.4	5.4	2.0	10.6
0.4	23.6	5.5	2.0	10.6
0.5	23.8	5.5	2.0	10.6

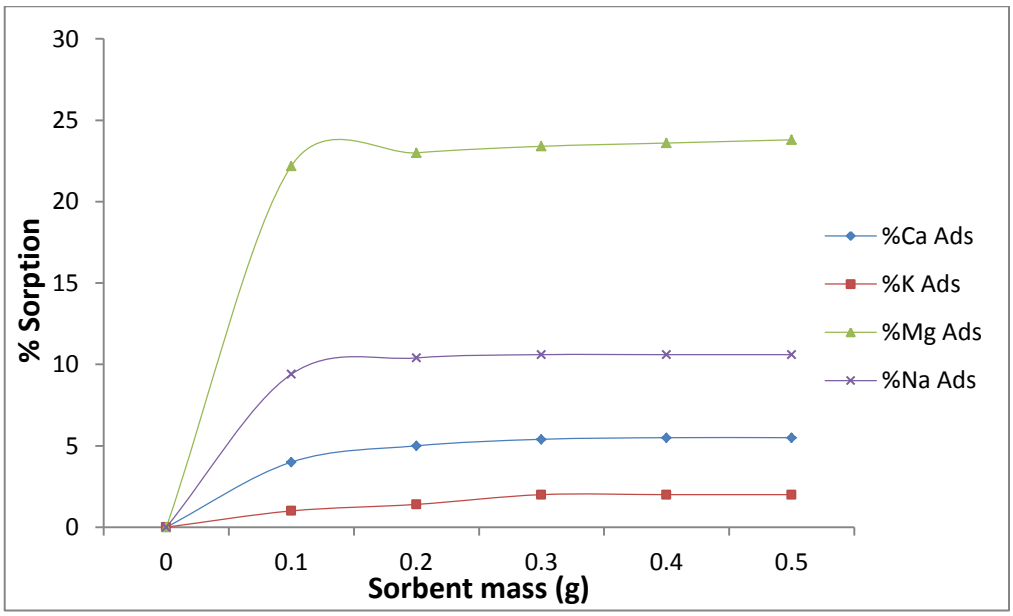

Figure 4.14: The percentage sorption of Mg^{2+}, Ca^{2+}, K^{+} and Na^{+} ions with PAN nanofibres as a function of sorbent mass.
(Metal ion concentration, 500 mg/L; Temperature, 25 $^{\circ}$C; volume, 25 mL; contact time 8 hours).

In the case of PAN+TiO_2 nanofibres, the results in Table 4.3 and Figure 4.15 reveal that as the sorbent dose increased, there was a slight increase in the sorption of metal ions from the solution. From these results, the optimum sorbent amount was found to be 12 g sorbent/L for the sorption of Mg^{2+}, Ca^{2+}, K^{+} and Na^{+} ions by PAN+TiO_2 nanofibres. The subsequent increase in the sorbent dose showed an insignificant increase in the percentage sorption of calcium, magnesium and sodium ions from the solution, this is perhaps due to exchange sites' saturation.

Table 4.3: Effect of the sorption dose on the sorption of Mg^{2+}, Ca^{2+}, K^{+} and Na^{+} ions from individual solutions by PAN+TiO_2 nanofibres.

PAN+TiO_2 mass(g / 25 mL)	Mg^{2+} sorption (%)	Ca^{2+} sorption (%)	K^{+} sorption (%)	Na^{+} sorption (%)
0.1	23.2	4.2	1.0	10.8
0.2	23.6	5.2	1.4	10.8
0.3	24.0	5.4	2.0	11.4
0.4	24.0	5.4	2.4	11.4
0.5	24.0	5.4	2.4	11.4

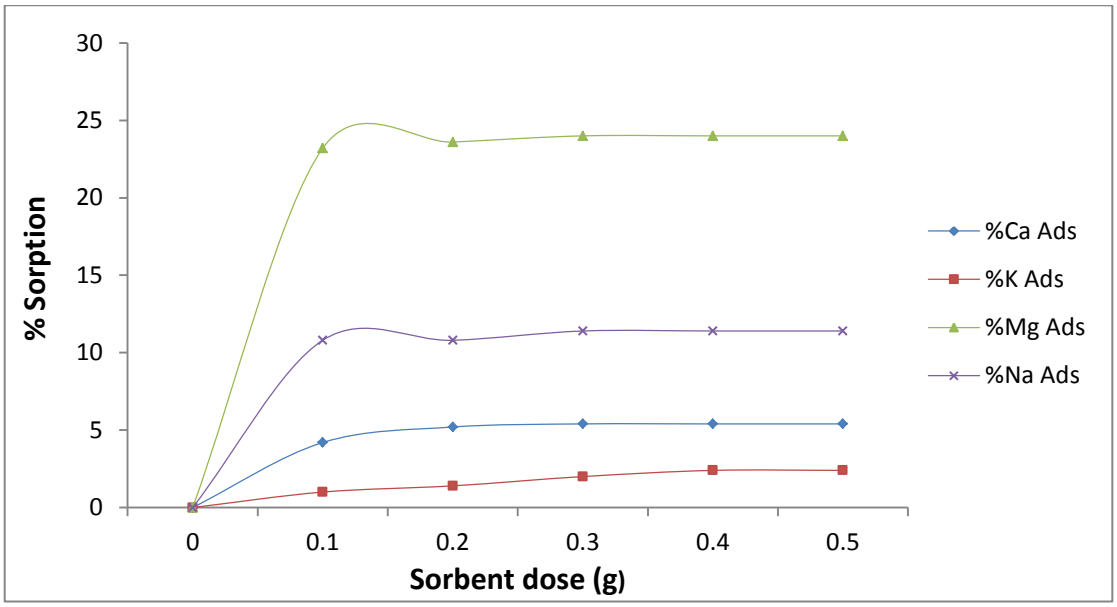

Figure 4.15: The percentage sorption of Mg^{2+}, Ca^{2+}, K^{+} and Na^{+} ions with PAN+TiO_2 nanofibres as a function of sorbent mass.
(Metal ion concentration, 500 mg/L; Temperature, 25 °C; volume, 25 mL; contact time 8 hours).

After the doping of PAN with TiO_2, the PAN+TiO_2 nanofibre when used for sorption showed a slight increase in the percentage of sorption of all the metal ions in solution compared to PAN nanofibres. Although there was a negligible increase in the sorption of metal ions when the various masses of the PAN+TiO_2 nanofibre were used in the sorbent dose experiments. This could be linked to exchange sites saturation, therefore, no sorption after a mass of 0.3 g sorbent.

PAN was also doped with zeolite and thereafter, it was used to carry out sorption for the individual metal ion solutions. It can be observed in Table 4.4 and Figure 4.16 that there was an increase in the percentage sorption of metal ions generally, compared with the PAN and PAN+TiO2 respectively. PAN+ZEOLITE showed an increased percentage sorption for both magnesium and calcium than what was obtained with PAN and PAN+TiO_2. The optimum sorbent dose for PAN+ZEOLITE nanofibre was found to be 8 g sorbent/L for the sorption of Mg^{2+}, Ca^{2+}, K^{+} and Na^{+} ions. Further increase in the sorbent dose showed no significant increase in the percentage of sorption.

Table 4.4: Effect of the sorption dose on the sorption of Mg^{2+}, Ca^{2+}, K^{+} and Na^{+} ions from individual solutions by PAN+ZEOLITE nanofibres.

PAN+ZEOLITE mass (g / 25 mL)	Mg^{2+} sorption (%)	Ca^{2+} sorption (%)	K^{+} sorption (%)	Na^{+} sorption (%)
0.1	24.4	6.4	0.4	5.6
0.2	25.0	7.0	0.6	5.8
0.3	25.0	7.6	1.4	6.0
0.4	25.2	8.8	1.4	6.2
0.5	25.2	8.4	1.4	6.2

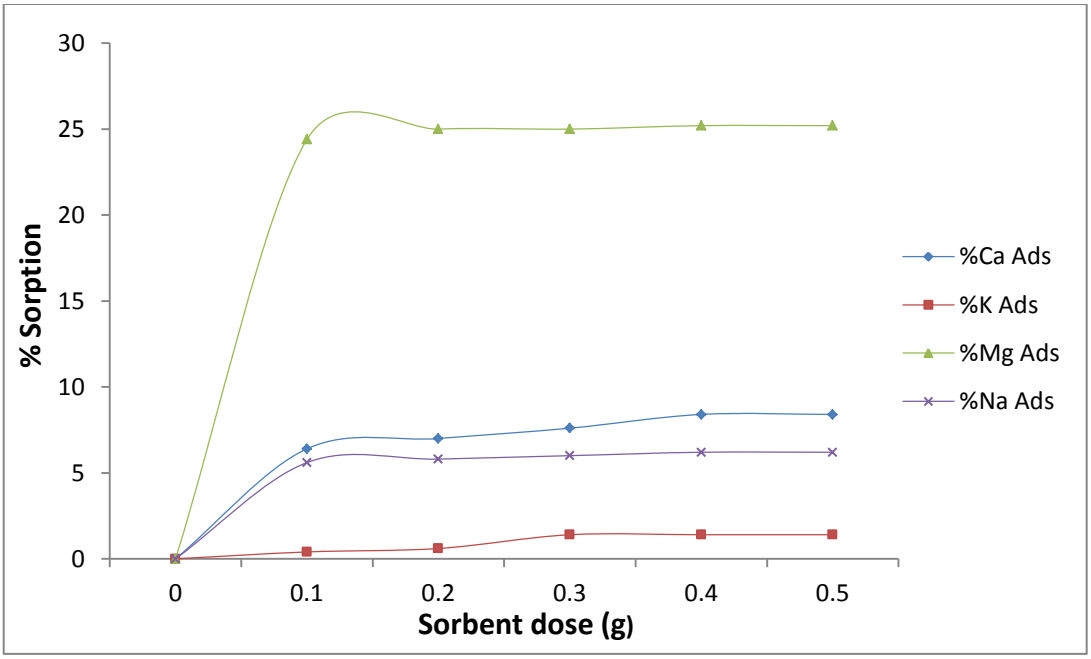

Figure 4.16: The percentage sorption of Mg^{2+}, Ca^{2+}, K^{+} and Na^{+} ions with PAN+ZEOLITE nanofibres as a function of sorbent mass.
(Metal ion concentration, 500 mg/L; Temperature, 25 °C; volume, 25 mL; contact time 8 hours).

4.2.2 The effect of contact time

The effect of contact time on sorption was investigated for each of the metal ions (Mg^{2+}, Ca^{2+}, K^+ and Na^+ ions) from their solutions which contained 100 mg/L metal ion concentration. The study was carried out by using Purolite S950 resin, and the nanofibres (PAN, PAN+TiO_2 and PAN+ZEOLITE). The sorbent masses (0.1 g) were added to 25 mL of the individual metal ion solutions at 25 $^{\circ}$C and subsequently shaken for 8 hours (see procedure in section 3.6.2).

Table 4.5 and Figure 4.17 show the quantity of sorption of each metal ion (Mg^{2+}, Ca^{2+}, K^+ and Na^+ ions) by Purolite S950 resin as a function of time. An increase in contact time from 60 to 120 minutes saw the sorption increase rapidly and that was just enough to reach the equilibrium. Further increase in time had no effect on the sorption of the metal ions. The optimum contact time of 120 minutes was enough for the sorption reaction by Purolite S950 to reach equilibrium. The quantities of calcium and magnesium sorbed from the solution were greater compared to potassium and sodium ions. The Purolite resin is more selective towards the divalent ions with 20.5 mg / g Ca^{2+}, 14.5 mg / g Mg^{2+}, 4.25 mg / g K^+ and 2 mg / g Na^+ respectively sorbed at equilibrium, these values correspond to 1.03 meq / g of calcium, 1.20 meq / g of magnesium, 0.11 meq / g of potassium and 0.09 meq / g of sodium.

In the case of PAN nanofibres, the optimum sorption contact time was 120 minutes to reach equilibrium in Table 4.6 and Figure 4.18. This results in the sorption of 1.45 mg / g, 1.25 mg / g, 1 mg / g and 0.45 mg / g of Mg^{2+}, Ca^{2+}, K^+ and Na^+ ions respectively which corresponds to the removal of the equilibrium amount of 0.12; 0.06; 0.03 and 0.02 meq / g respectively.

The PAN+TiO_2 nanofibre showed an improved performance towards potassium and sodium compared to that of PAN nanofibre. In Table 4.7 and Figure 4.19, the quantity sorbed at equilibrium for potassium and sodium are 1.75 mg / g and 3 mg / g respectively, compared to the 1.0 mg / g K^+ and 0.45 mg / g Na^+ achieved with PAN nanofibre.

Table 4.5: The effect of contact time on the sorption of Mg^{2+}, Ca^{2+}, K^{+} and Na^{+} ions from each model solution by Purolite S950 resin.

Time (mins)	Mg^{2+} sorbed (mg/g)	Ca^{2+} sorbed (mg/g)	K^{+} sorbed (mg/g)	Na^{+} sorbed (mg/g)
60	6.0	**7**	1.57	0.25
120	14.5	20.5	4.25	2
180	14.5	20.5	4.25	2
240	14.5	20.5	4.25	2
300	14.5	20.5	4.25	2
360	14.5	20.5	4.25	2
420	14.5	20.5	4.25	2
480	14.5	20.5	4.25	2

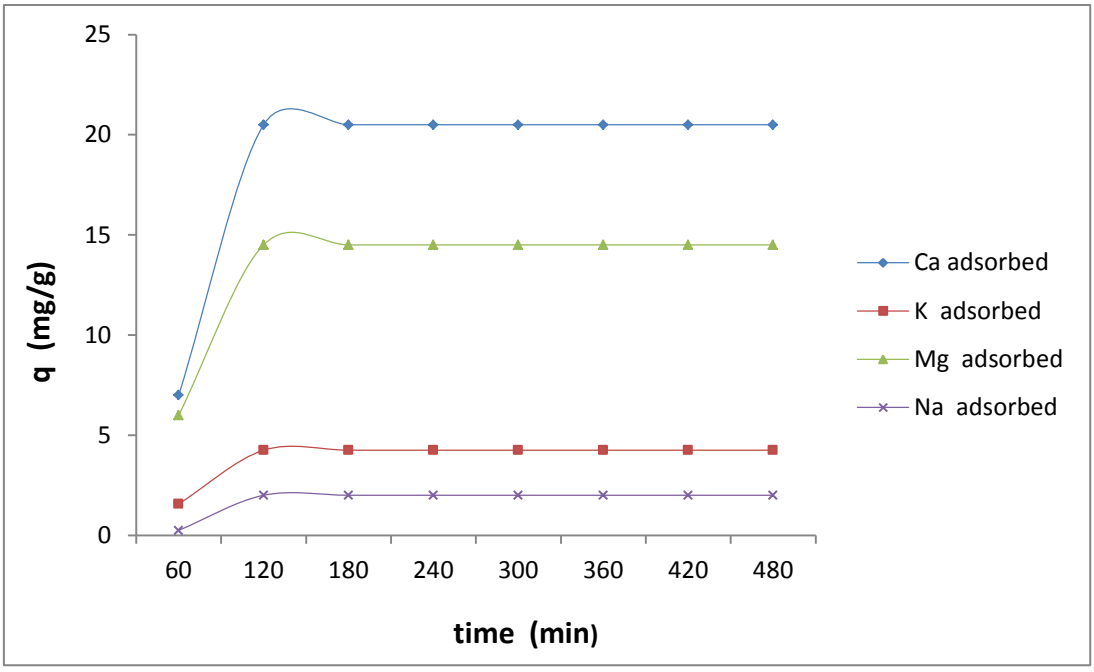

Figure 4.17: The effect of contact time on the sorption of Mg^{2+}, Ca^{2+}, K^{+} and Na^{+} ions from the individual model solutions by Purolite S950 resin
(Metal ion concentration, 500 mg/L; Resin mass, 0.1 g; Temperature, 25 ºC; Volume, 25 mL).

Table 4.6: The effect of contact time on the sorption of Mg^{2+}, Ca^{2+}, K^{+} and Na^{+} ions from each model solution by PAN nanofibre

Time (mins)	Mg^{2+} sorbed (mg/g)	Ca^{2+} sorbed (mg/g)	K^{+} sorbed (mg/g)	Na^{+} sorbed (mg/g)
60	0.75	0.5	0.25	0.15
120	1.45	1.25	1	0.45
180	1.45	1.25	1	0.45
240	1.45	1.25	1	0.45
300	1.45	1.25	1	0.45
360	1.45	1.25	1	0.45
420	1.45	1.25	1	0.45
480	1.45	1.25	1	0.45

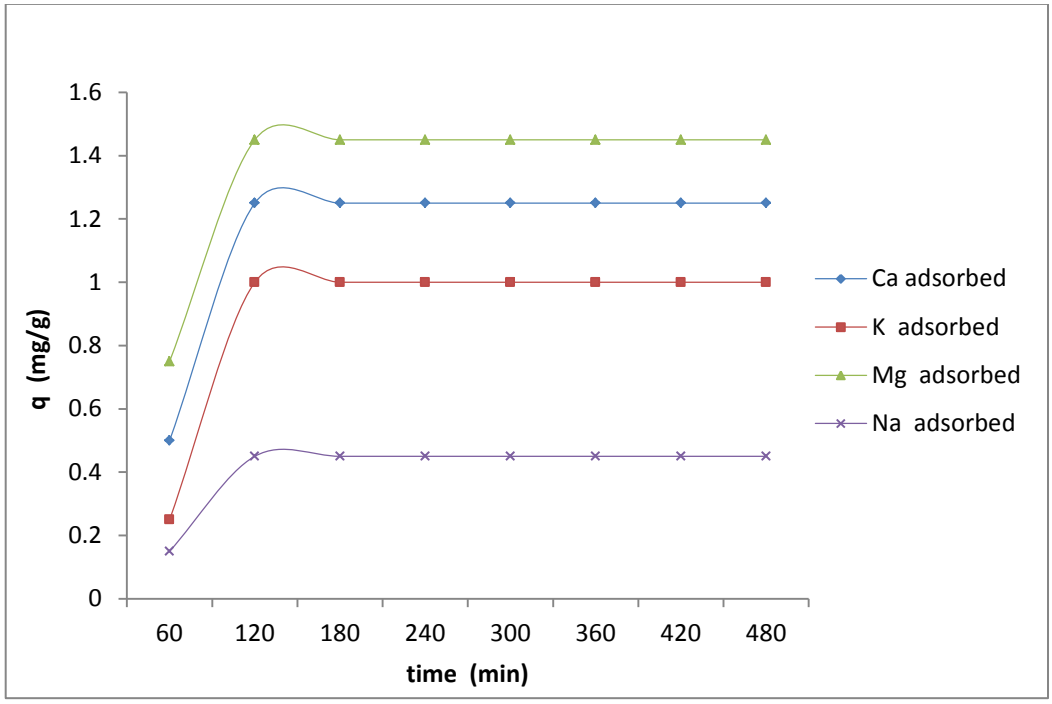

Figure 4.18: The effect of contact time on the sorption of Mg^{2+}, Ca^{2+}, K^{+} and Na^{+} ions from the individual model solutions by PAN nanofibres
(Metal ion concentration, 500 mg/L; Sorbent mass, 0.1 g; Temperature, 25 ºC; Volume, 25 mL)

Table 4.7: The effect of contact time on the sorption of Mg^{2+}, Ca^{2+}, K^{+} and Na^{+} ions from each model solution by PAN+TiO_2 nanofibres.

Time (mins)	Mg^{2+} sorbed (mg/g)	Ca^{2+} sorbed (mg/g)	K^{+} sorbed (mg/g)	Na^{+} sorbed (mg/g)
60	0.5	0.25	1.25	2.5
120	0.75	0.5	1.50	2.5
180	1.25	0.75	1.75	2.75
240	1.25	0.75	1.75	2.75
300	1.25	0.75	1.75	2.75
360	1.25	0.75	1.75	2.75
420	1.25	0.75	1.75	2.75
480	1.25	0.75	1.75	2.75

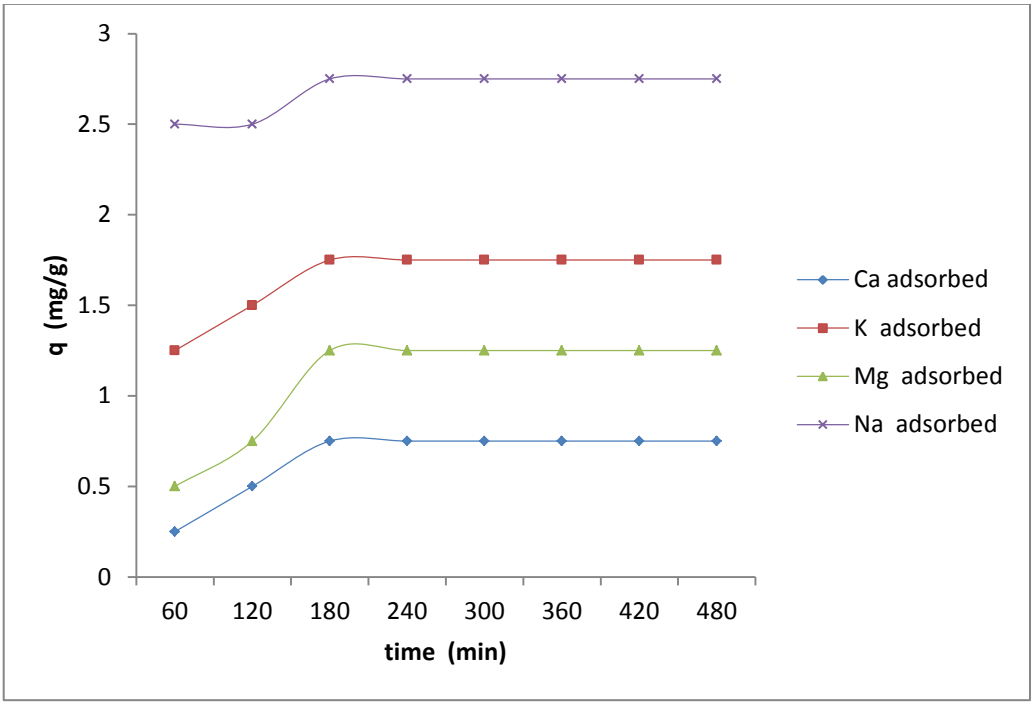

Figure 4.19: The effect of contact time on the sorption of Mg^{2+}, Ca^{2+}, K^{+} and Na^{+} ions from the individual model solution by PAN+TiO_2 nanofibre
(Metal ion concentration, 500 mg/L; Sorbent mass, 0.1 g; Temperature, 25 ºC; Volume, 25 mL)

Table 4.8: The effect of contact time on the sorption of Mg^{2+}, Ca^{2+}, K^{+} and Na^{+} ions from each model solution by PAN+ZEOLITE nanofibres.

Time (mins)	Mg^{2+} sorbed (mg/g)	Ca^{2+} sorbed (mg/g)	K^{+} sorbed (mg/g)	Na^{+} sorbed (mg/g)
60	0.75	0.5	1.0	0.75
120	1.25	1.0	1.25	0.75
180	1.75	1.25	1.25	0.75
240	2.5	1.75	1.25	0.75
300	2.5	1.75	1.25	0.75
360	2.5	1.75	1.25	0.75
420	2.5	1.75	1.25	0.75
480	2.5	1.75	1.25	0.75

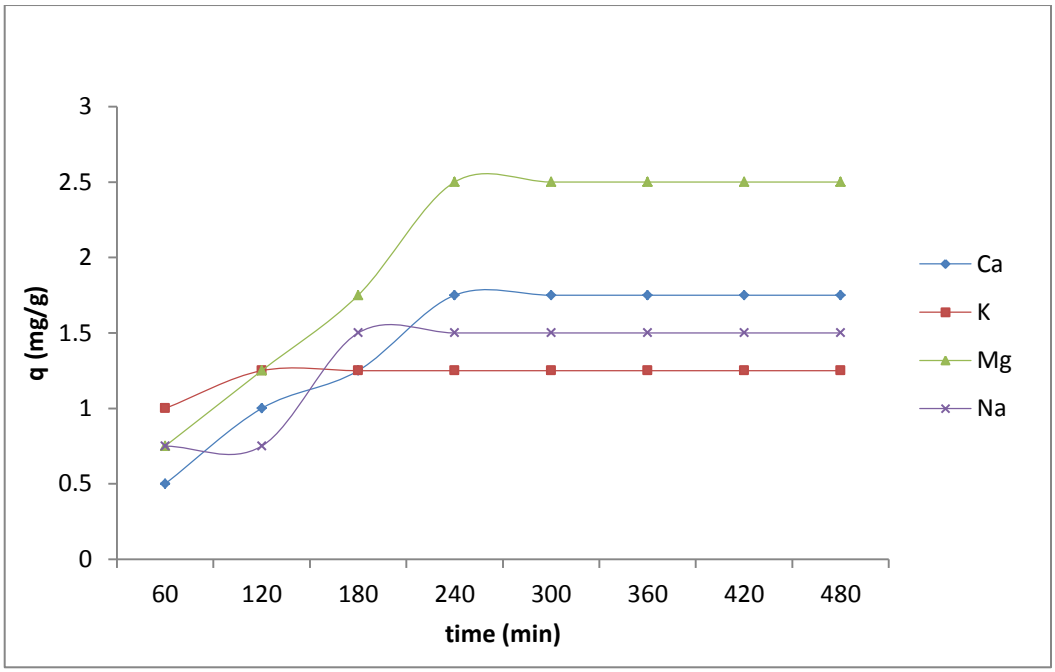

Figure 4.20: The effect of contact time on the sorption of Mg^{2+}, Ca^{2+}, K^{+} and Na^{+} ions from the individual model solutions by PAN+ZEOLITE nanofibres
(Metal ion concentration, 500 mg/L; Sorbent mass, 0.1 g; Temperature, 25 ºC; Volume, 25 mL)

In Table 4.8 and Figure 4.20, the sorption equilibria for Mg^{2+}, Ca^{2+}, K^{+} and Na^{+} ions by PAN+ZEOLITE nanofibres on the other hand was attained in 240 minutes for calcium and magnesium, 180 minutes for sodium and 120 minutes for potassium. This can be attributed to the rate at which the respective ions are binding onto the surface of the sorbent selectively, before reaching the equilibrium. The sorbed quantity of 2.5 mg/g, 1.75 mg/g, 1.25 mg/g and

1.5mg/g for Mg^{2+}, Ca^{2+}, K^{+} and Na^{+} ions respectively was achieved; corresponding to 0.21, 0.09, 0.03 and 0.07 meq/g ions respectively. PAN+ZEOLITE nanofibres were able to accomplish a greater quantity of sorption than both PAN and PAN+TiO_2 nanofibres except for potassium and sodium ions.

The rate of metal ion sorption is being governed by the kinetics, which is a vital feature that portrays how efficient the sorbent is. This is why the contact time needed to bring sorption process to completion is crucial, to give an insight into the process. At the same time, information is provided on the least time needed for reasonable sorption to occur as well as the mechanism for diffusion control between metal ions in moving from the solution towards the surface of the sorption or the pore matrix of the resin (Rengaraj et al., 2001).

Table 4.9: Cation exchange capacities of Purolite S950 resin, PAN, PAN+TiO_2 and PAN+ZEOLITE obtained in the contact time experiment

SORBENT	Mg^{2+} (meq/g)	Ca^{2+} (meq/g)	K^{+}(meq/g)	Na^{+} (meq/g)
Purolite resin	1.20	1.03	0.11	0.09
PAN	0.12	0.06	0.03	0.02
PAN+TiO_2	0.10	0.04	0.05	0.12
PAN+ZEOLITE	0.21	0.09	0.03	0.07

The summary of the various exchange capacities of the sorbents is given in Table 4.9. The Purolite S950 resin achieved the highest capacity owing to the aminophosphonic group attached to it. Its high sorption rate can be attributed to chelation of the ions by the aminophosphonic acid functional groups on the resin. The values for the cation exchange capacities were obtained after 120 minutes for the Purolite resin, 240 minutes for PAN+ZEOLITE, 180 minutes for PAN+TiO_2 and 120 for PAN nanofibres respectively. Therefore, the overall order of increasing capacity is PAN < PAN+TiO_2 < PAN+ZEOLITE < Purolite S950 resin. The Purolite resin was able to attain the highest capacity within 120 minutes because of the aminophosphonic group attached to its surface, whereby the metal ions were able to bind easily and faster. For the nanofibres, PAN+ZEOLITE achieved the greater capacity within 240 minutes for both magnesium and calcium, 180 minutes for sodium

and 120 minutes for potassium. This increase in time can be attributed to the mild blockage of the binding sites which makes it difficult for the metal ions to exchange into the sorbent rapidly, and of course, lack of a ligand to aid in sorption. PAN+ZEOLITE also shows selectivity for calcium and magnesium. PAN+TiO_2 nanofibre showed very little improvement compared to PAN itself except for sodium and was able to attain sorption equilibrium at 180 minutes and shows selectivity for sodium probably due to the changes in the physical structure as a result of titanium dioxide incorporation. PAN nanofibre attained sorption equilibrium at 120 minutes for all metal ions; this is due to the accessibility of the metal ions to the available binding sites without any blockage of other inorganic materials.

4.2.3 Effect of initial concentration

The initial concentration of the metal ion solutions (Mg^{2+}, Ca^{2+}, K^{+} and Na^{+} sorbates) was varied from 100 – 500 mg/L for the investigation of the sorption isotherms and the assessment of the sorption efficiency of the various sorptions (Purolite S950 resin, PAN, PAN+TiO_2 and PAN+ZEOLITE). The sorption conditions (temperature and the stirring speed) were kept constant while the optimal values of the contact time, pH and the masses of the sorbents were applied. The sorption isotherm equations of Langmuir and Freundlich models were subsequently applied for the modelling of the equilibrium data.

Figure 4.21 shows that the sorption equilibrium isotherm of Purolite S950 resin depicts that the equilibrium concentration is also directly proportional to the sorption capacity from 100 mg/L to 500 mg/L. The quantity of sorption increases gradually with the increase in the concentration of the solution. The resin showed an affinity for the divalent ions compared to the other cations. This is evident in the quantities of sorption shown towards the respective cations, while calcium and magnesium ions are still being sorbed from the solution at 28.25 and 31.25 mg/g quantities of sorption respectively, at the maximum sorbate concentration (500 mg/L), the other ions are already flattening out. Also, the Purolite resin has the highest capacity of sorption for calcium and magnesium compared to other sorptions. This can be attributed to the functional groups attached to the surface of the Purolite S950 resin, aiding a more favourable sorption.

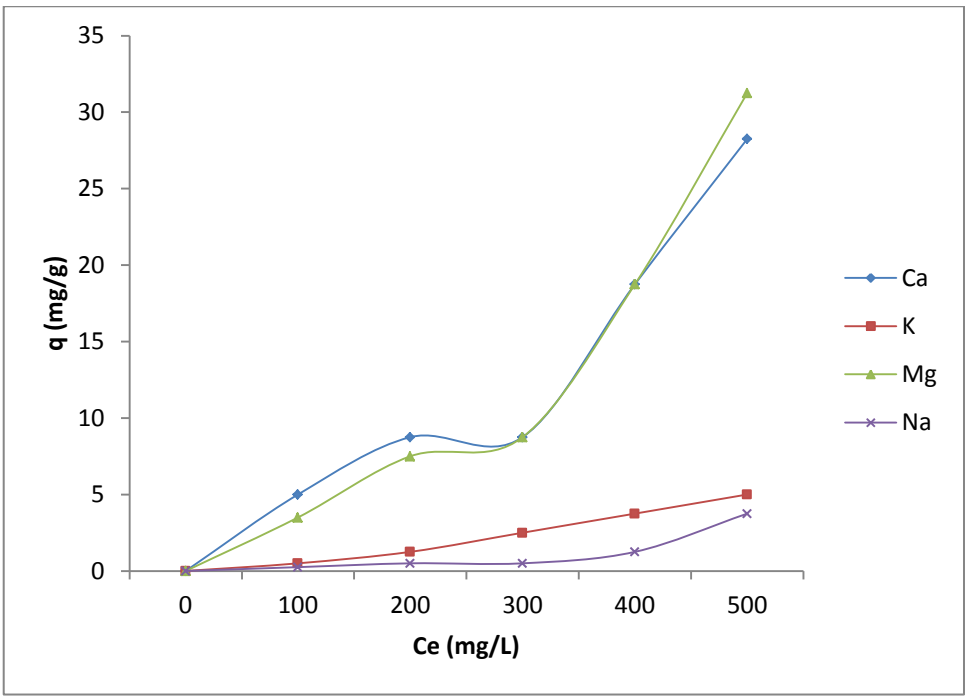

Figure 4.21: The equilibrium isotherm of Resin for the sorption of Mg^{2+}, Ca^{2+}, K^{+} and Na^{+} ions at increasing sorbate concentrations
(Sorbent mass, 0.1 g; Temperature, 25 ºC; Volume, 25 mL; Time, 60 mins)

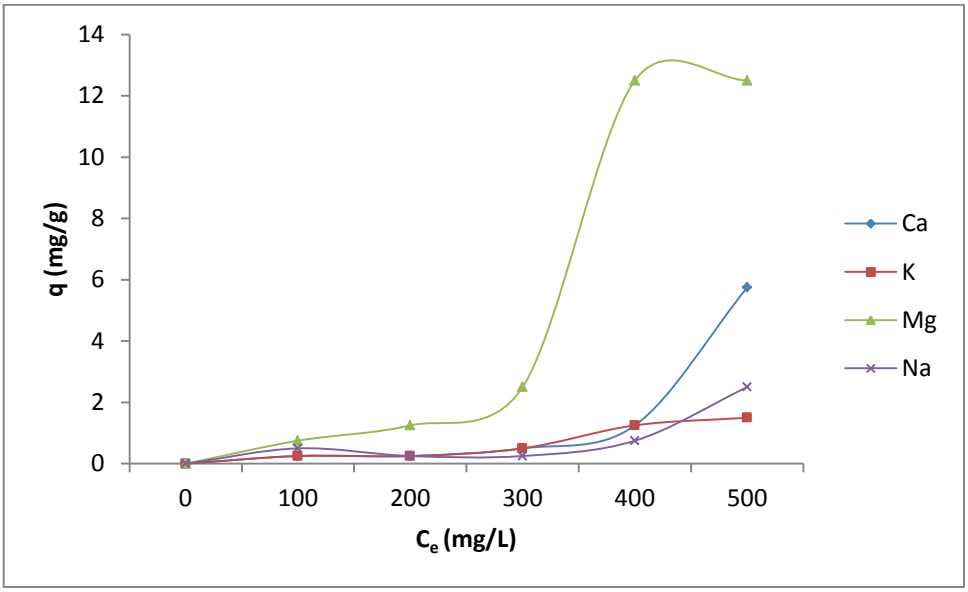

Figure 4.22: The equilibrium isotherm of PAN nanofibres for the sorption of Mg^{2+}, Ca^{2+}, K^{+} and Na^{+} ions at increasing sorbate concentration
(Sorbent mass, 0.1 g; Temperature, 25 ºC; Volume, 25 mL; Time, 60 mins)

In Figure 4.22, the result for the removal of Mg^{2+}, Ca^{2+}, K^{+} and Na^{+} ions at increasing concentrations using 0.1 g of PAN nanofibre shows that the equilibrium concentration is directly proportional to the sorption capacity from 100 mg/L to 500 mg/L. Both magnesium

and potassium ions already flattened out at 400 mg/L due to saturation of available sorption sites on the surfaces of the PAN nanofibres.

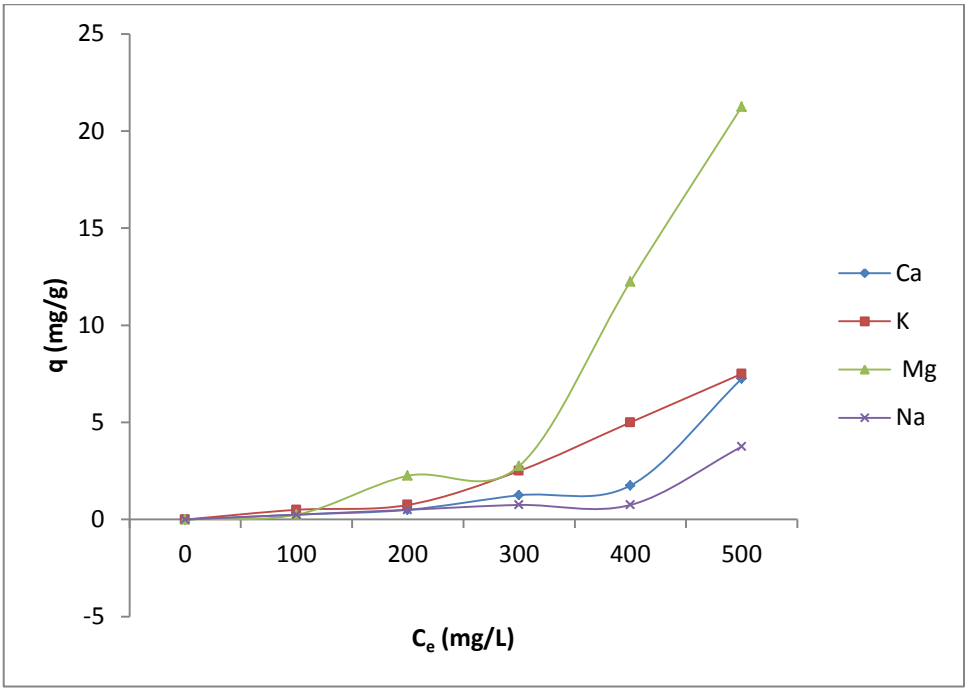

Figure 4.23: The equilibrium isotherm of PAN+TiO_2 nanofibres for the sorption of Mg^{2+}, Ca^{2+}, K^+ and Na^+ ions at increasing sorbate concentrations
(Sorbent mass, 0.1 g; Temperature, 25 ºC; Volume, 25 mL; Time, 60 mins)

For PAN+TiO_2 nanofibres, the efficiency of removal of Mg^{2+}, Ca^{2+}, K^+ and Na^+ ions at increasing sorbate concentration is presented in Figure 4.23. The sorption of Mg^{2+}, Ca^{2+}, K^+ and Na^+ ions increased with increasing concentration. At the initial stage of the sorption process, the sorption onto PAN+TiO_2 nanofibre was fairly constant from 100 – 300 mg/L for all the metal ions. Thereafter, there was a significant increase in the quantity of sorption. The sorption equilibrium isotherm for PAN+TiO_2 nanofibres also shows that the equilibrium concentration is directly proportional to the capacity of sorption.

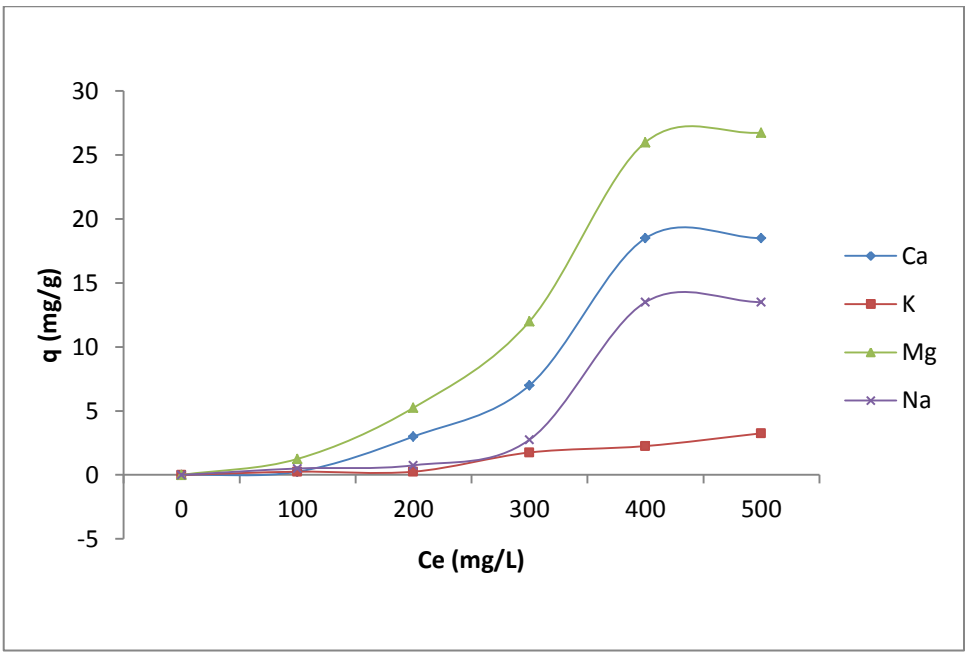

Figure 4.24: The equilibrium isotherm of PAN+ZEOLITE nanofibres for the sorption of Mg^{2+}, Ca^{2+}, K^{+} and Na^{+} ions at increasing sorbate concentrations
(Sorbent mass, 0.1 g; Temperature, 25 ºC; Volume, 25 mL; Time, 60 mins)

In the case of PAN+ZEOLITE nanofibres, Figure 4.24 shows the sorption equilibrium isotherm of PAN+ZEOLITE nanofibres and depicts that the equilibrium concentration is directly proportional to the sorption capacity as the sorbate concentration increased up to 400 mg/L. This suggests that there is an increase in the driving force due to the increase in the concentration gradient between the surface of the PAN+ZEOLITE nanofibres and the metal ion solution. The quantity of sorption increases gradually with the increasing concentration of the solution until it flattens out due to saturation of the active sites on the sorbent surface. Generally, PAN+ZEOLITE nanofibres show an improved sorption for all metal ions as the concentration of the solution increases compared to its performance at a lower concentration of metal ion solution.

4.2.3.1 Sorption Equilibrium Isotherm

The Langmuir and Freundlich model equations were applied to the sorption isotherm study of the metal ion solutions involving calcium, magnesium, potassium and sodium. In the Langmuir model, it is assumed that the uptake of metal ions occurs on a homogenous surface by monolayer sorption without any interaction between the ions sorbed. This model is expressed in the linearized form given as follows (Deng et al., 2003):

$$\frac{1}{q} = \left[\left(\frac{1}{k_1 q_m}\right)\left(\frac{1}{C_e}\right)\right] + \left[\frac{1}{q_m}\right] \quad (4.1)$$

Where q is the amount sorbed on the resin at equilibrium (mg/g), C_e is the equilibrium concentration of the sorbate (mg/L), and K_L is equilibrium constant related to the affinity of the binding sites for the metals or the Langmuir constant. q_m is the resin capacity (maximum possible amount of metallic ion sorbed per unit mass of sorption). Langmuir theory suggests that sorption takes place at specific homogenous sites within the sorption. It is then assumed that when a metal ion occupies a site, there cannot be any further sorption taking place at that site.

Whereas, in the Freundlich model, it is assumed that the uptake or sorption of metal ions takes place on a heterogeneous surface through monolayer sorption. Equation (4.2) describes the Freundlich model:

$$q = k_f (C_e)^{\frac{1}{n}} \quad (4.2)$$

$$lnq_e = \left(\frac{1}{n}\right) lnC_e + lnk_f \quad (4.3)$$

Where q_e is the amount sorbed (mg/g), C_e is the equilibrium concentration of the sorbate (mg/L), k_f ((mg/g)*(mg/L)^n) and n are the Freundlich constants related to sorption capacity and sorption intensity, respectively (Freundlich, 1926).

Here, the results of the sorption of calcium and magnesium ions by PAN+ZEOLITE and PAN+TiO_2 nanofibres were used to describe the sorption equilibrium isotherm and its modelling by the use of Freundlich and Langmuir models. The result of the isotherm parameters for the sorption of the metal ions (Mg^{2+}, Ca^{2+}, K^+ and Na^+) on the Purolite S950 resin and the nanofibres are given in Table 4.10 and the graphs are given in the Appendix 7.1.

Table 4.10: The isotherm parameters for sorption of Mg^{2+}, Ca^{2+}, K^+ and Na^+ ions onto Purolite S950 resin and the respective nanofibres.

Sorbent	Solution Conc (100 mg/L)	Freundlich Isotherms			Langmuir Isotherms		
		n	k_f	R^2	q_m	k_L	R^2
Purolite S950 resin	Mg^{2+}	1.464	0.829	0.96	181.8	0.0013	0.9904
PAN		1.279	0.511	0.9025	28.16	0.011	0.9799
PAN+TiO_2		1.263	0.469	0.8714	5.98	0.047	0.9466
PAN+ZEOLITE		1.362	0.665	0.9289	84.75	0.002	0.9756
Purolite S950 resin	Ca^{2+}	1.562	0.928	0.9786	136.98	0.0019	0.9909
PAN		1.187	0.363	0.8013	2.096	0.146	0.9797
PAN+TiO_2		1.259	0.409	0.8127	26.25	0.009	0.9926
PAN+ZEOLITE		1.224	0.478	0.909	12.36	0.023	0.9928
Purolite S950 resin	K^+	1.52	0.567	0.7931	29.24	0.009	0.9863
PAN		1.372	0.379	0.5793	4.179	0.068	0.9692
PAN+TiO_2		1.258	0.44	0.86	6.418	0.042	0.8676
PAN+ZEOLITE		1.252	0.395	0.7919	7.097	0.047	0.8675
Purolite S950 resin	Na^+	1.318	0.396	0.7101	3.476	0.079	0.9664
PAN		1.291	0.367	0.6445	11.24	0.025	0.9396
PAN+TiO_2		2.899	2.076	0.1257	25.51	0.01	0.9997
PAN+ZEOLITE		1.294	0.479	0.8535	28.49	0.009	0.9966

The linearized fitting curves for PAN+TiO_2 nanofibre sorption of Ca^{2+} and Mg^{2+} ions are given for Freundlich and Langmuir models in Figures 4.25, 4.26, 4.27 and 4.28 respectively.

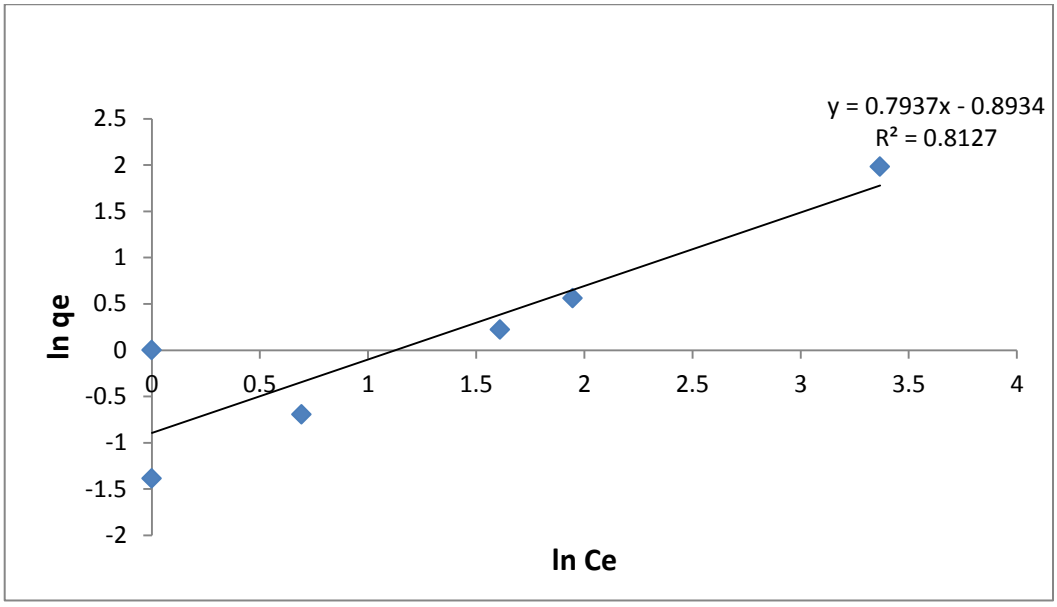

Figure 4.25: Linearized form of Freundlich model of PAN+TiO_2 nanofibre for the sorption of Ca^{2+} ions.

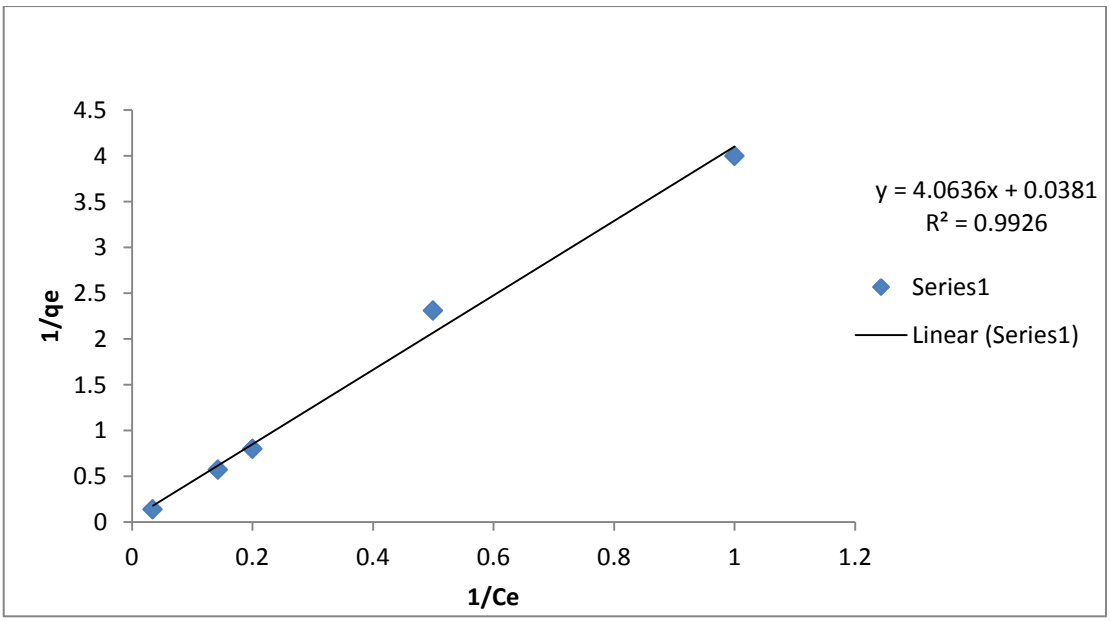

Figure 4.26: Linearized form of Langmuir model of PAN+TiO_2 nanofibre for the sorption of Ca^{2+} ions.

It is evident from the linear plots of ln q_e against ln C_e that Ca^{2+} ion sorption agrees with the Freundlich sorption isotherms. The same applies to the plots of $1/q_e$ against $1/C_e$ showing an agreement with the Langmuir sorption isotherm, but by comparing the correlation coefficient

values (R^2 values), Langmuir has a higher R^2 value which indicates that the Ca^{2+} ion sorption by PAN+TiO_2 nanofibre gives a better fit for the Langmuir isotherm model than Freundlich isotherm model. For the sorption of Ca^{2+} ions onto PAN+TiO_2 nanofibres, the correlation coefficients for the linear regression fit of Freundlich and Langmuir models are 0.8127 and 0.9926 respectively (Figures 4.25 and 4.26). This shows that PAN+TiO_2 nanofibre exhibits a better fit for the Langmuir model than Freundlich. The greater value of correlation coefficient for the Langmuir model over the Freundlich suggests that the sorption process was monolayer.

This means that the surface of the sorbent offers a homogeneous sorption process. Also, the evaluated values of the dimensionless separation parameter K_L for the PAN+TiO_2 nanofibre's sorption of the metal ions from the solution fall within the range 0 – 1, pointing to a favourable sorption. Subsequently, the values obtained for 'n' in the sorption study range within 1 – 10 which indicates a favourable sorption (Singh et al., 1998).

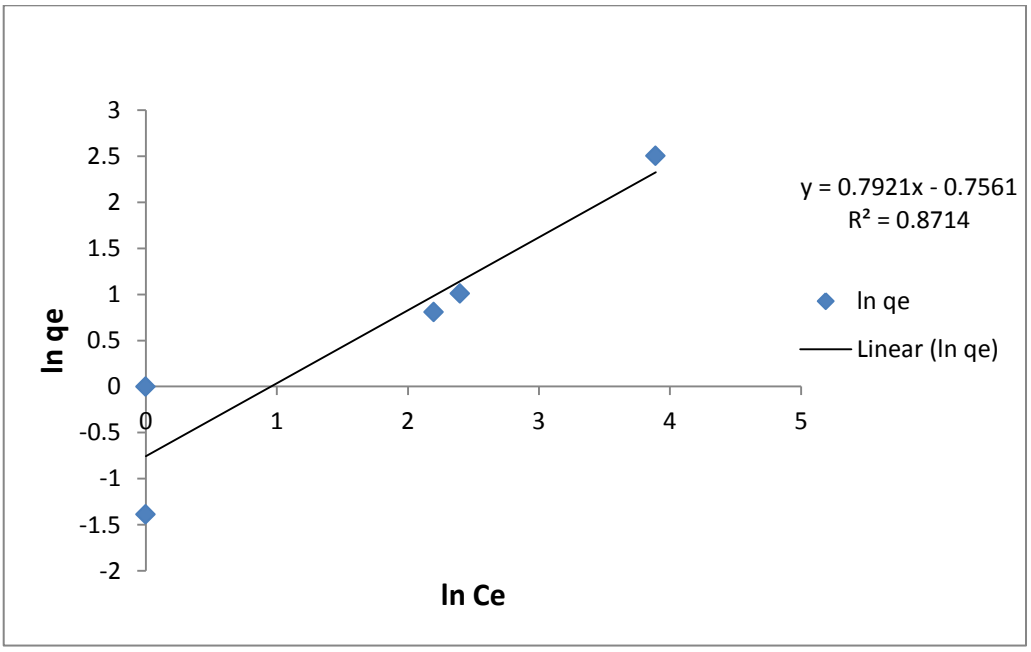

Figure 4.27: Linearized form of Freundlich model of PAN+TiO_2 nanofibre for the sorption of Mg^{2+} ions.

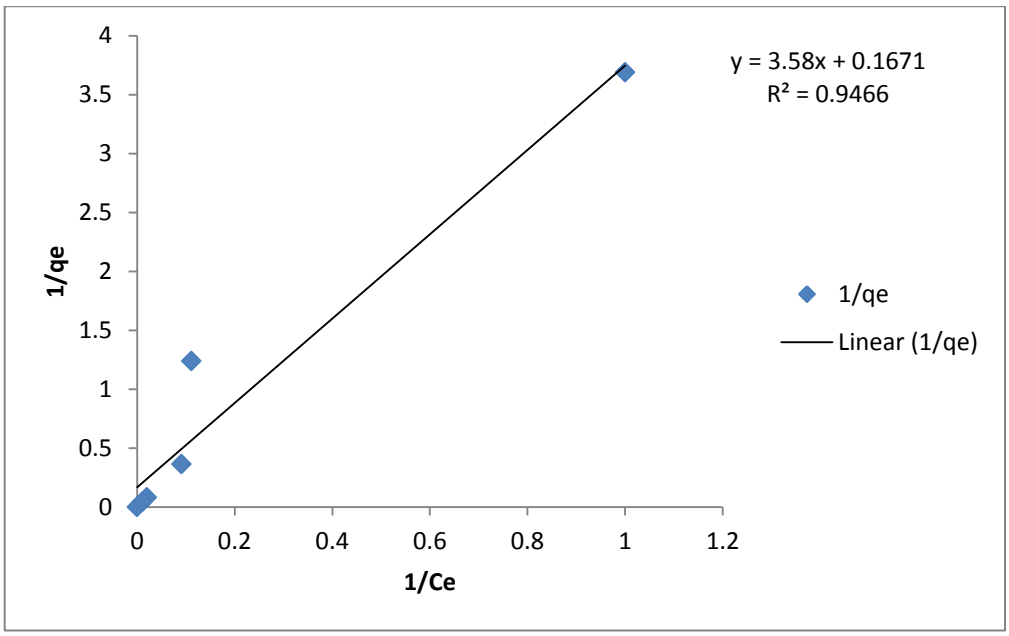

Figure 4.28: Linearized form of Langmuir model of PAN+TiO_2 nanofibre for the sorption of Mg^{2+} ions.

The sorption of Mg^{2+} ions onto the PAN+TiO_2 nanofibres can be described as monolayer. The correlation coefficients (R^2 values) for both Freundlich and Langmuir models (Figures 4.27 and 4.28) are 0.8714 and 0.9466 respectively, the greater R^2 value for Langmuir shows a better fit for Langmuir model over the Freundlich model. Also, the values of the dimensionless separation parameter K_L ranging 0 – 1 also signifies a favourable sorption.

The linearized fitting curves for PAN+ZEOLITE nanofibre sorption of Ca^{2+} and Mg^{2+} ions are given for Freundlich and Langmuir models in the Figures 4.29, 4.30, 4.31 and 4.32 respectively.

The correlation coefficients for the linear regression fit of Freundlich and Langmuir isotherm models were found to be 0.909 and 0.9928 for the sorption of Ca^{2+} ions onto PAN+ZEOLITE nanofibres (Figures 4.29 and 4.30), respectively. The sorption of Ca^{2+} ions onto the PAN+ZEOLITE nanofibres can be described as monolayer; this is because PAN+ZEOLITE showed a better fit for the Langmuir model than the Freundlich model by virtue of the greater R2 value. This is also due to the changes in the surface sorption properties in the binding of ions on the inner and outer surfaces, which becomes intense at higher initial concentrations, resulting in reduced number of available surface sites for ion exchange (Ndlovu-Yalala, 2010). The results show that the Langmuir isotherm model fitted the result so well, thereby suggesting a homogenous surface of the sorbent. The same explanation also applies to the sorption of Mg^{2+} ions onto PAN+ZEOLITE nanofibres.

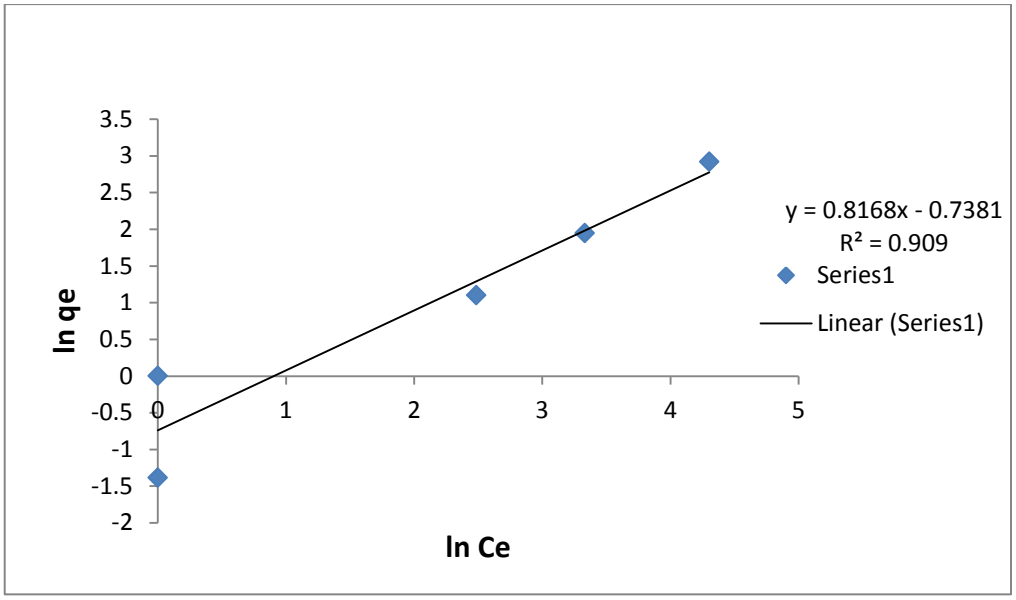

Figure 4.29: Linearized form of Freundlich model of PAN+ZEOLITE nanofibre for the sorption of Ca^{2+} ions.

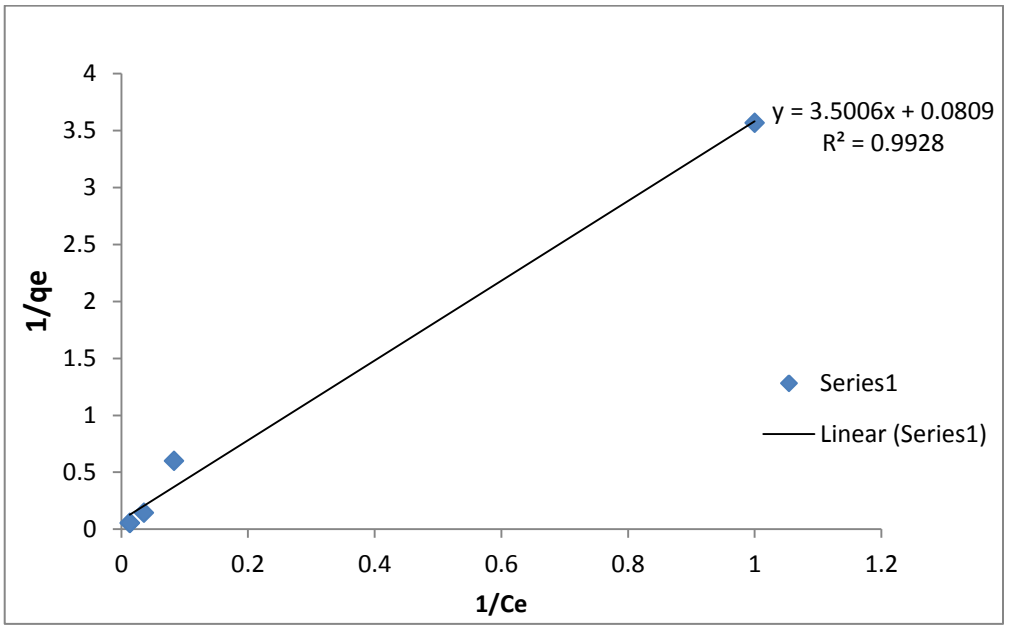

Figure 4.30: Linearized form of Langmuir model of PAN+ZEOLITE nanofibre for the sorption of Ca^{2+} ions.

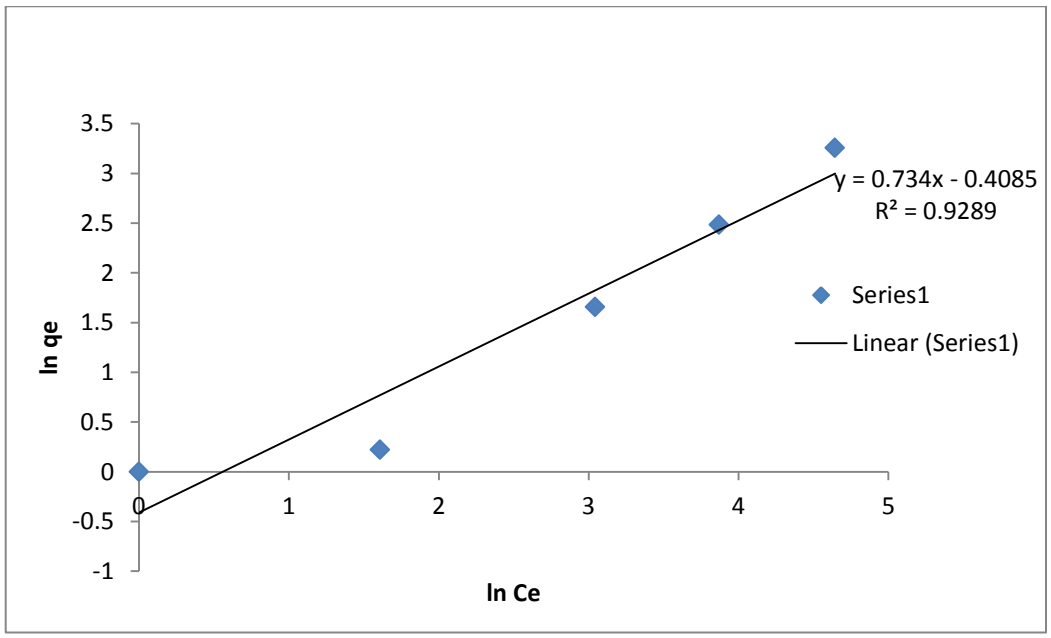

Figure 4.31: Linearized form of Freundlich model of PAN+ZEOLITE nanofibre for the sorption of Mg^{2+} ions.

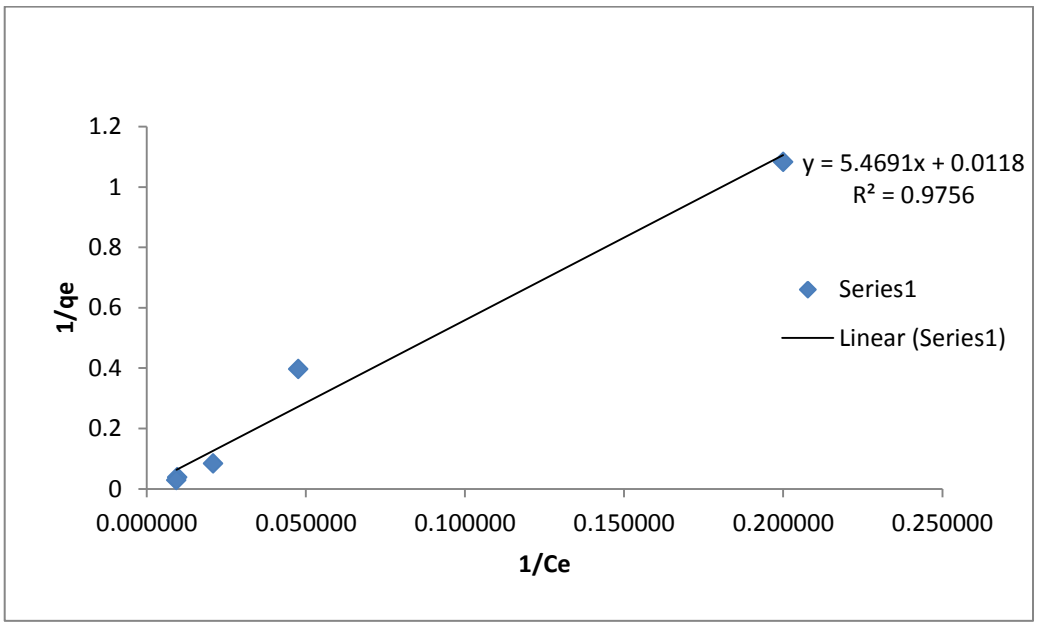

Figure 4.32: Linearized form of Langmuir model of PAN+ZEOLITE nanofibre for the sorption of Mg^{2+} ions.

The detailed data for the comparison of the Freundlich and Langmuir parameters for calcium, magnesium, sodium and potassium ions sorption equilibrium by the Purolite S950 resin, PAN, PAN+TiO_2 and PAN+ZEOLITE nanofibres are given in Table 4.10.

The correlation coefficient values (R^2 values) in Table 4.10 show that the Langmuir sorption isotherm offers a good model of sorption system. The Langmuir sorption constant, K_L, for calcium is higher than those for magnesium, potassium and sodium, while the sorption capacity, q_m, of magnesium is higher than that of calcium, potassium and sodium. Also, the maximum sorption capacity (mg/g) of the Purolite S950 resin is higher than those of the respective nanofibres. This is due to the functional groups attached to the surface of the resin polymer.

4.2.4 Effect of pH

The pH studies were carried out in accordance to the procedure presented in section 3.6.5, in the investigation of the effect of pH on the sorption of metal ions (Mg^{2+}, Ca^{2+}, K^+ and Na^+) from the bulk solution which contained 500 mg/L of Mg^{2+}, Ca^{2+}, K^+ and Na^+ ions with a fixed amount of the resin and the nanofibres (PAN, PAN+TiO_2 and PAN+ZEOLITE). The pH of the metal ion solutions was adjusted to the desired values using 0.1 mol/L acetic acid and 0.05 mol/L sodium hydroxide solutions. The experiment was separately conducted by shaking each of the metal ion solutions with 0.1 g of the respective sorbents for 8 hours at 25 ºC (see section 3.6.5 for the procedure). The determination of the quantity of sorption of Mg^{2+}, Ca^{2+}, K^+ and Na^+ ions separately from the aqueous solution by the Purolite S950 resin and the nanofibres (PAN, PAN+TiO_2 and PAN+ZEOLITE) was carried out as described in section 3.6.5. Table 4.11 shows that the pH does not play any significant role in the sorption of these metal ions. It can therefore be inferred from the results that the metal ion uptake is basically through the mechanism of ion exchange.

Table 4.11: The effect of pH on the sorption of Mg^{2+}, Ca^{2+}, K^{+} and Na^{+} ions by PAN nanofibre

pH	Mg^{2+} sorption (mg/g)	Ca^{2+} sorption (mg/g)	K^{+} sorption (mg/g)	Na^{+} sorption (mg/g)
2	27.00	10.25	3.75	7.25
3	27.00	10.13	3.88	7.25
4	27.50	10.00	3.95	7.75
5	28.25	10.75	4.00	7.75
6	28.75	10.75	4.13	7.76
7	28.50	11.00	4.13	7.78

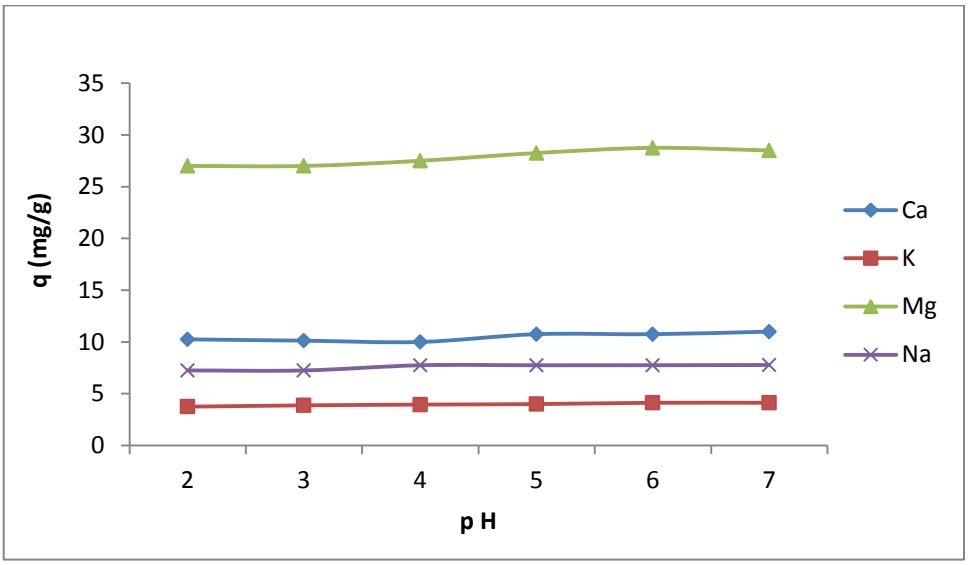

Figure 4.33: The effect of pH on the sorption of Mg^{2+}, Ca^{2+}, K^{+} and Na^{+} ions by PAN nanofibre.
(Sorbent mass, 0.1 g; temperature, 25 °C; volume, 25 mL, contact time, 8 hrs).

In Table 4.11 and Figure 4.33; Table 4.12 and Figure 4.34; Table 4.13 and Figure 4.35, it is evident from the results that the effect of pH does not play any significant role in the metal ions uptake. The optimum sorption was achieved between the pH values 5 and 6.

Table 4.12: The effect of pH on the sorption of Mg^{2+}, Ca^{2+}, K^{+} and Na^{+} ions by PAN+TiO_2 nanofibre.

pH	Mg^{2+} sorption (mg/g)	Ca^{2+} sorption (mg/g)	K^{+} sorption (mg/g)	Na^{+} sorption (mg/g)
2	28.00	5.75	2.00	12.75
3	27.50	6.75	2.50	12.50
4	27.00	6.80	2.00	11.75
5	28.25	7.00	1.25	12.50
6	28.75	7.25	1.75	13.00
7	28.75	7.50	1.93	12.75

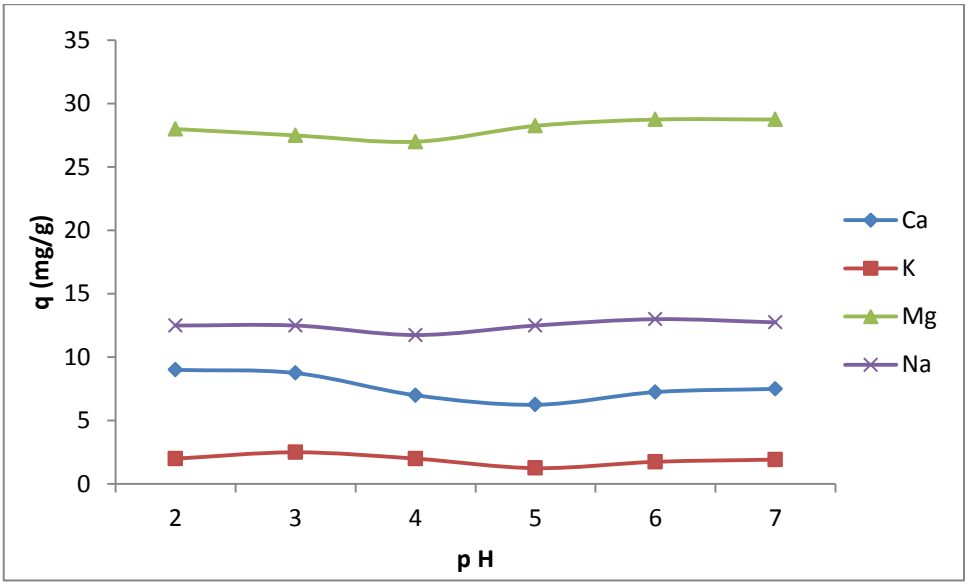

Figure 4.34: The effect of pH on the sorption of Mg^{2+}, Ca^{2+}, K^{+} and Na^{+} ions by PAN+TiO_2 nanofibre.
(Sorbent mass, 0.1 g; temperature, 25 °C; volume, 25 mL, contact time, 8 hrs).

Table 4.13: The effect of pH on the sorption of Mg^{2+}, Ca^{2+}, K^{+} and Na^{+} ions by PAN+ZEOLITE nanofibre.

pH	Mg^{2+} sorption (mg/g)	Ca^{2+} sorption (mg/g)	K^{+} sorption (mg/g)	Na^{+} sorption (mg/g)
2	30.00	12.75	3.25	4.50
3	30.10	13.00	3.5	5.25
4	29.25	12.81	2.75	5.25
5	29.75	13.00	2.88	5.34
6	29.75	13.25	3.00	5.48
7	30.05	13.75	3.00	5.75

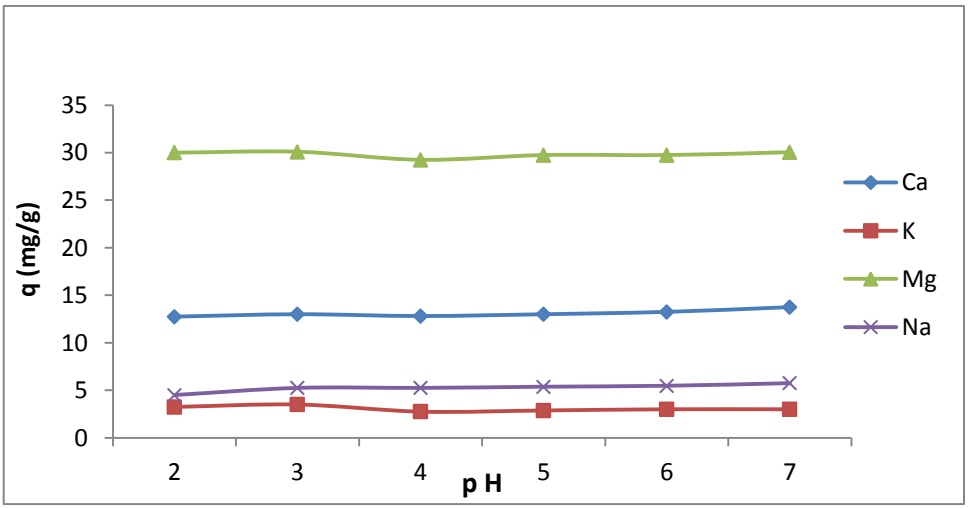

Figure 4.35: Effect of pH on the sorption of Mg^{2+}, Ca^{2+}, K^{+} and Na^{+} ions by PAN+ZEOLITE nanofibre.
(Sorbent mass, 0.1 g; temperature, 25 °C; volume, 25 mL, contact time, 8 hrs).

Table 4.14: The effect of pH on the sorption of Mg^{2+}, Ca^{2+}, K^{+} and Na^{+} ions by Purolite S950 resin.

pH	Mg^{2+} sorption (mg/g)	Ca^{2+} sorption (mg/g)	K^{+} sorption (mg/g)	Na^{+} sorption (mg/g)
2	32.50	22.50	3.75	16.25
3	35.50	23.25	4.00	19.50
4	35.75	23.50	5.00	16.00
5	36.25	23.75	5.50	19.75
6	36.35	23.75	5.50	19.75
7	35.00	23.56	5.25	18.75

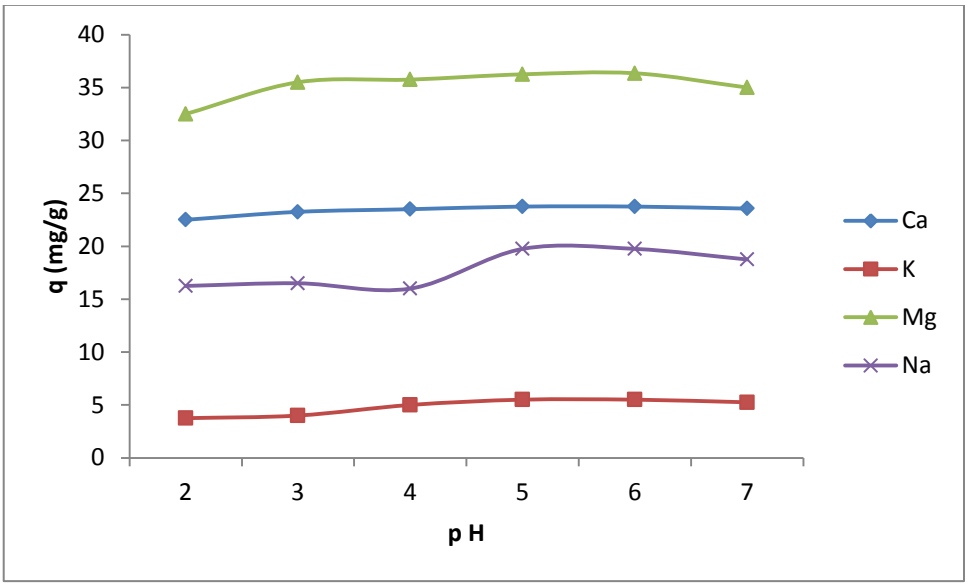

Figure 4.36: Effect of pH on the sorption of Mg^{2+}, Ca^{2+}, K^{+} and Na^{+} ions by Purolite S950 resin.
(Sorbent mass, 0.1 g; temperature, 25 °C; volume, 25 mL, contact time, 8 hrs).

In Table 4.14 and Figure 4.36, it can be seen that the degree of sorption was almost constant throughout the sorption process, but critically, the optimal uptake of metal ions takes place between the pH values of 4 and 6. At the pH of 7, there is a slight decline in the sorption quantities of the respective metal ions. These results are consistent with those reported by Alyuz & Veli, (2009), where ion exchange resins were used for the sorption of metals at pH values between 2 and 9.

In the investigation of the effect of pH on sorption, a major parameter that influences the ion-exchange process is the hydronium ion concentration. This is as a result of the hydrogen ions being part of the sorbate and strongly competing with other metals in the solution. Therefore, the pH of the solution affects the surface ionization of the functional groups and subsequently influences the sorption process (Alyuz & Veli, 2009).

At high pH values, the decline experienced in the quantity of sorption by resins is explained by the formation of metal hydroxides during the reaction of the respective metal ions with the hydroxide ions ($0H^-$) in the solution. In this situation, hydrolysis may occur and at the same time accompanied by metal hydroxide precipitation (Veli & Pekey, 2004). However, at very low pH values, the sorbent's surface is enveloped by the hydronium ions (H^+), which prevent the metal ions from reaching the binding sites of the sorbent (Wong *et al.,* 2003). It was found out in these experiments that the optimal uptake of the metal ions was realized at the pH values between 4 and 6 which justifies a higher pH value favourable for sorption.

Consequently, under highly acidic conditions (pH < 2), metal ion uptake is reduced. This is as a result of competition from the hydrogen ions. Alyuz & Veli, (2009), were able to achieve maximum sorption of Zn^{2+} and Ni^{2+} ions at a pH of between 5 and 6.

4.2.5 Sorption Kinetics

The sorption kinetics is used to describe the rate of metal ion uptake by the sorption process, the rate also leads to the determination of the equilibrium time. The procedure for investigating the sorption kinetics is shown in section 3.6.4.

Figure 4.37 shows that the Purolite S950 resin has faster kinetics in the sorption of Ca^{2+} ions than the respective nanofibres. This is due to the functional group attached to the surface of the resins which aids in bringing the sorption process to equilibrium ahead of the other sorbents, in addition to the fact that the Purolite S950 resin is more selective towards divalent ions. The sorption kinetics follows the order: Purolite S950 resin > PAN+ZEOLITE > PAN+TiO_2 > PAN. The equilibrium for Ca^{2+} ions sorption by the Purolite S950 resin was achieved within 60 minutes, whereas, the equilibrium for PAN+ZEOLITE was achieved within 120 minutes, while the equilibrium for PAN+TiO_2 and PAN was achieved within 180 minutes.

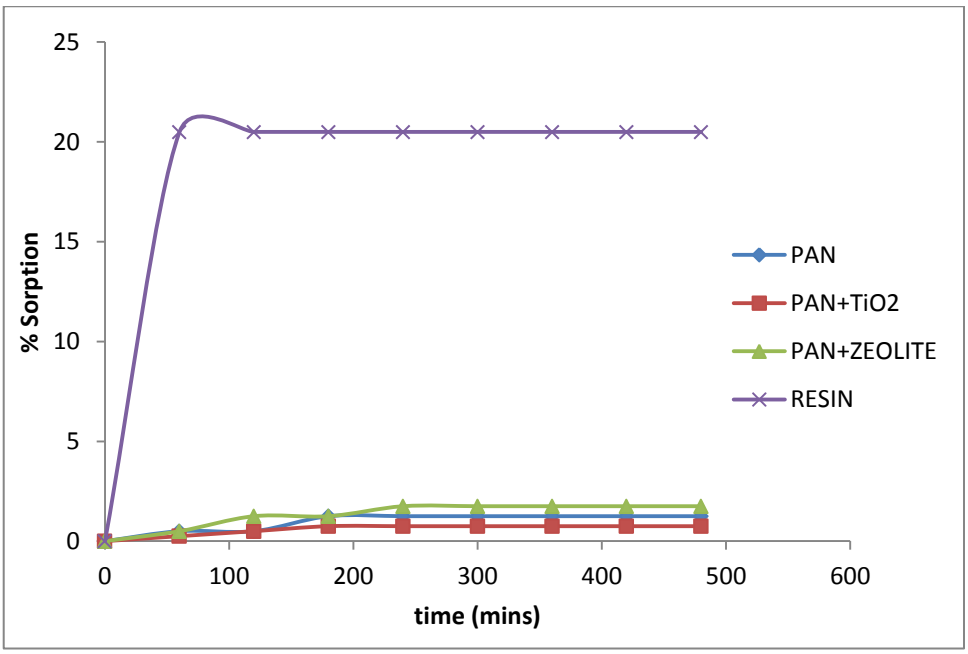

Figure 4.37: The comparison of the sorption kinetics curves of Ca^{2+} ions sorbed on Purolite S950 resin, PAN nanofibres, PAN+TiO_2 nanofibres and PAN+ZEOLITE nanofibres

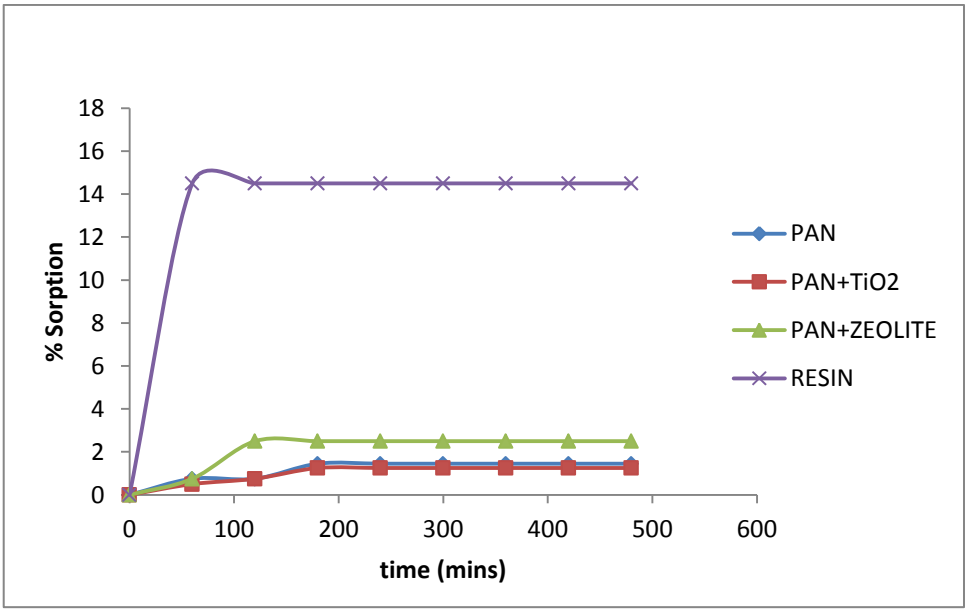

Figure 4.38: The comparison of the sorption kinetics curves of Mg^{2+} ions sorbed on Purolite S950 resin, PAN nanofibres, PAN+TiO_2 nanofibres and PAN+ZEOLITE nanofibres.

In the sorption kinetics of Mg^{2+} ions onto Purolite S950 resin, PAN, PAN+TiO_2 and PAN+ZEOLITE nanofibres, it is shown in Figure 4.38 that the Purolite S950 resin has faster kinetics in the sorption of Mg^{2+} than the other sorbents. The kinetics of sorption assumes a very similar trend as in the sorption of Ca^{2+} ions by the Purolite resin, PAN, PAN+TiO_2 and PAN+ZEOLITE nanofibres.

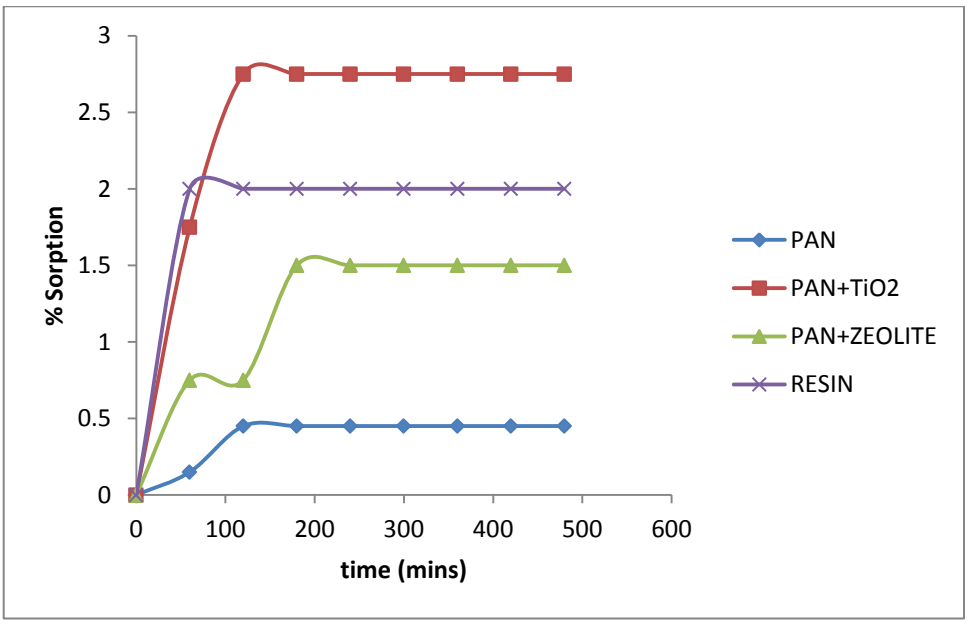

Figure 4.39: The comparison of the sorption kinetics curves of Na^+ ions sorbed on Purolite S950 resin, PAN nanofibres, PAN+TiO_2 nanofibres and PAN+ZEOLITE nanofibres

For the sorption of Na^+ ions onto Purolite S950 resin, PAN, PAN+TiO_2 and PAN+ZEOLITE nanofibres, Figure 4.39 shows that Purolite S950 resin had somewhat faster kinetics in the sorption of Na^+ ions than the nanofibres (PAN, PAN+TiO_2 and PAN+ZEOLITE respectively). The equilibrium for the sorption of Na^+ ions by Purolite S950 was achieved within 60 minutes. While for PAN and PAN+TiO_2 nanofibres, it was achieved within 120 minutes, whereas, equilibrium for PAN+ZEOLITE was achieved within 180 minutes. Kinetics for the sorption of Na^+ ions follows the order PAN+TiO_2 > Purolite S950 resin > PAN > PAN+ZEOLITE. Thereafter, the sorption proceeds at a slower rate.

In Figure 4.40, the sorption of K^+ ions onto Purolite S950 resin, PAN, PAN+TiO_2 and PAN+ZEOLITE nanofibres shows that Purolite S950 resin has faster kinetics than the nanofibres. The equilibrium for the sorption of K^+ ions the Purolite resin was achieved in 60 minutes, while the respective nanofibres attained equilibrium within 120 minutes.

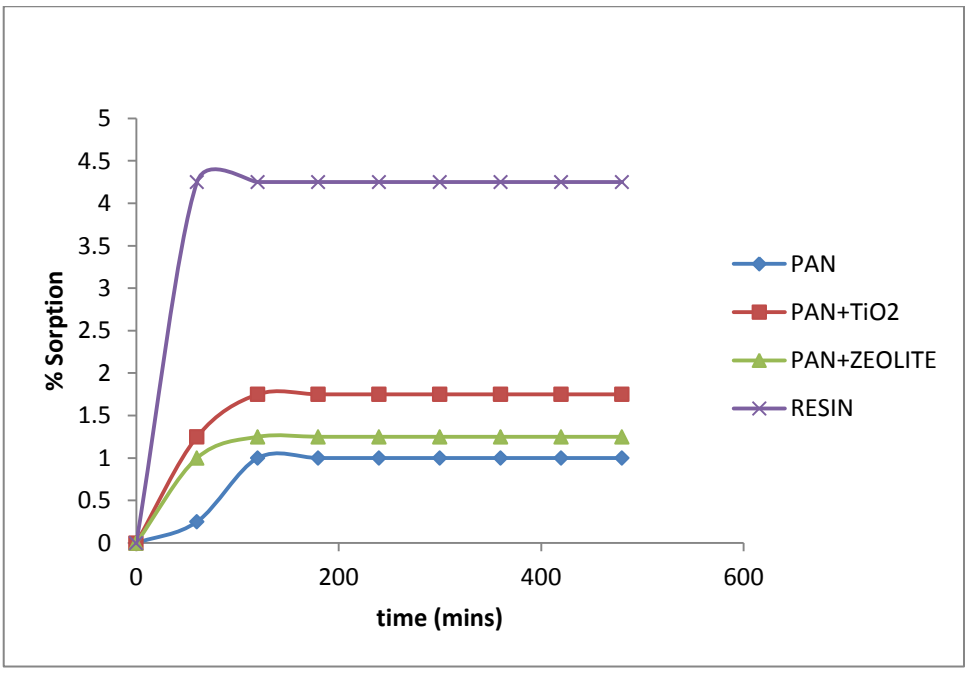

Figure 4.40: The comparison of the sorption kinetics curves of K^+ ions sorbed on Purolite S950 resin, PAN nanofibres, PAN+TiO_2 nanofibres and PAN+ZEOLITE nanofibres

After 60 minutes, 20.5 % sorption of Ca^{2+}, 14.5 % Mg^{2+}, 2 % Na^+ and 4.25 % K^+ were achieved by Purolite S950 resin. For PAN+ZEOLITE nanofibres, 0.5 % sorption of Ca^{2+}, 0.75 % sorption of Mg^{2+}, 0.75 % sorption of Na^+ and 1 % sorption of K^+ were achieved after 60 minutes. For PAN+TiO_2 nanofibres, 0.25 % sorption of Ca^{2+}, 0.5 % sorption of Mg^{2+}, 2.75 % sorption of Na^+ and 1.25 % sorption of K^+ respectively were achieved after 60 minutes. For PAN nanofibres, 0.5 % sorption of Ca^{2+}, 0.75 % sorption of Mg^{2+}, 0.15 % sorption of Na^+ and 0.25 % sorption of K^+ respectively were achieved after 60 minutes. This shows on an overall balance that the Purolite resins have faster kinetics of sorption followed by PAN+ZEOLITE, PAN+TiO_2 and PAN respectively.

It is necessary to predict batch sorption kinetics for the design of industrial sorption columns. Also, the nature of the sorption process depends on physical and chemical features of the sorption and on the conditions of the system. The sorption kinetics of Mg^{2+}, $Ca^{2+,}$ K^+ and Na^+ ions were modelled using the pseudo first order and pseudo second order equations.

4.2.5.1 Lagergren's Pseudo-First Order Kinetics

The pseudo first order kinetic model has been used widely to predict the kinetics of metal ion sorption. The metal ion kinetics of sorption that follows the pseudo-first order model is given by Ho & McKay, 1998; Sivaraj *et al.*, 2001.

$$\frac{dq}{dt} = k_1(q_e - q) \quad (4.4)$$

$$\log(q_e - q) = logq_e - \left(\frac{k}{2.303}\right) \times t \quad (4.5)$$

Where q_e is the amount of metal ion (M^{n+}) sorbed at equilibrium (mg/g), q_t amount of M^{n+} sorbed at time t (mg/g) and, k_1 the rate constant of pseudo-first order sorption (1/min). The value of k_1 can be obtained from the slope of the linear plot of log (qe - qt) vs. t.

The results of the pseudo-first order kinetics are presented in the Appendix 7.2. The plot of log (qe-qt) against time for the sorption of Mg^{2+}, Ca^{2+}, K^+ and Na^+ ions onto Purolite S950 resin and the nanofibres (PAN, PAN+TiO_2 and PAN+ZEOLITE) was obtained and the rate constant k_1 and the equilibrium capacity (q_e) were determined from the calculated slopes and intercepts form the plots. The values of k_1, q_e and the regression coefficient are provided in Table 4.15. It can be observed in Figures 4.37, 4.38, 4.39 and 4.30 respectively that the pseudo-first order kinetics (Lagergren's model) fits well for the first 60 and 120 minutes for the Purolite resin and the nanofibres respectively. After this period, the data deviated completely from the theory in both cases (Purolite resin and the nanofibres). Therefore, this model is only suitable for the initial sorption stages where the process is rapid, but it is not applicable to the whole process of sorption. This is similar to the observation made by Ho & Mackay, (1998) for dyes on peat particles. They observed that the sorption data fitted well to the Lagergren's pseudo-first order model but just for the initial stage of sorption within the contact time of 0 – 120 minutes.

Therefore, it can be confirmed that the Lagergren's pseudo-first order kinetic model cannot be used to predict the whole sorption period of the sorption kinetics of the metal ions (Mg^{2+}, Ca^{2+}, K^+ and Na^+), indicating that the model is applicable to an extent but inappropriate to describe the whole sorption process. So, in this work, the pseudo-first order model only applied to the initial 0–60 minutes sorption period for the Purolite resin and 0–120 minutes sorption period for the nanofibres (PAN, PAN+TiO_2 and PAN+ZEOLITE).

Table 4.15: Pseudo first order and pseudo second order rate constants for the sorption of Mg^{2+}, Ca^{2+}, K^{+} and Na^{+} ions on Purolite S950 resin, PAN, PAN+TiO_2 and PAN+ZEOLITE.

Sorbent	Solution Conc 100 mg/L	First Order Rate Expresssion		Second Order Rate Expression	
		k_1 (min^{-1})	R^2	k_2 (min^{-1})	R^2
Purolite Resin	Mg^{2+}	7.59×10^{-3}	0.9505	1.17×10^{-4}	0.9902
PAN		6.91×10^{-4}	0.0216	8.02×10^{-3}	0.9798
PAN+TiO_2		1.842×10^{-3}	0.3099	0.0149	0.7599
PAN+ZEOLITE		9.21×10^{-4}	0.2494	1.18×10^{-3}	0.9090
Purolite Resin	Ca^{2+}	0.0759	0.9548	9.92×10^{-5}	0.9868
PAN		1.38×10^{-3}	0.4737	0.01	0.9679
PAN+TiO_2		0.0023	0.4439	9.55×10^{-3}	0.9358
PAN+ZEOLITE		4.60×10^{-4}	0.0421	1.899×10^{-3}	0.9153
Purolite Resin	K^{+}	2.07×10^{-3}	0.3333	0.0162	0.9910
PAN		1.15×10^{-3}	0.7305	2.48×10^{-3}	0.9154
PAN+TiO_2		3.2×10^{-3}	0.536	0.0173	0.9967
PAN+ZEOLITE		1.84×10^{-3}	0.333	0.1023	0.9991
Purolite Resin	Na^{+}	3.22×10^{-3}	0.5714	0.011	0.9837
PAN		4.145×10^{-3}	0.7143	5.79×10^{-3}	0.8776
PAN+TiO_2		0.0253	0.4821	0.031	0.9994
PAN+ZEOLITE		6.91×10^{-4}	0.5714	5.497×10^{-3}	0.9254

4.2.5.2 Pseudo-Second Order Kinetics Model

Ho's pseudo-second order kinetics can be used to further analyse the sorption kinetics data (Ho, 2003).

$$\frac{dq}{dt} = k_2(q_e - q)^2 \qquad (4.6)$$

Where q = Amount of metal sorbed at any time (mg/g), (mol/g)

q_e = Amount of metal sorbed at equilibrium time (mg/g), (mol/g)

k_2 = Pseudo second order rate constant (g/mg.min), (g/mol.min)

The amount of metal ions on the surface of the sorption and the amount of metal ions sorbed at equilibrium are the major influence for pseudo-second order reaction (Ho & Mackay, 1998). Integrating equation (4.6) for the boundary conditions $t = 0$ to $t = t$ and $q = 0$ and $q = q_e$ gives the reaction rate expression for pseudo-second order as shown in the equation 4.7.

$$\frac{t}{q} = \frac{1}{k_2 q_e^2} + \frac{1}{q_e} \qquad (4.7)$$

A plot of t/q against t gives the value of the constants k_2 (g/mg h), (g/mole h) and also q_e (mg/g), (mole/g) can also be calculated.

The initial sorption rate h, can be calculated using the constant k_2 at $t \rightarrow 0$, as shown in equation 4.8.

$$h = k_2 q_e^2 \qquad (4.8)$$

Therefore, the rate constant k_2, the initial sorption rate h, and the predicted q_e can calculated from the plot of t/q against t at different sorbate concentrations by using equations (4.7) and (4.8) respectively.

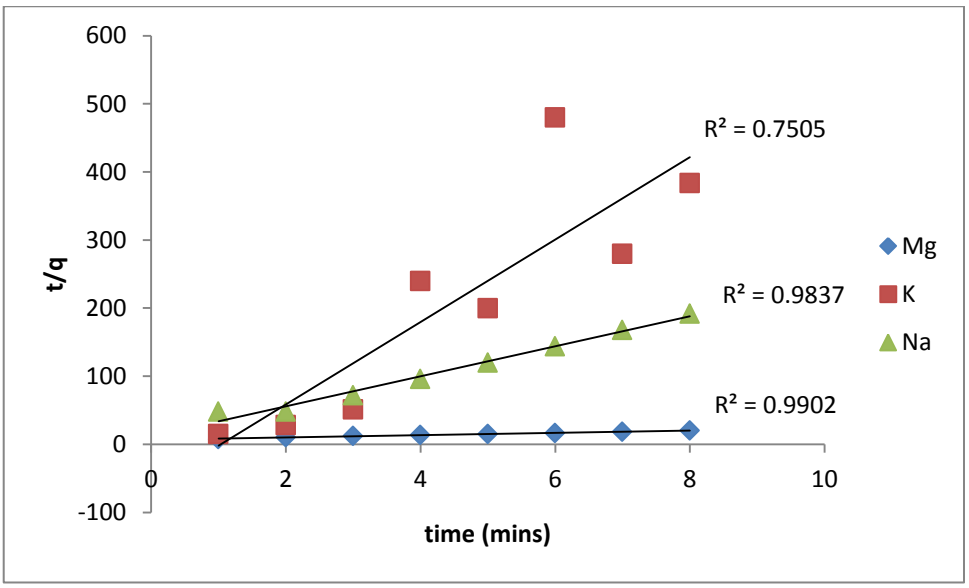

Figure 4.41: Pseudo-second order kinetics for Mg^{2+}, K^{+} and Na^{+} ions onto Purolite S950 resin
(Conditions: resin mass = 0.1 g; concentration: 100 mg/L).

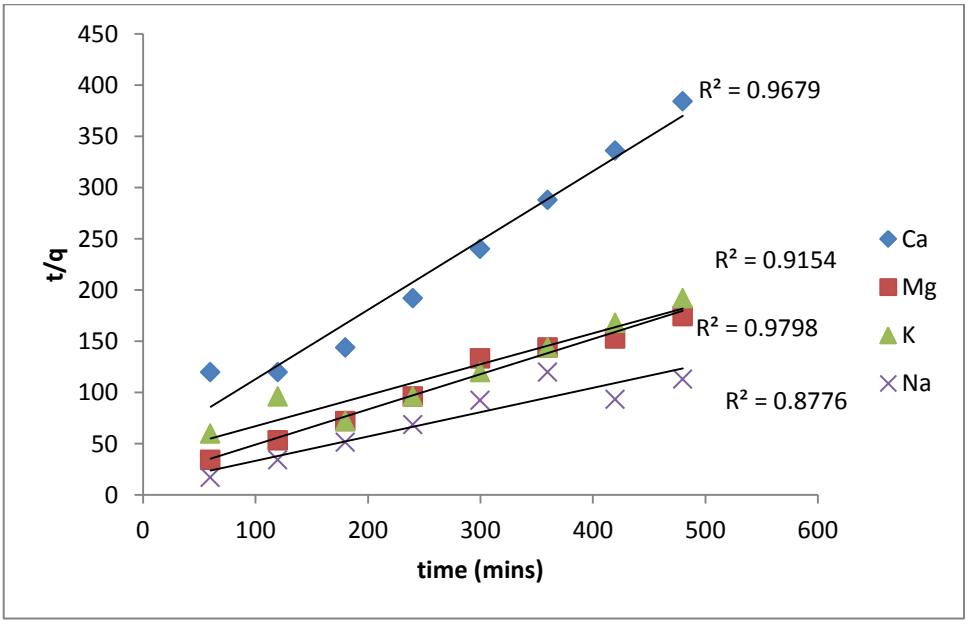

Figure 4.42: Pseudo-second order kinetics for Mg^{2+}, Ca^{2+}, K^{+} and Na^{+} ions onto PAN nanofibre
(Conditions: mass = 0.1 g; concentration: 100 mg/L).

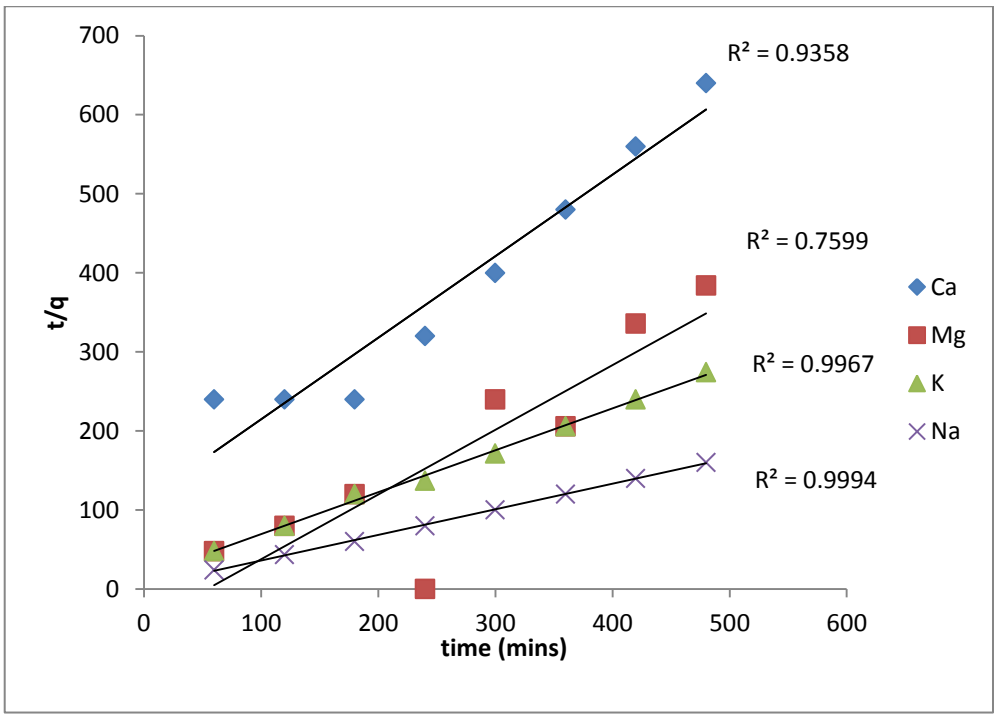

Figure 4.43: Pseudo-second order kinetics for Mg^{2+}, Ca^{2+}, K^{+} and Na^{+} ions onto PAN+TiO_2 nanofibre
(Conditions: mass = 0.1 g; concentration: 100 mg/L).

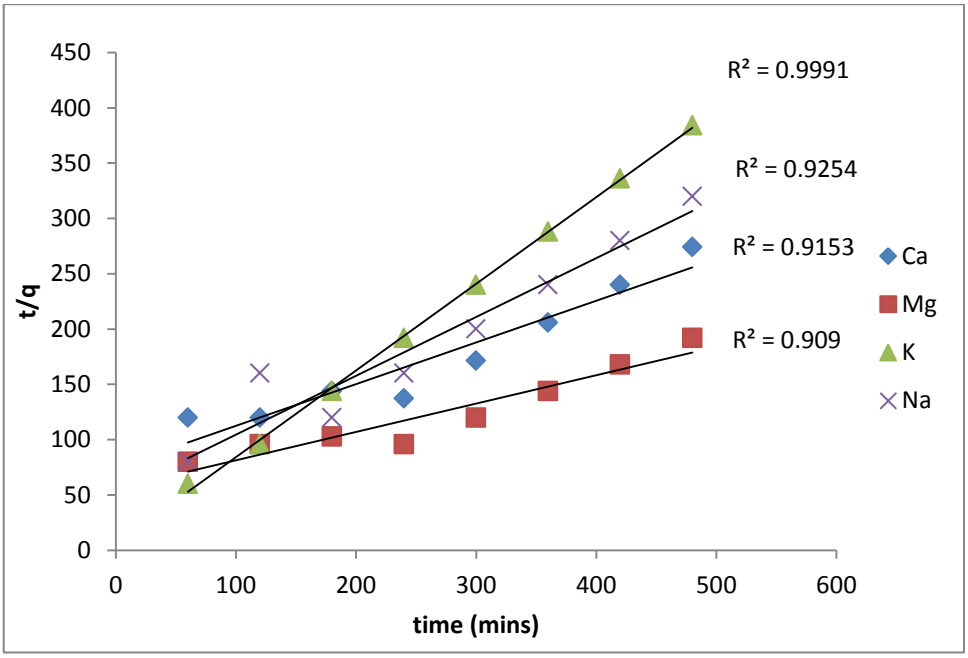

Figure 4.44: Pseudo-second order kinetics for Mg^{2+}, Ca^{2+}, K^{+} and Na^{+} ions onto PAN+ZEOLITE nanofibre
(Conditions: mass = 0.1 g; concentration: 100 mg/L).

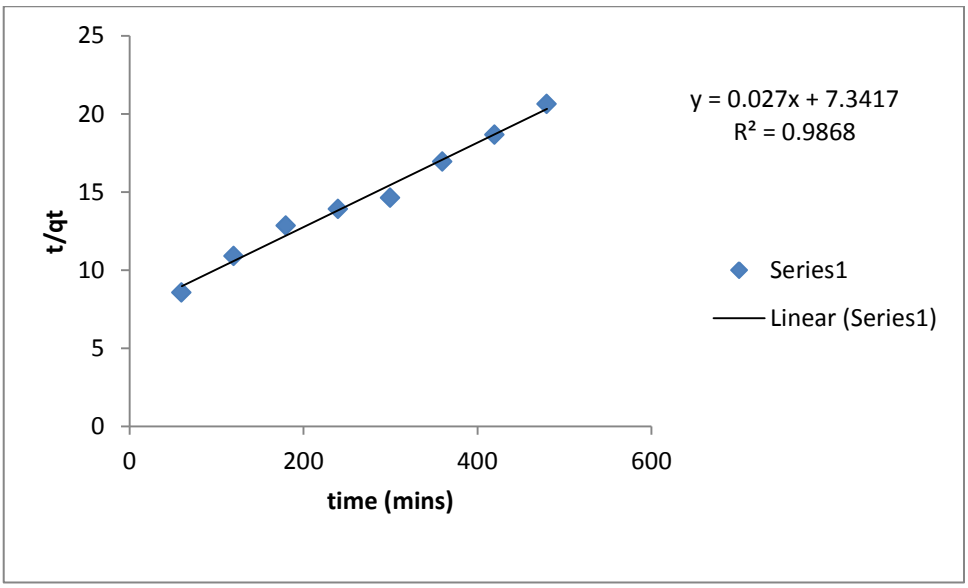

Figure 4.45: Pseudo-second order kinetics for Ca^{2+} ions onto Purolite S950 resin
(Conditions: resin mass = 0.1 g; concentration: 100 mg/L).

Figures 4.41, 4.42, 4.43 and 4.44, show the plots of the linearized form of the pseudo-second order kinetic model for the sorption of Mg^{2+}, Ca^{2+}, K^{+} and Na^{+} ions onto Purolite S950 resin, PAN, PAN+TiO_2 and PAN+ZEOLITE respectively. In the plots of t/q against time, for the pseudo-second order model, the linear regression correlation coefficients (R^2) are superior to that of the pseudo-first order model. It can therefore be concluded that the best fit for the sorption system is likely to be the pseudo-second order rate expression.

Table 4.15 shows the rate constants for pseudo-first and second order kinetics, the linear regression correlation coefficients for the two models. It is revealed that the pseudo-second order coefficients are superior to that of the pseudo-first order reaction. This implies that the sorption system is not of the first order and that the pseudo second order model fits best. Subsequently, the calculated values of q_e in the pseudo-second order reaction kinetics are closer to the experimental values, and the linear regression coefficients imply that the second-order model can be applied for the whole sorption process.

4.2.6 Effect of Temperature

The standard enthalpy change (ΔH°), standard entropy change (ΔS°) and the free energy change (ΔG°) are important thermodynamic parameters of sorption that are useful in defining whether the sorption reaction is endothermic or exothermic and to also determine the spontaneity of the sorption process. In section 2.6, it was given that the parameters can be calculated by the use of the following equations;

$$lnK_d = \frac{\Delta S^o}{R} - \frac{\Delta H^o}{RT} \quad (2.7)$$

$$K_d = \frac{q_e}{C_e} \quad (2.8)$$

$$\Delta G^O = -RTlnK_d \quad (2.9)$$

The distribution constant K_d, is an empirical equilibrium constant which has been used in the calculation of thermodynamic parameters in many studies, and is valid at specific initial concentration and other reaction conditions (Vadivelan & Kumar, 2005). The values for (ΔH°), (ΔS°) and (ΔG°) were calculated from the equations (2.7), (2.8) and (2.9). These thermodynamic parameters were obtained for the Mg^{2+}, Ca^{2+}, K^+ and Na^+ ions uptake on Purolite S950 resin, PAN, PAN+TiO_2 and PAN+ZEOLITE

4.2.6.1 Effect of Temperature on PAN

The result from batch sorption experiments of the effect of temperature on the sorption of Mg^{2+}, Ca^{2+}, K^+ and Na^+ ions using the PAN nanofibre is shown in Figure 4.46. It shows in this result that the percentage removal of the respective metal ions using PAN nanofibre increased with an increase in temperature. As a result of the temperature increase, the kinetic energy of the system increased leading to an increase in the degree of collision randomness between the sorbent and the metal ion in solutions. The order of removal of the metal ions by PAN nanofibre as the temperature increased was $Mg^{2+} > Na^+ > Ca^{2+} > K^+$. The Van't Hoff's plot for the sorption of Mg^{2+}, Ca^{2+}, K^+ and Na^+ ions onto PAN nanofibre are presented in Figures 4.47 – 4.50 respectively. The thermodynamic parameters are given in Table 4.16.

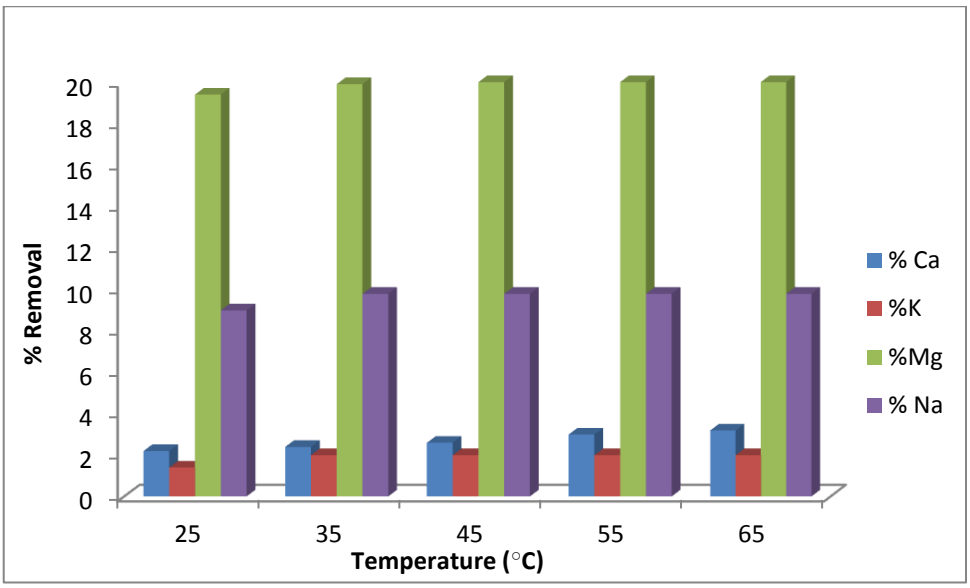

Figure 4.46: The effect of temperature on the sorption of Mg^{2+}, Ca^{2+}, K^{+} and Na^{+} ions onto PAN nanofibre.

From the graph in Figure 4.46, it can be observed that magnesium was more sorbed onto PAN nanofibre with an increase in temperature, and the lowest percentage removal was seen for the potassium ion.

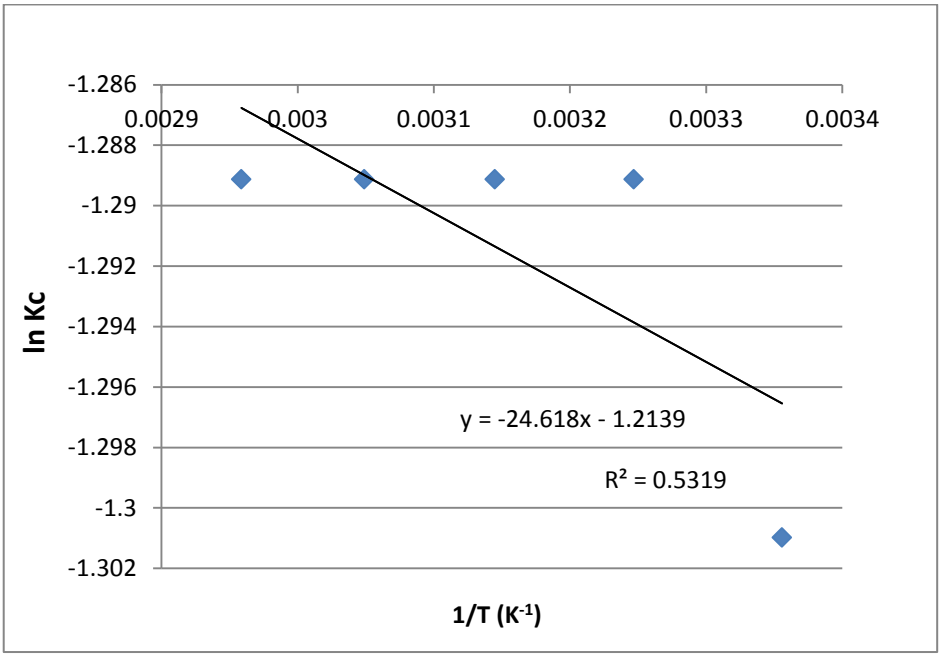

Figure 4.47: The Van't Hoff plot for the sorption of Mg^{2+} ions onto PAN nanofibre.

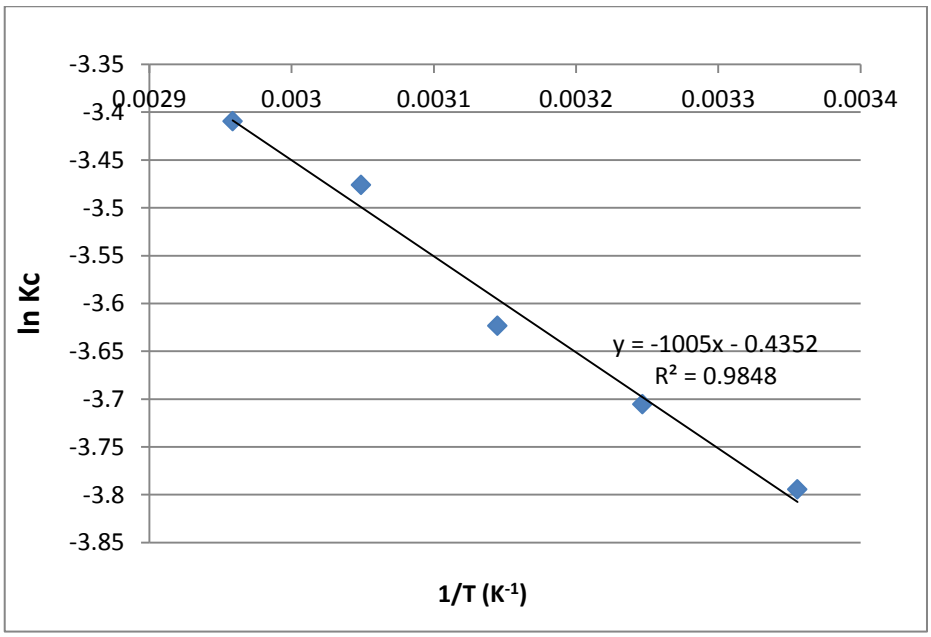

Figure 4.48: The Van't Hoff plot for the sorption of Ca^{2+} ions onto PAN nanofibre.

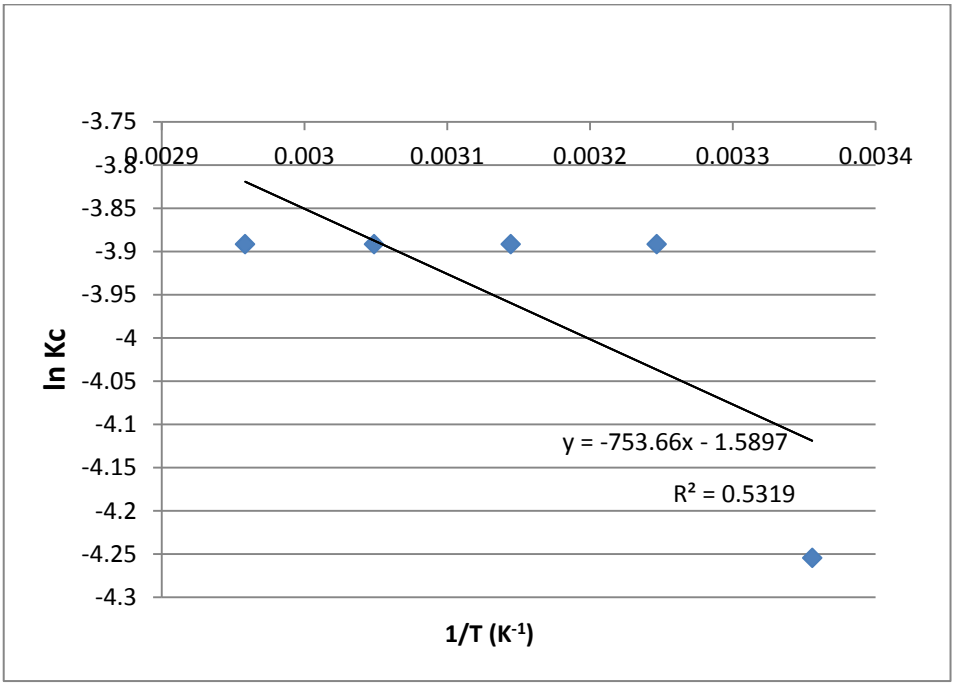

Figure 4.49: The Van't Hoff plot for the sorption of K^{+} ions onto PAN nanofibre.

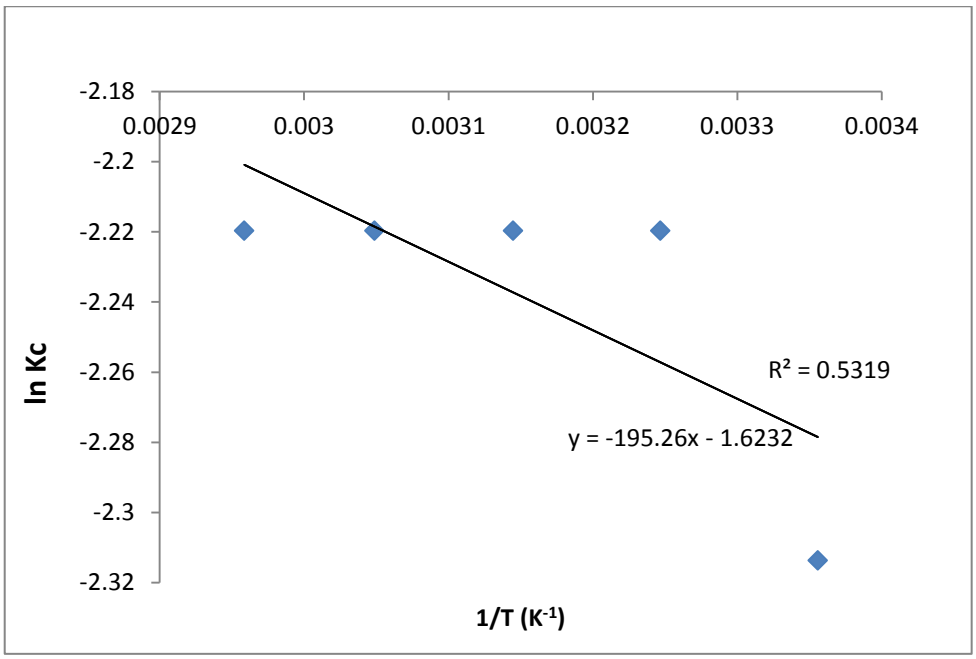

Figure 4.50: The Van't Hoff plot for the sorption of Na^+ ions onto PAN nanofibre.

Table 4.16: Values of ΔH^o, ΔS^o and ΔG^o calculated from the sorption data of Mg^{2+}, Ca^{2+}, K^+ and Na^+ ions onto PAN nanofibre.

Metal Ion	Conc (mg/L)	ΔH° (kJ/mol)	ΔS° (J/molK)	ΔG° (kJ/mol)			
				298 K	308 K	318 K	328 K
Mg^{2+}	500	0.21	-10.09	3.22	3.30	3.41	3.52
Ca^{2+}	500	8.36	-3.62	9.40	9.49	9.58	9.48
K^+	500	6.27	-13.22	10.54	9.97	10.29	10.61
Na^+	500	1.62	-13.49	5.73	5.68	5.87	6.05

In Table 4.16, the positive values of ΔH° show that the sorption process is endothermic and the sorption of Mg^{2+}, Ca^{2+}, K^+ and Na^+ ions onto PAN nanofibre will be favourable at high temperatures. To a large extent, physisorption and chemisorption can be classified by the magnitude of the enthalpy change. The bonding strengths of < 42 kJ/mol are accepted to be typically those of physical sorption type bonds, while chemisorption bond strengths range

from 42 to 125.4 kJ/mol (Aroguz, 2006). Chemical sorption is viewed as chemical bonding, when the enthalpy change is greater than 42 kJ/mol, while physical sorption is viewed as Van Der Waals interaction (< 42 kJ/mol) (Yang *et al.*, 2014). Based on this, the sorption of Mg^{2+}, Ca^{2+}, K^{+} and Na^{+} ions onto PAN nanofibre appears to be a physical sorption process. The corresponding values of ΔS° are negative for the sorption of the metal ions onto PAN nanofibre, indicating a decrease in the degree of freedom of the solid – sorbate interphase solution. The ΔG° values are positive, indicating that the sorption of Mg^{2+}, Ca^{2+}, K^{+} and Na^{+} ions onto PAN nanofibre is non-spontaneous (negative ΔG° values) (Aroguz, 2006). The efficiency and trend of sorption can also be explained by the standard enthalpy values with temperature increase, whereby, a lower value of ΔG° indicates a favourable sorption.

4.2.6.2 Effect of Temperature on PAN+TiO_2

The result from batch sorption experiments on the effect of temperature on the sorption of Mg^{2+}, Ca^{2+}, K^{+} and Na^{+} ions using the PAN+TiO_2 nanofibre is given in Figure 4.51. It is shown in this result that the percentage removal of metal ions using PAN+TiO_2 nanofibre increases with an increase in temperature. The increasing temperature increased the collision between the metal ions in the solution and the sorbent, thereby, enhancing the sorption process.

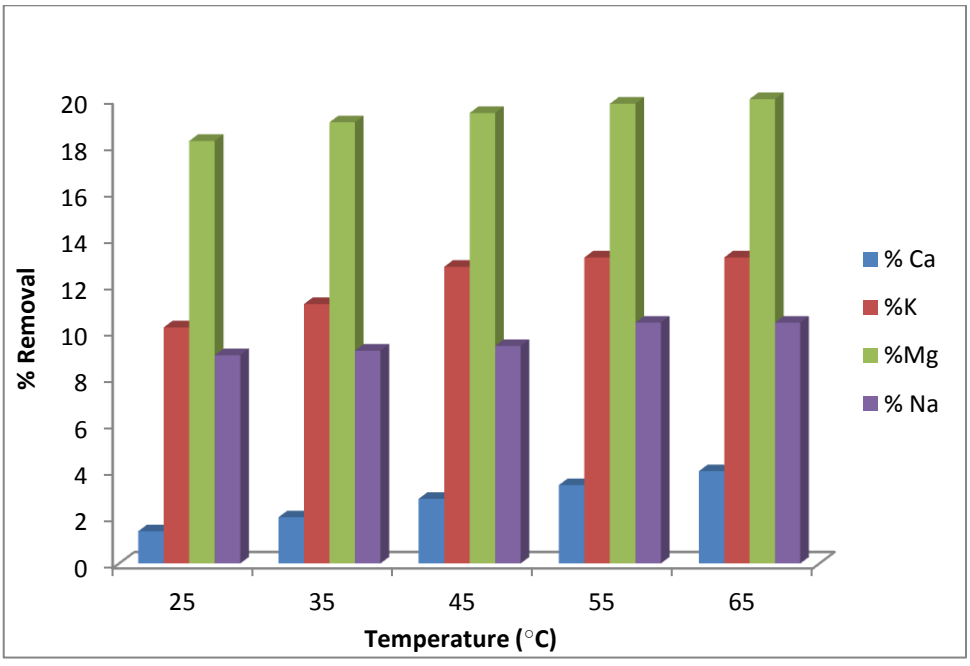

Figure 4.51: The effect of temperature on the sorption of Mg^{2+}, Ca^{2+}, K^{+} and Na^{+} ions onto PAN+TiO_2 nanofibre.

As a result of the temperature increase, the order of efficient removal of the metal ions (Mg^{2+}, Ca^{2+}, K^{+} and Na^{+}) by PAN+TiO_2 nanofibre was $Mg^{2+} > K^{+} > Na^{+} > Ca^{2+}$. From the graph in

Figure 4.51, it can be observed that magnesium was more sorbed onto PAN+TiO_2 nanofibre with an increase in temperature, and the lowest percentage removal was seen for calcium ion. The Van't Hoff's plot for the sorption of Mg^{2+}, Ca^{2+}, K^+ and Na^+ ions onto PAN+TiO_2 nanofibre are presented in Figures 4.52, 4.53, 4.54 and 4.55.

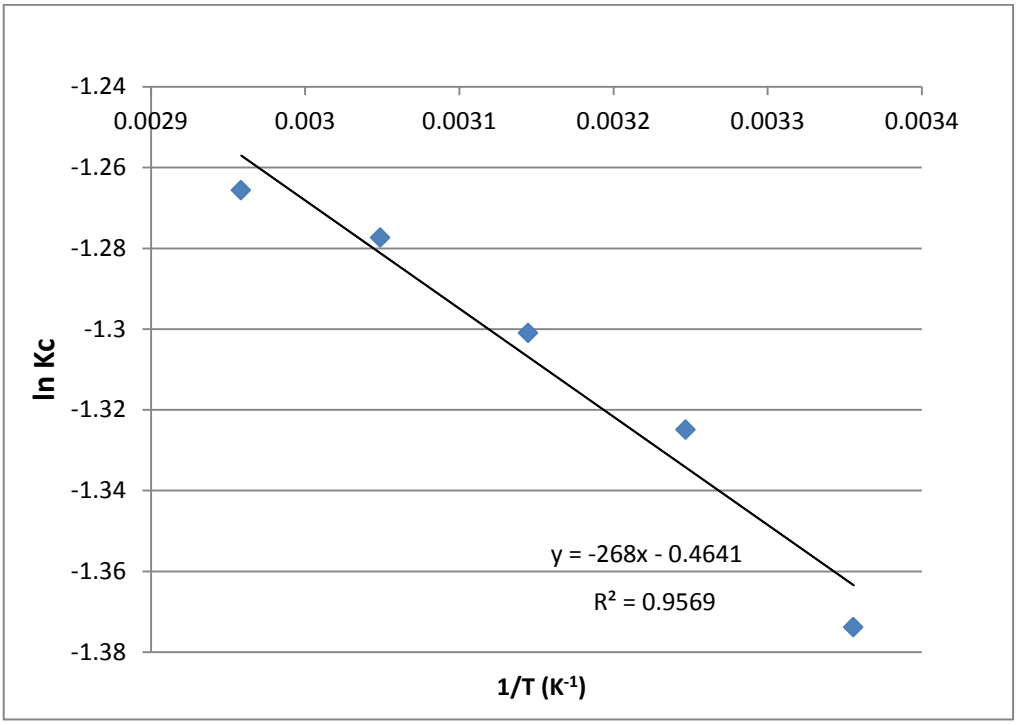

Figure 4.52: The Van't Hoff plot for the sorption of Mg^{2+} ions onto PAN+TiO_2 nanofibre.

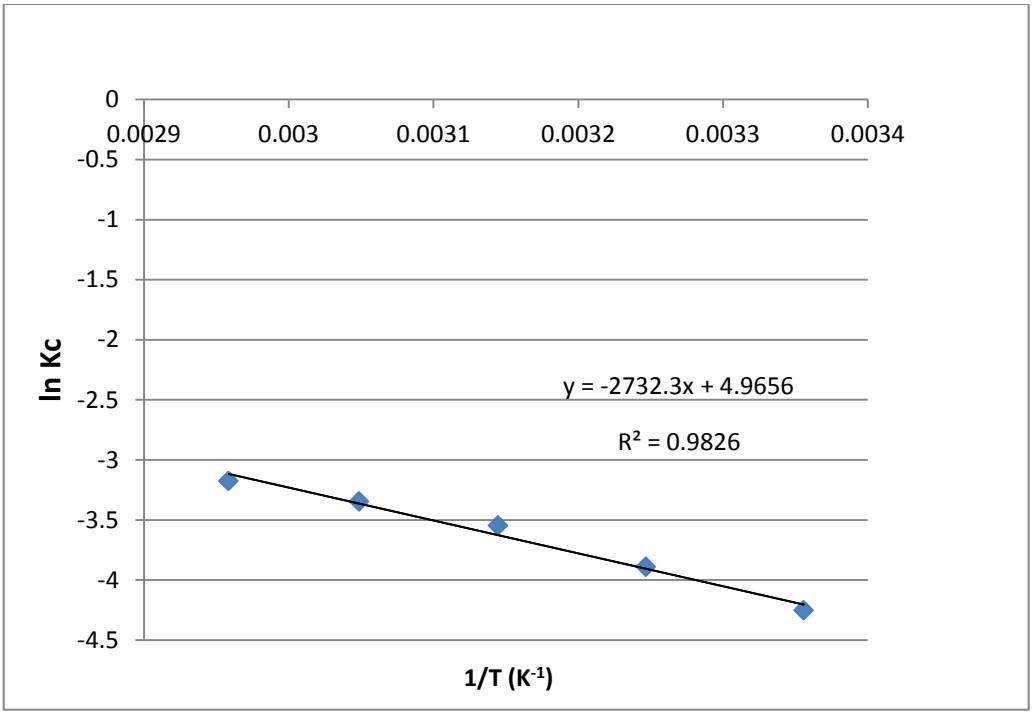

Figure 4.53: The Van't Hoff plot for the sorption of Ca^{2+} ions onto PAN+TiO_2 nanofibre.

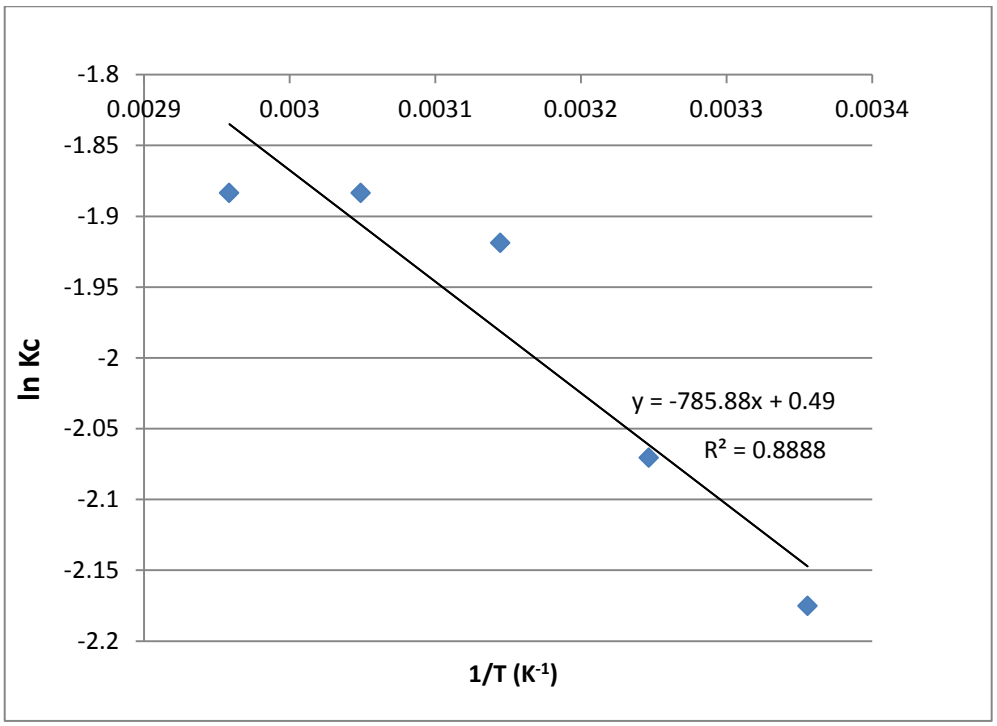

Figure 4.54: The Van't Hoff plot for the sorption of K^+ ions onto PAN+TiO_2 nanofibre.

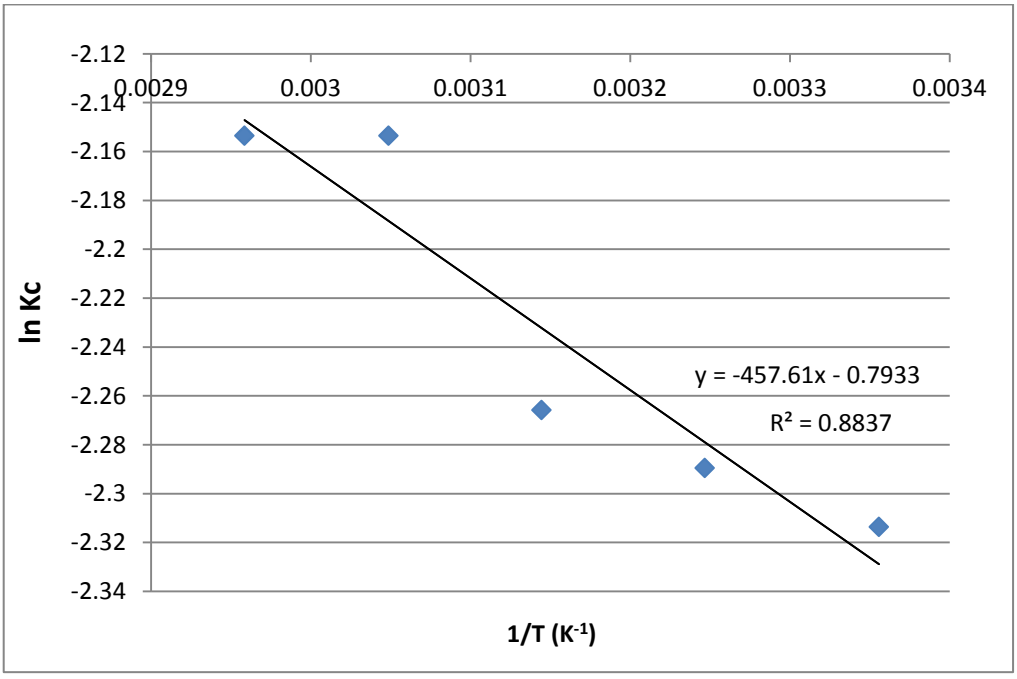

Figure 4.55: The Van't Hoff plot for the sorption of Na^+ ions onto PAN+TiO_2 nanofibre.

Table 4.17: Values of ΔH^o, ΔS^o and ΔG^o calculated from the sorption data of Mg^{2+}, Ca^{2+}, K^+ and Na^+ ions onto PAN+TiO_2 nanofibre.

Metal Ion	Conc (mg/L)	ΔH° (kJ/mol)	ΔS° (J/molK)	ΔG° (kJ/mol)			
				298 K	308 K	318 K	328 K
Mg^{2+}	500	2.23	-3.86	3.4	3.4	3.4	3.5
Ca^{2+}	500	2.3	41.28	10.54	9.97	9.38	9.13
K^+	500	6.53	4.07	5.39	5.30	5.07	5.14
Na^+	500	3.81	-6.60	5.73	5.86	5.99	5.87

In Table 4.17, the positive values of ΔH^o described a physisorption reaction (< 42 kJ/mol). The respective values of ΔH^o are less than 42 kJ/mol (Aroguz, 2006). The corresponding values of ΔS^o are negative for the sorption of Mg^{2+} and Na^+ ions, indicating a decrease in the degree of freedom; while the values are positive for the sorption Ca^{2+} and K^+ ions depicting an increase in the degree of disorderliness of the solid – sorbate interphase. The ΔG^o values are positive for the sorption of the metal ions onto the PAN+TiO_2 nanofibre, this indicates a non-spontaneous sorption process.

The decreasing ΔG^o values for Ca^{2+} and K^+ ions implies an increasing rate of sorption, spontaneity and thermodynamically favourable sorption process (Aroguz, 2006). This implies that the lower the value of ΔG^o, the higher the efficiency of sorption of the sorptions.

4.2.6.3 Effect of Temperature on PAN+ZEOLITE

The result from batch sorption experiments on the effect of temperature on the sorption of Mg^{2+}, Ca^{2+}, K^+ and Na^+ ions using the PAN+ZEOLITE nanofibre is given in Figure 4.56. The result also showed that the percentage removal of the metal ions (Mg^{2+}, Ca^{2+}, K^+ and Na^+) using PAN+ZEOLITE nanofibre increased with increasing temperature. The result is similar to the trend in other nanofibres. An increase in temperature increased the kinetic energy and subsequently increased the collision between sorbent and the metal ion solution.

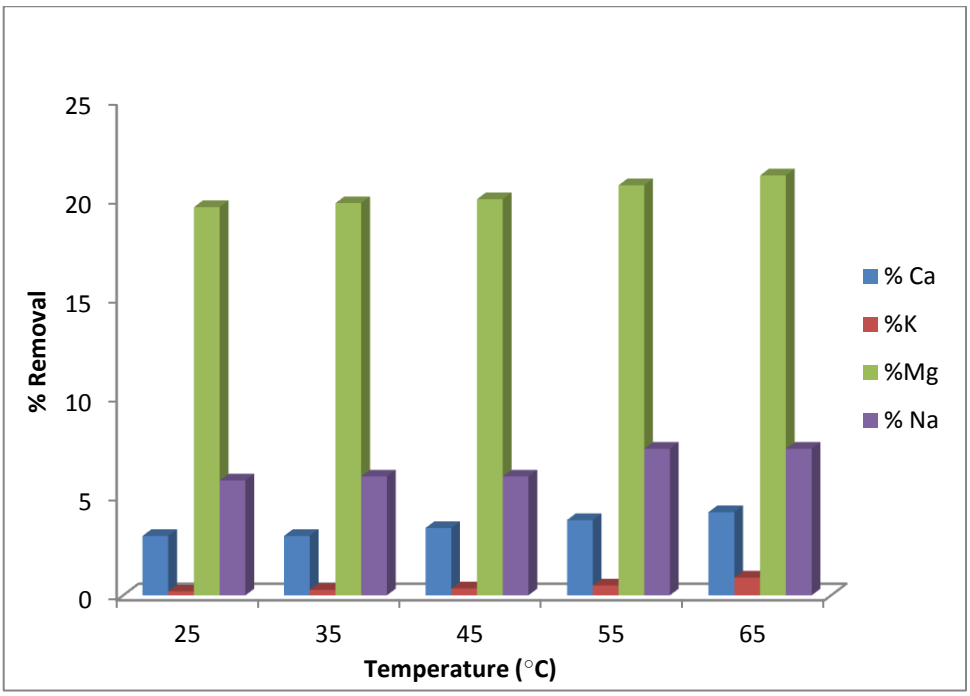

Figure 4.56: The effect of temperature on the sorption of Mg^{2+}, Ca^{2+}, K^{+} and Na^{+} ions onto PAN+ZEOLITE nanofibre.

As a result of the temperature increase, the order of efficient removal of the metal ions (Mg^{2+}, Ca^{2+}, K^{+} and Na^{+}) by PAN+ZEOLITE nanofibre was $Mg^{2+} > Na^{+} > Ca^{2+} > K^{+}$. From the graph in Figure 4.56, it can be observed that magnesium was more sorbed onto PAN+ZEOLITE nanofibre with an increase in temperature, and the lowest percentage removal was seen for the potassium ion. The Van't Hoff's plots for the sorption of Mg^{2+}, Ca^{2+}, K^{+} and Na^{+} ions onto PAN+ZEOLITE nanofibre are presented in Figures 4.57, 4.58, 4.59 and 4.60.

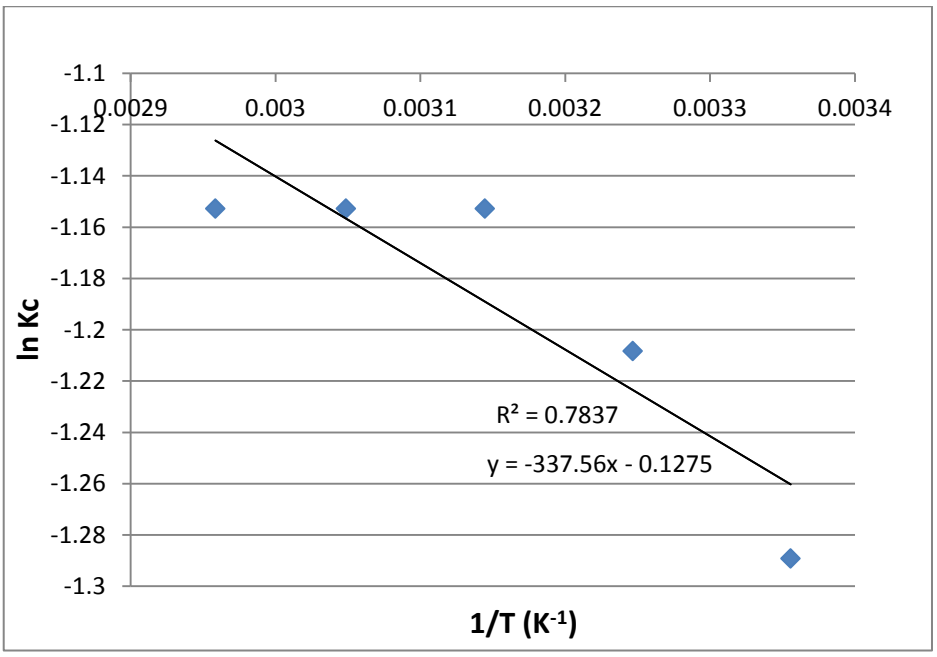

Figure 4.57: The Van't Hoff plot for the sorption of Mg^{2+} ions onto PAN+ZEOLITE nanofibre.

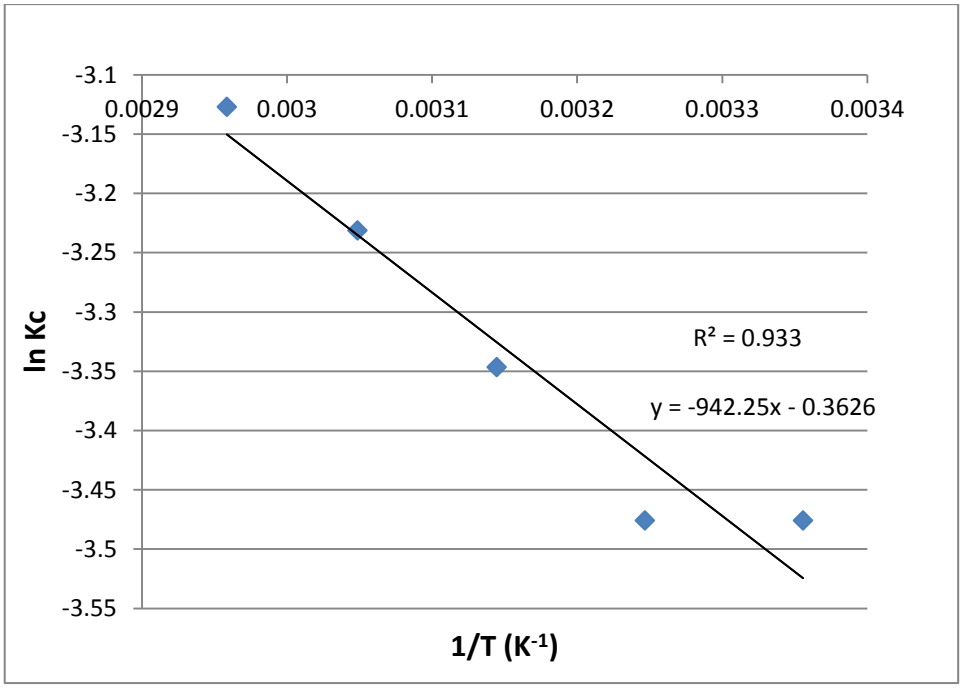

Figure 4.58: The Van't Hoff plot for the sorption of Ca^{2+} ions onto PAN+ZEOLITE nanofibre.

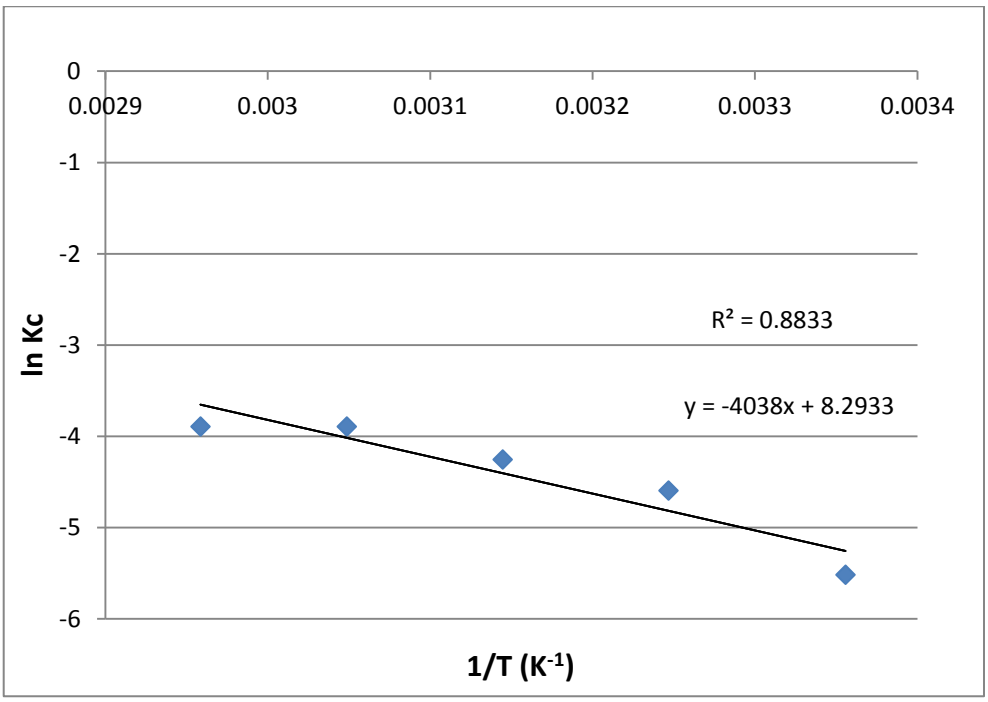

Figure 4.59: The Van't Hoff plot for the sorption of K^+ ions onto PAN+ZEOLITE nanofibre.

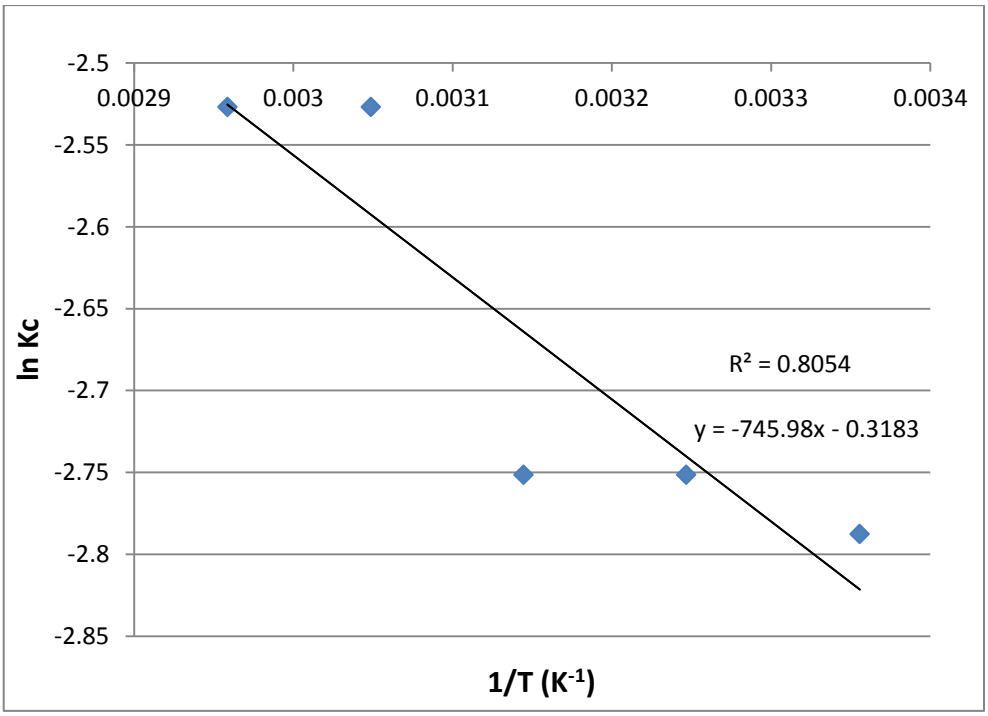

Figure 4.60: The Van't Hoff plot for the sorption of Na^+ ions onto PAN+ZEOLITE nanofibre.

Table 4.18: Values of ΔH^o, ΔS^o and ΔG^o calculated from the sorption data of Mg^{2+}, Ca^{2+}, K^+ and Na^+ ions onto PAN+ZEOLITE nanofibre.

Metal Ion	Conc (mg/L)	ΔH° (kJ/mol)	ΔS° (J/molK)	ΔG° (kJ/mol)			
				298 K	308 K	318 K	328 K
Mg^{2+}	500	2.81	-1.06	3.19	3.09	3.05	3.14
Ca^{2+}	500	7.83	-3.05	8.61	8.90	8.85	8.81
K^+	500	33.6	68.95	13.67	11.77	11.25	10.61
Na^+	500	6.20	-2.65	6.91	7.05	7.28	6.89

In Table 4.18, the values of ΔH^o are positive, which describes a physisorption reaction (< 42 kJ/mol) (Aroguz, 2006). The corresponding values of ΔS^o are negative for the sorption of Mg^{2+}, Ca^{2+} and Na^+ ions, which indicate a decrease in the degree of freedom; while the value is positive for the sorption K^+ ions depicting an increase in the degree of disorderliness of the solid – sorbate interphase. The ΔG^o values are positive for the sorption of the metal ions onto the PAN+ZEOLITE nanofibre, this indicates a non-spontaneous sorption process.

The decreasing ΔG^o values for Mg^{2+} and K^+ ions can be attributed to the increasing rate of sorption, spontaneity and thermodynamically favourable sorption process (Aroguz, 2006). Generally, the lower the ΔG^o values, the more favourable and spontaneous the sorption process, this implies that the lower the value of ΔG^o, the higher the efficiency of sorption.

4.2.6.4 Effect of Temperature on Purolite S950 Resin

For Purolite S950 resin, the result from the batch sorption experiments on the effect of temperature on the sorption of Mg^{2+}, Ca^{2+}, K^+ and Na^+ ions is shown in Figure 4.61. It can be seen that the removal efficiency of the metal ions onto the Purolite S950 resin increased with increasing temperature. The percentage of removal of the respective metal ions is proportional to the temperature increase, indicating the sorption of Mg^{2+}, Ca^{2+}, K^+ and Na^+ ions on Purolite S950 resin is endothermic (Yang *et al.*, 2014).

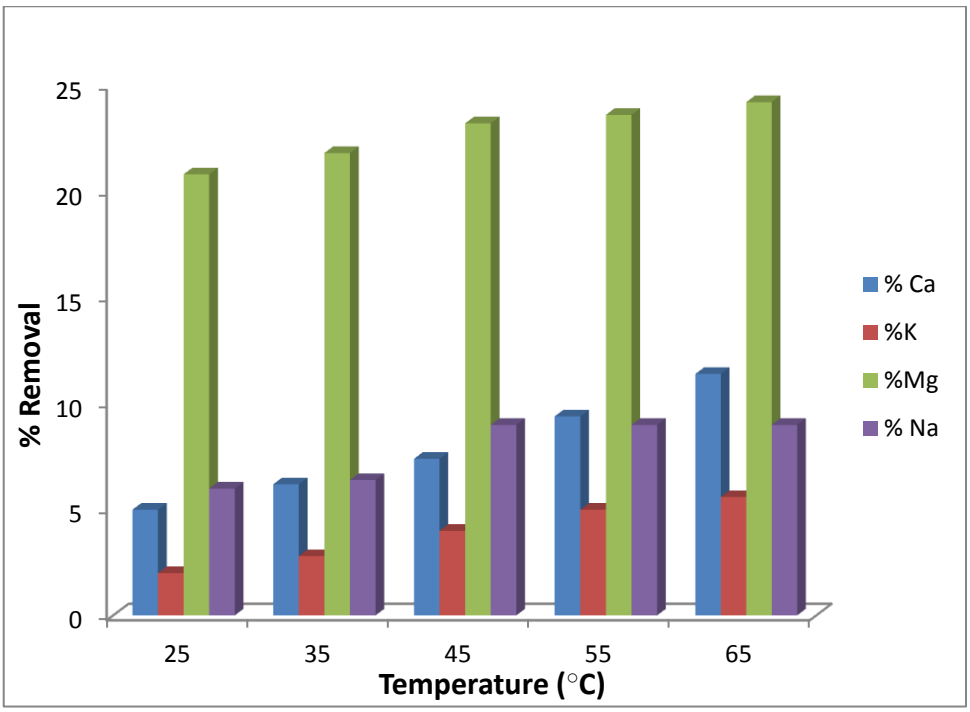

Figure 4.61: The effect of temperature on the sorption of Mg^{2+}, Ca^{2+}, K^{+} and Na^{+} ions onto Purolite S950 resin.

With an increase in temperature, the order of efficient removal of the metal ions by the Purolite S950 resin was $Mg^{2+} > Ca^{2+} > Na^{+} > K^{+}$. The Purolite S950 resin shows greater selectivity to the divalents compared to the monovalent cations, therefore the divalent Mg^{2+} and Ca^{2+} are highly sorbed onto the resin with the increase in temperature, and the lowest percentage removal was seen for potassium ion. The Van't Hoff's plot for the sorption of Mg^{2+}, Ca^{2+}, K^{+} and Na^{+} ions onto Purolite S950 resin are presented in Figures 4.62, 4.63, 4.64 and 4.65.

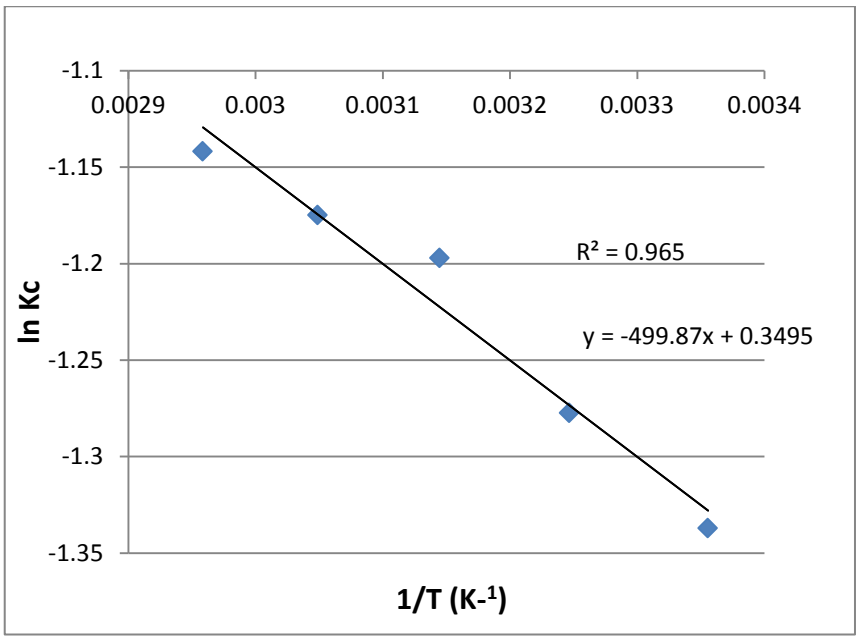

Figure 4.62: The Van't Hoff plot for the sorption of Mg^{2+} ions onto Purolite S950 resin.

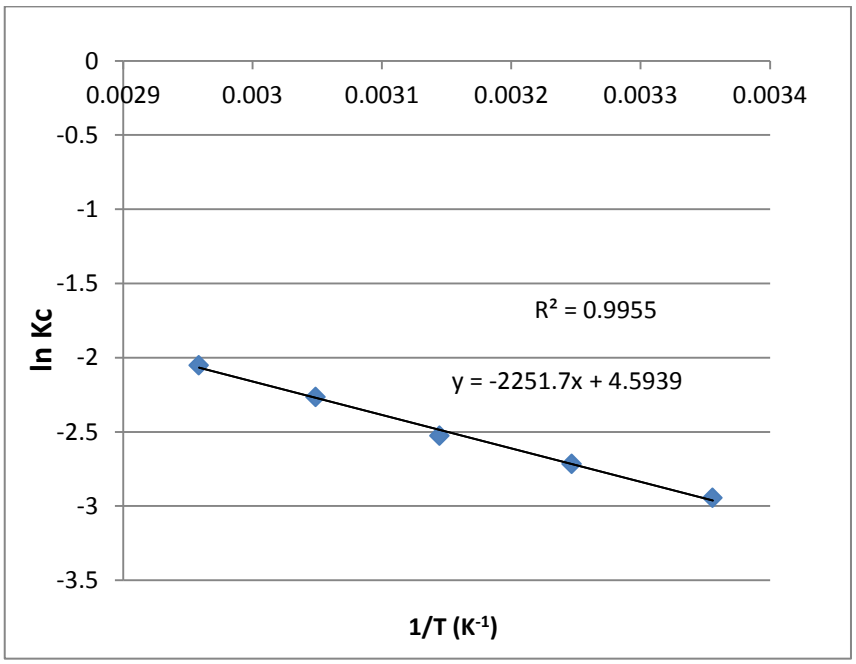

Figure 4.63: The Van't Hoff plot for the sorption of Ca^{2+} ions onto Purolite S950 resin.

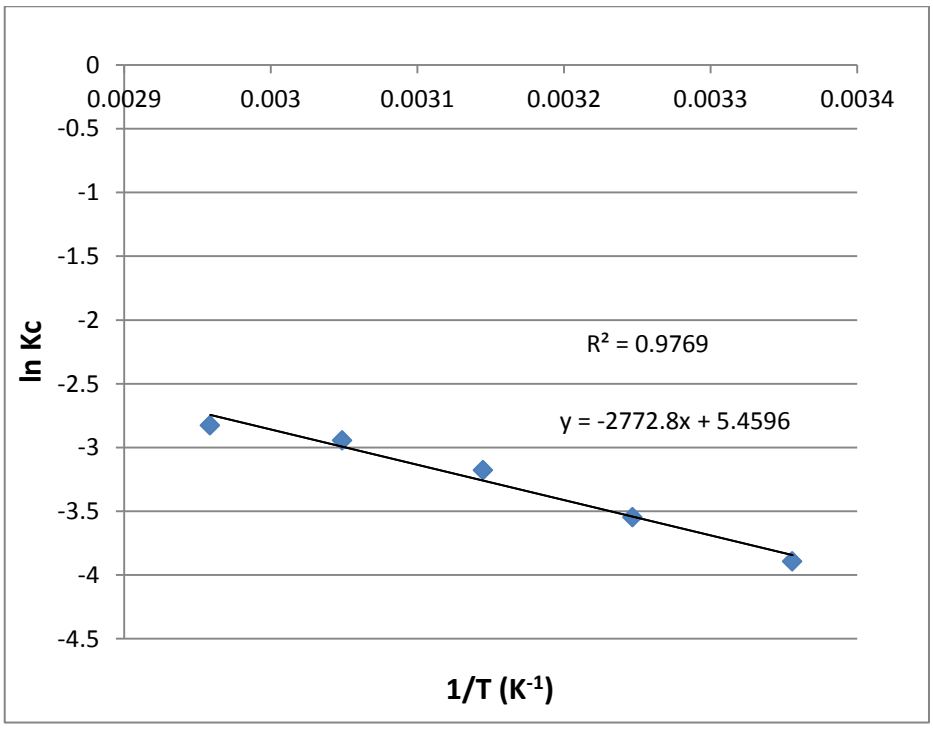

Figure 4.64: The Van't Hoff plot for the sorption of K^+ ions onto Purolite S950 resin.

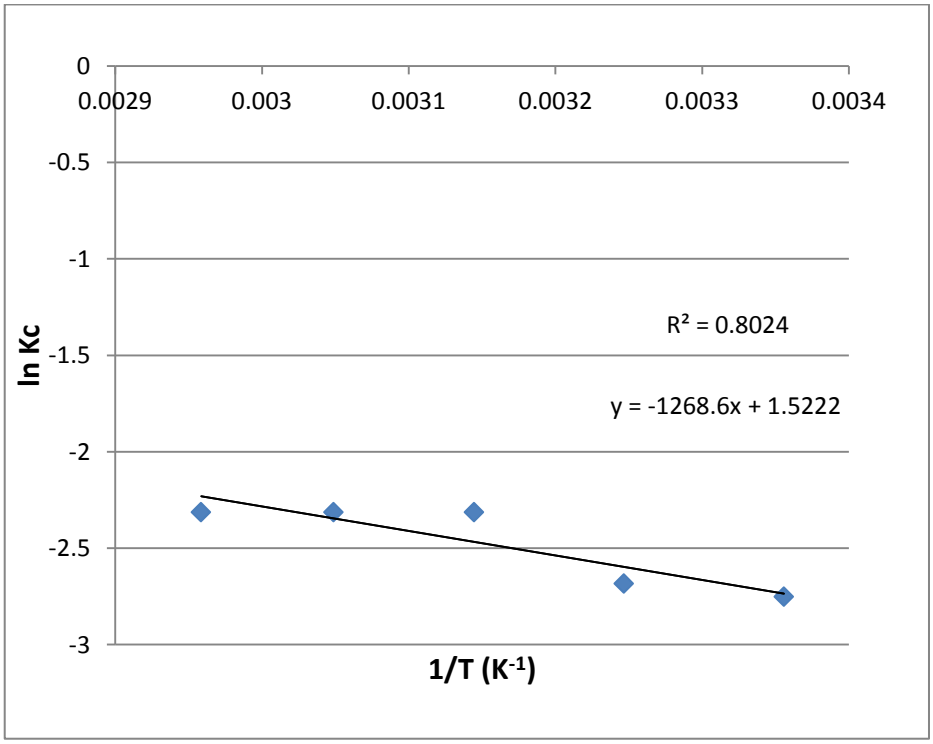

Figure 4.65: The Van't Hoff plot for the sorption of Na^+ ions onto Purolite S950 resin.

Table 4.19: Values of ΔH^o, ΔS^o and ΔG^o calculated from the sorption data of Mg^{2+}, Ca^{2+}, K^+ and Na^+ ions onto Purolite S950 resin.

Metal Ion	Conc (mg/L)	ΔH° (kJ/mol)	ΔS° (J/molK)	ΔG° (kJ/mol)			
				298 K	308 K	318 K	328 K
Mg^{2+}	500	4.16	2.91	3.31	3.27	3.17	3.20
Ca^{2+}	500	18.72	38.19	7.29	6.96	6.68	6.18
K^+	500	23.05	45.39	9.64	9.08	8.40	8.03
Na^+	500	10.55	12.66	6.82	6.87	6.12	6.31

In Table 4.19, the values of ΔH^o are positive and fall between 0 and 42 kJ/mol indicating that the sorption of Mg^{2+}, Ca^{2+}, K^+ and Na^+ ions onto Purolite S950 resin is endothermic, and that an increase in temperature favours the sorption process. It also describes a physical sorption reaction, with no chemical bond formation (< 42 kJ/mol) (Yang et al., 2014). The corresponding values of ΔS^o are positive for the sorption of Mg^{2+}, Ca^{2+}, K^+ and Na^+ ions, which indicate an increase in the degree of randomness of the solid – sorbate interphase. The ΔG^o values are positive for the sorption of the metal ions onto the Purolite S950 resin; this indicates a non-spontaneous sorption process.

The lower ΔG^o values for Mg^{2+} ions justify the higher efficiency of the resin in the removal of magnesium ions in solution. Potassium ions with the highest ΔG^o values were least sorbed from the metal ions solution at all temperatures.

4.2.7 Column Study

A column study was also carried out for the sorption of Mg^{2+}, Ca^{2+}, K^+ and Na^+ ions from the Emalahleni brine onto the Purolite S950 resin. The procedure for this experiment has already been described in section 3.4.2. The ICP-OES analysis of the Emalahleni brine is given in Table 4.20.

Table 4.20: ICP result for Mg^{2+}, Ca^{2+}, K^{+} and Na^{+} ions contained in Emalahleni brine.

Metal Ion	Mg^{2+}	Ca^{2+}	Na^{+}	K^{+}
Concentration (mg/L)	358.5	1213.4	3168.3	1004.1

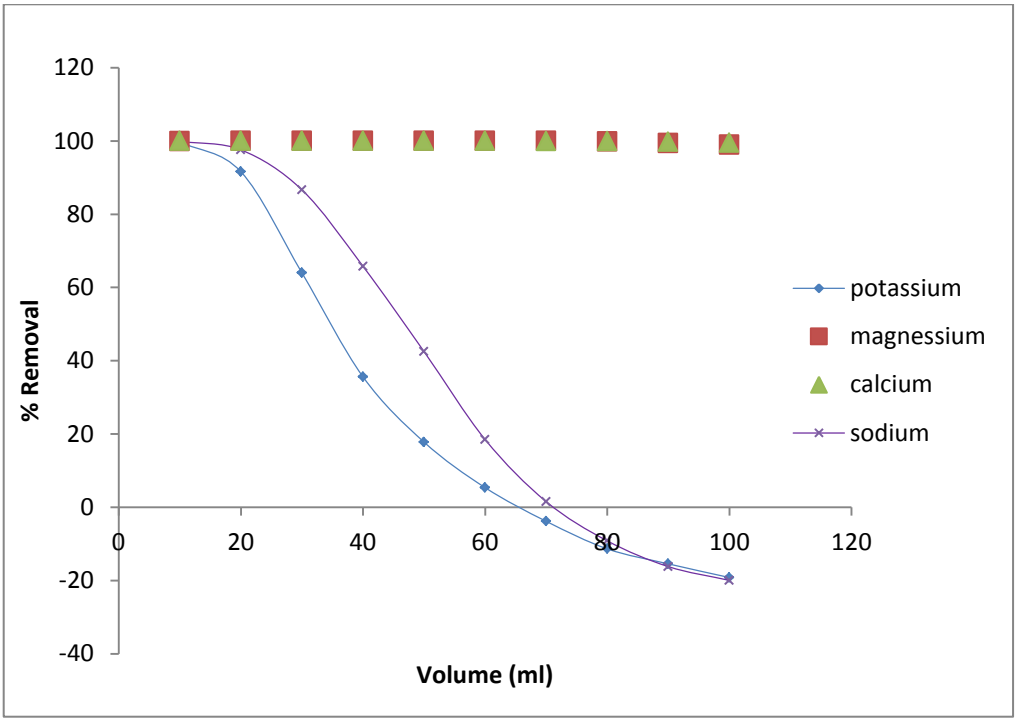

Figure 4.66: The sorption of Mg^{2+}, Ca^{2+}, K^{+} and Na^{+} ions onto Purolite S950 resin.

100 mL Emalahleni brine, having the various concentrations of metal ions highlighted in Table 4.20, was passed through a fixed column packed with 13.75 g of Purolite S950 resin filled to the 15 mL mark, at a flow rate of 2.5 mL per minute. The efficiency of the removal of the metal ions in a fixed bed mode is shown in Figure 4.66.

The removal of magnesium and calcium ions was greater than 99.9 % when 100 mL stock solution was passed through the column. The divalent Mg^{2+} and Ca^{2+} were sorbed at the same rate which makes their results overlap as shown in Figure 4.66. This is because the Purolite S950 resin is selective towards the divalent cations. The efficiency of potassium and sodium ions removal was greater than 99.9 % at 10 mL and 20 mL respectively. Thereafter, there was a sharp decline in the percentage removal (Figure 4.66).

The column study proves to be more effective in the sorption of metal ions, in spite of being carried out at the room temperature; this shows the non-complexity of the sorption process and the opportunity to selectively remove the Mg^{2+} and Ca^{2+} ions from the Emalahleni brine solution using the resin.

CHAPTER FIVE

5.0 Conclusion

5.1 General Conclusions

This study has been able to prove that hydrophilic materials like the nanofibres are capable of competing with the Purolite S950 resin in the removal and treatment of major ions (Mg^{2+}, Ca^{2+} K^{+} and Na^{+} ions) from brine effluents, in spite of the fact that no functional groups (ligands) were attached to its structure. The nanofibres have provided the advantage of their large surface area and many active sites coupled with the incorporation of inorganic materials (titanium dioxide and zeolite) in showing selectivity towards these ions. Sorption capacities of 0.21 meq/g for Mg^{2+}, 0.09 meq/g for Ca^{2+}, 0.03 meq / g for K^{+} and 0.07 meq / g for Na^{+} by PAN+ZEOLITE nanofibres; 0.1 meq / g for Mg^{2+}, 0.04 meq / g for Ca^{2+}, 0.05 meq / g for K^{+} and 0.12 meq / g Na^{+} by PAN+TiO_2 nanofibres; 0.12 meq / g for Mg^{2+}, 0.06 meq / g for Ca^{2+}, 0.03 meq / g for K^{+} and 0.02 meq / g for Na^{+} by PAN nanofibres and finally 1.20 meq / g for Mg^{2+}, 1.03 meq / g for Ca^{2+}, 0.11 meq / g for K^{+} and 0.09 meq / g for Na^{+} by Purolite S950 resins were achieved from the contact experiments.

FT-IR analysis of PAN nanofibre confirms the characteristic bands of nitrile (C≡N) at about 2250 cm^{-1}, carbonyl at about 1725 cm^{-1} indicating PAN as a copolymer. The FT-IR analysis reveals a broad peak at 470 cm^{-1} signifying the incorporation of titanium dioxide which is the only difference in the FT-IR spectrum of the PAN structure. The same applies to the incorporation of zeolite into the PAN structure where PAN+ZEOLITE nanofibre's FT-IR spectrum showed the peak at 460 cm^{-1} which is assigned to the insensitive internal structure TO_4 (T = Si or Al), indicating the tetrahedral bending peak of zeolite Y. Also, the peak at 685 cm^{-1} is assigned to the external linkage symmetrical stretching, while at around 1055 cm^{-1}, the peak indicates the external linkage asymmetrical of zeolite Y.

The XRD analyses for PAN+TiO_2 and PAN+ZEOLITE further complement the FT-IR spectra of the two nanofibres, showing that the titanium dioxide and the zeolite are incorporated in the PAN nanofibres.

Langmuir and Freundlich sorption equilibrium isotherm models were employed and their parameters were evaluated by fitting the model equations to data obtained from the batch experiments. The sorption mechanism for Mg^{2+}, Ca^{2+}, K^{+} and Na^{+} was found to follow Langmuir isotherm model. The respective sorbents (Purolite S950 resin, PAN nanofibres,

PAN+TiO_2 nanofibres and PAN+ZEOLITE nanofibres) displayed a better fit for the Langmuir model over the Freundlich model, subsequently depicting that the sorption capacities for Mg^{2+}, Ca^{2+}, K^+ and Na^+ ions indicated the sorption occurred at a particular homogeneous site within the sorbents, therefore, no subsequent sorption took place at that particular location once the metal ion occupied the site. This is called a monolayer adsorption.

The Purolite S950 resin had faster kinetics than the respective nanofibres showing that the sorption equilibrium could be reached within 60 minutes. Whereas, the respective nanofibres showed that the sorption equilibrium for the nanofibres could be reached in 120 minutes, having a slower kinetics compared to the Purolite resins. The sorption kinetics of Purolite S950 resin, PAN nanofibres, PAN+TiO_2 nanofibres and PAN+ZEOLITE nanofibres were also analysed for both pseudo-first order and pseudo-second order mechanisms. The rate-controlling step was chemical reaction dependent for all the systems. The pseudo-second order kinetics gave the best correlation of the experimental data, while the pseudo-first order model was only suitable for the initial sorption stages where the process is rapid, but not applicable to the whole sorption process. The pseudo-second order model however gives the best correlation for all the systems.

The enthalpy change (ΔH°) values for the sorption of Mg^{2+}, Ca^{2+}, K^+ and Na^+ ions onto Purolite S950 resin, PAN nanofibre, PAN+TiO_2 nanofibre and PAN+ZEOLITE nanofibre were positive. Therefore, the sorption processes are endothermic for all the sorbents. This means the sorption of the respective metal ions will be favourable at high temperatures. Consequently, the standard enthalpy change suggests that the sorption of Mg^{2+}, Ca^{2+}, K^+ and Na^+ ions onto Purolite S950 resin, PAN nanofibre, PAN+TiO_2 nanofibre and PAN+ZEOLITE nanofibre is basically governed by physisorption (enthalpy magnitude less than 42 kJ/mol). The free energy change (ΔG°) values for all the sorbents are positive, indicating that the sorption process onto the sorbents was non-spontaneous and thermodynamically unfavourable. The order of efficiency, performance and desired attributes of the sorbents can be given as: Purolite S950 resin > PAN+ZEOLITE > PAN+TiO_2 > PAN.

A column study was performed on the Purolite S950 resin using the real Emalahleni brine. Removal efficiency greater than 99.9 % was achieved for the divalent Mg^{2+} and Ca^{2+} ions in a fixed bed mode using 13.75 g of Purolite S950 resin and the passage of 100 mL brine solution through the column at a flow rate of 2.5 mL per minute. The divalent Mg^{2+} and Ca^{2+} ions were sorbed at the same rate. Thereafter, the efficiency of potassium and sodium ions removal was greater than 99.9 % at 10 mL and 20 mL respectively, after which a sharp decline was

observed indicating that some potassium and sodium ions were being eluted after saturation of the sorbent.

The Purolite S950 resins exhibit greater sorption capacity due to the attachment of a functional group (aminophosphonic group) on its surface. It also has faster kinetics and greater selectivity than the respective nanofibres.

5.2 Recommendation

It would be valuable to attach a suitable ligand onto the surface of the nanofibres and subsequently use it to carry out sorption experiments on the wastewater.

REFERENCES

Abufayed, A.A. & El-ghuel, M.K.A. 2001. Desalination process applications in Libya. *Desalination*, 138(1-3):47-53.

Ahmed, M., Arakel, A., Hoey, D. & Coleman, M. 2001. Integrated power, water and salt generation: a discussion paper. *Desalination*, 134(1-3):37-45.

Alaabdula'aly, A.I. & Al-saati. 1995. International Desalination Association Conference, pp 21.

Alexandratos, S.D. 2008. Ion-exchange resins: a retrospective from industrial and engineering chemistry research. *Industrial & Engineering Chemistry Research*, 48(1):388-398.

Alyuz, B. & Veli, S. 2009. Kinetics and equilibrium studies for the removal of nickel and zinc from aqueous solutions by ion exchange resins. *Journal of Hazardous Materials*, 167:482-488.

Al-Faifi, H., Al-Omran, A. M.,Nadeem, M., El-Eter, A.,Khater, H.A. & El-Maghraby,S.E. 2010. Soil deterioration as influenced by land disposal of reject brine from Salbukh water desalination plant at Riyadh, Saudi Arabia. *Desalination,* 250:479–484.

Ahn, Y.C., Park, S.K., Kim, G.T., Hwang, Y.J., Lee, C.G. & Shin, H.S. 2006. Development of high efficiency nanofilters made of nanofibres. *Current Applied Physics*, 6:1030–1035.

Anon, 1986. Management of the water resources of Southern Africa. Pretoria.

Annandale, J. G., Jovanovic, N. Z., Tanner, P. D., Benadé, N., Du plessis, H. M. 2002. The sustainability of irrigation with gypsiferous mine water and implications for the mining industry in South Africa. *Mine Water and the Environment*, 21:81-90.

Aroguz, Z. 2006. Kinetics and thermodynamics of adsorption of azinphosmethyl from aqueous solution onto pyrolyzed (at 600 $^{\circ}$C) ocean peat moss (Sphagnum sp.). *Journal of Hazardous Materials*, 135(1-3):100-105.

Awerbuch, L. & Weekes, M.C. 1990. Disposal of concentrates from brackish water desalting plants by means of evaporation technology. *Desalination*, 78(1):71- 76.

Baumgarten, P.K. 1971. Electrostatic spinning of acrylic microfibres. *Journal of Colloid and Interface Sci*ence, 36:71–9.

Bell, F.G., Bullock, S.E.T., Hälbich, T.F.J. & Lindsay, P. 2001. Environmental impacts associated with an abandoned mine in the Witbank Coalfield, South Africa. *International Journal of Coal Geology*, 45(2-3):195-216.

Bhardwaj, N. & Kundu, S.C. 2010. Electrospinning: A fascinating fibre fabrication technique. *Biotechnology Advances*, 28:325–347.

Boland, E.D., Wnek, G.E., Simpson, D.G., Pawlowski, K.J. & Bowlin, G.L. 2001. Tailoring tissue engineering scaffolds using electrostatic processing techniques: a study of poly (glycolic acid) electrospinning. *Journal of Macromolecular Science, Part A*, 38:1231–43.

Bolto, B. A. & Pawlowski, L. 1987. Wastewater Treatment by Ion exchange. London: McGraw-Hill.

Bourikas K., Hiemstra T. & Van Riemsdijk W.H. 2001. Ion pair formation and primary charging behavior of titanium oxide (anatase and rutile), *Langmuir*, 17(3):749-756.

Buchko, C.J., Chen, C., Shen, Y. & Martin, D.C. 1999. Processing and microstructural characterization of porous biocompatible protein polymer thin films. *Polymer*, 40:7397–7407.

Burhrmann, F., Van Der Walt, M., Hanekan, D. & Finlayson, F. 1999. Treatment of Industrial wastewater for reuse. *Desalination*, 124:263-269.

Calmon, C., 1981. Specific and chelate exchangers: new functional polymers for water and wastewaster treatment. *Journal American Water Works Association*, 73(12):652-656.

Casper, CL., Stephens, J.S., Tassi, N.G., Chase, D.B. & Rabolt, J.F. 2004. Controlling surface morphology of electrospun polystyrene fibers: effect of humidity and molecular weight in the electrospinning process. *Macromolecules*, 37:573–8.

Chanda, M. & Roy, S. K. 2006. *Plastics Technology Handbook*. 4th ed edn. United States: Taylor & Francis.

Chamier, J. 2007. Composite carbon membranes for the desalination of water. Published Master's thesis. Stellebosch: Stellebosch University. South Africa.

Chew, S.Y., Wen, Y., Dzenis, Y. & Leong, K.W. 2006a. The role of electrospinning in the emerging field of nanomedicine. *Current Pharmaceutical Design*, 12:4751–4770.

Chong, E.J., Phan, T.T., Lim, I.J., Zhang, Y.Z., Bay, B.H. & Ramakrishna S. 2007. Evaluation of electrospun PCL/gelatin nanofibrous scaffold for wound healing and layered dermal reconstitution. *Acta Biomaterialia,* 3:321–330.

Coaltech News. 2008. [Online]. Available: www.coaltech.co.za [Accessed 8th August 2011]

Colella, M.B. & Siggla, S. 1980. Poly(acrylamidoxime) Resin for Determination of Trace Metals in Natural Waters. *Analytical Chemistry*, 52(14):2347-2350.

Deitzel, J.M., Kleinmeyer, J., Harris, D. & Tan, N.C.B. 2001. The effect of processing variables on the morphology of electrospun nanofibres and textiles. *Polymer*, 42:261–272.

Demir, M.M., Yilgor, I., Yilgor, E. & Erman, B. 2002. Electrospinning of polyurethane fibers. *Polymer*; 43:3303–3309.

Deng, S., Bai, R. & Chen, J.P., 2003. Behaviours and mechanisms of copper adsorption on hydrolyzed polyacrylonitrile fibers. *Journal of colloid and interface science*, 260(2):265-272.

Desilva, J. 1999. Essentials of Ion Exchange, Presented at 25th W.Q.A. Annual Conference, 1999.

Ding, B., Kim, H.Y., Lee, S.C., Shao, C.L., Lee, D.R. & Park, S.J. et al. 2002. Preparation and characterization of a nanoscale poly (vinyl alcohol) fibre aggregate produced by an electrospinning method. *Journal of Polymer Science B, Polymer Physics*, 40:1261–8.

Doshi, J. & Reneker, D.H. 1995. Electrospinning process and applications of electrospun fibers. *J Electrost*; 35:151–6.

Dosunmu, O.O., Chase, G.G., Kantaphinan, W. & Reneker, D.H. 2006. Electrospinning of polymer nanofibres from multiple jets on a porous tubular surface. *Nanotechnology*, 17:1123–1127.

Economy, J., Dominguez, L. & Mangun, C.L. 2002. Polymeric Ion-Exchange Fibres. *Industrial & Engineering Chemistry Research*, 41(25):6436-6442.

Eichhorn, S.J. & Sampson, W.W. 2005. Statistical geometry of pores and statistics of porous nanofibrous assemblies. *Journal of the Royal Society Interface*, 2:309–318.

El-dessouky, H., Alatiqi, I. & Ettouney, H. 1998. Process synthesis: The multi-stage flash desalination system. *Desalination*, 115(2):155-179.

El-manharawy, S. & Hafez, A. 2003. A new chemical classification system of natural waters for desalination and other industrial uses. *Desalination*, 156(1-3):163-180.

Falkenmark, M., Lundqvist, J. & Widstrand, C. 1989. Macro-scale water scarcity requires micro-scale approaches: aspects of vulnerability in semi-arid development. *Natural Resources Forum*, 13:258–267.

Fang, X. & Reneker, D.H. 1997. DNA fibres by electrospinning. *Journal of Macromolecular Science, Physics B*, 36:169–73.

Feng, D., Van Deventer, J.S.J. & Aldrich, C. 2004. Removal of pollutants from acid mine waste water using metallurgical by-products slags. *Separation and purification technology*, 40:61-67.

Fenglin H., Yunfei X., Shiqin L., Dawei Y., You-Lo H. & Qufu W. 2013. Preparation of Amidoxime Polyacrylonitrile Chelating Nanofibres and Their Application for Adsorption of Metal Ions. *Materials*, 6(3):969-980.

Fisher, S. & Kunin, R. 1955. Routine Exchange Capacity Determinations of Ion Exchange Resins. *Analytical Chemistry*, 27:1191-1194.

Flanigen, E.M., Khatami, H. & Szymanski, H.A. 1971. Molecular Sieve Zeolites. *Advances in Chemistry Series* 101:201-229.

Fong, H., Chun, I. & Reneker, D.H. 1999. Beaded nanofibres formed during electrospinning. *Polymer*, 40:4585–4592.

Formhals, A. 1934. Process and apparatus for preparing artificial threads. U.S. Patent No. 1, 975:504.

Freundlich H., 1926. Adsorption. *Journal of Physical Chemistry*, 7:57-64.

Garg, B.S., Sharma, R.K., Bhojak, N. & Mittal, S. 1999. Chelating resins and their applications in the analysis of trace metal ions. *Microchemical Journal*, 61(2):94-114.

Georgaka, A. & N. Spanos. 2010. Study of the Cu (II) removal from aqueous solutions by adsorption on titania. *Global Nest Journal*, 12(3):239.

Geng, X., Kwon, O.H. & Jang, J. 2005. Electrospinning of chitosan dissolved in concentrated acetic acid solution. *Biomaterials*, 26:5427–5432.

Gibson, P., Schreuder-Gibson, H. & Rivin, D. 2001. Transport properties of porous membranes based on electrospunnanofibres. *Journal of Colloids and Surfaces* A: Physicochemical and Engineering Aspect, 187:469–481.

Glater, J. & Cohen, Y. 2003. Brines disposal from land based membrane desalination plants: A critical assessment. Prepared for the Metropolitan Water District of Southern California.

Gode, F. & Pehlivan, E. 2003. A comparative study of two chelating ion exchange resins for the removal of chromium(III) from aqueous solution. *Journal of Hazardous Materials*, 100(1-3):231-243.

Greig, J. A. 2000. Society of chemical industry (Great Britain), ed. *Ion Exchange at the Millennium: Proceeding of IEX 2000*. World Scientific.

Grenlee, L.F., Lawler, D.F., Freeman, D.B., Marrot, B. & Moulin, P. 2009. "Reverse osmosis desalination: Water sources, technology and today's challenges". *Water Research*, 43:2317-2348.

Gun'ko, V.M., Leboda, R., Skubiszewska-ziêba, J., Gawdzik, B. & Charmas, B., 2005. Structural characteristics of porous polymers treated by freezing with water or acetone. *Applied Surface Science*, 252(3):612-618.

Gunther, P. & Naidu, T. 2008. Mine Water reclamation: Towards zero disposal. Proceedings of the Biennial WISA Conference, Sun City, South Africa.

Gupta, P., Elkins, C., Long, T.E. & Wilkes, G.L. 2005. Electrospinning of linear homopolymers of poly(methylmethacrylate): exploring relationships between fibre formation, viscosity, molecular weight and concentration in a good solvent. *Polymer*, 46:4799–4810.

Hagfeldt, A. & Graetzel, M. 1995. Light-induced redox reactions in nanocrystalline systems. *Chemical Reviews*, 95(1):49-68.

Haghi, A.K. & Akbari, M. 2007. Trends in electrospinning of natural nanofibres. *Physica Status Solidi*, 204:1830–1834.

Hakkarainen, M. 2002. Aliphatic polyesters: abiotic and biotic degradation and degradation products. *Advanced Polymer Science*, 157:113–138.

Harland, C.E., 1994. Ion Exchange: Theory and Practice. 2nd ed. Cambridge, England: Royal Society of Chemistry.

Hayati, I., Bailey, A.I. & Tadros, T.F. 1987. Investigations into the mechanisms of electrohydrodynamic spraying of liquids. Effect of electric-field and the environment on pendant drops and factors affecting the formation of stable jets and atomization. *Journal of Colloid and Interface Science,* 117:205–221.

Helfferich, F.G. 1962. Ion Exchange. McGraw-Hill, pp. 5-9; 35-36; 72-94.

Henrich V.E. & Cox P.A. 1994. The Surface Science of Metal Oxides, Cambridge Univ. Press, Cambridge, UK.

Ho, B.C., Lee, Y.D. & Chin, W.K. 1992. Thermal degradation of polymethacrylic acid. *Journal of Polymer Science*: *Polymer Chemistry*, 30:2389–2397.

Ho, Y.S. 2003. "Removal of copper ions from aqueous solution by tree fern", *Water Research,* 37:2323–2330.

Ho, S. & McKay, G. 1998. "The kinetics of sorption of basic dyes from sphagnum. moss peat", *Canadian Journal of Chemical Engineering*, 76(4):822-827.

Hohman, M.M., Shin, M., Rutledge, G. & Brenner, M.P. 2001. Electrospinning and electrically forced jets. II. Applications. *Physics of Fluids*; 13:2221–2236.

Holmberg, B.A., Haunting, W., Joseph, M.N. & Yan Y. 2003. Controlling size and yield of zeolite Y nanocrystals using tetramethylammonium bromide. Microporous and Mesoporous Materials 59 (2003) 13–28. PMAA blends and PMMA-co-PMAA copolymers. *Polymer*, 44:2965–2974.

Houssin, C.J.M. 2003. Nanoparticles in zeolite synthesis. Proof script.

How, T.V., Guidoin, R. & Young, S.K. 1992. Engineering design of vascular prostheses, proceedings of the institution of mechanical engineers. Part H. *Journal of Engineering in Medicine*, 206:61–72.

Huang, C.F. & Chang, F.C. 2003. Comparison of hydrogen bonding interaction between PMMA/ PMAA blends and PMMA-co-PMAA copolymers. *Polymer,* 44:2965–2974.

Huang, L., Nagapud,i K., Apkarian, R.P., Chaikof, E.L. 2001a. Engineered collagen-PEO nanofibres and fabrics. *Journal of Biomaterial Science, Polymer Edition*, 12:979–993.

Huang, Z.M., Zhang, Y.Z., Kotaki, M. & Ramakrishna, S. 2003. A review on polymer nanofibres by electrospinning and their applications in nanocomposites. *Composite Science and Technology*, 63:2223–2253.

Hubicki, Z. & Kołodyńska, D. 2012. Selective removal of heavy metal ions from waters and waste waters using ion exchange methods. INTECH Open Access Publisher.

Hufschmidt, M.M. & Kindler, J. 1991. Approaches to Integrated Water Resources Management in Humid Tropical and Arid and Semiarid Zones in Developing Countries, UNESCO Technical Documents in Hydrology, UNESCO, Paris

Iqbal, M.,Saeed, A. & Zafar, S.I. 2007. Hybrid biosorbent: an innovative matrix to enhance the biosorption of Cd(II) from aqueous solution, *Journal of Hazardous Materials*, 148:47–55.

Jain, C.K., Singhal, D.C. & Sharma, M.K. 2004. Adsorption of zinc on bed sediment of River Hindon: Adsorption models and kinetics. *Journal of Hazardous Materials*, 114:231–239.

Jarusuwannapoom, T., Hongroijanawiwat, W., Jitjaicham, S., Wannatong, L., Nithitanakul, M. & Pattamaprom, C, et al. 2005. Effect of solvents on electro-spinnability of polystyrene solutions and morphological appearance of resulting electrospun polystyrene fibers. *European Polymer Journal*, 41:409–421.

Jiang, H.L., Fang, D.F., Hsiao, B.S., Chu, B. & Chen, W.L. 2004a. Optimization and characterization of dextran membranes prepared by electrospinning. *Biomacromolecules*, 5: 326–333.

Jun, Z., Hou, H., Schaper, A., Wendorff, J.H. & Greiner, A. 2003. Poly-L-lactide nanofibres by electrospinning - influence of solution viscosity and electrical conductivity on fibre diameter and fibre morphology. *e-Polym*ers, 9:1–9.

Khedr, M.G. 2008. Membrane methods in tailoring simpler, more efficient, and cost effective wastewater treatment alternatives. *Desalination*, 222(1-3):135-145.

Kelesoglu, S. 2007. Comparative adsorption studies of heavy metal ions on chitin and chitosan biopolymers. Unpublished Master's thesis. Izmir: Izmir Institute of Technology. Turkey.

Kenawy, E.R., Bowlin, G.L. & Mansfield, K. 2002. Release of tetracycline hydrochloride from electrospunpoly(ethylene-co-vinylacetate), poly(lactic acid), and a blend. *Journal of Control Release*, 81:57–64.

Khawaji, A.D., Kutubkhanah, I.K. & Wie, J. 2008. Advances in seawater desalination technologies. *Desalination*, 221(1-3):47-69.

Ki, C.S., Baek, D.H., Gang, K.D., Lee, K.H., Um, I.C. & Park, Y.H. 2005. Characterization of gelatin nanofibre prepared from gelatin-formic acid solution. *Polymer*, 46:5094–5102.

Kidoaki, S., Kwon, I.K. & Matsuda, T. 2005. Mesoscopic spatial designs of nano and microfibre meshes for tissue-engineering matrix and scaffold based on newly devised multilayering and mixing electrospinning techniques. *Biomaterials*, 26:37–46.

Kim M.S., Hong K.M. & Chung J.G. 2003. Removal of Cu(II) from aqueous solutions by adsorption process with anatase-type titanium dioxide. *Water Research*, 37(14):3524-3529

Korngold, E., Aronov, L. & Daltrophe, N. 2000. Electrodialyis of brine solutions discharged from RO plant. *Desalination*, 242:215-227.

Kunin, R. 1976. The Use of macroreticular polymeric adsorbents for the treatment of waste effluents. *Pure & Applied Chem*istry, 46:205-211.

Kurniawan, T.A., Chan, G.Y.S., LO, W. & Babel, S. 2006. Physico–chemical treatment techniques for wastewater laden with heavy metals. *Chemical Engineering Journal*, 118(1-2):83-98.

Lattemann, S. & Höpner, T. 2008. Environmental impact and impact assessment of seawater, *Desalination*, 220:1–15.

Lee, L.Y., Ng, H.Y., Ong, H.Y.S.L., Hu, J.Y., Tao, G., Kekre, K., Viswanath, B., Lay, W., & Seah, H. 2009. Ozone-biological activated carbon as a pretreatment process for reverse osmosis brine treatment and recovery. *Water Research*, 43:3948–3955.

Legrini O., Oliveros E. & Braun A.M. 1993. Photochemical processes for water-treatment, *Chemical Reviews*, 93(2):671-698.

Li, D. & Xia, Y. 2004. Electrospinning of nanofibres: reinventing the wheel. *Advanced Materials*, 16:1151–1170.

Lieser, K.H. 1979. New Ion Exchangers, Preparation, Properties and Application. *Pure & Applied Chemistry*, 51:1503–1517.

Liu, H.,Kameoka, J.,Czaplewski, D.A. & Craighead,H.G. 2004. Polymeric nanowire chemical sensor. *Nano Letters*, 4:671–675.

Liu, Y. & He, J.H. 2007. Bubble electrospinning for mass production of nanofibres. *International Journal of Nonlinear Sciences and Numerical Simulation*, 8:393–396.

Lloyd, P.J. 2002. Coal and the environment. JBA: Durban Energy Institute, University of Cape Town.

Ma, Z.W., Masaya, K. & Ramakrishna, S. 2006. Immobilization of Cibacron blue F3GA on electrospunpolysulphone ultra-fine fibre surfaces towards developing an affinity membrane for albumin adsorption. *Journal of Membrane Science*, 282:237–244

Mall, I.D. & Upadhyay, S.N. 1998. Studies on treatment of basic dyes bearing wastewater by adsorptive treatment using fly ash. *Indian Journal of Environmental Health*. 40:177.

Mauguin, G. & Corsin, P. 2005. Concentrate and other waste disposals from SWRO plants: characterization and reduction of their environmental impact. *Desalination*, 182(1-3):355-364.

Mickley, M., Hamilton, R., Gallengoes, L. & Truesdall, J. 1993. Membrane concentration disposal. Denver, Colorado: American Water works Association Research Foundation.

Miretzky, P., Saralegui, A. & Cirelli, A.F. 2006. Simultaneous heavy metal removal mechanism by dead macrophytes. *Chemosphere*, 62:247–254.

Mit-uppatham, C., Nithitanakul, M. & Supaphol, P. 2004. Ultrafine electrospun polyamide-6 fibers:effect of solution conditions on morphology and average fiber diameter. *Macromolecular Chemistry and Physics*, 205:2327–2338.

Mohamed, A. M. O., Maraqa, M. & Al Handhaly, J. 2005. Impact of Land Disposal of Reject Brine from Desalination Plants on Soil and Groundwater, *Desalination*, 182:411-433.

Mohammadi, M.R., Fray, D.J. & Cordero-Cabrera, M.C. 2007. Sensor performance of nanostructured TiO_2 thin films derived from particulate sol-gel route and polymeric fugitive agents. *Sensors and Actuatuators B: Chemical*, 124(1):74-83.

Moser, J.E., Bonnôte, P. & Grätzel M. 1998. Molecular photovoltaics. Coordination *Chemistry Reviews*, 171(1):245-250.

Mumpton, F.A. 1999. La roca magica, Uses of natural zeolites in Agriculture and industry. *Proceedings of National Academy of science*, 96:346-347.

Naiya T.K., Bhattacharya A.K. & Das S.K. 2009. Adsorption of Cd(II) and Pb(II) from aqueous solutions on activated alumina, *Journal of Colloid and Interface science*, 333(1):14-26.

Neghlani, P.K.; Rafizadeh, M. & Taromi, F.A.2011. Preparation of aminated-polyacrylonitrilenanofibre membranes for the adsorption of metal ions: Comparison with microfibres. *Journal of Hazardous Materials*, 186:182–189.

Ndlovu-Yalala, B. 2010. Ion exchange resins and functional fibres: A comparative Study for the treatment of brine. Unpublished Master's thesis. Bellville: University of the Western Cape. South Africa.

Oren, Y., Korngold, E., Daltrophe, N., Messalem, R., Volkman, Y., Aronov, L., Weisman, M., Bouriakov, N., Glueckstern, P. & Gilron, J. 2010. Pilot studies on high recovery BWRO-EDR for near zero liquid discharge approach, *Desalination*, 261:321–330.

Ohgo, K., Zhao, C., Kobayashi, M. & Asakura, T. 2003. Preperation of non- woven nanofibres for Bombyx mori silk, Samia cythia ricini silk and recombinant hybrid silk with electrospinnning method. *Polymer*, 44:841–846.

Ohkawa, K., Kim, H., Lee, K. & Yamamoto, H. 2004a. Electrospun non-woven fabrics of poly(ecaprolactone) and their biodegradation by pure cultures of soil filamentous fungi. *Macromolecular Symposia*, 216:301–306.

Olsson M., Jakobsson A.M. & Albinsson Y. 2003. Sorption of Pu(VI) onto TiO_2, *Journal of Colloid and Interface Science*, 266(2):269-275.

Pawlowski, K.J., Barnes, C.P., Boland, E.D., Wnek, G.E. & Bowlin, G.L. 2004. Biomedical nanoscience: electrospinning basic concepts, applications, and classroom demonstration. *MRS Proceedings* 827:17–28.

Pereira, L S., Cordery, I. & Iacovides, I. 2002. Coping with water scarcity. No. 58. Paris: UNESCO

Pesavento M., Biesuz, R. & Cortina J. L., 1994. Sorption of Metal Ions on a Weak Cation-Exchange Resin Containing Carboxylic Groups. *Analytica Chimica Acta*, 298:225-235.

Pham, Q.P., Sharma, U. & Mikos, A.G. 2006. Electrospinning of polymeric nanofibres for tissue engineering applications: A review. *Journal of Tissue Engineering*, 12:1197–1211.

Pierschbacher, M.D. & Ruoslahti, E. 1984. Cell attachment activity of fibronectin can be duplicated by small synthetic fragments of the molecule. *Nature*, 309:30–33.

Pruss, A., Kay, D., Fewtrell, L. & Bartram J. 2002. Estimating the burden of disease from water, sanitation, and hygiene at a global level. *Environmental Health Perspectives*, 110(5):537–542.

Ramakrishna, S., Fujihara, K., Teo, W.E., Yong, T., Ma, Z. & Ramaseshan, R. 2006. Electrospun nanofibres: solving global issues. *Materials Today*, 9:40–50.

Rao, N.S., Venkateswara, R.T.N., Rao, G.B. & Rao, K.V.G. 1990. Impact of reject water from the desalination plants on ground water quality. *Desalination*, 78:429–437.

Reneker, D.H. & Chun, L. 1996. Nanometre diameters of polymer, produced by electrospinning. *Nanotechnology*, 7:216–223.

Reneker, D.H., Yarin, A.L., Fong, H. & Koombhongse, S. 2000. Bending instability of electrically charged liquid jets of polymer solutions in electrospinning. *Journal of Applied Physics*, 87:4531–4547.

Rengaraj, S., Yeon, K. & Moon, S., 2001. Removal of chromium from water and wastewater by ion exchange resins. *Journal of hazardous materials*, 87(1-3):273-287.

Rijsberman, F.R., 2006. Water scarcity: Fact or fiction? *Agricultural Water Management*, 80(1-3):5-22.

Ryu, Y.J., Kim, H.Y., Lee, K.H., Park, H.C. & Lee, D.R. 2003. Transport properties of electrospun nylon 6 non-woven mats. *European Polymer Journal*, 39:1883–1889

Sadhwani, J. J., Veza, J. M. & Santana C. 2005. Case studies on environmental impact of seawater desalination, *Desalination*, 185:1–8.

Saeed, K., Haider, S., Oh, T.J. & Park, S.Y. 2008. Preparation of amidoxime-modified polyacrylonitrile (PAN-oxime) nanofibres and their applications to metal ions adsorption. *Journal of Membrane Science*, 322:400–405.

Saito, N., Okada, T., Horiuchi, H., Murakami, N., Takahashi, J. & Nawata, M. et al. 2001. Biodegradable polymer as a cytokine delivery system for inducing bone formation. *Nature Biotechnology*, 19:332–335.

Samczy ski Z. & Dybezy ski R. 1997. Some Examples of the Use of Amphoteric Ion-Exchange Resins for Inorganic Separations. *Journal of Chromatography A*, 789:157-167.

Sang, Y., Gu, Q. & Sun, T. 2008. Filtration by a novel nanofibre membrane and alumina adsorption to remove copper (II) from groundwater. *Journal of Hazardous Materials*, 153:860–866.

Schlacher, T. A. & Wooldridge, T. H. 1996. Ecological responses to reductions in freshwater supply and quality in South Africa's estuaries: lessons for management and conservation. *Journal of Coastal Conservation*, 2:115-130.

Schoeman, J.J. & Steyn, A. 2001. Investigation into alternative water treatment technologies for the treatment of underground mine water discharged by Grootvlei Proprietary Mines Ltd into the Blesbokspruit in South Africa. *Desalination,* 133(1):13-30.

Schwarzenbach, R.P, Gschwend, M.P. & Imboden, D.M. 2003. *Environmental Organic Chemistry*. (John Wiley & Sons, Inc. Publication, Canada).

Sekar, M., Sakthi, V. & Rengaraj, S. 2004. Kinetics equilibrium adsorption study of lead(II) onto activated carbon prepared from coconut shell. *Journal of Colloid and Interface Science*, 79:307–313.

Shin, D.H.,Ko, Y.G., Choi, U.S. & Kim, W.N. 2004. Design of high efficiency chelate fibres with an amine group to remove heavy metal ions and pH-related FT-IR analysis. *Journal of Industrial and Engineering Chemistry Research*, 43:2060–2066.

Shoushtari, A.M., Zargaran, M. & Abdouss, M. 2006. Preparation and characterization of high efficiency ion-exchange cross linked acrylic fibres. *Journal of Applied Polymer Science*, 101:2202–2209.

Sill, T.J. & Recum, H.A.V. 2008. Electrospinning: applications in drug delivery and tissue engineering. *Biomaterials*, 29:1989–2006.

Singh, A.K., Singh, D.P. & Singh, V.N. 1998. Removal of Zn(II) from water by adsorption on China clay. *Environmental Technology Letters*, 9:1153–1162.

Sivaraj, R., Namasivayam, C. & Kadirvelu, K. 2001. Orange peel as an adsorbent in the removal of acid violet 17 (acid dye) from aqueous solution. *Waste Management*, 21:105-110.

Son, W.K., Youk, J.H. & Park, W.H. 2004a. Preparation of ultrafine oxidized cellulose mats via electrospinning. *Biomacromolecules*, 5:197–201.

Son, W.K., Youk, J.H., Lee, T.S. & Park, W.H. 2004b. Electrospinning of ultrafine cellulose acetate fibres: studies of a new solvent system and deacetylation of ultrafine cellulose acetatefibres. *Journal of Polymer Science B, Polymer Physics*, 42:5-11.

Sonqishe, T., Balfour, G., Iwouha, E. & Petrik, L. 2009. Treatment of brines using commercial zeolites and zeolites synthesized from fly ash derivative. Proceedings of International Mine Water Conference, Pretoria, South Africa. 695-702.

Stankus, J.J., Guan, J., Fujimoto, K. & Wagner, W.R. 2006. Microintegrating smooth muscle cells into a biodegradable, elastomeric fibre matrix. *Biomaterials*, 27:735–744.

Stratton, C. L. & Lee, G. F. 1975. Cooling Towers and Water Quality. *Journal of Water Pollution Control Federation*, 47(7):1901-1912.

Subbiah, T., Bhat, G.S., Tock, R.W., Parameswaran, S. & Ramkumar, S.S. 2005. Electrospinning of nanofibres. *Journal of Applied Polymer Science*, 96:557–569.

Subramani, A., DeCarolis, J., Pearce, W. & Jacangelo, J.G. 2012. Vibratory shear enhanced process (VSEP) for treating brackish water reverse osmosis concentrate with high silica content, *Desalination*, 291:15–22.

Sukigara, S., Gandhi, M., Ayutsede, J., Micklus, M. & Ko, F. 2003. Regeneration of Bombyx mori silk by electrospinning. Part 1. Processing parameters and geometric properties. *Polymer*, 44:5721–5727.

Svensson, M. 2005. Desalination and the Environment: Options and considerations for brine disposal in inland and coastal locations. Yara International and Aqualying. SLU Uppsala. Department of Biometry and Engineering ISSN 1652-3245.

Szotsak, R. 1989. Molecular sieves, Principles of synthesis and identification. Van Nostrand Reinhold, New York.

Tahaei, P., Abdouss, M., Edrissi, M., Shoushtari, A.M. & Zargaran, M. 2008. Preparation of chelating fibrous polymer by different diamines and study on their physical and chemical properties. *Material. Science and Engineering Technology*, 39:839–844.

Tan, E.P.S., Ng, S.Y. & Lim, C.T. 2005a. Tensile testing of a single ultrafine polymeric fibre. *Biomaterials*, 26:1453–1456.

Tang, W. & Yong, H.Y. 2008. Concentration of brine by forward osmosis: Performance and influence of membrane structure. *Desalination*, 224(1-3):143-153.

Theron, S.A., Yarin, A.L., Zussman, E. & Kroll, E. 2005. Multiple jets in electrospinning: experiment and modeling. *Polymer*, 46:2889–2899.

Tsiourtis, N.X. 2001. Desalination and the environment. *Desalination*, 141(3):223-236.

Turek, M. 2004. Electrodialytic desalination and concentration of coal-mine brine. *Desalination*, 162:355-359.

Vadivelan, V. & Kumar, K.V. 2005. Equilibrium, kinetics, mechanism, and process design for the sorption of methylene blue onto rice husk. *Journal of Colloid and Interface Science*, 286:90-100

Valerdi-Perez, R., Lopez-Rodriguez, M. & Ibanez-Mengual, J.A., 2001. Characterizing an electrodialysis reversal pilot plant. *Desalination,* 137(1-3):199-206.

Vandenborre J., Drot R. & Simoni E. 2007. Interaction mechanisms between uranium(VI) and rutile titanium dioxide: From single crystal to powder, *Inorganic Chemistry*, 46(4), 1291-1296.

Varabhas, J.S., Chase, G.G. & Reneker, D.H. 2008. Electrospun nanofibres from a porous hollow tube. *Polymer*, 49:4226–4229.

Veli, S. & Pekey, B. 2004. Removal of copper from aqueous solutions by ion exchange resins. *Fresenius Environmental Bulletin*, 13:244-250.

Wallace, J.S. 2000. Increasing agricultural water efficiency to meet future food production. *Agriculture Ecosystems & Environment*, 82:105–119.

Wang, M., Hsieh, A.J. & Rutledge, G.C. 2005a. Electrospinning of poly (MMA-co-MAA) copolymers and their layered silicate nanocomposites for improved thermal properties. *Polymer*, 46:3407–3418.

Wang, Y., Lin, S. & Juang, R. 2003. Removal of heavy metal ions from aqueous solutions using various low-cost adsorbents. *Journal of hazardous materials*, 102(2-3):291-302.

Welle, A., Kroger, M., Doring, M., Niederer, K., Pindel, E. & Chronakis S. 2007. Electrospun aliphatic polycarbonates as tailored tissue scaffold materials. *Biomaterials*, 28, 2211–2219.

WHO see World Health Organization

Willis, J.P., 1987. Variation in the composition of South African fly ash. Ash – a valuable resource. *Council for Science and Industrial Research*, 3:2-6.

Winters, J.C. & Kunin, R., 1949. Ion Exchange in the Pharmaceutical Field. *Industrial & Engineering Chemistry*, 41(3):460-463.

Wnek, G.E., Carr, M.E., Simpson, D.G. & Bowlin, G.L. 2003. Electrospinning of nanofibres fibrinogen structures. *Nano Letters,* 3:213–216.

Wong, K.K., Lee, C.K., Low, K.S. & Haron, M.J., 2003. Removal of Cu and Pb by tartaric acid modified rice husk from aqueous solutions. *Chemosphere*, 50(1):23-28.

Wu, R.S.S. & Lau, T.C., 1996. Polymer-ligands: a novel chemical device for monitoring heavy metals in the aquatic environment. *Marine pollution bulletin*, 32(5):391-396.

Yang, J., Yu, M. & Qiu, T. 2014. Adsorption thermodynamics and kinetics of Cr(VI) on KIP210 resin. *Journal of Industrial and Engineering Chemistry,* 20:480–486.

Yarin, A.L. & Zussman, E. 2004. Upward needleless electrospinning of multiple nanofibres. *Polymer*, 45:2977–2980.

Yavuz, O., Altunkaynak, Y. & Guzel, F. 2003. Removal of copper, nickel, cobalt and manganese from aqueous solution by kaolinite. *Water Research*, 37(4):948-952.

Yuan, X.Y., Zhang, Y.Y., Dong, C.H. & Sheng, J. 2004. Morphology of ultrafine polysulfone fibers prepared by electrospinning. *Polymer International*, 53:1704–1710.

Zagorodgni, A.A. 2006. Ion Exchange Materials: Properties and Application. London: Elsevier Oxford.

Zamzow, M.J. & Murphy, J.E. 1992. Removal of metal cations from water using zeolites. *Separation Science and Technology,* 24 (14):1969-1984.

Zhang, C., Yuan, X., Wu, L., Han, Y. & Sheng, J. 2005b. Study on morphology of electrospun poly (vinylalcohol) mats. *European Polymer Journal*, 41:423–432.

Zhang, L., Kanki, T., Sano, N. & Toyoda, A. 2003. Development of TiO_2 photocatalyst reaction for water purification. *Separation and Purification Technology*, 31(1):105-110.

Zhao, H., Vance, G.F., Ganjegunte, G.K., Urynowioz, M.A. 2007. Use of zeolite for treating gas co-produces water in Wyoming in USA. *Desalination*, 228:263-276.

Zoumis, T., Calmano, W. & Forstens, U. 2000. Demobilization of heavy metals from mine waters. *Acta hydrochimica et hydrobiologica*, 24 (4):212-218.

Zuo, W.W., Zhu, M.F., Yang, W., Yu, H., Chen, Y.M. & Zhang, Y. 2005. Experimental study on relationship between jet instability and formation of beaded fibers during electrospinning. *Polymer Engineering and Science*, 45:704–709

Zussman, E., Theron, A. & Yarin, A.L. 2003. Formation of nanofibre crossbars in electrospinning. *Applied Phyicss Letters*, 82:973–975.

APPENDICES

7.1 Equilibrium Adsorption Isotherm

In this section, the equilibrium sorption isotherm results, table and graphs depicting the sorption for magnesium, calcium, potassium and sodium are presented. The Langmuir and Freundlich modeling results are also shown.

Appendix A: The equilibrium concentration versus metal ion adsorption for magnesium by Purolite S950 resin, PAN, PAN+TiO_2 and PAN+ZEOLITE

Concentration (mg/L)	**Purolite S950 Resin**		**PAN**		**PAN+TiO_2**		**PAN+ZEOLITE**	
	C_e	q_e	C_e	q_e	C_e	q_e	C_e	q_e
100	14	3.5	3	0.75	1	0.25	5	1.25
200	30	7.5	5	1.25	9	0.5	21	5.25
300	35	8.75	10	2.5	11	1.25	48	12
400	75	18.75	50	12.5	49	1.75	104	26
500	125	31.25	50	12.5	85	7.25	107	26.75

Appendix B: The equilibrium concentration versus metal ion adsorption for calcium by Purolite S950 resin, PAN, PAN+TiO_2 and PAN+ZEOLITE

Concentration (mg/L)	**Purolite S950 Resin**		**PAN**		**PAN+TiO_2**		**PAN+ZEOLITE**	
	C_e	q_e	C_e	q_e	C_e	q_e	C_e	q_e
100	20	5	1	0.25	1	0.25	1	0.25
200	35	8.75	1	0.25	2	0.5	12	3
300	35	8.75	2	0.5	5	1.25	28	7
400	75	18.75	5	1.25	7	1.75	74	18.5
500	113	28.25	23	5.75	29	7.25	74	18.5

Appendix C The equilibrium concentration versus metal ion adsorption for potassium by Purolite S950 resin, PAN, PAN+TiO_2 and PAN+ZEOLITE

Concentration (mg/L)	**Purolite S950 Resin**		**PAN**		**PAN+TiO_2**		**PAN+ZEOLITE**	
	C_e	q_e	C_e	q_e	C_e	q_e	C_e	q_e
100	2	0.5	1	0.25	2	0.5	1	0.25
200	5	1.25	1	0.25	3	0.75	1	0.25
300	10	2.5	2	0.5	10	2.5	7	1.75
400	15	3.75	5	1.25	20	5	9	2.25
500	20	5	6	1.5	30	7.5	13	3.25

Appendix D The equilibrium concentration versus metal ion adsorption for sodium by Purolite S950 resin, PAN, PAN+TiO_2 and PAN+ZEOLITE

Concentration (mg/L)	**Purolite S950 Resin**		**PAN**		**PAN+TiO_2**		**PAN+ZEOLITE**	
	C_e	q_e	C_e	q_e	C_e	q_e	C_e	q_e
100	1	0.25	1	0.25	1	0.25	2	0.5
200	2	0.5	1	0.25	2	0.5	3	0.75
300	2	0.5	2	0.25	3	0.33	11	2.75
400	5	0.2	3	0.75	3	0.33	54	13.5
500	15	0.07	10	2.5	15	0.066	54	13.5

Appendix E: (a) Linearized form of Langmuir and (b) linearized form of Freundlich for the sorption of K^+ ions by Purolite S950 resin.

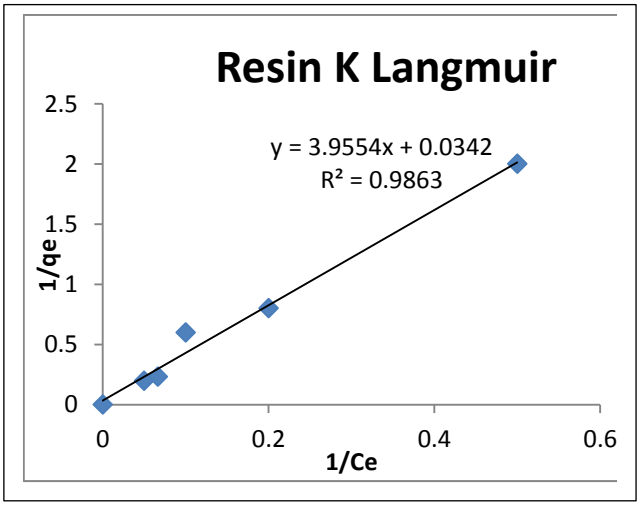

(a)

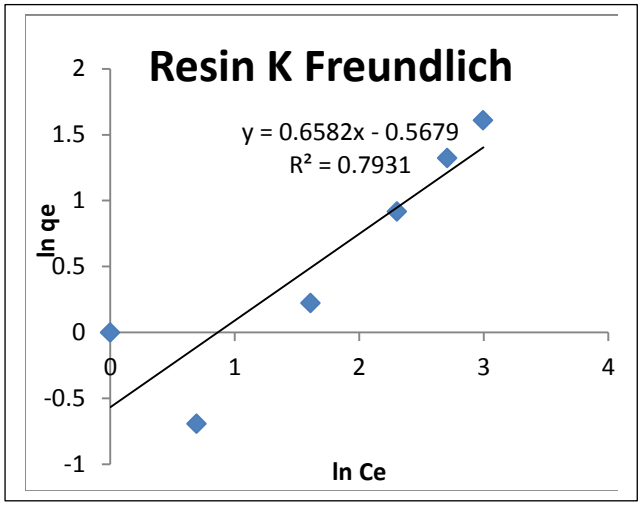

(b)

Appendix F: (a) Linearized form of Langmuir and (b) linearized form of Freundlich for the sorption of Na^+ ions by Purolite S950 resin.

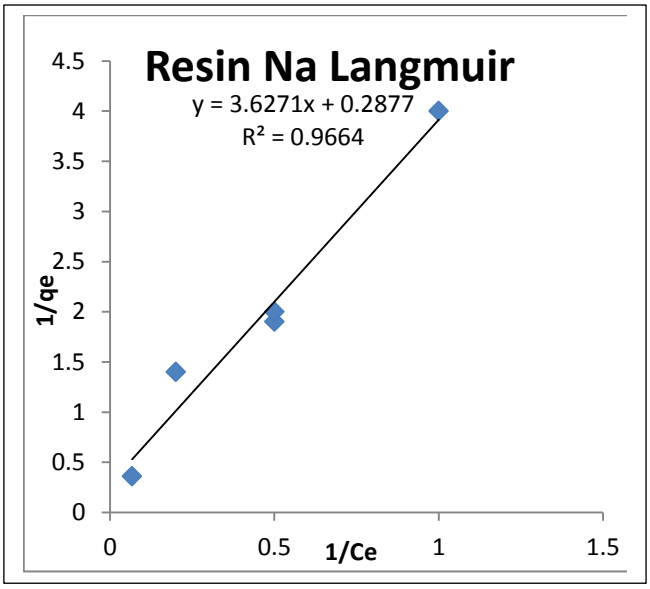

(a)

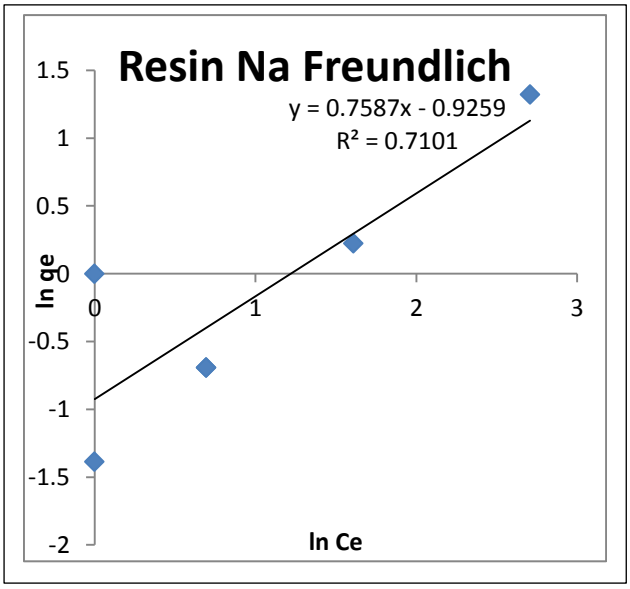

(b)

Appendix G: (a) Linearized form of Langmuir and (b) linearized form of Freundlich for the sorption of Ca^{2+} ions by Purolite S950 resin.

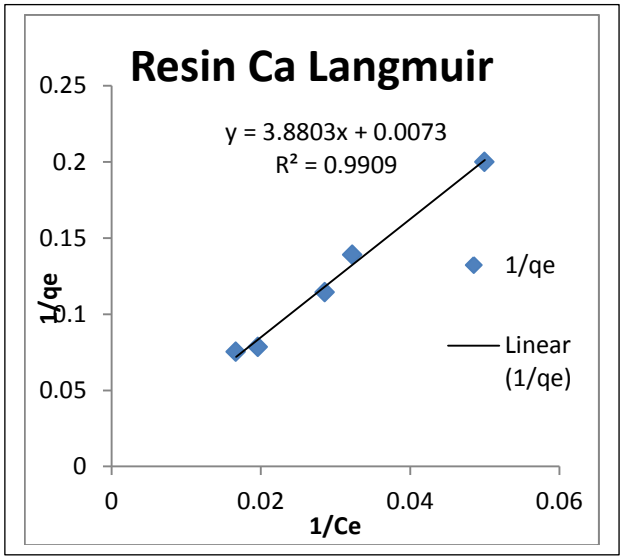

(a)

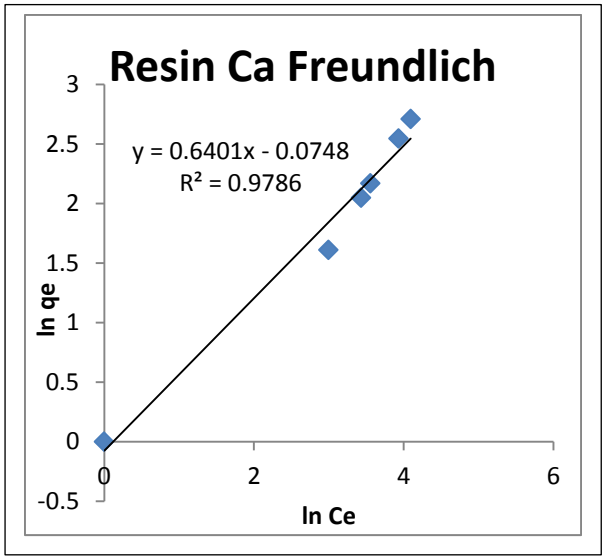

(b)

Appendix H: (a) Linearized form of Langmuir and (b) linearized form of Freundlich for the sorption of Mg^{2+} ions by Purolite S950 resin.

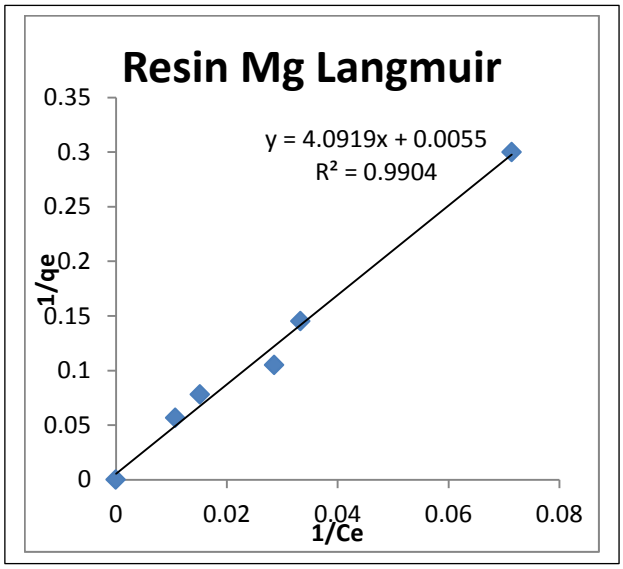

(a)

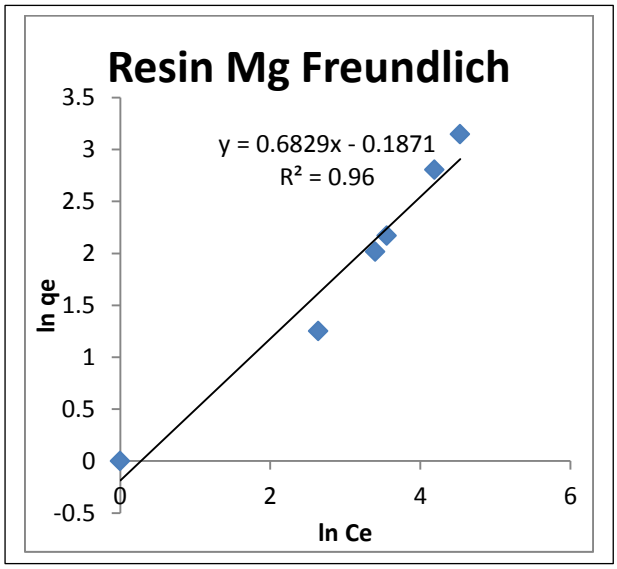

(b)

Appendix I (a) Linearized form of Langmuir and (b) linearized form of Freundlich for the sorption of Na^+ ions by PAN nanofibre.

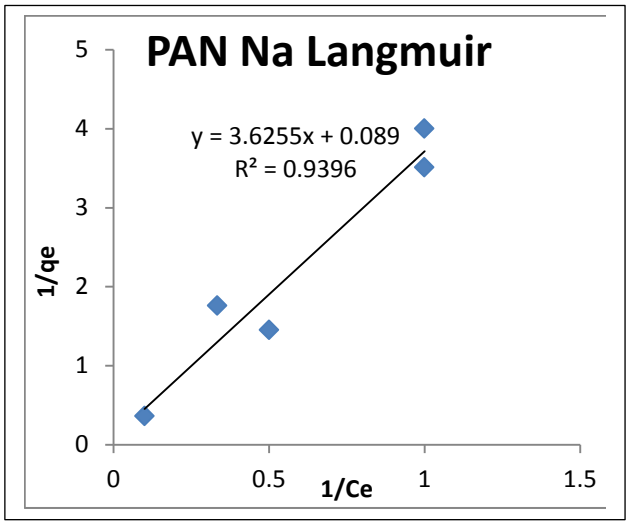

(a)

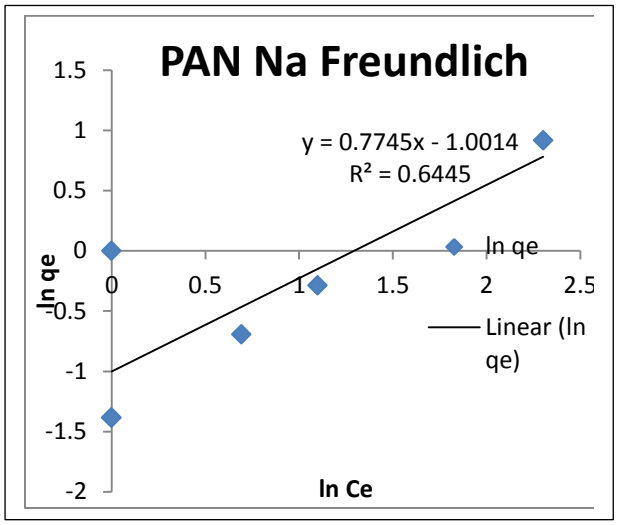

(b)

Appendix J (a) Linearized form of Langmuir and (b) linearized form of Freundlich for the sorption of K^+ ions by PAN nanofibre.

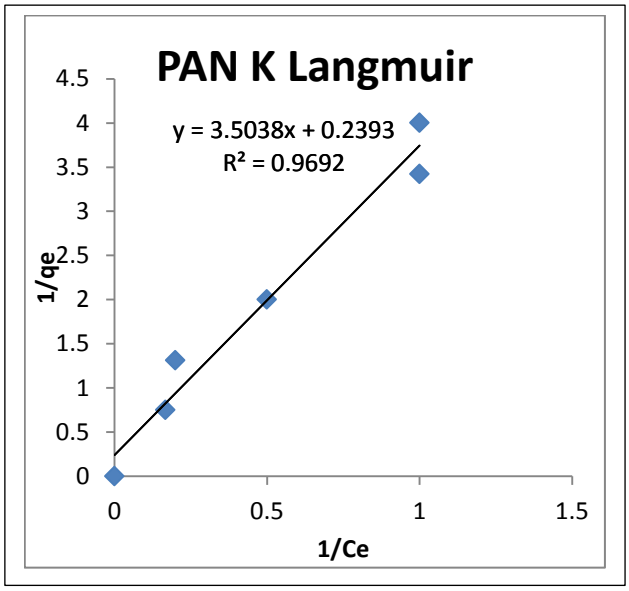

(a)

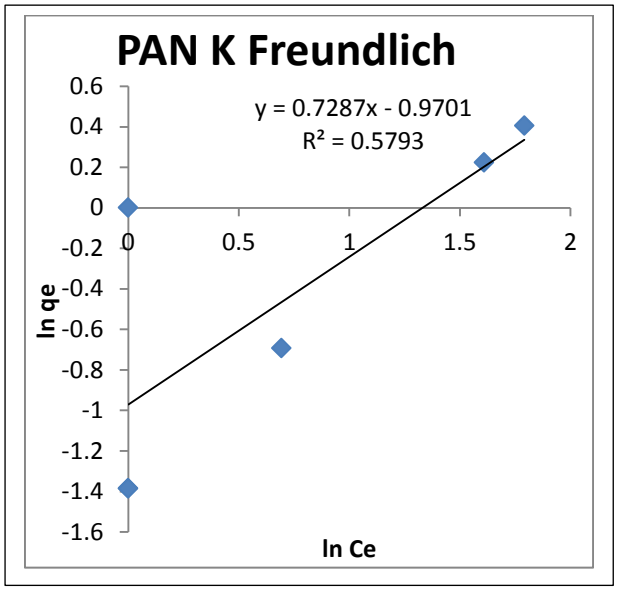

(b)

Appendix K: (a) Linearized form of Langmuir and (b) linearized form of Freundlich for the sorption of Ca^{2+} ions by PAN nanofibre.

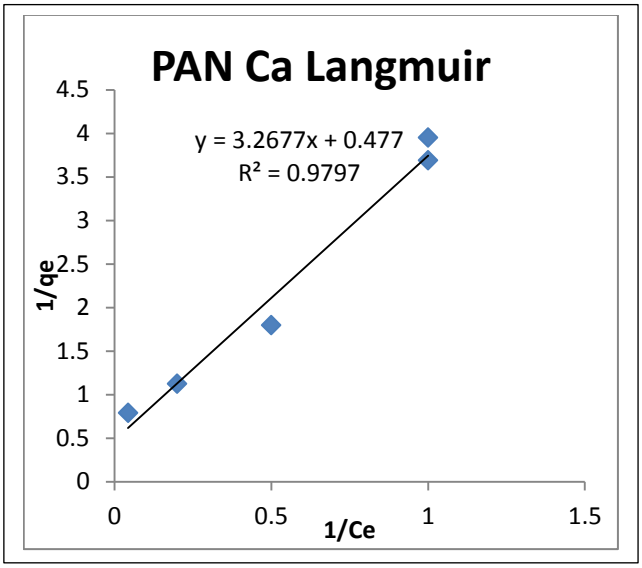

(a)

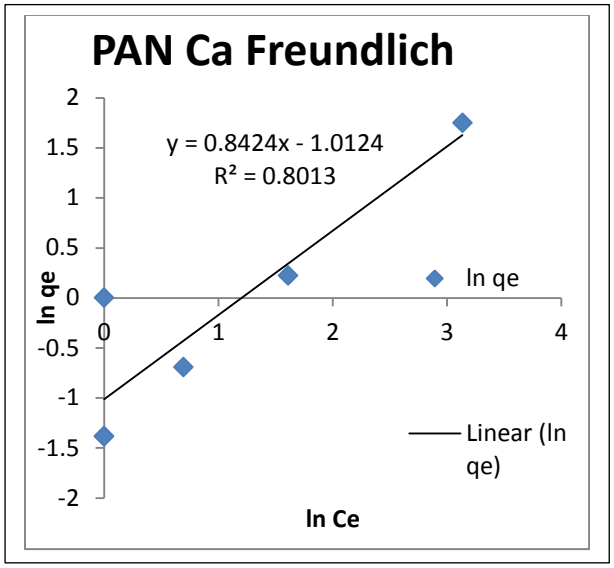

(b)

Appendix L: (a) Linearized form of Langmuir and (b) linearized form of Freundlich for the sorption of Mg^{2+} ions by PAN nanofibre.

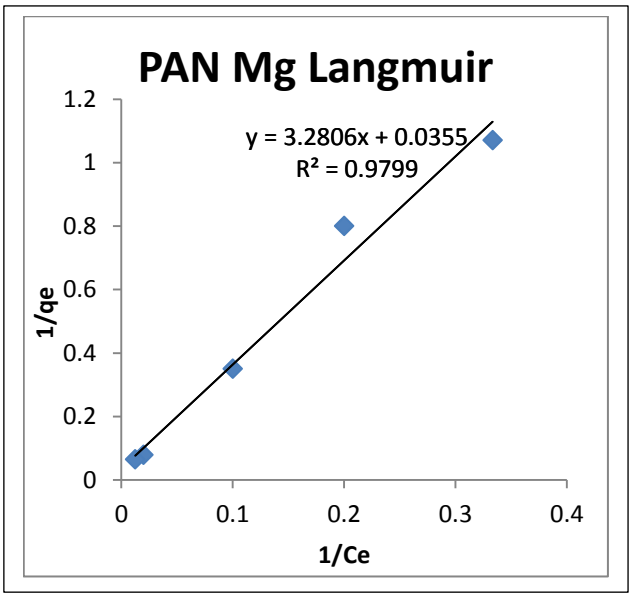

(a)

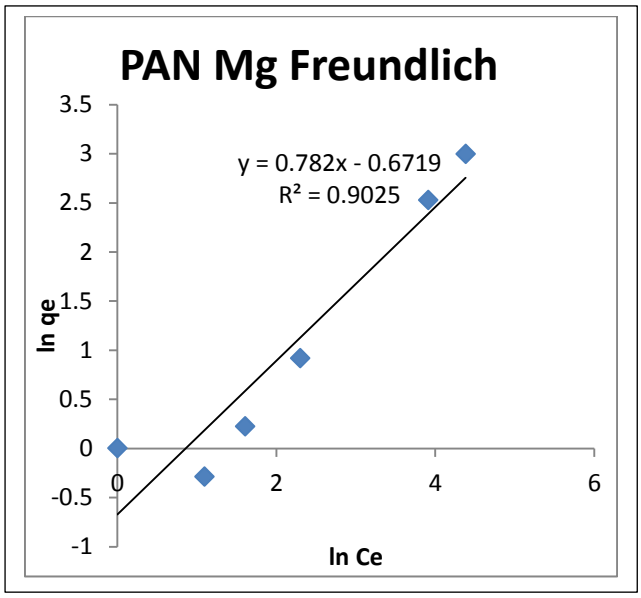

(b)

Appendix M (a) Linearized form of Langmuir and (b) linearized form of Freundlich for the sorption of Na^+ ions by PAN+ZEOLITE nanofibre.

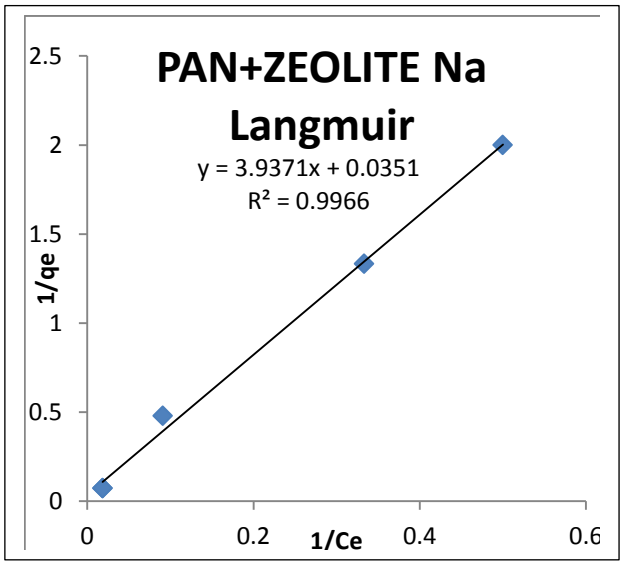

(a)

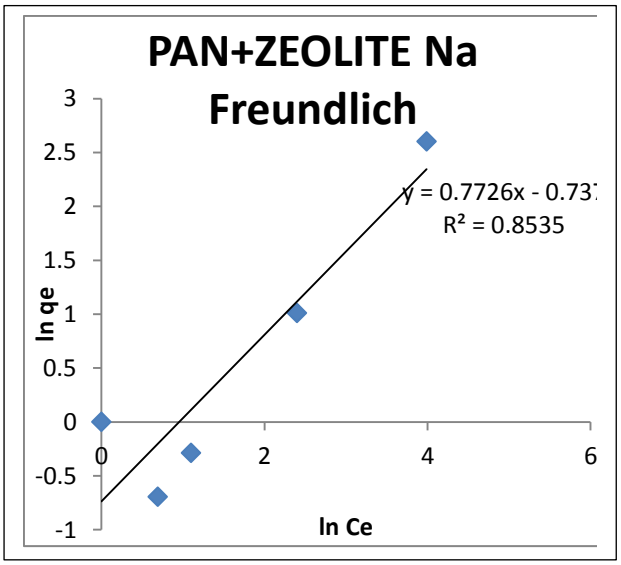

(b)

Appendix N: (a) Linearized form of Langmuir and (b) linearized form of Freundlich for the sorption of K^+ ions by PAN+ZEOLITE nanofibre

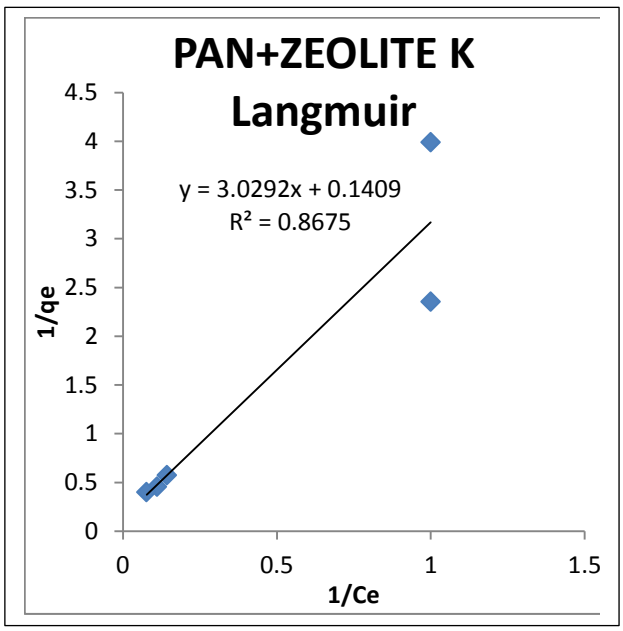

(a)

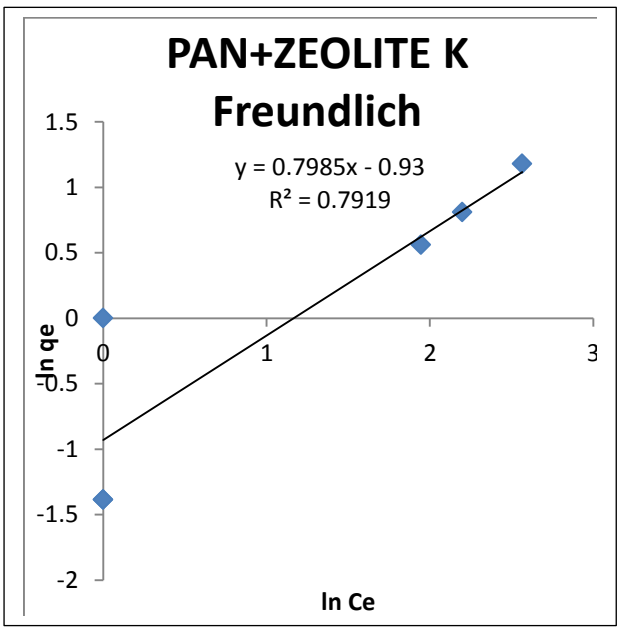

(b)

Appendix O: (a) Linearized form of Langmuir and (b) linearized form of Freundlich for the sorption of K^+ ions by PAN+TiO_2 nanofibre.

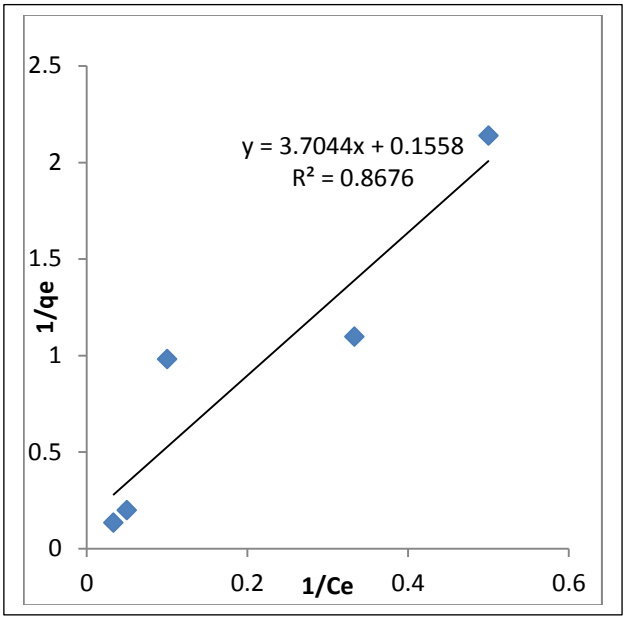

(a)

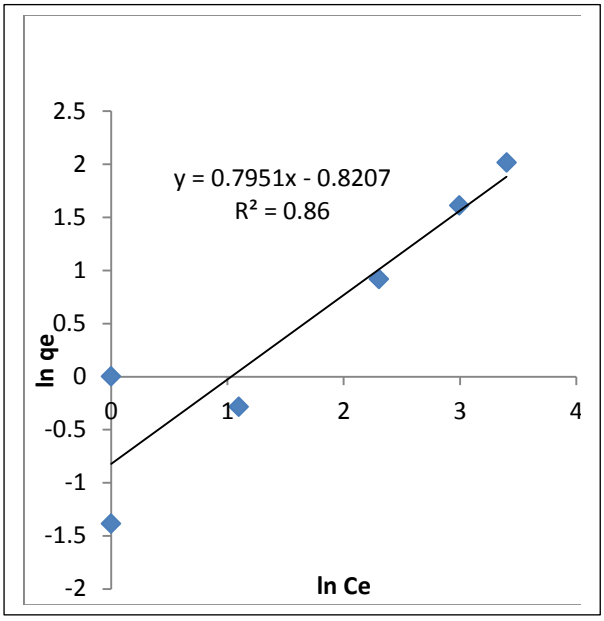

(b)

Appendix P: (a) Linearized form of Langmuir and (b) linearized form of Freundlich for the sorption of Na^+ ions by PAN+TiO_2 nanofibre.

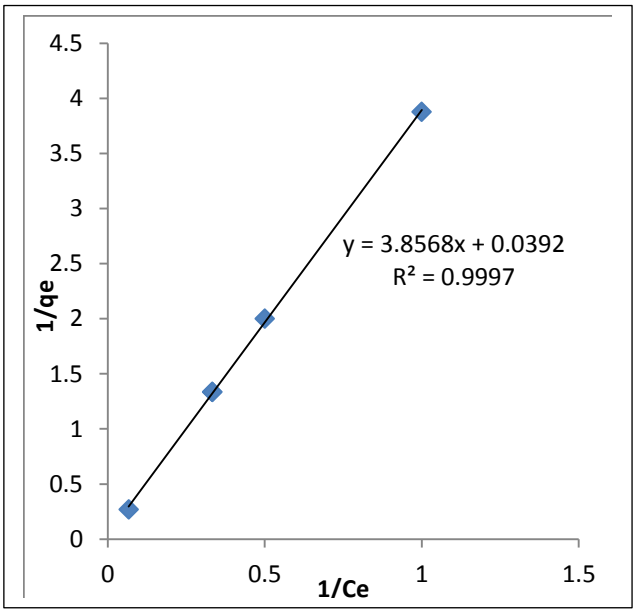

(a)

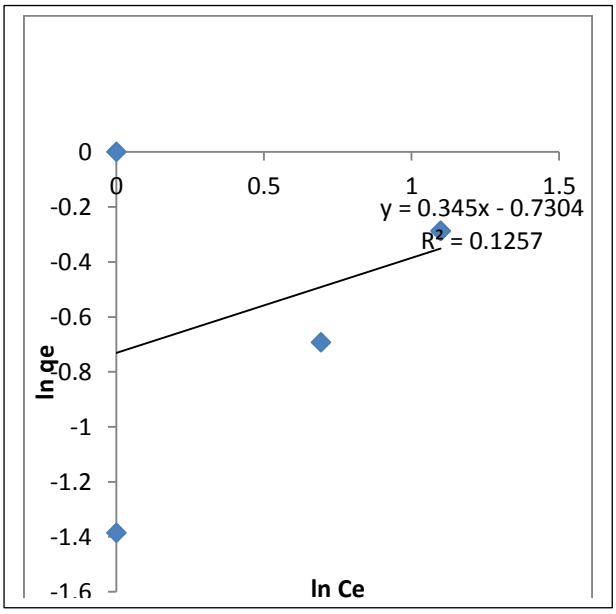

(b)

7.2 Kinetics of adsorption

In this section, the sorption kinetics table of results showing the sorption rates for Mg^{2+}, Ca^{2+}, K^{+} and Na^{+} ions by Purolite S950 resin, PAN, PAN+TiO_2 and PAN+ZEOLITE respectively is presented.

Appendix Q: Sorption kinetics for Mg^{2+} and Ca^{2+} for the respective sorbents

Time (mins)	**Mg^{2+} (mg/g)**				**Ca^{2+} (mg/g)**			
	Purolite S950 resin	**Pan**	**Pan+TiO_2**	**Pan+Zeolite**	**Purolite S950 resin**	**Pan**	**Pan+TiO_2**	**Pan+Zeolite**
60	7.75	1.75	0.5	0.75	7	0.5	0.25	0.5
120	11.25	1.45	0.75	1.25	11	1	0.5	1
180	14.25	1.45	1	1.75	14	1.25	0.75	1.25
240	17.5	1.45	1.25	2.5	17.25	1.25	0.75	1.75
300	19.75	1.45	1.25	2.5	20.5	1.25	0.75	1.75
360	21.5	1.45	1.25	2.5	21.25	1.25	0.76	1.76
420	22.75	1.45	1.26	2.5	22.5	1.25	0.75	1.75
480	23.5	1.45	1.25	2.5	23.25	1.25	0.76	1.75

Appendix R: Sorption kinetics for K^+ and Na^+ for the respective sorbents

Time (mins)	K^+ (mg/g)				Na^+ (mg/g)			
	Purolite S950 resin	**Pan**	**Pan+TiO_2**	**Pan+Zeolite**	**Purolite S950 resin**	**Pan**	**Pan+TiO_2**	**Pan+Zeolite**
60	1.57	1	1.25	1	1.25	3.5	2.5	0.75
120	4.25	1.25	1.5	1.25	2.5	3.51	2.75	0.76
180	4.25	2.5	1.5	1.25	2.5	3.51	3	1.5
240	4.25	2.5	1.75	1.25	2.5	3.52	3	1.5
300	4.25	2.5	1.75	1.25	2.5	3.5	3	1.5
360	4.25	2.6	1.75	1.25	2.5	4.25	3	1.5
420	4.25	2.5	1.75	1.25	2.5	4.25	3	1.5
480	4.25	2.5	1.75	1.25	2.5	4.25	3	1.5